THE UNIVERSITY
of EDINBURGH

Evaluation of the efficacy of bleomycin encapsulated within liposomes as novel, topical treatment for skin cancer in veterinary species and its potential for human medicine: an *in vitro*, *ex vivo* and *in vivo* study

Giulia Ferrari

Thesis submitted for the degree of Doctor of Philosophy (PhD)
The University of Edinburgh - 2020

THE UNIVERSITY *of* EDINBURGH

Doctor of Philosophy - The University of Edinburgh - 2020

Declaration

This thesis is submitted to the University of Edinburgh in accordance with the requirements for the degree of Doctor of Philosophy in the faculty of Medicine and Veterinary Medicine. The work presented is the work of the author except where stated otherwise by reference and/or acknowledgement. The candidate's contribution to the work in the publication is clearly stated in the manuscript. This work has not been submitted for award or degree at any other University.

Signed:

Giulia Ferrari

Table of Contents

List of Figures

List of Tables

List of Abbreviations

5-FU 5-Fluorouracyl

ANOVA Analysis of variance

ATP Adenosine triphosphate

ATM Ataxia-telangiectasia mutated

ATR Ataxia-telangiectasia and Rad3 related

BCC Basal cell carcinoma

BCG Bacillus Calmette–Guérin

BER Base excision repair

BPV Bovine papilloma virus

BLMH Bleomycin hydrolase

BSA Bovine serum albumin

cDNA Complementary DNA

CLSM Confocal laser scanning microscope

CO_2 Carbon dioxide

DAMP Damage-associated molecular pattern

DAPI 4,6-diamidino-2-phenylindole

DCM Dichloromethane

DMEM Dulbecco's modified Eagle's medium

DMSO Dimethyl sulfoxide

DNA Deoxyribonucleic acid

DSB Double-strand break

DTT Dithiothreitol

DUSP Dual-specificity phosphatase

ECL Enhanced chemiluminescence

ECT Elechtrochemotherapy

EGR4 Early growth factor-4

ERK Extracellular signal-regulated kinase

ES Enrichment score

F-Bleomycin Fluorescently labelled bleomycin

F-Bleosome Fluorescently labelled Bleosome

FACS Fluorescence activated cell sorting

FAD Flavin adenine dinucleotide

FDA Food and drug administration

FDR False discovery rate

FFPE Formalin-fixed-paraffin-embedded

FNA Fine-needle aspiration

FSC Forward scatter

HPLC High-performance liquid chromatography

HRR homologous recombination repair

IHC Immunohistochemistry

IC_{50} Half maximal inhibitory concentration

kDa Kilodalton

logFC Logarithm Fold change

EGR4 Early growth factor-4

FBS Fetal bovine serum

GAPDH Glyceraldehyde 3-phosphate dehydrogenase

GLM General linear model

GSEA Gene set enrichment analysis

HPLC High-Performance liquid chromatography

HRP Horseradish peroxidase

HYAL1 Hyaluronidase-1

IFN Interferon

IL Interleukin

IRF5 Interferon regulatory factor-5

IPA Ingenuity pathway analysis

MAPK Mitogen-activated protein kinase

ml Millilitre

mM Millimolar

MP Multiphoton microscope

MyD88 Myeloid differentiation primary response 88

MW Molecular weight

MS Mass spectrometry

NAD Nicotinamide adenine dinucleotide

NBF Neutral buffered formalin

NF Nuclear factor

NHEJ Non-homologous end joining

NMSC Non melanoma skin cancer

p- Phosphorylated

PAGE Polyacrylamide gel electrophoresis

PAMP Pathogen-associated molecular pattern

PBS Phosphate buffered saline

PCA Principal component analysis

PCR Polymerase chain reaction

PGE Prostaglandin E

PI3K Phosphatidylinositol-4,5-bisphosphate 3-kinase

R(D)SVS Royal (Dick) School of Veterinary Studies

RIN RNA integrity number

RNA Ribonucleic acid

RNS Reactive nitrogen species

ROS Reactive oxygen species

RPM Rotations per minute

RT Room temperature

SCC Squamous cell carcinoma

SDS Sodium dodecyl sulphate

SSB Single-strand break

SSC Side scatter

TEM Transmission electron microscopy

TLR Toll-like receptor

TNF Tumour necrosis factor

UD Ultra-deformable

VERC Veterinary ethical review committee

µL Microlitre

µM Micromolar

Acknowledgements

Firstly, I would like to thank my supervisors: Professor David Argyle and Dr Lisa Pang. I feel truly grateful to David, who has always been an inspiration to me, for giving me the opportunity to join his lab, for his guidance and help during good and bad times of my PhD, and for his constant support also after this experience. I don't think I have enough words to thank you Lisa, you have been such a wonderful supervisor and a fundamental guide. Thank you for giving me the confidence to trust in my ideas, for your infinite patience and availability, for your care about me as a student and person and for all your constant support. You are amazing for me and this PhD would have not be the same without you.

Many thanks to Dr Sunil Chopra and Dr Andrew Higgins for having supported this project and for the joy and passion demonstrated for this work.

Huge thanks to Bob Fleming, the wizard of the microscopy, for all his patience and guidance. Scott Maxwell for his generous help and for how fun it has been working with him, despite his extensive expertise. Steve Mitchell, for helping me through the TEM, always smiling and being kind with me. Mark Vendrell's group, especially to Fabio, for the kind collaboration. Many thanks to Jorge Del Pozo for having been so supportive and helpful every time I needed it. Greg Markby for all the help and advice, especially with qRT PCR and for RNA seq! A big thank you to Dr Maciej for your constant help with all the troubles I have encountered and for welcoming me every morning with your smiley 'buongiorno'!

Thanks to all the present and past brilliant scientists and wonderful persons of the Argyle Lab; you made my experience at the Roslin really unforgettable. Many thanks in particular to Rhona, I really don't know how I could have made this without you, you guided me since the first day I arrived and shared the joys and pains of the lab techniques with me!! Thanks Ylenia, for your help in starting this journey. Thanks to my lab mate/little sister Chantell, for the laughs, walks, chats and aerial classes together, I could not be more happy to have shared this experience with you crazy lady! Taty, for all the support and laughs together, all in all, we are from the same

(Italian-Brazilian) place! I can't thank you enough Erika (MIMI!!!), you are the most incredible person that I have met here and I really need to thank the Roslin Institute for that! I feel so blessed for having shared our ups & downs, 'fresh air' moments and our lives during the last 3 years.

Thanks to all the wonderful people that I have met at the Roslin Institute, for being such an inspiring and friendly bunch of people. Thanks to Bruno, for having trusted me since the very beginning, when I did not have any confidence in being able to do it. Gianluigi, for our funny and sometimes deep chats inside and outside the Roslin, thank you so much also for your help and all the never-ending working questions you always had an answer to. Anna! I feel so lucky to have found such a unique friend in you. I cannot thank you enough for being there for me every time, for your understanding, for all our laughs, and for all your help with every single working question I had (we can do it!!).

A big thank you to the clinicians and the nurses of the oncology division at the Small Animal Hospital of the Vet School, for giving me the possibility to join their fabulous team and helping with my research. Thanks to Richard Reardon, from the Dick Vet Equine Hospital for the patience and kindness in sharing data and for all your time.

During the last three years, Edinburgh gave me the incredible gift of meeting some beautiful people and I really want to thank them all, the past and the present ones, as they are part of my 'family' now. Many thanks to Lorenzo 'Ciaurello', for our trips, laughs, chats and special connection, Angelo for having been so kind and nice with me during all our adventures. Many thanks also to Marco, Franci, Stefano and Giorgia. Then, my favourite complainer Luca 'Musi'! Thank you for all our long chats, trips and dinners, and for our several 'debates' too!!! I can't really tell how important you have been for me during these Scottish years!

Thank you Jamie, for keeping me laughing, for being there for me, and lifting me up when I felt lost, with always the right words and cares; thank you for keeping the rhythm of my life in these last months!

Then, there are a few very special people that have been with me for a long time, and, as always, I have to thank them, as they are my ‘safe place’. In particular, thanks to Gina, for listening to me and understanding me always, thank you Giulia, you have been there for me every single day, every single time, and the way you are thoughtful and caring about me is extraordinary. The completion of this PhD is yours as much as it is mine. Thank you Gigio, you are my other side and my brother, and, as always, thank you for your constant presence and support.

Lastly, I want to thank my real family (my father, my aunts, my uncles and all my cousins) for the support and love they always show me. Most of all, thanks to Nella, my aunt, for being there for me always: thank you for listening to me and for making me feel that I have a ‘place to be’.

This work is entirely dedicated to my mother.

Lay Summary

Non-melanoma skin cancers (NMSC) are very common skin tumours that develop slowly on the upper layers of the skin and are usually removed by surgery but this can lead to disfiguring scars. Better treatments are needed for NMSC to minimise scarring and prevent the cancer from returning. Bleomycin is a drug used to treat different types of cancer in both people and animals, including NMSC. It is currently injected into patients but this leads to the drug also being distributed to other healthy tissues, and can cause severe side-effects that, in few cases, can lead to fatal lung damage. Ideally, we would like to apply bleomycin directly on to the skin tumour but bleomycin is a big molecule and cannot pass through the skin or directly enter into cancer cells to kill them. Therefore, we need to find new ways of packaging the drug to get it inside cancer cells. Once inside cancer cells bleomycin can kill them by damaging their DNA. However, we currently do not understand how bleomycin causes DNA damage.

Liposomes are small artificial bubbles of spherical shape that can be filled with pharmaceutical drugs. Liposomes are made up from the same building blocks, cholesterol and phospholipids, which make up our skin and cell membranes and are proposed to be able to pass through our skin and into our cells, to directly deliver the drugs into the cancer cells. In this study, we propose that liposomes can assist the drug delivery of bleomycin by improving absorption and penetration through the skin. We are using a new compound called Bleosome, which contains liposomes packed with bleomycin. Bleosome is a cream that can be applied directly to the surface of the skin and may be used in the management of NMSC in human and veterinary medicine. The main goal of this project was to evaluate the effect of Bleosome as a non-invasive and innovative therapy. Hence, we aimed to assess if Bleosome was able to penetrate through the skin and reach the target tumour, to evaluate how cancer cells respond to the treatment and what happens when we use Bleosome on real patients such as horses with sarcoids, a form of skin tumour. We found that: (1) Bleosome penetrated further through healthy skin, reaching a much deeper level than bleomycin. We repeated this experiment on skin removed from dogs, horses and humans and obtained similar results; (2) we confirmed using a number of different cancer cell lines, cancer cells

grown on plastic dishes in the laboratory, that Bleosome can kill cancer cells and that the amount of cancer cell death increases with increasing doses of the drug; (3) to better understand how Bleosome works we used a special technology called RNA-Seq to reveal changes in the activity of lots of genes at the same time after treatment with Bleosome. We observed that cells were not able to repair their DNA and eventually died by a process called autophagy; and (4) we treated a cohort of horses bearing cutaneous sarcoids, a type of skin cancer, with Bleosome after the bulk of the tumour was removed by surgery and showed that Bleosome was tolerated by the patients and lacked painful and harmful side-effects. In conclusion, Bleosome can effectively penetrate through the skin, kill cancer cells and is well-tolerated by horses with skin cancer. These are promising results indicating that Bleosome may be an effective treatment, with easy application and limited side-effects, to treat skin cancer that affects both humans and our pets.

Abstract

Bleomycin is a potent anticancer agent that is able to induce single and double stranded breaks in DNA. It is effective against several types of cancer, including cutaneous skin tumours, in both human and veterinary medicine. However, due to its molecular characteristics, including polar charge and high molecular weight, it is unable to effectively penetrate the skin barrier and freely cross the plasma membrane. Bleomycin can be administered systemically but is known to carry severe side effects such as fatal pulmonary fibrosis, which is the most concerning one and represents the main limiting factor to its potential use in clinical applications. Furthermore, several studies claim that bleomycin causes cell death in a cell-type dependent manner, although to date, the actual mechanism of action is not fully elucidated.

Advances in cancer therapy aim to minimise the side effects of treatments and improve the quality of life of patients. Within the context of developing minimally invasive treatments, liposomes have become highly valued for their ability to deliver payload drugs to the target tumour tissues and to be applied topically therefore decreasing systemic toxicity. Bleosome is a novel formulation of bleomycin where the cytotoxic agent bleomycin has been encapsulated in ultra-deformable (UD) liposomes. In this study, we evaluated Bleosome as a topical, non-invasive treatment for non-melanoma skin cancer (NMSC).

This PhD project also aimed to evaluate the mechanism of action and efficacy of Bleosome *ex vivo*, *in vitro* and *in vivo*. We hypothesised that encapsulation of bleomycin within nanoparticles, namely UD liposomes, enhances the penetration of the drug through the skin, and we tested this in three model systems: canine, equine, and human skin explants. Firstly, we optimised an imaging technique that allowed us to directly visualise the liposomes using the transmission electron microscope, and effectively fluorescently labelled bleomycin, prior to encapsulation within liposomes, to visualise penetration through skin and equine patient-derived sarcoids, using multiphoton microscopy. We concluded that lipid nanoparticles could act as penetration enhancers, carrying the entrapped bleomycin through the channels of the

outermost *stratum corneum* and subsequently releasing the drug and allowing it to penetrate deeper in the skin. At the cellular level, we determined the effect of Bleosome on cell viability on a panel of canine, feline and human cancer cell lines in vitro. Using live cell imaging, we showed that Bleosome is taken up by cancer cells more efficiently than free bleomycin. We also compared the variation in protein and gene expression in two canine cancer cell lines after 8 and 24 hours post-Bleosome treatment. Preliminary data showed that the response to Bleosome is cell type dependent, and the transcriptomic profiling of a canine cancer cell line treated with a time course of Bleosome revealed that these specific cells are unable to repair the DNA lesions, produced by Bleosome treatment. Lastly, we administered Bleosome to equine patients bearing cutaneous sarcoids, in an adjuvant setting, following laser excision. After surgical excision of the sarcoids, Bleosome was applied topically on the site of the scar in 12 horses, twice a day, for a mean length of 4 weeks. To date, after an overall follow-up of 12 months, 5 patients were in complete remission (41.6%), 4 experienced recurrences (33.3%), and 3 failed to follow up (25%). The treatment was overall very well tolerated and the study was still on going at the time of writing.

Overall, the findings of my PhD provide compelling evidence of the mechanism of action, efficacy and clinical benefit of Bleosome as topical, non-invasive treatment for NMSC.

Chapter 1 Introduction

1.1 Background

Non-melanoma skin cancers (NMSC) are the most common skin tumours currently diagnosed in Caucasian people (Simonetti et al. 2009). In veterinary species, within this cathegory of neoplasms, basal cell carcinoma (BCC) and squamous cell carcinoma (SCC) are the most frequently encountered in the canine and feline oncology cases (Amadori and Marconato 2012); while in horses, cutaneous sarcoids are the most common diagnosed cutaneous malignancies (Bergvall 2013). In both human and veterinary medicine, these tumours share similar features and outcomes. Although overall mortality from this cathegory of skin cancer is generally low in both humans and pets, NMSC causes considerable morbidity, particularly on the face in men, and can cause severe discomfort and impaired performance in dogs, cats and horses (Amadori and Marconato 2012; Knottenbelt 2019). Conventional therapies for NMSC include surgery, electrochemotherapy (ECT), radiotherapy, topical formulation of different cathegories of compounds alone or in combination (Galiczynski and Vidimos 2011; Amadori and Marconato 2012). However, all these standard therapies currently available can cause potential functional impairments and/or undesirable cosmetic outcomes (Burns and Brown 2005). Moreover, all these treatments are highly invasive, painful and, in some cases, require general anaesthesia. To address this unmet clinical need, our research focused on the evaluation of a novel compound called Bleosome. Bleosome consists of the anticancer agent bleomycin encapsulated within ultra deformable (UD) liposomes.

1.2 Overview of the key characteristics of bleomycin and potential benefit of liposomes encapsulation

Bleomycin is an anticancer agent belonging to the family of glycopeptide antibiotics. It was originally isolated from *Streptomyces verticillus* in 1966, by Umezawa and colleagues (Umezawa et al. 1966). Bleomycin is a phase-specific agent, exerting its maximum toxicity during M and G2 phases of the cell cycle, and hampering cell cycle progression during S to G2 transition (Riviere and Papich 2009). The principal target of bleomycin is the DNA, carrying out single (SSB) and double strand (DSB) breaks (Chen and Stubbe 2005).

Bleomycin is used as a first-line agent in human medicine, directed against malignant lymphomas and embryonal testicular tumours; bleomycin has also led to good results in the treatment of head and neck malignancies, cervical and skin tumours, including squamous cell carcinomas (Chen and Stubbe 2005). Despite its proved efficacy in human oncology patients, the use of bleomycin in veterinary medicine is still poorly established (Marconato 2009). It is highly valued in multidrug regimens because its toxicity does not overlap that of other anticancer drugs (Riviere and Papich 2009). However, bleomycin toxicity is dose-dependent and includes pulmonary inflammation, which has been reported to develop into fatal lung fibrosis in 1% to 3% of patients (Sleijfer 2001). This led to the development of new therapeutic strategies aimed to overcome this issue, therefore bleomycin started to be used in topical therapeutic regimens against skin tumours. The most exploited method in both animal and human patients is ECT, a topical treatment that employs the use of short electric pulses coupled with the administration of bleomycin. It has been successful in the management of skin tumours in humans (Zygogianni et al. 2016) and in pets (Impellizeri et al. 2016). Although, this method reduces the major systemic side effects of bleomycin, it also carries some adverse reactions and requires veterinary patients to undergo general anaesthesia.

Recently, the trend in cancer treatment is towards the development of more targeted and non-invasive therapies. To this purpose, particular attention has been focused on liposomes, which are nanocarriers able to deliver a wide range of drugs with reduced side effects and enhancing their therapeutic power. Given that bleomycin delivered by ECT enhanced the clinical outcome against skin tumours, a novel formulation of bleomycin was created by encapsulating bleomycin inside UD liposomes, a new generation of liposomes specifically designed to penetrate into the skin. This new

product is called Bleosome and is proposed to be a topical, non-invasive formulation of bleomycin, active in the management of cutaneous malignancies.

To date, few studies have been performed with bleomycin liposomal formulation (Lau et al. 2005; Arndt et al. 2001; Alomrani et al. 2011; Chiani et al. 2017). Although they have demonstrated that this type of bleomycin can be effective against different types of cancer cell lines there is a need to prove its therapeutic power and its benefit in reducing the severe toxicity *in vivo*. This may lead to the clinical use of Bleosome in the management of cutaneous tumours in veterinary and in human patients, and successful clinical trials in veterinary medicine may be an optimal basis for translating this therapy into human medicine. The innovative potential of the Bleosome resides in its lack of side effects as a non- or low-invasive treatment of skin tumours, resulting in the increased well-being of the patients and improved quality of life.

1.3 Bleomycin chemical structure

The molecular structure of bleomycin is composed of three functional domains: the N-terminal metal-binding domain, the C-terminal DNA-binding domain (encompassing the bithiazole tail), and the carbohydrate moiety. The linker region, situated between metal and DNA binding domains, has a key role in inducing DNA DSBs (figure 1.1) (Ramotar and Wang 2003). The N-terminal domain is flexible and can bind both redox-active and non-redox-active metal ions, such as iron and cobalt, respectively (Ehrenfeld et al. 1985). Among the metal ions, iron is predominantly used in clinical preparations of bleomycin, as it enhances the production of DNA lesions (Winkler et al. 1986). The metal ion is required to enable contact between bleomycin and DNA, and is able to produce radical species by activation of oxygen (Ramotar and Wang 2003). The pyrimidine moiety and the C-terminus domain of bleomycin are involved in selective DNA cleavage, by binding to N3- and N2- amino groups of the guanine 5’ to the pyrimidine cleavage site (5’-GC-3’) (Abraham, Zhou, and Hecht 2001; Hecht 2000; Chen and Stubbe 2004). Many studies have been conducted to evaluate the role of bleomycin domains showing that the whole molecule is bigger

than the sum of its parts, and that one single molecule of the drug is able to produce efficient lesions on both strands of DNA. Moreover, modifications of either the metal-binding domain, the linker region or the bithiazole group lead to reduced effects on the DNA cleavage ability of bleomycin (Chen and Stubbe 2005). Conversely, the role of the carbohydrate moiety still remains unclear. Recent studies demonstrated that removal of the carbohydrate moiety from bleomycin (creating deglycobleomycin) has little effect on its ability to cleave DNA *in vitro* (Leitheiser et al. 2000). However, a study demonstrated that deglycobleomycin appears to be about 100 times less toxic to Chinese hamster fibroblasts than the unmodified bleomycin (Tounekti et al. 2001) and there is evidence that it has a higher uptake in some cancer cells (Schroeder et al. 2014). Thus, a better understanding of the transport mechanism of bleomycin into the cells and developing strategies to increase its uptake are likely ways to enhance the anti-tumour effects of this drug.

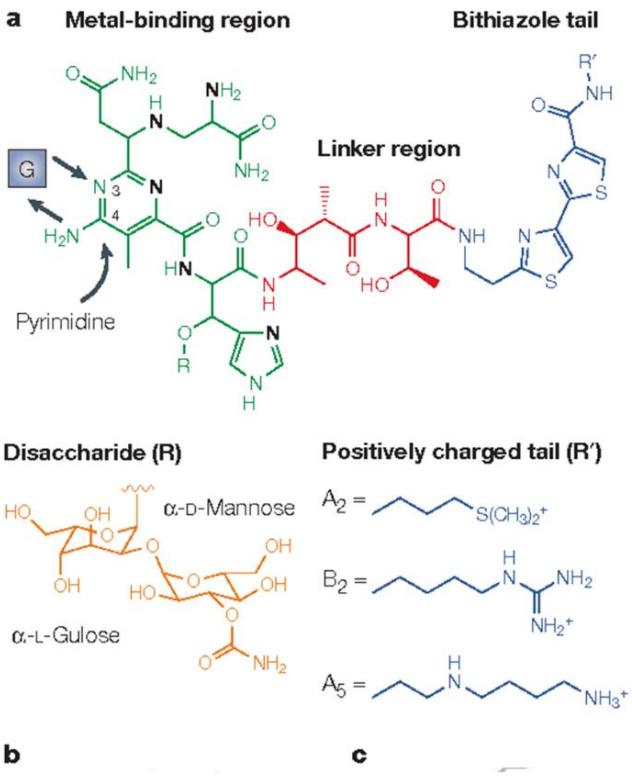

Figure 1.1 *Molecular structure of bleomycin. (a) The metal-binding region is in green, arrows show the pyrimidine moiety responsible DNA guanine; the linker region in red is connected to the bithiazole tail in blue.(b) The disaccharide moiety, in orange, may be involved in cellular uptake. (c) Three different positively charged tails are shown and they are responsible for the slight difference among pharmaceutical preparations of bleomycin, which are most commonly employed for clinical purposes. (Chen and Stubbe 2005).*

1.4 Bleomycin induced lesions in DNA and RNA

1.4.1 Single Strand DNA cleavage

The basis of bleomycin sequence specificity and its specific binding to DNA is attributed to the H-bonds between the pyrimidine (N3 and N4 amino group) in the metal-binding domain of bleomycin and the guanine, that is 5' to the cleavage site (2-amino group and the 3-N). The pyrimidine moiety is planar and aromatic, binds to the nucleic bases and intercalates between bases. Positively charged moieties distal to the bithiazole group penetrate the major groove and may provide ionic interactions with DNA phosphates (Chen and Stubbe 2005).

To be able to effectively cleave nucleic acids, bleomycin needs to be in its activated form (metallobleomycin) by binding transition metals (Fe(II) or CU(II)) and oxygen, in the presence of a one-electron reductant. This leads to the formation of the activated bleomycin, (BlmFe (III)-OH) (figure 1.2 (a)). The generated DNA damage is similar to that caused by ionising radiation (Chen and Stubbe 2005).

The activated bleomycin has a half-life of minutes and is responsible for commencing DNA damage. (Chen and Stubbe 2005; Richard M. Burger 1998 (B)). Depending on the presence of oxygen, this generated radical intermediate can be rearranged to produce different types of DNA lesions which are closely related to the ones produced by ionising radiation (Ramotar and Wang 2003). One of these products includes an apurinic\ apyrimidinic (AP) site, where the entire base is lost. The unstable sugar is also able to perform a DNA SSB where 3' end is terminated with a portion of the deoxyribose ring to form a 3' phosphoglycolate (3'-PG). It has been shown that this lesion is able to block DNA synthesis by DNA polymerase. The remaining portion of the fragmented sugar exists in the free base propenal form, which has the ability to react with DNA to form base adducts (Figure 1.2) (Chen and Stubbe 2005; Hecht 1986).

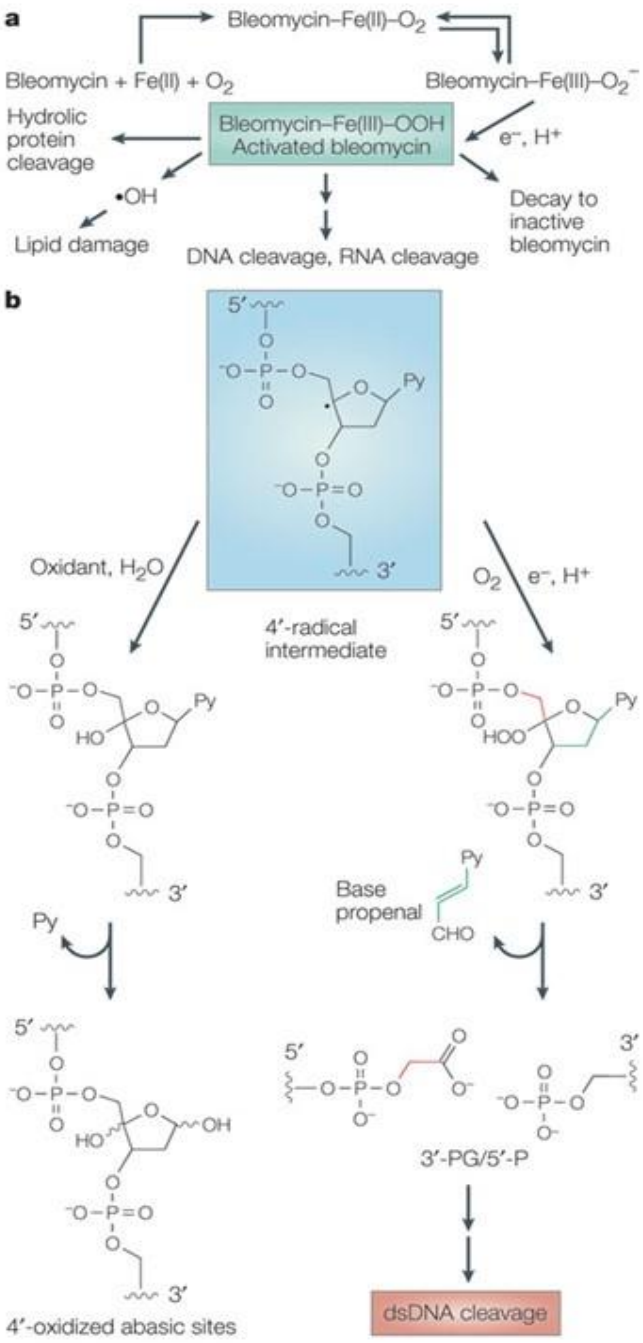

Figure 1.2 *Mechanism of DNA damage generated by bleomcyin. (a) bleomycin bond to transitional metal (Fe), forming the activated metallobleomycin. Depending on the availability of O2, this 4'-radical intermediate (blue box) can partition between two pathways (b). In the pathway on the left, the 4' radical intermediate is oxidized to a 4'-carbocation to which H2O is added, generating the 4'oxyidised abasic site. In the pathway on the right, the 4'-radical intermediate reacts with O2 to form a 4'peroxy radical. The resulting 4'-hydroperoxide then undergoes a complex series of chemical transformation, ultimately generating a gapped DNA 3' phosphoglycolate/ 5' phosphate (3'PG/5'P) ends and a pyrimidine propenal. (Chen and Stubbe 2005)*

1.4.2 DNA Double Strand breaks

Bleomycin also produces bi-stranded DNA lesions at certain specific sequences, such as CGCC, which are generated when the Fe-bleomycin complex creates an AP site on one strand and a directly opposed SSB on the complementary strand (Absalon et al. 1995). The spontaneous cleavage of the AP site by primary amines (e.g., histone amine) *in vivo* converts the bi-stranded lesion into a DSB (figure 1.3) (Absalon et al. 1995). However, DSB of DNA is affected by a single bleomycin molecule and consequently requires reactivation of bleomycin (figure 1.2 (b) right-hand side pathway) and bleomycin reorganisation during or after the cleavage of the first strand of DNA (figure 1.3) (Chen and Stubbe 2005).

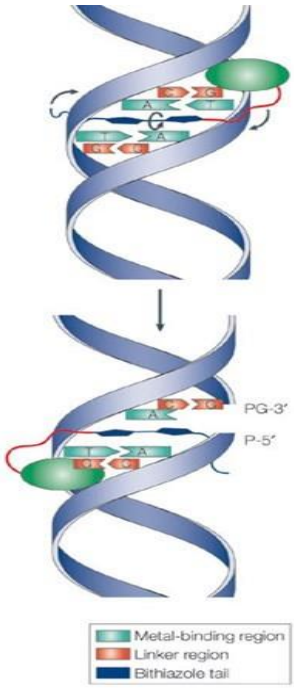

Figure 1.3 *Rearrangement of the bleomycin molecule during DSB. Stubbe et al, have proposed a model for reorganisation of bleomycin from one strand to the cleavage site in the second strand, based on structural information from bleomycin-CO(III)-OOH bound to a hot spot for DNA DSB. The key to the reorganisation is proposed to be the linker region and the flexibility of the bithazole tail that is bound by partial intercalation. The rotation around the bond between the two thiazole rings in the tail of bleomycin, together with the other motions, make the peroxide of the activated drug available for interaction with the second DNA strand (Chen and Stubbe 2005).*

In general, bleomycin-induced DNA lesions are mutagenic (Bennett, Swerdlow, and Povirk 1993) and some factors, rather than oxygen, may affect the nature of the bleomycin induced lesions, including the structure of the DNA (Kane et al. 1995). Moreover, when bleomycin is used in a clinical protocol including other DNA-damaging agents, it may cause irreparable DNA lesions (Chen and Stubbe 2005). Treatment of isolated nuclei from normal and cancer cell lines with bleomycin and analysis of DNA cleavage demonstrated that bleomycin preferentially damages internucleosome linker regions rather than nucleosome structure themselves (Kuo and Yang 2008).

1.4.3 RNA damage

Bleomycin also has the ability to cleave ribonucleic acids, including mRNA, tRNA and rRNA, with similar mechanisms to those targeting DNA (Hecht 1994). The cleavage of RNA is likely to occur at 5'-GU-3' sequences. However, despite the fact that *in vitro*, all the main classes of RNA can be cleaved by metallobleomycins (Burger et al.1981(A)), the extent of RNA lesions is significantly less than that of DNA (Chen and Stubbe 2004). Moreover, Abraham et al. (2001) have demonstrated that bleomycin can lead to the inhibition of protein synthesis in a rabbit reticulocyte cell-free system and in *Xenopus* oocytes. This may be due to the RNA damage promoted by bleomcyin. However, to effectively maintain a blockage of protein synthesis, high concentrations of bleomycin is needed. In summary, evidence that RNA is a therapeutic target in biological systems *in vivo* has received limited support (Hecht 1994; Ramotar and Wang 2003).

1.5 Resistance to bleomycin

The extent of the response of cancer cells to bleomycin is dependent on the tumour type. The reason why this drug seems to be more efficient against some malignancies rather than other is not well understood. A possible explanation for this could reside in the mechanism of drug resistance and in the different mechanisms of cellular uptake (Chen and Stubbe 2005; Pron et al. 1999). Bleomycin causes mutational lesions and it is likely that the normal cells of a cancer patient exposed to bleomycin rely on mechanisms that lead to repair the drug-induced lesions (Ramotar and Wang 2003). Several studies have identified repair pathways involved in repair of bleomycin induced lesions; among these, Xu et al. (1998) claimed that the SSB of DNA could be rescued by the base excision repair pathway using apurinic/apyrimidinic endonuclease 1 (APE1) and polymerase-β (POLβ). APE1 has an important role in processing the oxidised abasic sites. Furthermore, increased levels of APE1 in germ cell lines have been shown to correlate with bleomycin resistance (Chen and Stubbe 2005). In the case of POLβ, studies on cultured mouse macrophage cells (P388D1) showed that the inhibition of POLβ sensitised the cells to bleomycin damage, supporting a role of POLβ in the base excision repair pathway (Chen and Stubbe 2005). Moreover, as bleomycin is also capable of producing DNA DSB, it is likely that specific DS-lesion repair pathways are involved, such as non-homologous end joining (NHEJ) and homologous recombination repair (HRR) (Chen and Stubbe 2005). Other DNA protective factors include Hap1, a DNA repair enzyme (Robertson et al. 2001) and the integrin protein receptor family. This is consistent with a study that showed that yeasts are protected from the lethal effect of bleomycin by their cell walls. In animal cells, the family integrin proteins exert functions analogous to the yeast cell wall and can trigger signal transduction pathways similar to the one generated during yeast cell wall maintenance, and may activate a defence mechanism against bleomycin (Ramotar and Wang 2003). However, despite these insights, the mechanism of celluar resistance to bleomycin currently lacks of consensus.

1.5.1 Bleomycin hydrolase

Several studies identified bleomycin hydrolase (BLMH), a neutral cysteine protease, as another key factor in the bleomycin resistance. It is proposed to metabolically inactivate bleomycin in normal and cancer tissues (Umezawa et al. 1974). It plays an important role in antigen presentation, hydrolysis of homocysteine-thiolactone, breakdown of deaminated filaggrin into amino acids N-terminal proteolysis of huntingtin, and it is involved in other pathological processes such as atopic dermatitis, keratinization disorders and Alzheimer's disease (Wang et al. 2013). To better understand the role of BLMH the enzyme was shown to be able to hydrolyse the amino-alanine amide moiety at the C-terminus of bleomycin, generating the inactive de-amino metabolite (Sebti et al. 1991). Using a specific thiol protease inhibitor (E64) that blocks BLMH activity, it was shown that mammalian cells exposed to E64 become more sensitive to bleomycin (Sebti et al. 1991). However, recent studies in the yeast orthologue gene, BLH1, showed that it does not affect cytotoxicity of bleomycin in the organisms when deleted or overexpressed. Thus, the role of BLMH in producing tumour resistance is controversial (Ramotar and Wang 2003). On the basis of the ongoing studies, it would appear that BLMH has a more general role in cells to degrade proteins, and to indirectly regulate gene expression by degrading specific transcription factors (Koldamova et al. 1999). If this is the case, the bleomycin resistance observed by expression of yeast BLH1 protein in mammalian cells may be explained, for example, by the degradation of pro-apoptotic factors thus preventing cell death (Ramotar and Wang 2003).

1.6 Bleomycin transport

Bleomycin is a large hydrophilic molecule (MW 1.5 kDa), which is unable to passively diffuse through the cell plasma membrane effectively (Pron et al. 1999). It has been hypothesised that bleomycin cellular uptake may involve a specific receptor-mediated endocytosis mechanism. Based on models derived from Chinese hamster

fibroblasts and human head and neck carcinoma cell lines, the internalisation process depends on the number of "bleomycin receptors" on the cell surface and on the endocytic activity of the cells. After its uptake, bleomycin is internalised into vesicles but it is still unknown how bleomycin is released from the intracellular vesicles into the cytoplasm, and why only a few molecules of bleomycin reach the DNA under standard use of the drug (Pron et al. 1999). No further characterisation of this putative receptor or the endocytosis pathway has been reported. Identification of the plasma membrane receptor and its expression in different tissue could be the key to determining why there is differential toxicity of bleomycin between tumour cells and cells of the lung (Chen and Stubbe 2005). Other studies revealed that altered transport may be the general mechanism conferring bleomycin resistance, and bleomycin uptake might require *de novo* protein synthesis. A study claimed that bleomycin might share a pathway with spermidine uptake, which is blocked by the PTK2 kinase mutant, and that the drug was ultimately sequestered in the vacuoles (Aouida et al. 2004). The authors argued that sequestering bleomycin into vacuoles is a possible detoxification pathway and the observed cytotoxicity of bleomycin comes from non-sequestered drug, which diffuses from the cytosol into the nucleus. Schroeder et al. (2014) claimed that the uptake mechanism involves one or more cell surface receptors involved in glucose transport in tumour cells, which are upregulated in tumour cells to support their enhanced use of glycolysis. Recent studies suggest that the selective tumour cell targeting of the bleomycin is due to the disaccharide moiety of the drug (Yu et al. 2013; Madathil et al. 2014). At the present, there is no general consensus on either the efficiency of uptake into the cells or into the nucleus of cells. Furthermore, there is no consensus about the mechanism of uptake and about which part of the bleomycin molecule is essential for this process (Chen and Stubbe 2005). Given the importance of uptake and cellular distribution to differential cytotoxicity of bleomycin, further studies to elucidate these mechanisms are required.

1.7 Cellular response to bleomycin-induced DNA damage

Bleomycin is proposed to induce two distinct types of tumour cell death, which are dependent on the concentration of bleomycin within cells and, consequently, the

degree of DNA damage caused by DSBs. At low therapeutic doses of bleomycin, cells accumulate in G2/M phase, generating a mitotic cell pathway. At high doses, bleomycin causes extensive DNA damage by DSBs, leading to an apoptosis-like process (Tounekti et al. 2001; Chen and Stubbe 2005). However, the specific cell-death pathway induced by bleomycin is proposed to be cell-type dependent (Fulda et al. 2001). Studies in cell culture support a role for ATM in bleomycin-induced DNA damage. ATM is a phosphatidylinositol- 3-kinase-like kinase proposed to function as both a damage sensor and signal transducer. ATM is proposed to be required for the efficient activation of the DNA-repair pathway in response to bleomycin-induced DNA damage in mammalian cells. ATM activates the tumour suppressor protein p53, which has been heralded as the guardian of the genome for its role in mediating cell cycle inhibition, DNA repair, and apoptosis (Lu et al. 2017).Lee et al. (2010) found that bleomycin induces necrosis and apoptosis in wild-type p53 human non-small cell lung and colon cancer cells, and that p53 expression affected the sensitivity of these tumours to bleomycin.

Bugaut et al. (2013) also showed that bleomycin has an immunogenic effect by triggering the "immunogenic cell death" (ICD) whereby the DNA damage and the oxidative stress induced by bleomycin may trigger an event cascade that leads IFN gamma and CD8+ T cells to mount a response against the tumour cells. Furthermore, bleomycin may have a dual effect, as it also induces the production of TGF-beta by tumour cells leading to regulatory T cells (T-regs) accumulation, which limits anti-tumuor efficacy (Bugaut et al. 2013). In summary, preferential activation of these different cell-death pathways in different tumour cells lines could potentially account for differential cytotoxicity and cell-type dependent differences (Chen and Stubbe 2005).

1.8 Pharmacokinetic and clinical use

1.8.1 Systemic treatment

The main components of bleomycin sulphate, the form of the drug used for injection, are bleomycins A2 and B2, which differ in the terminal amine substituent of the common structural unit (figure 1.4) (Hospira 2013).

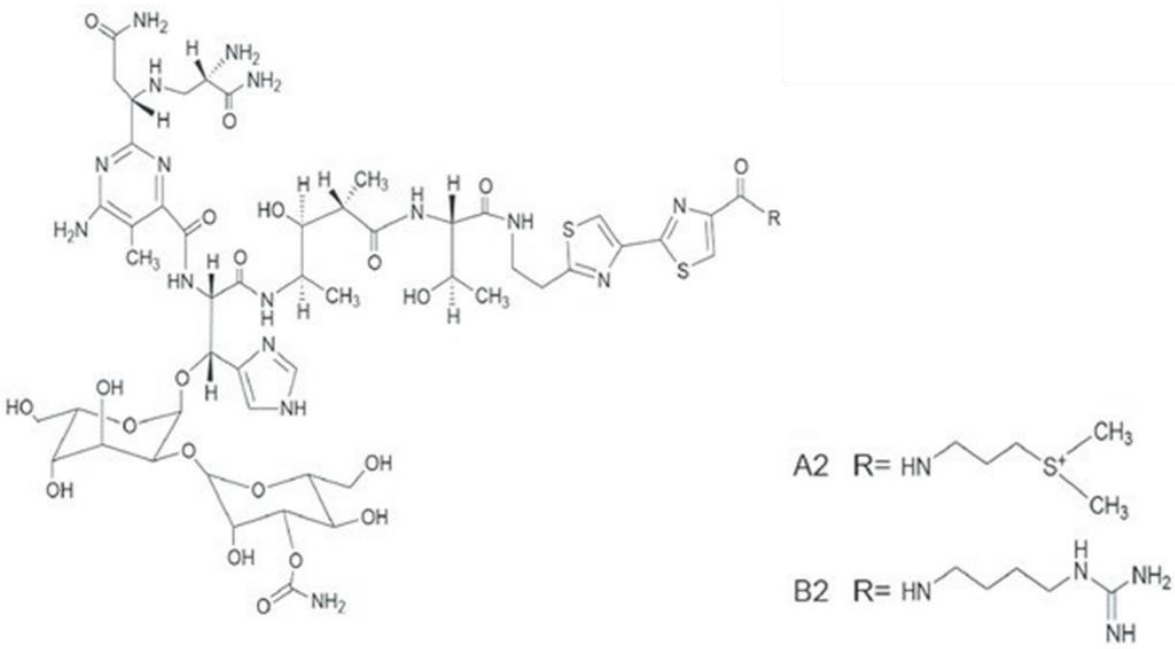

Figure 1.4 *Chemical structure of Bleomycin sulphate, including the A2 and B2 terminal amine substituents (He et al. 2016)*

In human medicine, bleomycin is commonly designed to be delivered as systemic drug. It can conventionally be administered by intramuscular, intravenous or subcutaneous injection (Hospira 2013). In veterinary medicine, it is essentially administered by subcutaneous, intralesional, and rarely, by intracavitary injection (Marconato 2009). However, its use is restricted by its intrinsic pulmonary toxicity (Froudarakis et al. 2013). After injection, bleomycin reaches a peak of plasma concentration in 30 to 60 minutes and it is homogeneously delivered in the body. However, it does not cross the blood–brain barrier, but it does pass through the placenta (Froudarakis et al. 2013). The primary route of elimination is via the kidneys. About 65% of the administered intravenous dose is excreted in urine within 24 hours with a mean terminal half-life of 2 hours following intravenous bolus administration (Hospira 2013). Indeed, renal dysfunction leads to significantly increased drug exposure (Froudarakis et al. 2013). At a cellular level, the inactivation of bleomycin

may involve BLMH. This enzyme is widely distributed in normal tissues with the exception of the skin and lungs, and this may explain the severe toxicity of bleomycin in these two tissues (Chen and Stubbe 2005).

Systemic use of bleomycin has been shown to be useful in the management of several neoplasms either as a single agent or in combination with other chemotherapy drugs. In human medicine, the tumours treated include lymphomas (Hodgkin's disease, non-Hodgkin's lymphoma), testicular carcinoma (embryonal cell, choriocarcinoma, and teratocarcinoma), SCC of head and neck (including mouth, tongue, tonsil, nasopharynx, oropharynx, sinus, palate, lip, buccal mucosa, gingivae, epiglottis, skin, and larynx), penis, cervix, and vulva (Hospira, 2013). Bleomycin has also been shown to be successful in the management of malignant pleural effusion as it has been proven to be an effective sclerosing agent for this disorder and in the prevention of recurrent pleural effusions (Hospira 2013). Although it has marked anticancer potential, bleomycin also causes severe side effects when administered systemically (Marconato 2009): skin adverse reactions have been reported in approximately 50% of treated patients consisting of erythema, rash, striae, vesiculation, hyperpigmentation, and tenderness of the skin. Hyperkeratosis, nail changes, alopecia, pruritus, and stomatitis have also been reported. It was necessary to discontinue bleomycin therapy in about 3% of treated patients because of these toxicities (Hospira 2013). The most serious side effects are pulmonary adverse reactions, occurring in approximately 10% of treated patients. The most frequent presentation is pneumonia, occasionally progressing to pulmonary fibrosis and approximately 3% of treated patients died of pulmonary fibrosis (Hospira 2013). This represents the main limiting factor to its clinical use, especially for veterinary patients. The molecular basis of bleomycin-induced lung injury (BILI) involves cytokines and free radicals as key effectors, and they are related also to low levels of BLMH in the lung, particularly in type II pneumocytes. This feature makes lung cells vulnerable to toxic effects of bleomycin during mitosis. Acute inflammation is central to development of BILI. Inflammatory exudate consists mainly of mononuclear macrophages, lymphocytes and neutrophils (Froudarakis et al. 2013). Continued exposure of lungs to bleomycin can lead to increase collagen synthesis and deposition of various matrix proteins including collagens, elastin, and proteoglycans. Moreover, bleomycin-activated alveolar

macrophages stimulate the synthesis of hyaluronic acid, a connective tissue molecule that is seen in fibrotic lungs (Froudarakis et al. 2013). Other side effects rarely seen in human patients and, to a lesser extent in animals include idiosyncratic reactions, vascular abnormalities (such as Raynaud's phenomenon), gastrointestinal disorders and pain at the local tumour injection site (Hospira 2013). In veterinary medicine, the use of bleomycin as systemic agent is poorly described, and its main utilisation is in the treatment of feline SCC (Marconato 2009).

1.8.2 Topical treatment

Bleomycin is an extremely toxic agent once inside the cell, but its high intrinsic cytotoxicity is restricted by the inability of bleomycin to freely diffuse through the plasma membrane (Gothelf, Mir, and Gehl 2003). This limiting factor along with its systemic toxicity, has highlighted the need for a new route of administration, aimed to potentiate its anti-cancer activities, enhance cellular penetration and reduce side-effects. Previously, several attempts to develop topical administration of this antibiotic were made in both human and veterinary medicine, including intralesional administration, photochemical internalization and the most efficient and well-studied ECT (Mir and Orlowski 1999; Glass et al. 1996; Rodrıguez-Cuevas et al. 2001; Spugnini, Citro, and Baldi 2009 (A); Tozon, Tamzali, and Cemažar 2017).

1.8.3 ECT

ECT is based on coupling electroporation with chemotherapy agents (Impellizeri et al. 2016). The structure of the cell membrane prevents the influx of hydrophilic drugs, macromolecules and peptides. By applying an electric current, it is possible to overcome this barrier by allowing the cells to become permeable to these molecules, which normally would not be able to cross the cell membrane. This method is called electroporation (Impellizeri et al. 2016). When electroporation is combined with certain chemotherapy drugs, the cytotoxicity of these drugs is increased by several-fold, leading to a dramatic improvement in the response of the treated tumour

(Impellizeri et al. 2016). Ideal drugs for ECT use are lipophilic, non-permeant or poorly permeant molecules with a high intrinsic toxicity (Mir and Orlowski 1999). Bleomycin is a non-permeant molecule, which cannot diffuse across the cell membrane because of its size, physical and chemical properties. When administered via parenteral route, cellular uptakes of bleomycin is dependent on transmembrane proteins, this mechanism is restricted by the number of proteins involved and by the speed at which these proteins can withdraw from the cell membrane. Electroporation enables almost free diffusion of bleomycin into the cells for as long as the cells remain permeable (up to 60 minutes). The cytotoxic effect of bleomycin can be increased by up to 700-fold when used in ECT (Mir and Orlowski 1999; Impellizeri et al. 2016). Bleomycin can be applied intralesionally or systemically before the electroporation (Impellizeri et al. 2016).

1.8.3.1 Human clinical applications

Substantial amounts of clinical data are published on the application of electroporation in human patients. The European Standard Operating Procedures for Electro-Chemotherapy (ESOPE) achieved an objective response rate of ~85% with a single treatment in a wide variety of skin tumours (melanoma, head and neck cancer, SCC, breast cancer skin metastases, cutaneous Kaposi's sarcoma) of 3 cm in diameter or smaller (Bertino et al. 2016; Dolinsek et al. 2016; Campana et al. 2016). Clinically, the application of ECT has been mainly focused on the treatment of cutaneous or semi-cutaneous tumours with palliative intent including melanoma, head and neck cancer, SCC, BCC, breast cancer skin metastases, cutaneous Kaposi's sarcoma. Among these, several studies have demonstrated that BCCs are one of the most responsive malignancies to ECT treatment using bleomycin (Glass et al. 1996; Rodriguez-Cuevas et al. 2001). However, ECT has been proved to be a useful palliative therapy in melanoma, breast cancer skin metastasis, and SCCs (Rodriguez-Cuevas et al. 2001). Moreover, ECT is one of the treatments of choice for tumours refractory to conventional treatment and can be used as cyto-reductive therapy before standard therapy. Finally, ECT can be adopted to treat haemorrhagic or painful nodules and it can be applied in previously irradiated areas (Giardino et al. 2006).

1.8.3.2 ECT in veterinary medicine

Several studies support the veterinary use of ECT coupled with bleomycin in the treatment of tumour types traditionally known to have limited or no treatment options, or to be poorly responsive to standard therapy (Spugnini, Citro, and Baldi 2009 (A); Tozon, Tamzali, and Cemažar 2017). Furthermore, Impellizeri et al (2016) achieved a good outcome in the management of unresectable tumours or those in inaccessible anatomical areas.

1.8.3.2.1 Canine studies

In canine patients, a wide range of neoplasms such as lymphosarcoma, hemangiopericytoma, neurofibrosarcoma, liposarcoma, acanthomatous epulis, melanoma, were responsive to ECT and bleomycin (Spugnini and Porrello 2003). One study, conducted on 9 dogs bearing different types of cutaneous tumours, achieved 38% of complete response for more than 5 months and 50% of partial response up to 19 months (Spugnini and Porrello 2003). Moreover, ECT and bleomycin has been a beneficial treatment for mast cell tumours (MCTs) when combined with surgery (Spugnini et al. 2006). Even with recurrence and re-treatment with ECT, survival ranged from 6 to more than 28 months. Coupling surgery with bleomycin delivered by ECT, there has been success in the treatment of a canine perianal gland adenoma, achieving a complete response after treatment, which lasted for more than 18 months (Tozon et al. 2005). This method of treatment could be ideal against tumours with behaviour limited to local recurrence (Impellizzeri et al. 2016). Furthermore, Reed et al. (2010) achieved a complete remission, treating an oral SCC and an acanthomatous ameloblastoma in dogs by coupling bleomycin with IL-12 gene therapy, delivered by ECT.

1.8.3.2.2 Feline studies

The main target of ECT in feline patients is SCC. In one study, ECT has elicited favourable responses against cutaneous SCC in cats treated with bleomycin administrated intravenously before electroporation (Tozon, Tamzali, and Cemažar 2017). Furthermore, Spugnini et al. (2015) conducted a non-randomised prospective study to evaluate the efficacy of bleomycin with electroporation compared to bleomycin alone in the treatment of 21 feline cases of periocular carcinoma, comprising 17 SCC and 4 anaplastic carcinomas, as well as to 26 cases with advanced SCC of the head. In the periocular cohort, 12 were treated with bleomycin and electroporation, and 9 received bleomycin alone. In the advanced SCC group, 14 received ECT, while 12 had bleomycin only. Of the 26 ECT treated cases, there were 21 complete responses and 2 partial responses, with the treatment being well tolerated and reported to have minimal toxicity. In contrast, the bleomycin only group (21 cases) had four complete responders and three partial responses. This finding is significant and supportive of the central role that cellular uptake may play in the efficacy of bleomycin treatment.

1.8.3.3 Side effects of ECT

ECT with bleomycin has shown to be a promising and efficient therapeutic option in the management of skin tumours. However, it produces some side effects, although milder compared to the systemic use of the drug, including painful underlying muscle contractions (Campana et al. 2016). In human patients, commonly local analgesia is sufficient to treat the pain, although in the treatment of multiple nodules, general anaesthetic is also described (Campana et al. 2016). In animal patients general anaesthetic is always mandatory, and for some patients classified in a critical ASA class, it can be a restricting factor for the use of ECT (Impellizzeri et al. 2016). Local side effects after ECT are erythema and slight oedema at the site of the treated lesions, which occurred in most of the patients and disappeared in a few days (Spugnini et al. 2009 (B)). In the study of Spugnini et al (2015), when ECT was performed in cats bearing periocular carcinoma and advanced SCC, they found that two cats in the advanced head SCC ECT group had local inflammation involving the deep subcutaneous connective tissues, which led to compulsive scratching. All of the cats that underwent ECT experienced transient muscular contractions at the time of treatment. Haematological toxicity was not observed in the 26 cats of the ECT study, except for mild neutropenia on day 7 in two cats (grade I according to VCOG-CTAE guidelines) (Spugnini, Pizzuto et al, 2015). Cardiac arrhythmias and respiratory dysfunction treatment-induced are also rare side-effects (Chaudhary and Rajuria 1995).

1.9 Novel therapeutic approach

Advancement in the management of cancer is focusing more on precise medicine and on delivering therapies specifically targeted against cancer cells, and diminishing the cytotoxicity to healthy cells. These attempts in reducing systemic side-effects have resulted in the development of less invasive treatments and major patient compliance. In 1906, Paul Ehrlich coined the phrase “magic bullet” to describe the liposomes as novel tools that are able to deliver the chemotherapy payload directly to the cancer cells (Utku 2011). The theoretical benefits of carrier-mediated drugs include greater

solubility, longer duration of exposure, selective delivery of entrapped drug to the site of action, superior therapeutic index and the potential to overcome resistance associated with the regular anti-cancer agent (Zamboni 2008). Early evidences in veterinary medicine on the efficacy of liposomes as novel selective carriers for chemotherapy were obtained in 1989, when MacEwen and colleagues assessed that the systemic treatment with muramyl tripeptide-phosphatidylethanolamine encapsulated in liposomes resulted in delayed metastatic disease in dogs bearing osteosarcoma following surgical amputation, and in significantly prolonged median survival times compared to patients receiving liposomes alone; authors reported also the lack of severe side effects following the liposomal chemotherapy treatment (MacEwen et al. 1989).

For these reasons, entrapping bleomycin in liposomes may improve the efficacy of this drug, allowing a targeted therapeutic approach and reducing systemic toxicological risks.

Bleomycin delivered by ECT has shown to be effective against skin tumours in both animals and human beings. Therefore, the compelling idea was to develop a new non-invasive treatment for this class of neoplasms, such as a topical skin treatment, using bleomycin encapsulated inside liposomes: the Bleosome. The hypothesis behind Bleosome's manufacture was to highlight the anti-cancer properties of bleomycin and to avoid the drawbacks of electroporation. Moreover, Bleosome could be formulated as cutaneous cream, which would have far-reaching applications as a completely non-invasive tool for both human and for animal patients. This PhD study is focused on testing the efficacy of this new formulation against NMSC.

1.9.1 Liposomes

Liposomes are valued for their biological and technological advantages as they are able to encapsulate ions and molecules inside their membranes (Bozzuto and Molinari 2015). Several types of liposomes are in clinical use and, to date, notable progress has been made in their formulation. Furthermore, new biomedical applications of liposomes are either in clinical trials or about to be put on the market (Bozzuto and Molinari 2015).

Liposomes are mainly composed of phospholipids, amphiphilic molecules that have a hydrophilic head and two apolar hydrophobic chains. Thanks to their amphipathic nature, when phospholipids are dispersed in aqueous solutions, they have a strong tendency to form membranes: the polar heads interact with the aqueous environment, whereas, their long apolar aliphatic chains promote interaction with one another forming two lipid layers (figure 1.5) (Papahadjopoulos, Cowden, and Kimelberg 1973). The hydrophobic chains of each layer face each other forming a lipophilic inner compartment that avoids the loss of the entrapped molecules, acting as a permeability barrier, both inward and outward. (Bozzuto and Molinari 2015). These lipid bilayers, indeed, are kept together by hydrophobic interactions, and the van der Waals forces are responsible for the interaction between long hydrocarbon tails, thus strengthening this architecture. Furthermore, hydrogen bonds and polar interactions between the water molecules of the aqueous environment and the polar heads of lipids stabilise this organisation. The final architecture of lipids relies on their nature, concentration, temperature, and geometric form (Bozzuto and Molinari 2015).

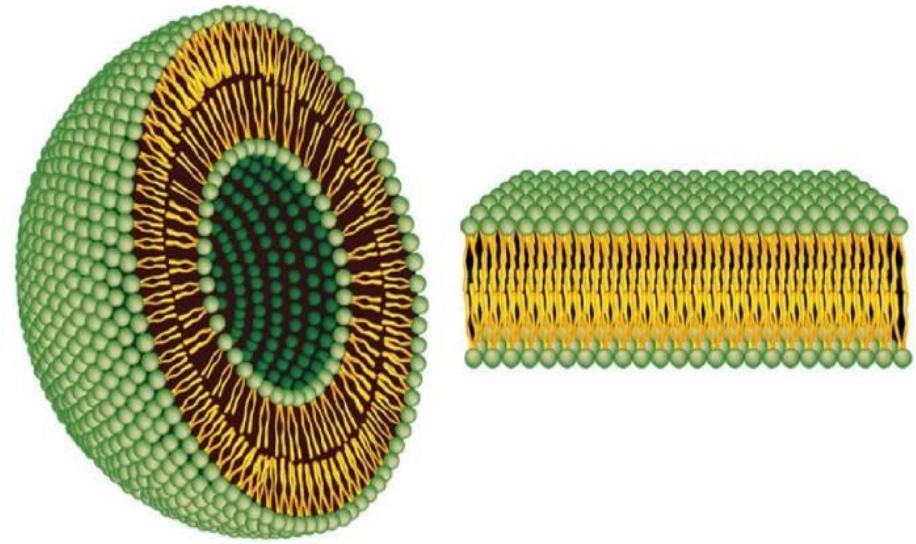

Figure 1.5 *Structure of a liposome (left), and a lipid bilayer (right). Liposomes are composed of a lipid bilayer, forming a membrane, with hydrophilic heads facing outward and hydrophobic chains interacting inward. From Bozzuto and Molinari 2015*

Liposomes can be classified on the basis of the preparation method (reverse-phase evaporation vesicles or vesicle extruded technique), size (small, intermediate, or large), and lamellarity (uni-, oligo-, and multilamellar vesicles) (Alavi et al. 2013). All liposomes have in common a structure that renders them capable of encapsulating both hydrophilic and hydrophobic drugs. The entrapment efficiency of a molecule in a liposome depends on its polarity and partition coefficient, which also determines its localisation in the liposomal membrane. If a drug is hydrophobic in nature, it resides in the acyl hydrocarbon chain of the liposome, whereas if a drug is polar or hydrophilic, it tends to localise in the aqueous central core or adjacent, near the polar head groups of the liposome (Noonan et al. 2014). Liposomes act like a protecting environment for the encapsulated drug, and, thanks to their properties, they avoid enzymatic degradation and immunologic and chemical inactivation of the carried molecule. Therefore, liposomes prevent a drug from being metabolised prior to reaching the target tissue and they minimise the exposure of healthy tissue to the encapsulated drug during its circulation in the blood. Both these effects contribute to an increase in the therapeutic index. In fact, high levels of the active form of a drug are delivered to the tumour site, enabling the expected cytotoxic effect to be achieved (Bozzuto and Molinari 2015). A characteristic of solid tumour tissues is the formation of a new vascular network with an increased vascular permeability. The enhanced permeation and retention (EPR) effect is a phenomenon characterising malignant tissues by which nanocarriers of an appropriate size can pass through tumour-vessel walls and enter the neoplastic lesion. In particular, the new vasculature, created by solid tumours, consists of a discontinuous endothelium with wide fenestrations, which enable large molecules (of about 4,000 kDa or 500 nm) to enter the interstitial space (Torchilin 2011). Liposomes can satisfy the size conditions needed to pass through tumour vessels and concentrate in the target site. This mechanism represents the major targeting principle for intravenously administered liposomes (Bozzuto and Molinari 2015). Another encouraging feature of liposomes is that they diminish systemic toxicity of the chemotherapy drugs. Therefore, when a therapeutic agent is encapsulated into these nanocarriers, it adopts the carrier's pharmacokinetics until the drug is released. As a consequence, liposomes modify both the tissue distribution and the rate of clearance of the loaded drug, thus any undesirable side-effects of the loaded

drug are dramatically reduced compared to the free form (Bozzuto and Molinari 2015). Despite this knowledge, the exact mechanism undergoing the pharmacokinetic and pharmacodynamics variability of these agents remains unclear, but most likely includes the mononuclear phagocyte system (Zamboni 2008). Elimination of liposomes takes place in different ways. The first involves absorption of plasma proteins on the surface of liposomes and then their recognition by the mononuclear phagocyte system. This event results in the excretion of the cargo at the hepatic level and its subsequent metabolism by Kupffer cells. Furthermore, liposomes are metabolised by splenic macrophages (Ishida, Harashima, and Kiwada 2002).

Physicochemical characteristics of the liposomes, however, influence the pharmacokinetics of the loaded drug; they can differ in lipid composition, size, membrane lipid packing, steric stabilisation, surface charge, dose, and route of administration. This confers to these carriers the advantage to well suit with the final therapeutic goal (Bozzuto and Molinari 2015). For this reason, a broad range of liposomes differing in formulation have been designed including: PEG-coated (or stealth) liposomes, which are able to better escape from mononuclear phagocyte system uptake and to circulate in bloodstream for a longer time compared to the non-PEG coated ones (Alavi et al. 2013); immunoliposomes, generated by coupling antibodies to the liposomal surface and allowing an active tissue targeting through the bond to tumour cell-specific receptors (Paszko and Senge 2012); dual function liposomes; and thermosensitive liposomes (Bozzuto and Molinari 2015). However, there are some drawbacks that inevitably affect the efficacy of liposomes; the most relevant ones include short half-life, instability, and the possibility of phospholipids undergoing oxidation and hydrolysis-like reactions, the leakage and fusion of encapsulated drug, and high production costs (Alavi et al. 2013).

1.9.2 Challenges to applicability of liposomes

An optimal delivery system for active drug needs to satisfy several necessary conditions including high encapsulation efficiency, long-term stability, small particle size with narrow size distribution. Although it has been assumed that liposomes have

a great potential for delivery of active principles, their applicability in clinics has faced many challenges (Van Tran, Moon, and Lee 2019).

Two of the major problems limiting liposomes utilisation in practical applications are their low physical and chemical stabilities (Takeuchi et al. 2001). The physical instability of liposomes can be explained by two parameters: changed particle size and size distribution due to the aggregation and fusion of vesicles and leakage of the entrapped drug (Grit and Crommelin 1993). Such destabilisations will happen at a faster rate when the surface charges of liposomes are decreased by pH or the presence of strong ions. It has been reported that liposomes with no or weak surface charges will tend to aggregate more readily than strongly charged ones (Van Tran, Moon, and Lee 2019).

The leakage of encapsulated drug strongly depends on the particle size and structural compositions of the liposomes. To ensure the physical stability of liposomes, therefore, increasing the surface charge and optimising the structural compositions and particle size will be necessary approaches (Van Tran, Moon, and Lee 2019). As for the chemical instability of liposomes, it has been suggested that oxidation and hydrolysis of the phospholipids may be one of the main pathways causing this problem (Grit and Crommelin 1993). Also, temperature and pH are the two major parameters that can significantly influence the chemical stability of liposomes, and it recommended that for long-term stability, liposomes should be stored at a low temperature (4-6 °C) and neutral pH (6.5) (Van Tran, Moon, and Lee 2019).

Another problem limiting the clinical application of liposomes is the low encapsulation efficiency of some molecules, especially hydrophilic ones such as vitamin C. It has been shown that by using conventional methods (thin-film, ethanol-injection methods) to prepare liposomes, hydrophilic substances may be easily dissolved in the external aqueous phase of liposomes, and as they are encapsulated in the aqueous cores of liposomes, this leads to low efficiency (Eloy et al. 2014). In addition, the conventional methods are based on the self-assembly of phospholipids in an aqueous environment and thus, because of the random nature of bilayer folding, these techniques will produce vesicles non-uniform in size and shape (Van Tran, Moon, and Lee 2019).

Large-scale production is also a major challenge. It has been reported that liposomes used for drug delivery can be fabricated by various techniques including mechanical

methods, such as thin-film, sonication, microfluidisation, extrusion; and techniques using aqueous solution to replace organic solvents, such as ethanol injection and reverse-phase evaporation (Van Tran, Moon, and Lee 2019). For large-scale production, however, it seems that majority of the methods are unsuitable, due to difficulties in scaling-up and limitated cost-effectiveness. Therefore, novel techniques that improve industrial production of nanoparticles for medical purposes are sought-after (Van Tran, Moon, and Lee 2019).

1.9.3 Skin cancers and liposomes as carrier for topical treatment

Liposomes have been utilised to encapsulate several types of drugs and designed to successfully deliver anticancer, antibacterial, antifungal, immunomodulation, diagnostics, ophthalmic, vaccines, enzymes and genetic elements. This enhances the therapeutic power and reduces the side effects of the encapsulated agents (Alavi, Karimi, and Safaei 2017). Focusing on cancer therapy, successful outcomes have been achieved by encapsulating very harmful drugs such as doxorubicin, oxaliplatin, cytarabine and paclitaxel (Zamboni 2008). Bleosome was designed to deliver the therapeutic benefit of bleomycin with reduced systemic toxicity. Based on the excellent results that ECT using bleomycin has achieved in the management of skin tumours, the primary aim of this study is to prove the efficacy of bleomycin encapsulated in liposomes in the treatment of NMSC in both veterinary and human patients.

1.10 NMSC

1.10.1 Human patients

In human medicine, NMSC are the most common type of cancer affecting Caucasian populations (Simonetti et al. 2009). They include, among others, BCC, the most commonly diagnosed skin tumour with 75% of incidence, and SCC (Anthony 2000). They both derive from epidermal keratinocytes. The major predisposing factor for the

development of these types of tumours is chronic sunshine exposure, followed by fair skin, other forms of ionising radiations, immunosuppression, previous skin malignancy and premalignant states, such as multiple actinic keratosis (Newlands et al. 2016). BCCs have several clinical presentations: the nodular lesions are the most frequently diagnosed and may have cystic or pigmented variants. Morphoeic BCCs are typically found on the skin of the head and neck, while superficial forms are predominantly located on the trunk (Newlands et al. 2016). BCCs are unlikely to rapidly grow and rarely disseminate (Daphu et al. 2014). However the Royal College of Pathology dataset, in 2014, established the term 'infiltrative BCC' for all high-risk histological variants and noted that many BCCs contain both high and low risk subtypes (Newlands et al, 2016).

The first clinical evidence of SCC is skin induration. The affected area may be plaque-like, verrucous, tumid or ulcerated, sometimes even without evidence of keratinisation (Daphu et al. 2016). Cutaneous SCC of the nasal vestibule or of the ear canal is often diagnosed late, resulting in poor prognosis. Conventional surgical excision, curettage and cautery, cryosurgery, Mohs micrographic surgery and radiotherapy are the most common invasive treatments for NMSC (Daphu et al. 2016).

Current topical treatments for NMSC include semi-solid formulations of 5-fluorouracil (5-FU), imiquimod and photodynamic therapy (PDT) (Barrera and Herrera 2007). 5-FU is a chemotherapeutic agent that blocks DNA synthesis and prevents cell proliferation (Galiczynski and Vidimos 2011). This medication has some side-effects, including an intense local inflammatory reaction that results in a lack of patient compliance. Other disadvantages are the relative long treatment period and partial inefficacy of the treatment to penetrate into the deep layers of skin (Barrera and Herrera 2007). Imiquimod is an immune response modifier that directly and indirectly interacts with the immune system (Perrotta, Giordano, and Malaguarnera 2011). Studies have revealed that almost all patients treated with imiquimod exhibit some degree of local inflammation at the application site. In FDA studies, patients presented some degree of erythema, oedema, ulceration or erosion (Burns and Brown 2005). PDT involves the administration of a photosensitising drug. Subsequent activation by light of a specific wavelength leads to the formation of highly reactive singlet oxygen (1O2), destroying the cells via chemical, biological and physiological reactions

(Araujo, Thomazine, and Lopez 2010). However, a 5-year follow up, multicentre study, demonstrated that PDT was less efficacy in the treatment of skin tumours compared to surgery (Rhodes et al. 2007).

1.10.2 Veterinary patients

BCCs are rarely observed in dogs and cats, with an incidence of 4-12% and 15-26% of the overall cutaneous tumours, respectively. BCCs are a low grade type of tumour. In animal patients, the aetiology is unknown and these malignancies can be found on the skin of head, neck, trunk and, occasionally on the nasal planum of cats. Clinically, BCC can be found in the solid, cheratinic and, in cats, clear cell form. Usually, the lesion is a single, hyperpigmented, cystic and sometimes ulcerated nodule (Amadori and Marconato 2012). The standard treatment for BCC involves mainly surgical excision, coupled with chemotherapy and radiotherapy for metastatic disease (Amadori and Marconato 2012).

SCC is more frequent, with an incidence of 5-15% of all cutaneous tumours in veterinary patients. It arises from keratinocytes and the aetiology is not well understood, although, like in humans, it is likely to be dependent from the action of sun exposure and from immunological disorders. In canine patients, the clinical presentation is a cauliflower-like lesion on the anatomical areas that are more exposed to the sun (ear, nose, ventral abdomen) and it is commonly a single lesion. It is well known that white haired cats are the most predisposed to develop this kind of malignancies, and the most commonly affected areas of the body are nasal planum, pinna, eyelids and lips. In this species, SCC is sometimes presented as multiple lesions (Amadori and Marconato 2012). SCCs are locally invasive with a low metastatic rate (Amadori and Marconato 2012). SCC are commonly treated with surgery, cryosurgery and in some cases, radiotherapy. Topical treatment for feline patients, like for humans, includes PDT and imiquimod, although they are not yet established treatment option for pets. It has been shown that they can carry side-effects similar to human medicine (Marconato et al. 2013). After PDT, hyperaemia, oedema, cyanosis and pruritus are reported. Moreover, for patients undergoing this treatment, general anaesthetic is needed (Marconato et al. 2013). In one study, 12 cats treated with imiquimod

manifested adverse reactions suspected to be associated with the use of the cream, including local erythema (25%), increased liver enzymes and neutropenia (8%), and partial anorexia and vomiting (Gill et al. 2008).

Sarcoids are the most common skin tumours in horses worldwide. The pathogenesis of this neoplasm is multifactorial, and the tumour is associated with bovine papillomavirus types 1 and 2 (Bergvall 2013). Clinical presentation varies and includes 6 types of lesions: occult, verrucous, nodular, fibroblastic, mixed, and malignant (malevolent) types (Knottenbelt 2019). This tumour does not normally spread to distant areas of the body, but can become very aggressive locally. Multiple tumours are common and all clinical types can be present in the same horse (Bergvall 2013). The tumour has a high risk of recurrence. Large, recurrent lesions carry a worse prognosis (Bergvall 2013). To date, there is no consensus on the optimal treatment for equine sarcoids (Knottenbelt 2019). The most common techniques involve the use of surgery, chemotherapy, immunotherapy, gene therapy, radiotherapy, photodynamic and phytotherapy. All of these therapeutic options are invasive or locally aggressive and painful for the patients, and several studies have concluded that none of them, even in combination, achieves a durable remission in a high proportion of patients (Knottenbelt 2019).

NMSC in both veterinary and human medicine share similar features in terms of biological behaviour and response to treatment; of note, despite the different nature of sarcoids, arising from mesenchymal cells compared to BCCs and SCCs that are epithelial tumours, this class of malignancies tends to have low rate of distance metastasis but is characterised by locally aggressiveness and by the tendency of relapsing after the treatment.

The limitations of the standard treatments of NMSC highlight the clinical need of developing new less invasive formulations, which are able to ensure optimal drug penetration through the skin and effective anticancer activity. Semi-solid conventional formulations, such as creams, ointments and gels, have been used for topical administration of drugs for many years (Fleury and Vianna Lopez 2011). Simple application of the formulations on the surface of the skin, however, is not sufficient to allow the drug to reach the site of action. This means that it is important for the

formulation to be capable to penetrate through the different skin layers to reach the tumour site (Schmid and Korting 1996). Nanocarriers, such as liposomes, could improve NMSC targeting, by enhancing the ability of the drug to reach and penetrate through the skin and into the tumour. Moreover, nanocarriers can improve drug stability and reduce skin irritation by avoiding direct contact of the drug with the skin surface (Schimid and Korting 1996). UD liposomes have been developed to efficiently traverse the *stratum corneum* and be effective drug carriers through skin layers (Jain et al. 2003).

1.11 Skin structure

The skin is the largest organ of the body and is composed of three main layers: the epidermis, dermis and hypodermis. The epidermis plays an important role in the defence against external environment and in the penetration of substances into the skin. It is the outer, avascular layer of the skin, primarily composed of keratinocytes. Due to cellular differentiation, the epidermis is divided into different layers, which are formed by the division of basal cells in the *stratum basale*, from the lower part of the skin toward the surface. Thus, basal cells undergo progressive maturation, giving rise to the spinous layer composed of squamous cells. From this stage, cells differentiate again, creating the granular layer and finally the *stratum corneum*, which is the outermost layer of the skin (Fleury and Vianna Lopez 2011).

The *stratum corneum* is the major barrier for the penetration of substances through the skin because of its heterogeneous composition, packed organisation of corneocytes and intercellular lipid matrix. The corneocytes are flat anucleated squamous cells, made essentially of keratin and encircled by a lipid matrix composed primarily of ceramides, cholesterol, and free fatty acids (Bouwstra et al. 2003).

In the *stratum basale*, there are two other cell types that are important in the context of skin tumour composition, melanocytes and Langerhans cells. Melanocytes are dendritic cells capable of melanin production, and Langerhans cells are antigen-presenting cells that are responsible for the immune response in the skin (figure 1.6) (McGrath and Uitto 2010).

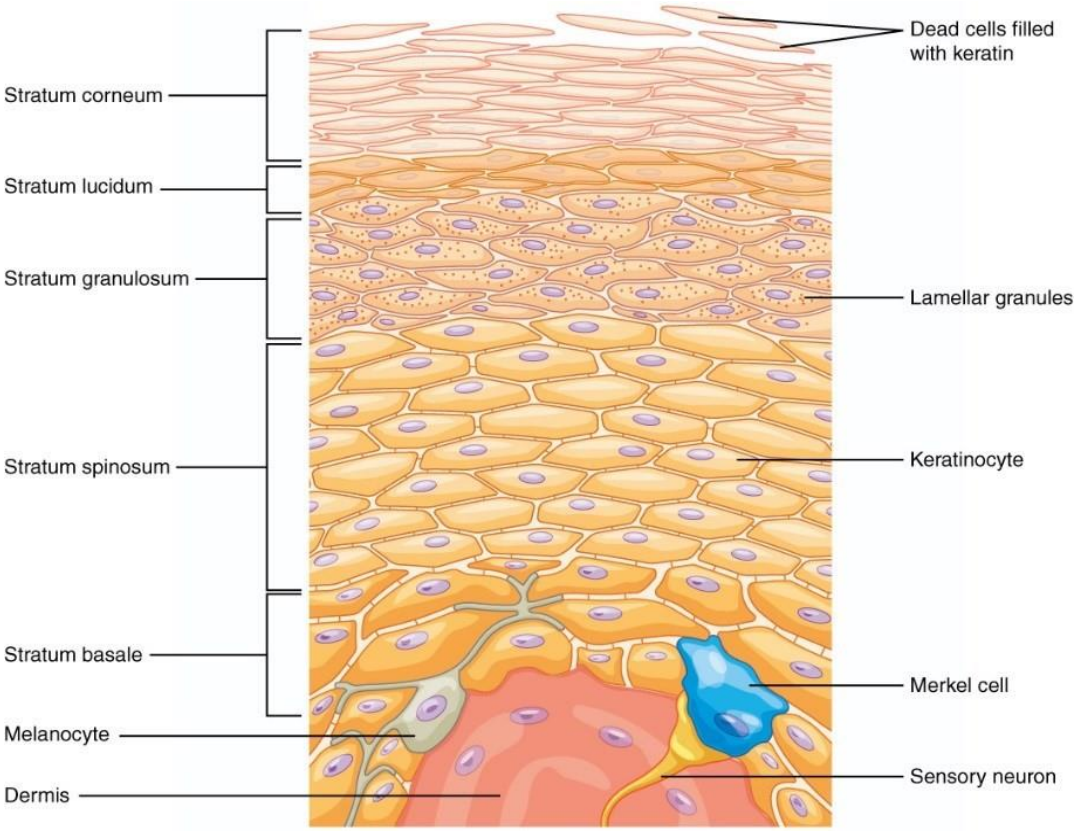

Figure 1.6 *Layers of the epidermis. The epidermis is the outermost part of the skin and consists of five layers of keratinocytes that start from the basal layer, mature and differ first in the keratinocytes of the spinous layer then in those of the granular layer to eventually become anucleated cells (corneocytes) in the stratum lucidum and finally in the stratum corneum. This maturative keratinization of the epidermis in a healthy subject takes about 3 weeks to occur. Corneocytes are the largest layer (approximately 85%) of keratinocytes and are securely held together by secretion of intercellular lipids from the same keratinocytes and, in the least, by sebaceous glands (Betts et al. 2013)*

The skin is a heterogeneous organ and contains a wide variety of cell types that can generate several types of benign and malignant tumours. For instance, SCC and BCC originate from keratinocytes (Fleury and Vianna Lopez 2011).

Over the past two decades, significant attention has been paid to understanding the mechanisms by which drugs penetrate through the skin. It is well known that substances usually penetrate the skin by three different routes: through the *stratum corneum* between the corneocytes (intercellular route); through these cells and the intervening lipids (intracellular route); or through the skin appendages, such as hair follicles and sweat glands (Moser et al. 2001). Molecules with adequate solubility in water and oil, with a log of oil/water partition coefficients between 1 and 3 (Mitragotri

et al. 2011) and a molecular weight lower than 0.6 kDa (Alnasif et al. 2014; El Maghraby, Williams, and Barry 2001 (B)) may penetrate through the skin. Therefore, topical administration is limited to hydrophobic and low-molecular weight drugs. Because most anticancer drugs are hydrophilic (like bleomycin), have low oil/water partition coefficients, high molecular weights and ionic characters, they do not easily penetrate the *stratum corneum* (Simonetti et al. 2009).

1.12 UD liposomes for skin penetration

Conventional liposomes are composed mainly of phospholipids (section 1.9.1). Liposomes formed with different components have been developed in an attempt to ameliorate the stability of the vesicles and their ability to penetrate through different membranes, especially the *stratum corneum*. Thus, elastic liposomes, also called UD or flexible liposomes were developed (Fleury and Vianna Lopez 2011). Conventional liposomes have limited ability to pass through skin layers and are deposited in the outermost cutaneous layer, whereas UD liposomes can penetrate intact skin, carrying therapeutic concentrations of drugs through the skin but only when applied under non-occluded conditions(Cevc and Blume 1992). Elastic liposomes were the first generation of elastic vesicles introduced by Cevc and Blume (1992) with an average particle size of 140.6 ± 19 nm. Their novel composition includes an edge activator added to phospholipid bilayers. An edge activator is often a single chain surfactant, having a high radius of curvature, that destabilizes lipid bilayers, increasing the deformability of the vesicle (Cevc et al. 1998; Cevc and Blume 2001; Honeywell-Nguyen and Bouwstra 2003(A)). Edge activators include sodium cholate, sodium deoxycholate, Span 60, Span 65, Span 80, Tween 20, Tween 60, Tween 80 and dipotassium glycyrrhizinate (Cevc et al. 1998; El Maghraby, Williams, and Barry 2001 (B)). Several studies investigated the likely mechanism by which flexible vesicles could improve delivery of drugs through the skin. Two mechanisms were proposed (Honeywell-Nguyen and Bouwstra 2003 (B)). First, vesicles can act as drug carrier systems, whereby intact vesicles enter the *stratum corneum* carrying vesicle-bound drug molecules into the skin (mechanism 1). Second, vesicles can act as

penetration enhancers, whereby vesicle bilayers enter the *stratum corneum* and subsequently modify the intercellular lipid lamellae. This will enable the penetration of free drug molecules into and across the *stratum corneum* (mechanism 2) (figure 1.7).

In more detail, the first mechanism was put forward by Cevc and colleagues for UD liposomes (Cevc, Schätzlein, and Richardsen 2002). They claimed that intact UD liposomes penetrated through the *stratum corneum*, under the influence of the naturally occurring transcutaneous hydration gradient (Cevc and Blume 2001). The driving force for UD liposomes penetration into the skin is xerophobia: the tendency of phospholipids to avoid dry surroundings (Cevc and Blume 2001). To remain fully swollen, UD liposomes need to move into the more hydrated layers of skin (epidermis and dermis), and this movement is driven by the hydration gradient across the layers of the skin, therefore UD liposomes can penetrate the intact skin because of their high deformability (Romero and Morilla 2013). In contrast, conventional liposomes become dehydrated and fuse to the dry surface of the *stratum corneum* and are able to only lie on the upper layers of this external surface, and do not pass beyond the first micron of the skin. UD liposomes are sensitive to the transdermal hydration gradient and can also exploit virtual channels in the skin barrier to enhance their penetration. These channels are also known as hydrophilic pores through which water can evaporate (Cevc, Schätzlein, and Richardsen 2002).

Mechanism 2 suggests that UD liposomes can enhance general penetration of encapsulated drugs through the skin. Verma et al (2003) found that these vesicles were able to carry both the entrapped and the non-entrapped hydrophilic fluorescent compound, carboxyfluorescein, into the *stratum corneum* and possibly to deeper layers of the skin, suggesting a penetration enhancing effect (Verma et al. 2003). However, in this study, the authors treated skin with carboxyfluorescein encapsulated in UD liposomes and with UD liposomes and free carboxyfluorescein outside of the vescicles. They observed that, when entrapped in UD liposomes, carboxyfluorescein penetrated into deeper skin layers than did when it was applied in its free form, separated by the UD liposomes. This might confirm the hypothesis of intact vesicle permeation, although the total amount of encapsulated carboxyfluorescein that penetrated into deeper skin layers and into the receiver compartment did not exceed

0.2% of the applied dose (Verma et al. 2003). In another study, flexible liposomes with ketotifen only on the outside of the vesicles significantly improved ketotifen skin permeation and deposition over deformable liposomes with ketotifen entrapped inside the vesicles, suggesting that the penetration enhancing effect may be of greater importance in the enhanced skin delivery of ketotifen by deformable liposomes (Elsayed et al. 2006).

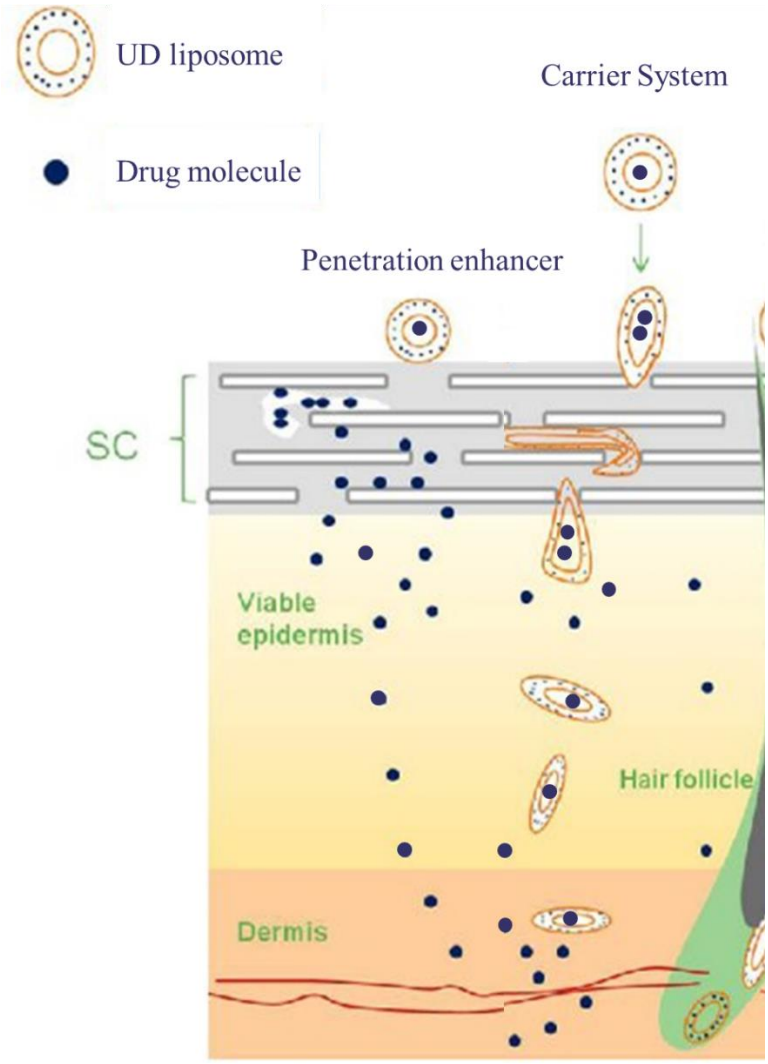

Figure 1.7 *Schematic representation of the two mechanisms of action of UD liposomes through the skins layers. On the right, the representation of the mechanism number 1 and on the left the mechanism number 2 proposed by Verma and colleagues are shown. Modified from Guo et al. 2015.*

Overall, the current experimental evidence suggests that both mechanisms may play a role in the enhanced skin penetration of drugs delivered using UDs. Closely related to this subject is the mechanism of drug release from vesicles. Entrapment might result in slow transdermal flux and suboptimum permeation. Once released, drug diffusion in skin must occur; thus, the fate of the released drug is dependent on its solubility in the tissue (Romero and Morilla 2013).

In summary, liposomes have been shown to be an innovative method to carry the entrapped drug to the target tissue and it appears that UD liposomes may enable their cargo to penetrate through the skin. However, the exact mechanism of improved skin penetration of entrapped drugs is still poorly elucidated and some reports describe liposome instability and drug leakage during the storage period (Fleury and Vianna Lopez 2011). *In vivo* experiments on patients should be performed to demonstrate the potential of flexible liposomes loaded with different anticancer drugs for topical skin cancer treatment (Fleury and Vianna Lopez 2011).

1.13 Preliminary evidence on the efficacy of Bleosome *in vitro*

Despite the potential clinical benefits of encapsulating bleomycin in UD liposomes, only a few studies have been conducted to test the efficacy of this novel formulation *in vitro*.

Arndt et al (2001) found that the encapsulation of bleomycin into liposomes strongly enhanced its antitumor activity against P388 leukemia and the Lewis lung carcinoma cell lines *in vitro*, and that its activity was comparable for liposomal and free drug in the B16 melanoma cells (Arndt et al. 2001). Another study investigated the effect of liposome composition on the cytotoxic efficacy of bleomycin against Daudi cell line from Burkitt's lymphoma, and showed that the efficacy of this formulation relied on the composition of liposomes, comparing fusogenic, flexible and pegylated vesicles (Alomrani et al. 2011). Furthermore, Chiani et al (2017) demonstrated that the

bleomycin encapsulated in PEG liposomes had lower toxicity compared to the free drug against TC-1 (mouse lung) and HFLF-P15 (human fetal lung fibroblasts) cells, but the cytotoxicity against LLC1 cells was significantly higher than that of unencapsulated bleomycin (Chiani et al. 2017). Furthermore, bleomycin entrapped in UD liposomes can effectively target SCC cell line *in vitro* (Lau et al. 2005).

These studies confirm the retained efficacy in killing cancer cell lines of liposomal bleomycin, compared to the free form, however they also highlight that there is still a the lack of consensus in literature about the different mechanism of action of free and encapsulated bleomycin. Moreover, they valide, the hypothesis of a cell-type dependent response to the treatment, and of the importance of the type of nanocarriers used for the delivery of bleomycin, according to the lesion to target. Further efforts are required to elucidate the molecular mechanisms triggered by Bleosome in particular cell lines, in order to improve the formulation of the compound and to potentially target mechanisms of resistance to bleomycin treatment.

1.14 Preliminary evidence on the clinical efficacy of Bleosome

Pilot studies have been conducted to determine the efficacy of Bleosome as topical, non-invasive therapy for NMSC. Firstly, Chopra and colleagues encapsulated the bleomycin in a film of UD liposomes and they checked the particle size and the entrapment efficiency of the novel composition over a time course (S. Chopra, personal communication). The size of the nanoparticles were stable up to 40 days, and thereafter began to slightly increase in size, going from initial 200 nm to 230 nm; however, this increase was low compared to the placebo formulation of liposomes, used as control, whose dimension increased up to 500 nm. When the entrapment efficacy was checked, the liposomal bleomycin relative entrapment curve indicated a loss of 50% of the original concentration of bleomycin (1mg/ml at day 0) within the liposomes at day 15. Following day 15, the curve continued downwards, showing a

gradual decrease to almost a fifth of the original concentration (0.53mg/ml to 0.11mg/ml) and the amount of the bleomycin outside the liposomes increased from 0.52 mg/ml to 0.65 mg/ml. In percentage, the amount of bleomycin in the liposome on day 13 was 45.5%, which subsequently decreased to 16.7% on day 69, resulting in a loss of 38.8% of active principle over 56 days (S. Chopra, personal communication). Chopra et al (in preparation) performed a pilot study on the clinical application of Bleosome, treating 60 named patients bearing NMSC including large BCCs, facial keratoachantoma and multiple actinic keratosis and reported 100% positive response to the treatment, with 97% of clearance rate, and concluded that Bleosome was well tolerated, painless, cost-effective and easy to apply (S. Chopra, unpublished data).

Furthermore, a study on the efficacy of Bleosome on equine sarcoids compared the efficacy of 5-FU or tazarotene alone and in combination with the topical application of Bleosome, and found that, the combination of treatments resulted in a much-improved outcome, and demonstrated the lack of side-effects of the liposome-encapsulated bleomycin, when administered topically to equine patients (Knottenbelt et al. 2018)

1.15 Conclusions

Skin cancer is the most common type of cancer affecting Caucasian populations. It has a very high rate of incidence, exceeding the sum of all other cancers combined (Simonetti et al. 2009). NMSC are not fatal but can destroy facial sensory organs such as the nose, ear and lips (Alam et al. 2011). Ideally, these lesions should be treated using non-invasive techniques.

There are some well-established treatments for NMSC, such as curettage, surgery, cryotherapy and chemotherapy. However, these conventional treatments lead to severe inflammation, pain and unappealing scars in human medicine (Lopez et al. 2004). Whereas in veterinary medicine the most common treatments involve

sometimes destructive surgical techniques. Moreover, pets must undergo general anaesthetic in the majority of the cases (Amadori and Marconato 2012).

To increase patient compliance and to reduce surgical costs and undesirable scars, the topical administration of anticancer drugs has been investigated. The topical administration of anticancer drugs is an interesting alternative for reducing side effects and for increasing drug targeting and therapeutic benefits (Fleury and Vianna Lopez 2011). Bleomycin is a potent anticancer agent that is able to induce SSB and DSB in DNA. It has proved to be effective against several types of tumours, including cutaneous ones. Because of its molecular characteristics (polar charge, high molecular weight, and system of cellular uptake) it is unable to freely cross the plasma membrane and efficiently reach the site of action. Treatment with high dose of bleomycin, also leads to severe side-effects, limiting its clinical application.

To address these issues, in the recent years, there has been an increasing interest in the development of new topical administration of bleomycin. Bleomycin administered through ECT regimen carried excellent outcome in the management of skin tumours, and the common target tumours in both veterinary and human medicine were NMSC. However, this technique can be invasive and may require a general anaesthetic.

For this reason, this study is focused on exploring the potential of Bleosome, a novel topical compound composed of bleomycin encapsulated in UD liposomes, as innovative non-invasive treatment for NMSC in veterinary and human medicine.

UD liposomes have the power to effectively ameliorate the drugs cellular uptake, to carry polar molecules through the skin, and to diminish the negative side effects of systemic chemotherapy. Moreover, it is likely that they act selectively in the tumour site. Despite this therapeutic potential there are few studies on the effectiveness of bleomycin encapsulated into liposomes *in vitro*.

We hypothesise that coupling UD liposomes with the potent anticancer agent bleomycin, it may improve the tumour targeting, lessen adverse reactions and create a non-invasive method to cure skin tumours in both humans and animals.

Experimental skin penetration study *in vitro, ex vivo* and *in vivo* will enable a mutli-layer understanding of the effective power of this new bleomycin formulation, the

extent of skin penetration and the efficacy against NMSC. This study may potentially impact veterinary and human medicine. Furthermore, NMSC as first class of target tumours may be the starting point in the effective management of skin cancers, as bleomycin had proven to be efficient against a wide type of tumours, including lymphoproliferative disorders and MCTs.

1.16 Rationale of the study: hypotheses and objectives

NMSC are very common tumours in humans and companion animals. Clinical challenges are often associated with definitive treatment of NMSC in veterinary species, and the management of this class of tumours often involves destructive and painful therapeutic interventions. Bleomycin encapsulated within UD liposomes is a promising novel minimally invasive anti-cancer therapy. Considering the similar clinical and pathological features of human and animal NMSC, veterinary patients could not only benefit from this easy and safe treatment, but also represent a comparable model for translating the application of the Bleosome into human medicine.

This PhD study aimed to test the following hypotheses:

1. Bleomycin is a large and hydrophilic molecule, which is not able to freely pass through cellular membrane and skin barrier. Hence, we propose that UD liposomes will facilitate and highly improve the penetration of the entrapped bleomycin through plasma membrane and through several layers of the skin.
2. Bleosome is comparable to the efficacy of bleomycin against several types of tumour.
3. Bleomycin acts in a tumour-type dependent manner and that is due to cell-type dependent response to bleomycin treatment.
4. Bleosome will enable the penetration of the active principle into the target cutaneous cancer lesion and avoid the systemic toxicity.

The objectives to be addressed in this PhD are:

1. To investigate the ability of Bleosome to penetrate through human, canine and equine skin and cellular membrane, and to determine the underlying mechanism driving penetration of Bleosome through the skin.
2. To determine the efficacy of Bleosome in inhibiting the cell viability in a panel of canine, feline and human cancer cell lines *in vitro*.
3. To investigate the signalling pathways and mechanisms activated at the molecular level in cancer cells in response to Bleosome treatment.
4. To clinically evaluate the efficacy and safety of Bleosome as topical therapy in the management of NMSC in veterinary medicine.

Chapter 2 Materials and methods

2.1 General materials and methods

General reagents, solutions and buffers are listed in Appendix 1 Buffers and Solutions. Phosphate buffered saline (PBS) was prepared by the Central Service Unit at the Roslin Institute (Midlothian, UK). Unless stated otherwise, cells were grown in T25, 75 and T175 cell culture flasks for adherent cells (Thermo Scientific, Paisley, UK). Falcon tubes (15 and 50 ml) were from Greiner Small 0.5 and 1.5 ml tubes were from Eppendorf (Loughborough, UK). Pipette tips were form Starlab. Centrifugations of 0.5 and 1.5 ml tubes were completed using the centrifuge 5415R (Eppendorf, Loughborough, UK) and 15 and 50 ml tubes using the 5810R (Eppendorf, Loughborough, UK). Reagents were weighed using a L2200S+ or BP210D balance (Sartorius, Goettingen, DE).

2.1.1 Cell lines

Six cell lines were used for this study. CML10 is a canine melanoma cell line, characterised and kindly provided by Lauren Wolfe (Auburn University, USA). REM134 and MCF7 are canine and human mammary carcinoma respectively, the first was characterised by Else et al (1982) (Edinburgh, UK) and the second was purchased from European Collection of Authenticated Cell Cultures (ECACC) (UK). C2 is a canine mastocytoma cell line with KIT tandem duplication of a 48bp sequence variation (reference: RRID:CVCL_1R44) (CA, USA). SSCF1 and SMG cell lines are both derived from feline squamous cell carcinoma (SCC), the first was characterised from a laryngeal lesion by T.J. Rosol (Ohio State University, USA) and the latter from an oral SCC carcinoma, by Erika Abbondati (The University of Edinburgh, UK). REM134 and MCF7 cells were grown in in Dulbecco's modified Eagle's medium (DMEM) (high glucose (HG) (ThermoFisher Scientific, Paisley, UK), while CML10 was grown in DMEM low glucose (LG), both supplemented with 10% foetal bovine

serum (FBS) and 1% penicillin/streptomycin (ThermoFisher Scientific, Paisley, UK). SMG and SSCF1 cells were grown in DMEM –HG (ThermoFisher Scientific), supplemented with 10 ng/ml EGF.
C2 cells were grown is Eagle DMEM (ThermoFisher Scientific) supplemented with 5% FBS,1% Non-essential amino acid, 1% Glutamax and 25 mg of Gentamicin. All cell cultures were maintained at 37°C in a humidified 5% CO_2 incubator.

2.1.2 Thawing cells

Cells were revived from frozen vials kept at -180°C. Cells were quickly defrosted in a 37°C water bath, transferred into a falcon tube containing 4 ml of warmed cell culture media and centrifuged at 5000 g for 5 minutes. The supernatant was discarded and the cell pellet re-suspended in 6 ml of warmed cell culture media before transfer into a T25 cell culture flask. Cells were incubated until ~ 80% confluence in a humidified 37°C, 5% CO_2 incubator and transferred to a T75 flask for further culture as described above.

2.1.3 Passaging cells

Cells were routinely passaged at 70 - 100% confluency every 4-5 days (REM134, MCF7, C2, CML10, SMG, SCCF1). To passage cells, cell culture media was removed and cells were washed twice with 5 ml of PBS. Cells were then incubated with 1-3 ml of 0.25% Trypsin-EDTA (ThermoFisher Scientific, Paisley, UK) at 37°C 5% CO_2 for 5-15 minutes until detached. Trypsinization was terminated by adding at least twice the trypsin volume of cell culture media containing FBS to the cells and washing well to ensure efficient cell collection. Cells were seeded at the required cell number into new cell culture vessels with fresh warmed cell culture media.

2.1.4 Counting cells

A haemocytometer was used to manually count cells. Following trypsinization as described in section 2.1.3, the cell suspension was centrifuged at 500 g for 5 minutes and the pellet resuspended in 1 ml of PBS. The cell suspension was mixed in a 1:1 ratio with Trypan Blue stain (ThermoFisher Scientific, Paisley, UK) and added to the counting chamber of the haemocytometer. Live cells (not stained blue by Trypan stain) were counted in the 5 x 5 square counting chamber and the total cell number was calculated by the following formula:

Cells / ml = (Number of cells in 5 x 5 counting chamber $\times$ 2 (dilution factor)) $\times$ 10^4

2.1.5 Freezing cells

Cells were grown to near confluency (~ 90%), trypsinised, and the total number of cells calculated as above. Each cell line was frozen down at approximately 3 x 10^6 cells in 0.5 ml of freezing media per cryogenic vial. The cell suspension was centrifuged at 500 g for 5 minutes and re-suspended in the appropriate volume of freezing media. The cell suspension was then aliquoted into cryogenic vials, placed into a Mr Frosty™ freezing container (ThermoFisher Scientific, Paisley, UK) (which contains 100% isopropyl alcohol for a steady freezing rate of 1°C per minute) and frozen in a -80°C freezer for at least 12 hours. Vials were then transferred to a -180°C freezer for long-term storage.

2.1.6 Harvesting cells

To harvest adherent cells, cell culture media was removed and cells were washed twice with chilled PBS. Depending on the size of the cell culture vessel, cells were then scraped with a cell scraper in 200 µl to 1 ml of ice-cold PBS (6 well plate to T75 flask) and collected in 1.5 ml Eppendorf tubes. The cell suspension was centrifuged at 1500

g for 3 minutes at 4°C. The supernatant was discarded and the cell pellet was snap frozen on dry ice and stored at -80°C.

2.1.7 Cell lysis

To lyse harvested cell pellets, 2-3 times the volume of urea lysis buffer (Appendix 1, Buffers and Solutions) was added to the frozen cell pellet (no more than 100 µl per pellet). The mixture was pipetted up and down until all particles of the cell pellet were dissolved, and the lysate solution was incubated on ice for 30 minutes. The solution was centrifuged at 13000 g for 10 minutes at 4°C. The supernatant (cell lysate) was transferred to a new tube, snap frozen on dry ice and stored at -80°C.

2.2 Cytotoxic drug treatment

Bleosome 0.2% is a compound containing bleomycin encapsulated in Ultra-Deformable (UD) liposomes designed to be delivered topically. Bleomycin aqueous solution (cream) 0.2% is made by bleomycin dissolved in aqueous solvent in the form of cream. Bleovet 0.2% is made by bleomycin dissolved in aqueous solvent in the form of gel. All the formulation were manufactured and provided by Ascot Laboratories LTD, London, UK. Bleosome and bleomycin aqueous solution were supplied in a cream, and Bleovet in a gel form containing 1.32221 mM (2mg/ml) of active principle (bleomycin). All compounds were stored at 4°C (fridge temperature) before and after use.

2.2.1 Cell viability assay

The CellTiter-Glo® Luminescent Cell Viability Assay kit (Promega, Madison, USA) was used to determine the viability of cells after treatment with indicated titrations of Bleosome and bleomycin aqueous solution. The kit determines the number of viable cells in culture based on the quantity of ATP present. A luminescent signal is produced

proportional to the amount of ATP present, which is directly proportional to the number of viable cells. Experimentally, cells were trypsinised and seeded as single cells in opaque 96-well plates (Corning, CA, USA) at 500 cells per well and incubated for 24 hours. Then, either serial dilutions of Bleosome and aqueous cream bleomycin were added in triplicate wells. Cell viability was measured 72 hours post-treatment. According to the manufacturer's instructions, the CellTiter-Glo® Substrate and CellTiter-Glo® Buffer were thawed at room temperature and mixed in a 1:1 ratio into a homogenous solution by inverting to form the CellTiter-Glo® Reagent. The 96–well cell culture plate was allowed to equilibrate to room temperature for 30 minutes prior to the addition of 100 µl of CellTiter-Glo® Reagent to each well. An ATP standard curve was produced in the same 96-well cell culture plate. ATP concentrations used to form the standard curve were 10 µM, 1 µM, 100 nM and 10 nM. CellTiter-Glo® Reagent is also added to the ATP standard wells. The cell culture plate was mixed for 2 minutes on an orbital shaker and incubated at room temperature for 10 minutes. Luminescence was recorded for 1 second per well by a spectrophotometer (WPA Biowave, Biochrom, Massachusetts, USA) using the Viktor3 software. Data was averaged and normalized against the average signal of vehicle control treated samples and a dose-response curve was produced.

2.2.2 Colony formation assay

To determine colony forming ability, cells were trypsinised into single cells and seeded at 1000 cells / 10 cm plate (CML10) or at 500 cells / 10 cm plate (REM134). Three concentrations of Bleosome and aqueous cream bleomycin were added to media immediately after cell seeding. Plates were incubated at 37°C in humidified 5% CO_2 incubator for 10-14 days. When colonies were visible, media were removed, and the cells were washed twice in PBS. Five ml of cold methanol were then added to each plate and incubated at RT for 5 minutes. The methanol was removed, and 10 ml of 10% Giemsa stain (Sigma-Aldrich, USA) was used to stain the colonies for 20 minutes. The plates were rinsed thoroughly in tap water and air-dried. For each

concentration tested, plates were set up in triplicate. The total number of colonies was manually counted and the average number of colonies for each condition calculated.

2.3 Protein analysis

2.3.1 Protein quantification – Bradford assay

A Bradford Assay was used to quantify total protein concentration of samples. Briefly, a 1:5 dilution is made of each cell lysate sample at the point of lysing. In a 96-well plate, 5 µl of the 1:5 cell lysate sample is transferred to a well, with each sample tested in triplicate. As a control 1 µl of each BSA standard solution (0.125, 0.25, 0.5, 1, 2 and 4 mg/ ml) was assayed, also in triplicate at the same time. To each well containing a sample, standard and to three blank wells, 250 µl of Quick Start™ Bradford 1x Dye Reagent (Bio-Rad, Watford, UK) was added and mixed well. After 5 minutes, the plate was read for absorbance (optical density at 560 nm) using a spectrophotometer (WPA Biowave, Biochrom) using the Viktor3 software (PerkinElmer). A standard curve was produced by plotting the standards (a linear relationship was determined). The equation of the line was used to calculate the concentration of the samples.

2.3.2 Western blotting by SDS page

Proteins were resolved based on their molecular weight by SDS polyacrylamide gel electrophoresis (SDS PAGE) (Laemmli 1970), transferred to Amersham™ Hybond-C™ nitrocellulose membrane (Amersham Pharmacia Biotech, Buckinghamshire, UK) and hybridised to an appropriate primary antibody and HRP-conjugated secondary antibody for subsequent detection by enhanced chemiluminescence (Amersham™ ECL™, Buckinghamshire, UK).

2.3.3 Gel preparation

The polyacrylamide gels were prepared and assembled using the Biorad Protean II mini-gel system. Cover slips and 1 mm spacer plates were cleaned with 70% ethanol and the casting frame was assembled. The plates were checked for leaking by incubating with water for 5 minutes and emptying. The resolving gel was prepared by combining 6 or 12% acrylamide (depending on the size of the protein of interest), along with 5% stacking gels, Resolving gel was made up using 30% acrylamide/ 0.8% bisacrylamide solution (National Diagnostics, USA), 1.5 M Tris-HCl pH 8.8 and 10% SDS at 10 ml per gel and the stacking gel by combining 30% acrylamide, 1.5 M Tris-HCl pH 6.8 and 10% SDS at 5 ml per gel (refer to table 2.1 for recipes). When ready to pour the resolving gel, 10% ammonium peroxidisulphate (APS) and TEMED (tetramethylethylenediamine, Signma-Aldrich, Gillingham, UK) were added to the resolving gel, which initiates polymerisation. Approximately 7 ml of resolving solution was poured to 2/3 of the height of Mini-Protean glass plates and isopropanol was added on top to remove air bubbles. The gel was allowed to set at room temperature for approximately 20 minutes. The isopropanol was then removed and the stacking gel preparation was completed by adding 10% APS and TEMED. The stacking gel was then dispensed on top of the resolving gel (approximately 3 ml) and a comb was immediately inserted. The gel was allowed to set at room temperature for approximately 20 minutes. Once set, the gel was removed from the casting frame and the comb was gently removed. The wells were washed gently with dH_2O from a water bottle, placed into a running module and immersed in SDS-PAGE running buffer prior to protein sample loading.

For 10 ml resolving gel:

Solution component	Volume for 6% gel (ml)	Volume for 12% gel (ml)
H_2O	5.3	3.2
30% acrylamide	2.0	4.0
1.5 M Tris-HCl pH 8.8	2.5	2.6
10% SDS	0.1	0.1
10% APS	0.1	0.1
TEMED	0.008	0.004

For 5 ml stacking gel

Solution component	Volume for 5% gel (ml)
H_2O	3.4
30% acrylamide	0.83
1.5 M Tris-HCl pH 6.8	0.63
10% SDS	0.05
10% APS	0.05
TEMED	0.005

Table 2.1 *SDS-PAGE resolving and stacking gel recipes. Recipes for producing 10 ml resolving gels and 5 ml stacking gels for SDS-PAGE western blotting. The percentage of the resolving gel was chosen based on the size of the protein of interest; for small proteins, a higher percentage gel was used and vice versa. Stacking gels were always produced as 5%.*

2.3.4 Protein sample loading

The concentration of protein in each sample had been previously determined by a Bradford assay (see above). The protein samples were prepared by adding the appropriate volume of 4 x SDS sample buffer (see Buffers and Solutions appendix for recipe. 1 M DTT is added to 4 x SDS sample buffer prior to mixing with samples in a 1:4 ratio) to cell lysates (volumes calculated from the Bradford assay). Prior to loading, each sample was heated to 100°C for 2 minutes to denature the proteins. Each sample was loaded into wells in the stacking gel at 10 µl of sample per well. The size standard used was Precision Plus Protein Dual Colour (5 µl, Bio-Rad, Watford, UK) was loaded into 1 well at 10 µl. The gel was subject to electrophoresis at 120 V for approximately 75-90 minutes.

2.3.5 Protein transfer to nitrocellulose membrane

One piece of 10 cm x 5 cm Amersham™ Hybond-C™ nitrocellulose membrane (Amersham Pharmacia Biotech) was prepared per gel, along with 2 pieces of blotting paper at 10 cm x 6 cm per blot. A shallow dish was half filled with 1 x transfer buffer and 2 sponges are soaked along with the blotting paper. A transfer cassette was placed into the shallow dish black side down and assembled as follows: 1 sponge, 1 piece of blotting paper, the gel, the nitrocellulose membrane, 1 piece of blotting paper and 1 sponge. The gel was removed from the electrophoresis module when the run was completed and the glass plates separated to remove the gel by inserting a wedge and lifting gently. The stacking gel was discarded and the resolving gel was removed from the glass plate and placed gently on the blotting paper soaking in transfer buffer. The remaining layers of membrane, blotting paper and sponge were added on top and the bubbles between the layers were removed by rolling a 15 ml falcon tube over the top sponge. The cassette was closed and inserted into a transfer holder, ensuring the black side of the cassette faces the black side (cathode) of the holder. An ice block was inserted into the holder and the module was filled with 1 x transfer buffer. The transfer was run at 100 V for 1 hour at room temperature.

2.3.6 Immunoblotting

The nitrocellulose membrane was removed from the transfer cassette and checked for protein marker transfer. The membrane was placed into a square petri dish and stained using Ponceau red (Ponceau S Sigma-Aldrich, CA, USA), 0.5 g dissolved in 1 ml glacial acetic acid) for 30 seconds with rotation. The membrane was washed with distilled water until the bands were visible, then, washed with PBS Tween (0.1%) 2 x 5 minutes. Subsequently, the membrane was blocked for non-specific antibody binding by incubating with 5% milk for 1 hour at RT. After blocking, the membrane was probed with primary antibody diluted in blocking agent (3 ml per membrane) overnight at 4°C and washed for 3 x 5 minutes in PBS Tween. After washing, the secondary antibody conjugated to horseradish peroxidase (HRP) was diluted in blocking agent at 10 ml per membrane and incubated at room temperature for 1 hour on an orbital shaker. Finally, the blot was washed 3 x 15 minutes in PBS Tween. See Table 2.2 for antibody dilutions.

2.3.7 Chemiluminescent protein detection

After washing, the membrane was subject to chemiluminescent protein detection. The Amersham™ ECL™ reagents (GE Healthcare) were combined in a 1:1 ratio at 2 ml per blot and incubated on the membrane for 1 minute at room temperature. The excess reagent was removed and the membrane covered with clingfilm (Saran), ensuring no bubbles. In the dark room, the membrane was exposed to a radiograph film (GE Healthcare) for 30 seconds to 30 minutes (depending on the protein being detected) inside a closed cassette. The film is then developed using the X-Ograph SRX-101A developer and the resultant film shows bands of protein that can be aligned with the weight marker on the blot for identification.

2.3.8 Antibodies

2.3.8.1 Primary antibodies

All primary antibodies are listed in table 2.2, including the final dilution used for immunoblotting and the suppliers.

Target protein	Clonality	Supplier	Dilution
ATM (D2E2)	Rabbit monoclonal	Cell Signaling	1:500
BLMH (ab188371)	Rabbit polyclonal	Abcam	1:500
BRCA1 C-terminal (ab191042)	Rabbit polyclonal	Abcam	1:500
DNA PKs [Y393] (ab 32566)	Rabbit monoclonal	Abcam	1:1000
Gamma H2A.X (phosphoS139) antibody [9F3] (ab26350)	Mouse monoclonal	Abcam	1:500
Ku70 + Ku80 C-terminal (ab 166822)	Rabbit polyclonal	Abcam	1:250
P21 (R.229.6)	Rabbit monoclonal	ThermoFisher	1:500
P53	Rabbit monoclonal	ThermoFisher	1:1000
Rad51 [EPR4030(3)] (ab133534)	Rabbit monoclonal	Abcam	1:500
Phospho ATM (Ser1981) (D6H9)	Rabbit monoclonal	Cell Signaling	1:500
Phospho-p53 (Ser15) (16G8)	Mouse monoclonal	Cell Signaling	1:500
Beta Actin [AC-15] (ab6276)	Mouse monoclonal	Abcam	1:5000

Table 2.2 *Table of antibodies. List of primary antibodies used in this study. The clonality, supplier and dilution of each primary antibody are listed.*

2.3.8.2 Secondary antibodies

Secondary antibodies were HRP-conjugated swine anti-rabbit IgG and rabbit anti-mouse IgG (Dako, Agilent Technologies, CA, USA). Both of them were diluted 1:1000.

2.4 Quantitative real-time polymerase chain reaction (RT-qPCR)

2.4.1 Primer design

Primers were designed against BLMH, ATM, RAD51, BRCA1, PRKDC, XRCC4. GAPDH was used as a reference gene (see Table 2.3 for details of primers). All DNA oligonucleotides were purchased from Eurofins MWG Operon. Canine specific primers were designed based on the canine specific gene sequences obtained from the Ensembl genome browser (http://www.ensembl.org/Canis_familiaris/Info/Index/). The entire transcript was uploaded to Primer3Plus online program (https://primer3plus.com/cgi-bin/dev/primer3plus.cgi), with introns annotated. Primer sequences were selected based on: proximity to 3' end of sequence, spanning large introns, avoiding multiple G and C nucleotide repeats, low GC% and a T_m near 60°C. The parameters mentioned were quantified using the "general settings" tool of the program. To ensure the specificity of selected sequences for the genes of interests, forward and reverse primers were then uploaded in the "BLAST/BLAT" command of the Ensembl genome browser, searching against canine genome. All primers were delivered as lyophilised powders and were resuspended in nuclease free water to a concentration of 100 pmol/µl

Gene	Forward primer	Reverse primer
BLMH	5′ TAGTGGAGCGACCAAAGGAG 3′	5′ CCCAGGTGAATGTCTCTGGT 3′
ATM	5′ CCCTTCACTGCCAGAAGAAA 3′	5′ TGGGTCCAAGAACTTTTCCA 3′
RAD51	5′ GCCTATGCACCAAAGAAGGA 3′	5′ GCAGTAGTGAAACCCATTGGA 3′
BRCA1	5′ CCTGAGTCTGATCCCTCGTC 3′	5′ AACGCAGAGGTTGAAGTTGG 3′
PRKDC	5′ TTACCCAGCCTTGACGGATA 3′	5′ GCAGCCTGAGAAAGTGCTG 3′
XRCC4	5′ TGCCTAATCCCTCTGTGTCG 3′	5′ CCATTTTCGGTTCTGTTCCA 3′
GADPH	5′ GGGAAGATGTGGCGTGAC 3′	5′ GAAGGCCATGCCAGTGAG 3′

Table 2.3. *Primer sequences. The primers utilised in this study for each gene are described above. For each gene, the forward and reverse primer sequences are shown.*

2.4.2 Primer efficiency testing

Serial dilutions of cDNA were mixed from stock to 1:1000 and reactions were performed in technical triplicate with each primer set. The efficiency was calculated according to the Pfaffl method, where cycling threshold values were plotted against the cDNA dilution, and the slope of the graph calculated. Efficiency (E) was calculated by:

$$E = 10^{-1/slope}$$

Efficiency values of approximately 2.00 are required as the comparative ΔΔCt method of data analysis utilised here assumes efficiency of 100% (i.e. a single doubling of the template for each reaction cycle).

2.4.3 RNA extraction

RNA was extracted from C2 and CML10 cell lines treated with Bleosome according to chapter 4. Lysates were prepared as described in 2.1.7. The supernatant was removed from the harvested cell pellet, the pellet was loosened by flicking the tube

and the cells were resuspended in Buffer RLT (350 µl for < $5x10^6$ cells or 600 µl for $5x10^6$ – $1x10^7$ cells). The cell lysate was mixed by pipetting or vortexing and homogenised by processing through a QIAshredder spin column (Qiagen, CA, USA) and centrifuged for 2 minutes at 16,100 g One times volume of 70% ethanol was added to the homogenised lysate and mixed by pipetting. Up to 700 µl of sample was transferred to an RNeasy spin column in a 2 ml collection tube and centrifuged for 15 seconds at ≥ 11,200 g. The flow through was discarded. DNase digestion was completed by adding 350 µl of Buffer RW1 to the RNeasy spin column and centrifuging for 15 seconds at ≥ 11.200 g to wash the membrane. DNase 1 stock solution (Qiagen, CA, USA) was diluted in Buffer RDD (10 µl: 70 µl respectively) and the DNase mixture was added to the RNeasy spin column and incubated for 15 minutes at RT. Buffer RW1 (350 µl) was added to the RNeasy spin column and centrifuged for 15 seconds at ≥ 11,200 g. Buffer RPE (500 µl) was added to the RNeasy spin column and centrifuged for 15 seconds at ≥ 11, 200 g, then repeated for a longer spin (2 minutes at ≥ 11,200 g). The RNeasy spin column was placed into a new 2 ml collection tube and centrifuged for 1 minute at 16,100 g. To elute the RNA, 30-50 µl of RNase free water was dispensed onto the RNease spin column and centrifuged for 1 minutes at ≥ 11,200 g into a new 1.5 ml RNase free collection tube. A Nanodrop (NanoDrop™ 2000/2000c Spectrophotometer Thermofisher Scientific, Paisley, UK) was used to measure the yield of RNA from each extraction, and the A260:A280 ratio as a measure of contamination in the samples. Ratios of approximately 2.0 were considered optimal. RNA was stored at -80°C until use.

2.4.4 Reverse transcription

RNA extracted from cells was reversed transcribed to cDNA using Omniscript Reverse Transcriptase (Qiagen, CA, USA). For each RNA sample, 7 µl of RNA was mixed with 10x Buffer RT (2 µl), 5mM dNTP mix (2 µl), 1 µM Oligo-dT primer (0.2 µl), 5 units/µl RNase inhibitor (0.25 µl), Omniscript Reverse Transcriptase (1 µl), 100µM dTT (2 µl) and RNase free water (5.55 µl) to give a total volume of 20 µl. The cDNA mixture was gently vortexed for no longer than 5 seconds, centrifuged briefly

to collect contents at the bottom of the tube and incubated for 60 minutes at 37°C. cDNA was stored at -20°C until use.

2.4.5 RT-qPCR set up and analysis

All RT-qPCR were performed using the Roche LightCycler® 480 instrument with LightCycler® 480 Multiwell Plate 96 according to the manufacturers protocol. The reactions were performed with QuantiNova™ Sybr® Green (Qiagen, CA, USA) master mix. Briefly, 20 µl reaction volumes were used; 12.5 µl of mastermix, 1 µl of primer mix (containing forward and reverse primers) 0.05 µl of ROX (for normalisation of fluorescent signals) and 6.45 µl of nuclease free water. The cycling conditions are summarised in Table 2.4.

PCR step	Temperature (◦C)	Time	Number of cycles
PCR initial activation step	95	2 seconds	1
	95	5 seconds	
Amplification	60	11 seconds	40
	72	5 seconds	
Melting curve analysis	As machine	As machine	As machine

Table 2.4 *RT-qPCR cycling conditions. The cycling parameters for the Roche LightCycler® 480 that were used for RT-qPCR analysis are described. The temperature and length of time for each cycling step is stated, as is the number of cycles run per condition.*

All data analysis was performed by exporting .txt files of crossing point data from the Roche LightCycler® 480 software to Microsoft Office Excel 2011 (Microsoft Corporation). Statistical analysis was performed using Minitab© 16 Statistical Software (Minitab Ltd). Changes in gene expression between experimental samples

were analysed through relative quantitation using the Livak 2-ΔΔCt method. To measure the relative quantitation, reference gene was assayed alongside every reaction (GAPDH). This method assumes that the target and reference genes are amplified with efficiencies approaching 100% and within 5% of each other. The following steps were taken to calculate fold changes in gene expression:

1. The ΔCt was calculated by subtracting the geometric mean of all reference gene crossing point values to the mean of the experimental crossing point values. This is performed for both the experimental samples and the reference control samples therefore x2 ΔCt values are obtained.
2. The ΔΔCt values were calculated by normalising the ΔCt of the experimental sample to the reference sample.
3. The gene expression ratios were calculated by raising the negative of the ΔΔCt above the power of 2 (2-ΔΔCt).
4. The result is the fold change value of the target gene expression normalised to the internal calibrator provided by the reference gene. By using the internal calibrator variation in the amount of cDNA tested can be overcome.

2.5 RNA sequencing using Next Generation Sequencing (NGS)

2.5.1 RNA quality control

All sequencing was performed by The University of Edinburgh sequencing service (Edinburgh Genomics, Ashworth Laboratories, King's Buildings, Edinburgh). Samples were prepared in labelled RNase free tubes. Samples were checked for quality by the Agilent 2200 Tapestation with the RNA analysis screen tape (Agilent) (Stockport, UK). This method provides an accurate and objective assessment of total RNA degradation as indicated by the RNA integrity number (RIN). The RIN is a software output that estimates the integrity of total RNA samples based on the entire

electrophoretic trace of the RNA sample rather than just the ratio of the ribosomal bands, 28S and 18S. This includes the presence or absence of degradation products. The assigned RIN is independent of sample concentration, instrument and analyst, and therefore it is considered a *de facto* standard for RNA integrity (Griffin et al. 2012). Concentrations of RNA within the samples were also assessed by fluorometric quantitation, using Qubit 4 Fluorometer (ThermoFisher Scientific, Paisley, UK). Samples sent for sequencing fulfilled all the following requirements: RIN > 7; concentration >37 ng/ul; A260:280 >2, amount > 2200 ng, volume >60 ul (figure 2.1). Good quality and quantity of RNA is critical for obtaining optimal sequencing results.

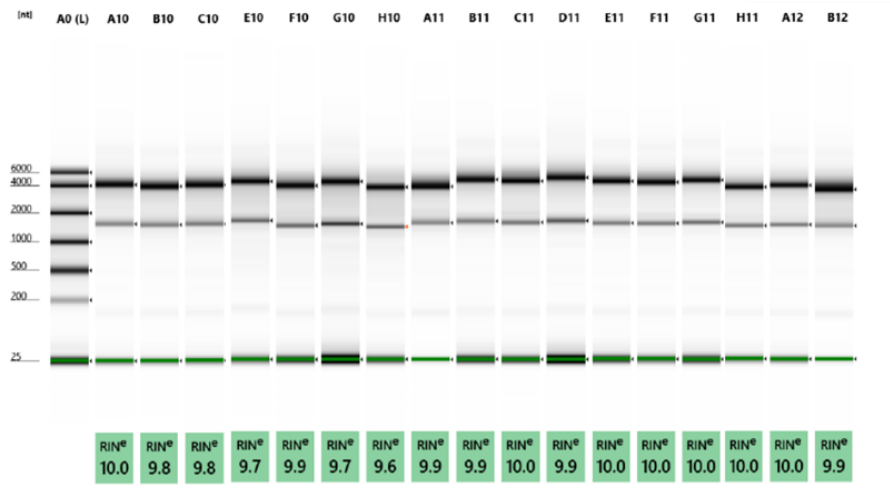

Well	RINe	28S/18S (Area)	Conc. [ng/µl]	Sample Description
A0	-	-	84.9	Electronic Ladder
A10	10.0	2.8	118	11755AD0001_1:1
B10	9.8	2.7	141	11755AD0002_1:1
C10	9.8	2.5	123	11755AD0003_1:1
E10	9.7	2.5	101	11755AD0005_1:1
F10	9.9	2.6	69.6	11755AD0006_1:1
G10	9.7	2.0	38.1	11755AD0007_1:1
H10	9.6	2.3	80.0	11755AD0008_1:1
A11	9.9	3.2	359	11755AD0009_1:1
B11	9.9	2.6	56.4	11755AD0010_1:1
C11	10.0	3.2	66.8	11755AD0011_1:1
D11	9.9	2.4	34.8	11755AD0012_1:1
E11	10.0	2.7	54.6	11755AD0013_1:1
F11	10.0	3.3	79.3	11755AD0014_1:1
G11	10.0	2.9	51.9	11755AD0015_1:1
H11	10.0	3.0	94.5	11755AD0016_1:1
A12	10.0	2.9	91.5	11755AD0017_1:1
B12	9.9	3.5	405	11755AD0018_1:1

Figure 2.1 *RNA-sequencing data quality analysis using RNA Integrity Number of some of the samples used in this study (Agilent 2200 Tapestation).*

2.5.2 Library preparation for RNA sequencing

Library preparation from mRNA before sequencing is necessary to obtain a clear view of the coding transcriptome with strand-specific information (Corney 2013). The mRNA library was prepared by The University of Edinburgh sequencing service (Edinburgh Genomics, Ashworth Laboratories, King's Buildings, Edinburgh) using Tru Seq Stranded mRNA Library Prep Kit (Illumina, CA, USA). Library preparation consists of the following steps:

1. RNA fragmentation: mRNAs are typically fragmented to smaller pieces of RNA to enable sequencing.
2. Reverse transcription: first and second strand cDNA is reverse transcribed from fragmented RNA using random hexamers or oligo(dT) primers.
3. Adapter ligation: the 5' and 3' ends of cDNA are repaired, and adapters (containing sequences to allow hybridization to a flow cell) are ligated.
4. Library clean-up and amplification: libraries are enriched for correctly ligated cDNA fragments and amplified by PCR to add any remaining sequencing primer sequences.
5. Library quantification, quality control and sequencing: library concentration is assessed using qRT-PCR and Bioanalyzer and is ready for sequencing (Corney 2013).

2.5.3 Sequencing

Illumina RNA-sequencing uses a "sequencing by synthesis" (SBS) approach (Metzer et al., 2010). Libraries are denatured and undergo a process known as "bridge amplification" to create clonal clusters of single-stranded DNA molecules. Briefly, once the fragments attach on the flow cell, DNA is sequenced by adding polymerase resulting in a covalently bound full-length complementary copy of the cDNA fragment. The cDNA fragment obtained is subjected to several rounds of PCR amplification to produce clones that can be optically resolved during sequencing. Obtaining optimal cluster density is critical since it will determine the number of reads

obtained. Therefore, the cDNA is labelled with dNTPs (nucleoside triphosphate). Each of the dNTPs is labelled with a specific fluorescent colour. After laser excitation, different emitted fluorescent waves are recorded for each cluster. Based on the fluorescence emission the base of each cluster is identified and because the clusters contain identical DNA sequences the entire cluster is read as one base. A camera records these base reads across the entire flow cell. This takes place between 50 and 100 cycles to create about 150-200 million 50 bp to 100 bp reads. When two separate read cycles occur in both directions, it is called paired-end reads. This kind of read will provide data about both sides of the fragment of interest (Metzker 2010). In this study, we sequenced fragments of 75 bp to a yield of at least 290 milion paired-end reads using an Illumina HiSeq 4000 machine.

2.5.4 Bioinformatic NGS analysis

Bioinformatic analyses were performed by The University of Edinburgh sequencing service (Edinburgh Genomics, Ashworth Laboratories, King's Buildings, Edinburgh). The process of analysis is described as follows:

1. Trimming: reads were trimmed using Cutadapt (version cutadapt-1.9.dev2). Reads were trimmed for quality at the 3' end using a quality threshold of 30 and for adapter sequences of the TruSeq stranded mRNA kit (AGATCGGAAGAGC). Reads after trimming were required to have a minimum length of 50.
2. Reference: the reference used for mapping was the Canis familiaris (CanFam3.1) genome from Ensembl. The annotation used for counting was the standard GTF-format annotation for that reference (annotation version 84).
3. Reads were aligned to the reference genome using STAR (version 2.5.2b) specifying paired-end reads and the option --outSAMtype BAM Unsorted. All other parameters were set at the standard option.
4. Read counting by feature: reads were assigned to features of type 'exon' in the input annotation grouped by gene_id in the reference genome using featureCount (version 1.5.1). featureCounts assigns counts on a 'fragment' basis as opposed to individual

reads such that a fragment is counted where one or both of its reads are aligned and associated with the specified features. Strandedness was set to 'reverse' and a minimum alignment quality of 10 was specified. In addition to the counts matrix used in downstream differential analysis, a matrix of Fragments Per Kilobase of transcript per Million mapped reads (FPKM) values was generated, using the rpkm() function of edgeR (Robinson et al, 2010) (version 3.20.9) and normalized effective library sizes. Gene lengths for the FPKM calculation were the number of bases in the exons of each gene (only counting bases once where they occur in multiple exon annotations). FPKM values may be useful in analyses requiring accurate gene-gene (as opposed to sample-sample) comparisons. Gene names and other fields were derived from input annotation and added to the count/expression matrices.

5. Count processing:

5.1 Filtering: The raw counts table was filtered to remove genes consisting predominantly of near-zero counts, filtering on counts per million (CPM) to avoid artefacts due to library depth. Specifically, a row of the expression matrix was required to have values greater than 0.1 in at least 3 samples, corresponding to the smallest sample group as defined by Group, once any samples were removed (where applicable).

5.2 Normalisation: Reads were normalised using the weighted trimmed mean of M-values method5, passing 'TMM' as the method to the calcNormFactors method of edgeR.

6. Differential gene set analysis: Differential gene set analysis was carried out with the ROAST method from the Limma package (version 3.34.9) of Bioconductor, using the same models and contrasts as used in differential expression. The following gene sets were used:

- Gene Ontology Biological Process, downloaded from Ensembl version 98
- Reactome Pathways, downloaded from Ensembl version 98

ROAST was executed using 9,999 rotations (randomisations). Each gene set was annotated with those genes individually differential (in the same direction as indicated for the gene set) to an unadjusted p-value of 0.05.

2.6 Immunohistochemistry (IHC)

Equine sarcoids and skin were treated and fixed as detailed in chapter 4. Once ready, samples were sent to the Pathology Unit of the Royal (Dick) Veterinary School of the University of Edinburgh, where immunohistochesmistry (IHC) was performed by Dr Scott Maxwell. Briefly, the procedure was performed as follow:

1.Processing: samples were processed on an Excelsior AS processors (ThermoScientific, Paisley, UK) according to the following program: 1X (1hour and 30 minutes) 10% NBF; 6X (3 hours each) absolute alcohol; 3X (3 hours each) Histoplast IM wax (ThermoScientific, Paisley, UK);
2.Embedding: samples were embedded on the HistoStar (ThermoScientific, Paisley, UK) using Histoplast IM wax;
3.Cutting/Microtomy: all blocks were cut at 4µ on a Finesse microtome (ThermoScientific, Paisley, UK). All sections were floated onto Thermo Plus Slides and placed in a low temperature drier overnight. An hematoxylin and eosin (H&E) staining was initially performed on each block. H&E staining was carried out on the Varistain Gemini (ThermoScientific, Paisley, UK) using the in-house staining program;
4.Antigen retrieval: the Autostainer 360 (Thermo Scientific, Paisley, UK) was used and the antigen retrieval was carried out offline using a microwave- Histos 5 (Milestone, Sorisole, IT). The fluid used was Antigen Unmasking Solution by Vector (H-3301). Retrieval was carried out at 110°C for 5 minutes (with an overall time including getting up to temperature of 12 minutes);
5. IHC Staining: Anti-BLMH antibody (ab204584, abcam, Cambridge, UK) was the antibody anti bleomycin hydrolase used, and it was also stained using a Vector Red (Immpact Nova Red Vector SK-4805, Novus Biologicals, CO, USA) chromagen. The staining was carried out on the Thermo Autostainer 360 according to the program detailed in supplementary data (8.2.1).

2.7 Fluorescence-activated cell sorting (FACS)

Fluorochrome-conjugated probes have been used to label and then sort CML10 and C2 cell lines using BD Fortessa cell analyser (BD Biosciences, USA). Specific fluorophores are detailed in table 2.5. Following a general protocol, cells were harvested, washed and adjusted to a concentration of 0.5-1x 10^6cells per condition in ice cold PBS. Cells were strained using 70 µm cell strainers to avoid clumps that could block the flow cytometer. Cells were then stained in polystyrene round-bottom 12x75 mm tubes. Control samples (cells incubated with equivalent concentration of nuclear marker, dead cell marker, fluorescent drugs) were evaluated for each experiment. At least 100,000 events were acquired for analysis.

All the procedures were performed at 4°C protected from light, according to the relative manufacturer's protocol. Cells were then analysed in the flow cytometer by a laser at different wavelengths depending on the conjugated fluorochrome. Cells were gated by adjusting the size (forward scatter (FSC)) and granularity or complexity (side scatter (SSC)) of the cells to the middle of an FSC × SSC graph. Post-acquisition analysis was performed using FlowJo (Treestar, USA). Results were analysed after setting the gate on the cellular population, eliminating debris. The percentage of positive cells was determined by comparison to the control cells (unstained) and excluding dead cells (percentage of cells positively stained with dead cell marker in control).

Fluorescent probe	Manufacturer	Excitation Wavelength (nm)	Emission Wavelength (nm)
Zombie Yellow	BioLegend	396	572
LysoTracker Deep red	LifeTechnology	647	668
Hoechst 33342	ThermoScientific	350	461

CellLight Lysosomes RFP BacMam 2.0	LifeTechnology	555	584
Bodipy-FL		503	512

Table 2.5 *List of fluorescent probes with relative emission and excitation spectra*

2.8 Bleomycin fluorescent labelling process assessed by High-Performance Liquid Chromatography/ Mass Spectrometry (HPLC/MS)

In order to visualise Bleosome and bleomycin activity within cells and skin tissues by microscopy, 120 mg of bleomycin sulphate (A2-B2) were coupled with a green fluorophore, the Bodipy-FL. Monitoring of the reaction and characterization of the final product were achieved by means of High-Performance Liquid Chromatography/ Mass Spectrometry (HPLC/MS). The whole process was conducted in collaboration with the the group of Dr. Marc Vendrell at The Queen's Medical Research Institute (QMRI), the University of Edinburgh.

2.8.1 High-Performance Liquid Chromatography/ Mass Spectrometry - HPLC/MS

High-Performance Liquid Chromatography (HPLC) is a highly improved form of column chromatography. Instead of a solvent being allowed to flow through a column under gravity, it is pushed through under high pressures of up to 400 atmospheres. This increases the speed of the process (Clark and Frank 2016). Reverse phase HPLC is the most commonly used form of HPLC and it was used in this study.

2.8.*2* Solubility tests to establish the process for the purification of the labelled compound

Bodipy-FL (Edinburgh, UK) might bind the amine groups of bleomycin, releasing N-hydroxisuccinimide (succinimide-OH). In order to obtain a pure fluorescent labelled compound, free from other fluorescent impurities and succinimide-OH, different trials were conducted to find a solvent in which succinimide-OH, but not bleomycin, could be dissolved: this enabled to separate the undissolved fluorescently labelled bleomycin by mechanically removing the solution containing succinimide-HO. Solubility tests showed dimethyl sulfoxide (DMSO) to be the only solvent in which bleomycin sulphate was dissolved, while succinimide-OH was found to be very soluble in dichloromethane (DCM), which was thus chosen for the purification of the final compound.

2.8.3 Coupling bleomycin sulphate with Bodipy-FL

The mass and absorbance profiles of bleomycin sulphate and Bodipy-FL were evaluated by HPLC in order to achieve references for the two starting materials, prior to commencing the coupling process.

Bodipy-FL is supposed to bind to the amine groups of the metal binding domain of the bleomycin sulphate, releasing the succinimide-OH leaving group. The main concern about the coupling process was that the fluorophore could have tagged all of the three amine groups of bleomycin. Therefore, the labelling could have potentially affected the ability of bleomycin to bind and intercalate the DNA of cancer cells, thus affording a final compound with reduced overall efficacy. Hence, the first aim was to establish the right amount of fluorophore to use in order to obtain the highest possible amount of mono-labelled bleomycin (bleomycin sulphate bound to one amine group), by minimizing double and triple labelling of the drug. Initially, a small-scale trial using 0.9 equivalents of fluorophore was conducted to evaluate reaction conditions.

Subsequently, according to the findings of this preliminary experiment (images shown in section 3.4.3), a larger batch of drug was coupled using less Bodipy (0.7 equivalents), i.e. a 8.1 mg amount was reacted with 45 mg of bleomycin sulphate, according to the following equation:

mmol of bleomycin sulphate: 45 mg / 1512.62 bleomycin MW= 0.03 mmol bleomycin

mmol of Bodipy-FL: 1 e.g, bleomycin : 0.03mmol bleomycin = 0.7 e.g. :x = 0.021 mmol Bodipy-FL

mg of Bodipy-FL = 0.021 mmol Bodipy-FL x Bodipy-FL MW 389.16 = 8.1 mg

	Molecular Weight	e.g. (equivalents)	Mmol	mg
BODIPY-FL	389.16	0.7	0.021	8.1
BLEOMYCIN	1512.62	1	0.03	45

Table 2.6 *Molecular weight (MW), equivalents (e.g.), millimoles (mmol) and milligrams (mg) of Bodipy-FL and bleomycin sulphate (bleomycin) employed in the first coupling reaction with 45 mg bleomycin sulphate (corresponding to roughly half of the total amount of drug to be labelled).*

45 mg of bleomycin sulphate were dissolved in DMSO, and put in an Eppendorf equipped with a stirring bar; subsequently, Bodipy-FL dissolved in DMSO, was added to the bleomycin solution dropwise over 20 minutes. The addition process was conducted slowly to prevent multiple tagging of the drug.

The reaction was checked by HPLC after 30 minutes, 1.5 hours and 3 hours; the reaction was then left running overnight (images are shown in section 3.4.3).

The remaining 81 mg of bleomycin sulphate were coupled with 0,8 equivalents of Bodipy-FL according to table 2.7, following the same calculation made for the first coupling process.

	Molecular Weight	e.g. (equivalents)	Mmol	Mg
BODIPY-FL	389.16	0.8	0.0376	14.6
BLEOMYCIN	1512.62	1	0.047	71

Table 2.7 *Molecular weight (MW), equivalents (e.g.), millimoles (mmol) and milligrams (mg) of Bodipy-FL and bleomycin sulphate (bleomycin) put in the second coupling reaction with 71 mg bleomycin sulphate (corresponding to roughly half of the total amount of drug to be labelled).*

2.8.4. Lyophilisation and purification

Both batches of Bodipy-tagged bleomycin were lyophilised to remove the DMSO: the reaction mixture was diluted with water, snap-frozen in dry ice, and the solvents were removed overnight by means of a freeze dryer.

In order to remove impurities and succinimide-OH, 5ml of DCM (according to section 2.8.2) were added and the resulting suspension was allowed to sit for 15 minutes, until undissolved solid settled. Subsequently, the supernatant (succinimide-OH and DCM) was removed using a syringe. This process was performed five times until the removed supernatant resulted colourless (meaning that no residues of fluorescent impurities were left). After drying under vacuum, the final compound resulted in a fine, red powder (figure shown in section 3.4.3), whose composition was assessed by HPLC.

2.8.5 Fluorescently labelled Bleosome and bleomycin (F-Bleosome and F-bleomycin)

The final powder was sent, refrigerated and protected from light, to the *Ascot Laboratories Ltd* (London, UK), to be encapsulated into ultra-deformable liposomes and to have a final fluorescent Bleosome (F-Bleosome) in the form of a 0.2% cream. A small amount (20 mg) was saved to create the aqueous form of non-encapsulated fluorescent bleomycin (F-bleomycin), used as comparison with F-Bleosome in penetration and cellular up-take experiments. Briefly, 0.02 g of fluorescent bleomycin powder were dissolved in 9.98 ml of PBS, vortexed and stored at 4°C protected from light.

2.9 Skin and equine sarcoid samples used for penetration studies.

2.9.1 Skin samples

2.9.1.1 Canine and equine skin

2.9.1.1.1 Sample collection

Skin samples were collected from animal cadavers donated from The Edinburgh Cat and Dog Home to the Royal (Dick) Veterinary School of the University of Edinburgh. Specimens were withdrawn from flank and abdomen of cadavers, previously shaved with an electric clipper. As soon as the euthanasia was performed, cadavers were brought to the post-mortem and the skin was immediately removed from each animal using a knife, the section was attached to a square cork block and kept tense by pins, subcutaneous fat was subsequently removed by a scalpel. Immediately after the

procedure, each sample was wrapped in aluminium foil, stored in a sealed plastic bag, snap frozen in dry-ice, and stored at -70◦C or -20◦C.

2.9.1.1.2. Skin sample processing for Bleosome penetration study performed with Confocal Laser Scanning Microscopy (CLMS)

Skin samples were thawed by washing 3x in PBS at RT. They were cut by a scalpel into 2x2 square centimetres. Thickness of sections were measured using an electronic calliper. Sections staining and treatments are detailed in relative chapters.

2.9.1.1.3 Skin sample processing for Bleosome penetration study performed with fluorescent microscopy

Skin samples were treated as in 2.9.1.1.2. Samples were then treated with indicated dose of Bleosome at the indicated time points. To obtaining cryosectioned slides to be visualised with the fluorescent microscope, samples were processed as follow:

1. Snap-freezing:: at the relative time point, each skin section was cut in four equally sized slices using a scalpel. Each slice was positioned, oriented on the edge, in a 20x20x5 metal cryomold, with the longer side parallel to the longer side of the cryomold and the epidermis facing the right side. The cryomold was filled with Tissue-Tek® O.C.T.™ Compound (Sakura, USA) in a sufficient amount to embed the whole tissue. Subsequently, the slice was snap-frozen using a metal beaker filled for 2/3 with isopentane and placed in a box containing liquid nitrogen. The cryomold was positioned, but not fully submerged, in the isopentane using forceps, until frozen and then wrapped in aluminium foils, sealed in plastic bags, positioned in dry-ice and subsequently stored at -70 ◦C. This protocol was modified by Peters 2010.
2. Cryosectioning: samples were transferred into the cryostat (Cryostat CMI900, Leica, Stantonbury, UK) and mounted on the chuck with O.C.T. compound. Temperature in the cryostat was set at -20◦C and thickness of sections was set at 10

µm. The blade used was MB35 Premier, microtome blade 340/80 mm (ThermoScientific, Paisley, UK) and the sample was oriented with the epidermis perpendicular to the blade (figure 2.2).

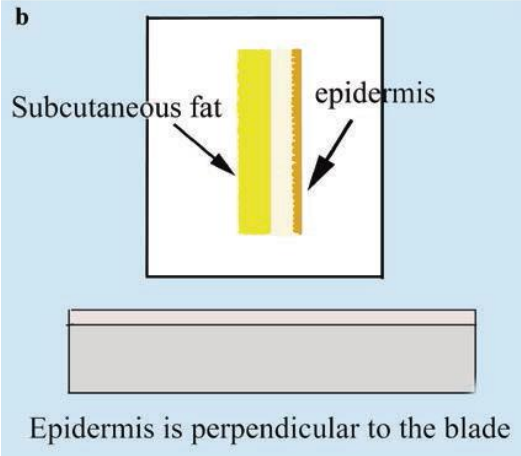

Figure 2.2 *Orientation of the sample for cryosectioning.(Peters 2010)*

Once cut, sections were impressed on a slide (Superfrost Plus Microscope Slide, ThermoScientific, Paisley, UK), dried at RT for 3 hours covered by aluminium foil, to avoid light exposure. Samples were stored at -20◦C. This protocol was modified by Fisher et al, 2006.

3. Fixation and mounting: slides were exposed at RT for 30 minutes and then fixed with neutral buffered formalin (NFB) 10%, for 10 minutes; subsequently slides were rinsed in PBS for 5 minutes, this procedure was performed twice. Half of the slides were pre-treated with TrueBlack™ Lipofuscin Autofluorescence Quencer (Biotinum, CA, USA) as per manufacturer instruction. All the slides were stained with DAPI nuclear counterstaining (ThermoFisher, Paisley, UK) following the manufacturer protocol; subsequently, they were rinsed in PBS, dried and coverslipped with ProLong™ Gold Antifade Mountant (ThermoFisher, Paisley, UK) and then dried at RT overnight, covered by aluminium foils to avoid light exposure.

2.9.1.1.4 Skin sample processing for Bleosome penetration study performed with Transmission Electron Microscopy (TEM)

Skin samples were thawed X3 in PBS at RT. They were cut by a scalpel in 2x2 square centimetres as in 2.9.1.1.2., and, treated with Bleosome according to chapter 3.

At the indicated time point, each sample was cut in to 1 centimetre thick slices that were fixed in 3% glutaraldehydein 0.1 M Sodium Cacodylate buffer, pH 7.3, for 2 hours, then washed in 0.1M Sodium Cacodylate 3x 10 minutes. Samples were subsequently sent to the microscopy unit at the King's Buildings Institute, The University of Edinburgh, where they were processed, in order to be visualised with the TEM. Briefly, Specimens were post-fixed in 1% Osmium Tetroxide in 0.1M Sodium Cacodylate for 45 minutes, then washed 3x 10 minutes in 0.1 M Sodium Cacodylate buffer. These samples were then dehydrated in 50%, 70%, 90% and 100% ethanol (X3) for 15 minutes each, then in two 10-minute changes in Propylene Oxide. Samples were then embedded in TAAB 812 resin. Sections 1 μm thick were cut on a Leica Ultracut ultramicrotome, stained with Toluidine Blue, and viewed in a light microscope to select suitable areas for investigation. Ultra-thin sections 60 nm thick were cut from selected areas, stained in Uranyl Acetate and Lead Citrate then viewed in a JEOL JEM-1400 Plus TEM.

2.9.1.2 Human skin

2.9.1.2.1 Sample collection

Human skin was collected from patients undergoing reductive plastic surgery. Patients were presented with an informative leaflet and agreed, by signing a consent form, to donate the surplus skin removed by surgery to this study (supplementary data 8.2.2 and 8.2.3). After the surgical excision, a surgeon removed the subcutaneous fat from

the skin tissue with a scalpel and the samples were snap frozen in dry-ice and subsequently stored at -70◦C.

2.9.1.2.2. Sample processing

At the time of the experiment, skin samples were thawed and processed as 2.9.1.1.2.

2.9.2 Equine sarcoids

2.9.2.1 Sample collection

All equine sarcoids included in this study were kindly provided by the equine veterinary surgeons of the Royal (Dick) Veterinary Equine Hospital at The University of Edinburgh. Owners consented to include their horses in this study signed a consent form, after being explained all the procedures and provided with a dedicated information leaflet (Supplementary data). This study entitled: "Evaluation of the efficacy of Bleosome as a topical treatment for equine sarcoids" received the approval of the Veterinary Ethical Review Committee (VERC) with the VERC reference number is 6.19. Sarcoids were surgically removed from patients, as part of their standard therapeutic protocols, by CO_2 laser or excision. Immediately after the excision, sarcoids were wrapped in aluminium foils, stored in sealed plastic bags and snap frozen in dry-ice, to be stored at -70◦C or -20◦C.

2.9.2.2 Sample processing

Sarcoids were thawed by washing 3x in PBS at RT. They were treated, cut or treated and cut according to the experiment performed (procedures are detailed in relative chapters).

2.10 Microscopy

2.10.1 Fluorescence microscopy

In this study, Leica DMLB upright phase/fluorescent microscope (Strantonbury, UK) with quad pas emission filter/ Lumencor LED light engine with 6 bandpass excitation filters and Hamamatsu low light mono camera for quantification use was used. Objective lenses used were 20x (Green Ring) Type Fluotar Ph2, na 0.50 and 40x (Green/Blue Ring) Type Fluotar Ph3, na 0.75. For the bleomycin green fluorescence the Cyan Lumencor Exciter filter (202/324 band-pass) was used (configuration: 485/20), with 200msec exposure time; for the visualisation of DAPI stained structures, the Violet Lumencor Exciter filter (201/401 band-pass) was used (configuration: 390/18), with 30 msec exposure time.

2.10.2 Transmission Electron Microscopy (TEM)

In this study, TEM was used to visualize the liposomes through the skin, after the Bleosome treatment. Samples were prepared according to section 2.9.1.1.4; samples were viewed in a JEOL JEM-1400 Plus TEM (USA). Representative images were collected on a GATAN OneView camera at different magnification.

2.10.3 Confocal Laser Scanning Microscopy (CLSM)

2.10.3.1 CLSM settings for the equine sarcoids penetration study

Equine sarcoids (Bleosome treated and untreated) were cut in 2 mm slices using a coronal mouse brain matrix (rbma 600c acrylic brain matrix for rat 300g-600g coronal

slices, World Precision Instrument, USA). Slices were put on a glass slide and kept flat by positioning another glass on the top (see chapter 5). All images were collected using a Zeiss LSM 710 AxioObserver Confocal Microscope (Cambourne, UK) equipped with EC Plan-Neofluar 20x/0.50 M27 objective lens. Imaging was performed with a 20x 0.8 na oil lens using a 488 argon laser (4.0% laser power) for BODIPY-FL (493-598 nm band pass filter), with 716v detector gain; and a 405 nm diode laser (9.9% laser power) for Hoechst 33342 (410-492 nm band pass filter), with 878.14v detector gain. Picture of the whole sample were acquired using the tile-scan tool. Fluorescence intensities and Bleosome particles position were assessed using Zen lite 3.0 (Blue edition, Zeiss, Cambourne, UK).

2.10.3.2 CLSM settings for live-cell imaging study

Cells were grown in 2-well chamber slides (Nunc Lab-Tek II Chambered Coverglass, 1.5 borosilicate glass, ThermoFisher, Paisley, UK) according to chapter 4, and were placed under a Zeiss LSM 880 Confocal microscope Airyscan/Fastscan with 32 sensitive GaAsP detectors, equipped with an incubation chamber, which is maintained at 37 °C with controlled CO_2 flow. Images were acquired using a using a 488 argon laser (0.5% laser power) for BODIPY-FL (500-651 nm band pass filter), with 983.2v detector gain; and a 405 nm diode laser (1.1 laser power) for Hoechst 33342 (411-499 nm band pass filter), with 681.86v detector gain. Cells were captured in single images, moreover, images were also acquired for 10 seconds, for 60 cycles creating a 10 minutes time-course video for each time point and treatment.

2.10.4 Multiphoton microscopy

In this study, all images were collected with a Zeiss LSM7 MP intravital multiphoton microscope equipped with W Plan-Apochromat 20x/1.0 DIC D=0.17 M27 75mm objective lens and a Coherent chameleon ultraII pulsed laser with OPO (wavelength tunable 690 to 1400nm) (Cambourne, UK). Imaging was done with a 20x upright,

water dipping lens, big detector (binary GASP detector) with the green (NDD R4) and blue (NDD R3) filters set up was used (figure 2.3).

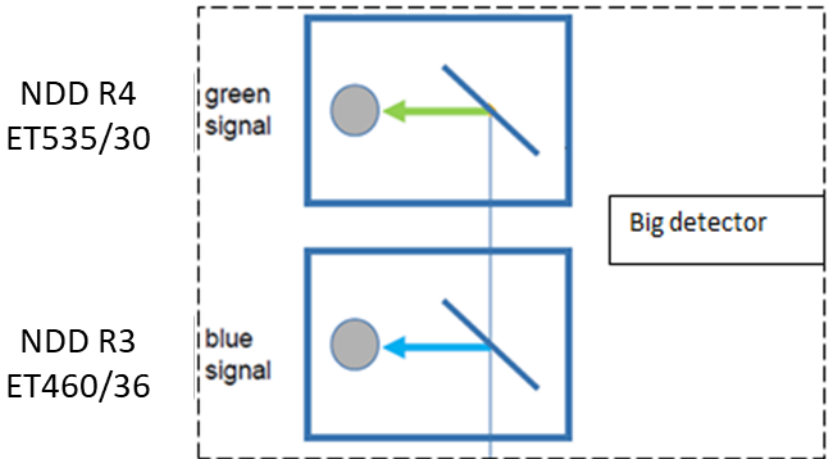

Figure 2.3 *Green (NDD R4) and Blue (NDD R3) filters used in this study.*

780 nm laser line and 22% laser power were used. NDD R4 master gain was 541, NDD R3 master gain was 653; laser gain was 22.0 and 1.0 was set as digital gain.

Multidimensional acquisition was performed with the Z-stack tool, setting 150 slices as average with an interval of approximately 3 µm.

3-D images were visualised, processed and interpreted using Imaris Biplane (9.1.2 version) (Zurich, CH) software.

2.11 Statistical analysis

Quantitative analysis was based on a minimum of three replicates. Data were analysed using Minitab® 17 Statistical Software (Minitab Ltd., Coventry, UK) and all graphs and diagrams were generated using Microsoft Office 2011 software (Microsoft Corporation). P-values <0.05 were considered statistically significant. Normality test was performed using Minitab® 17 Statistical Software. When data followed a normal distribution, two sample t-tests were used to compare differences between two

samples, or one-sample t-tests to determine whether the sample mean was statistically different from a known or hypothesised mean. General linear model (2-way ANOVA-analysis of variance) was used to understand if in two groups there was an interaction between two independent variables on the dependent variable.

IC_{50} values were calculated using GraphPadPrism 6 (GraphPad Software, La Jolla, CA, USA).

Chapter 3. A comparative study of the potentional of a novel formulation of bleomycin to penerate through canine, equine and human skin

3.1 Abstract

Advances in cancer therapy are focused on minimising the side-effects of treatments and improving the quality of life of patients. Minimally invasive treatments are sought after and liposomes are highly valued for their ability to topically deliver a payload of drugs to target tumour tissues, and decrease systemic toxicity. To this extent, we evaluated Bleosome (bleomycin encapsulated in ultra-deformable (UD) liposomes) as topical treatment for non-melanoma skin cancer (NMSC) in veterinary and human medicine. Although, liposomes have been extensively studied as a vehicle of drug delivery to the skin, the exact mechanism employed by UD lipid vesicles in penetrating the skin barrier remains controversial. In this study, we investigated the mechanism of penetration of Bleosome through the skin by developing and optimising a direct imaging technique. Initially, we attempted to utilise the autofluorescent property of Bleosome itself to estimate the rate and peak of penetration of Bleosome through animal skin using fluorescent microscopy, however, the intrinsic autofluorescence of the compound was comparable to the autofluorescence of skin, and we therefore concluded that this method was not suitable. We subsequently visualised both the liposomes and the entrapped bleomycin through the skin after topical application of Bleosome using two different methodologies: (1) we visualised the penetration of liposomal nanoparticles through the skin over a time course using the transmission electron microscope (TEM) and concluded that UD liposomes are able to penetrate the outermost *stratum corneum* of the skin only, without reaching deeper layers; and (2) we fluorescently labelled the entrapped bleomycin with Bodipy-FL, packaged into UD liposomes and visualised the penetration of the drug molecules within canine, equine and human skin, using multiphonon microscope (MP). Here, we found that, in all species tested the entrapped bleomycin, after several hours of Bleosome topical

application to the skin, crossed the *stratum corneum* and passed through deeper layers of the epidermis. Moreover, we found that length of treatment had a significant impact on the rate of penetration and that Bleosome penetrated significantly deeper through canine, equine and human skin, compared to free bleomycin. We concluded that, in the case of Bleosome, UD liposomes act as penetration enhancers: they cross the first layer of the skin, interact with intercellular lipid lamellae, and pass through tortous virtual channels between keratynocytes. We propose that this may cause damage to the lipidic bilayers of the liposomes enabling the release of bleomycin and deeper penetration of the drug through the skin compared to unencapsulated drug.

3.2 Introduction

Non-melanoma skin cancers (NMSC) are a group of cutaneous tumours including basal cell carcinoma (BCC) and squamous cell carcinoma (SCC) (Simonetti et al. 2009).
The incidence of NMSC has steadily increased in human medicine, making it a major challenge in terms of management of public health (Fleury and Vianna Lopez 2011).

In veterinary medicine, SCC is more frequent in dogs and cats than in humans, with an incidence of 5-15% of all cutaneous tumours. SCCs are locally invasive with a low metastatic rate (Amadori and Marconato 2012). In horses, sarcoids are locally invasive, fibroblastic skin tumours and represent the most common tumour in equids worldwide (Taylor and Haldorson 2013). Treatment for NMSC in both human and veterinary medicine includes several standard treatments, such as curettage, surgery, cryotherapy, radiotherapy and chemotherapy (Amadori and Marconato 2012); Fleury and Vianna Lopez 2011). However, these conventional treatments lead to severe inflammation, pain and unappealing scars (Lopez et al. 2004). To increase patient compliance and to reduce surgical costs and undesirable scars, particularly in cases where the cancer has spread over large areas of the body, the topical administration of anti-cancer drugs has been investigated. This is an interesting alternative for reducing side effects and for increasing drug targeting and therapeutic benefits. The major challenge of this kind of treatment is to increase penetration of the anti-neoplastic drug

through the skin in sufficient quantity to kill tumour cells (Fleury and Vianna Lopez 2011)

Bleomycin is a potent anti-cancer agent that is able to induce single and double stranded breaks in DNA. It is effective against several types of tumours, including cutaneous ones. Because of its molecular characteristics, including polar charge, high molecular weight, hydrophilic molecule and system of cellular uptake, it is unable to efficiently cross the plasma membrane and lipophilic skin barriers and reach the site of action (J. Chen and Stubbe 2005a). Furthermore, systemic treatment with high dose of bleomycin, leads to severe side effects (1.8.1), limiting its clinical application (Sleijfer 2001). To address these issues, there has been an increasing interest in the development of a novel formulation of bleomycin for topical administration. Bleomcyin administered through electrochemotherpy (ECT) regimen produced excellent outcomes in the management of NMSCs. However, this technique is invasive (1.8.3). Furthermore, when administered to animals and, in some cases to human patients, general anaesthesia is required (Enrico P. Spugnini, Citro, and Baldi 2009 (A)). For this reason, we focused our interest on liposomes as a potential carrier of bleomycin through the skin.

Skin is an excellent barrier and has evolved to provide protection against the external environment, and to limit the absorption of exogenous molecules (Fleury and Vianna Lopez 2011). Nanotechnologies have been proposed to escape the defenses of the skin, taking advantage of some defects of the *stratum corneum*, which at the microscopic level is a poorly permeable nanoporous membrane (Gregor Cevc and Gebauer 2003). In fact, in some regions the corneocytes do not perfectly overlap and channels, like pores with a higher water content, are formed and contributes to the tiny hydrophilic furrows (0.4−36 nm large) present in the intercellular spaces between the polar heads of the *stratum corneum* lipids (Gregor Cevc and Gebauer 2003). Among nanocarriers, liposomes, owing to their particular composition, are considered as the most suitable means to enhance the skin penetration of drugs because of a number of intrinsic characteristics. However, it is now recognised that conventional liposomes, having a rigid bilayer, mostly disassemble on the skin surface and fail to enhance skin drug absorption (Elsayed et al. 2007). Thus, novel generations of lipid vesicles have

been proposed to solve this issue (Elsayed et al. 2007). Among them, flexible or ultra-deformable (UD) liposomes are of increasing interest. These vesicles are composed mainly of amphiphilic molecules forming bilayers with the addition of non-ionic, single chain surfactants with high curvature radius, which have deformable properties. In contrast to conventional liposomes, flexible liposomes can adapt their structure to support relatively high stress because the surfactant relocates in the zones of maximum pressure allow shape changes at minimum energetic cost (G. Cevc and Blume 1992). However, their mechanism of penetration is still undefined (Perez et al. 2016) and there is limited evidence of a correlation between the level of flexibility of the liposomes and their qualitative and quantitative penetration potential into human skin (Franzé et al. 2017). Two mechanisims have been proposed to explain how deformable vesicles improve delivery of drugs through the skin (Honeywell-Nguyen and Bouwstra 2003 (B); Honeywell-Nguyen, Arenja, and Bouwstra 2003 (A)). Firstly, vesicles can act as drug carrier systems, passing through the virtual channels of the *stratum corneum* and carrying vesicle bound drug molecules into the skin (mechanism 1). Alternatively, vesicles can act as penetration enhancers, where their lipidic bilayers interact with corneocytes and subsequently modify the intercellular lipid lamellae. This would cause the damage of the nanocarriers membrane and facilitate penetration of free drug molecules into and across the *stratum corneum* (mechanism 2).

In support of mechanism 1, Cevc et al. (1998) suggested that there are two different penetration pathways: the intercluster pathway and the intercorneocyte pathway. The authors claimed that these regions contained structural irregularities within the intercellular lipid lamellae, and that these irregularities can function as 'virtual channels' through which elastic vesicles can penetrate, and that intact deformable liposomes penetrated through the *stratum corneum* and through the underlying viable skin into blood circulation (Gregor Cevc, Schätzlein, and Richardsen 2002).

However, in another study, deformable liposomes were able to carry both the entrapped and the non-entrapped hydrophilic fluorescent compound, carboxyfluorescein, into the *stratum corneum* and possibly to deeper layers of the skin (Verma et al. 2003) suggesting also a possible penetration enhancing effect (mechanism 2). Another study also showed that deformable liposomes improved only the skin deposition of dipotassium glycyrrhizinate, as skin fluxes were below detection

limit, whereas skin deposition increased 4.5-fold in comparison to an aqueous control (Trotta et al. 2002). UD liposomes also improved only skin deposition of 5-fluorouracil with little or no effect on the drug permeation, according to El Maghraby et al. (2001 (A)), and therefore only useful for dermal delivery of these drugs. The limited partitioning into the acceptor phase used in the experiment indicates that deformable vesicles are not carrying the associated drug into the acceptor phase. In addition, the percentage of 5-fluorouracil that penetrated the skin was higher than the drug entrapment efficiency which strongly suggested that liposome components may have altered skin structure, thus enhancing 5-fluorouracil transmission through human epidermis (mechanism 2) (El Maghraby et al. 2001 (A)). Hence, some studies showed improved transdermal permeation, while others showed little or no effect (El Maghraby et al. 2001 (A); Trotta et al. 2002) after encapsulating drugs into UDs. El Maghraby et al (2008) suggested that the reasons for the variation in reported results, regarding improvement of skin permeation, may arise from different vesicle compositions, alternative methods of preparation, and the selection of skin membranes from different species (El Maghraby, Barry, and Williams 2008).

The aim of the present study was to investigate if Bleosome could penetrate through the skin of dogs, horse and humans and to elucidate the mechanism by which UD liposomes could improve delivery of the bleomycin through the skin, under non-occlusive conditions. We hypothesised that, if able to penetrate through deep layers of the epidermis, Bleosome could be used as topical agent in the treatment of cutaneous tumours. To achieve these aims we labelled bleomycin with a fluorescent probe and then encapsulated the fluorescently labelled drug into UD liposomes to create fluorescently labelled Bleosome. Subsequently, we treated live canine, equine and human skin tissues with the fluorescently labelled Bleosome and visualised the position of the entrapped drug within the skin over a time course by multiphoton microscopy (MP). In parallel, we treated comparable canine skin sections with unlabelled Bleosome and analysed samples using the trasmission electron microscopy (TEM), with the aim of visualising the liposomal nanocarriers within the skin. Hence, we optimised a novel method of directly visualising both liposomes and entrapped bleomycin inside live skin tissues after the Bleosome treatment. We found that Bleosome penetrated through equine, canine and human skin significantly deeper than

free bleomycin and we speculated that UDs, when carry bleomycin for skin delivery, might act as penetration enhancers.

3.3 Materials and methods

3.3.1. Skin collection and storage

3.3.1.1 Animal skin

The skin was collected in the *post mortem* department of the Royal (Dick) School of Veterinary Study, The University of Edinburgh, from euthanised dogs and horses. Skin samples were withdrawn from the abdomen and flank area of the carcasses. Equine and canine penetration studies were performed at least twice using skin from different animals (different breed, age and sex). Before excision, the hair of the target areas was removed using electric clippers. Skin was collected by a knife and afterwards, the subcutaneous fat and muscles were removed with a scalpel. Subsequently, according to the OECD guidelines, skin samples were snap-frozen in dry ice and stored at -20°C or -70°C until ready for the experiment, as detailed in section 2.9.

3.3.1.2 Human skin

Human skin was collected from patients undergoing reductive plastic surgery who voluntarily agreed to take part to this study. Detailed information can be found in section 2.9.1.2.1

3.3.2 Fluorescent microscopy

3.3.2.1 Processing canine skin sections

The skin was cut by a scalpel in three sections sized 2 cm x 2 cm, at a thickness of approximately 1 mm, and orientated with the epidermis side facing upward in a sterile 100 x 15 mm Petri Dish (Corning™) filled with DMEM to a level suitable to prevent the subcutaneous side of the skin section from drying out (figure 3.1). Two time points (2 hours (2h) and 4 hours (4h)) plus the control ((0h), untreated skin) were set-up, and the skin sections were treated with 0.1 ml of Bleosome, administered by insulin-syringes without needle, in the middle of the top surface, within a rubber "O" ring.

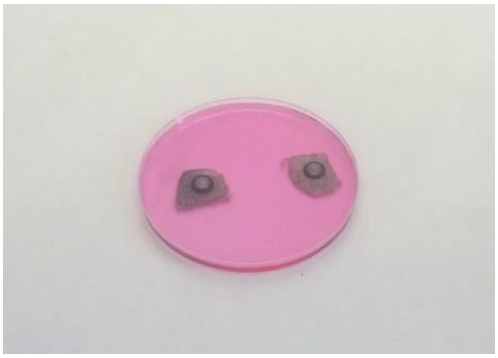

Figure 3.1 *Skin sections (2 cm^2) treated with Bleosome, moistened in cell medium. The two sections correspond to the 2h and 4h time points.*

At each time point, the Bleosome left on the surface was gently rinsed using a cotton swab and the respective sample was snap-frozen in isopentane cooled by liquid nitrogen. Each section was then cut into thin slices, placed in a cryomold to be cryosectioned at 10 µm thick sections and impressed on slides (detailed protocol in 2.9.1.1.3). Several experiments were conducted to optimise the protocol:

1) In the first experiment, samples were left drying overnight at RT and were then fixed with pre-cooled acetone and stained with DAPI (ThermoFisher Scientific) according to the manufacturer's instruction. This experiment was performed in duplicate.

2) For the second experiment, half of the samples were fixed with 10% neutral buffered formalin (NBF) and half with acetone, and stained with DAPI (ThermoFisher Scientific) according to the manufacturer's instruction. This experiment was performed one time.

3) In the third experiment, samples were fixed with 10% NBF, subsequently, half samples were pre-treated with TrueBlack® (a quencher agent), prior to staining with DAPI (for details refer to 2.9.1.1.3). This experiment was performed in duplicate.

4) A further experiment was conducted by treating the skin sections for 2 and 4 h with either 0.1 ml of bleomycin aqueous cream (0.2 %), bleomycin ointment (Bleovet 0.2%), or Bleosome. All samples were pre-treated with TrueBlack. Bleomycin aqueous cream and Bleovet ointment contain non-encapsulated bleomycin, and they have different moisture contents (2.2) (figure 3.2). This experiment was performed one time.

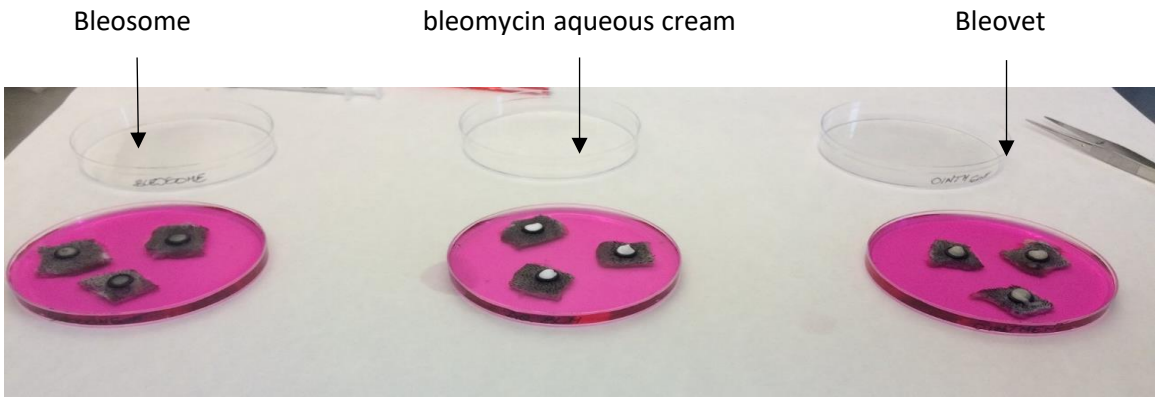

Figure 3.2. *Skin sections treated with either Bleosome, bleomycin aqueous cream or bleovet ointment for 0h, 2h and 4h. All sections were moistened in cell media.*

3.3.2.2 Fluorescent Microscope visualisation

Slides were visualised at the Leica DMLB upright phase/fluorescent microscope, at 20x and 40x magnification. To evaluate the inherent green fluorescence of bleomycin, the Cyan Lumencor Exciter filter (202/324 band-pass) was used. To visualise DAPI stained structures the Violet Lumencor Exciter filter (201/401 band-pass) was used (microscope settings and specification are detailed in 2.10.1).

3.3.3 Transmission electron microscopy (TEM)

3.3.3.1 Treatment of canine skin sections

Each experiment conducted with TEM was performed using the skin withdrawn from a single dog, randomly chosen from the frozen skin library, which was used in that study only; hence all the penetration studies were conducted using canine skin sections belonging to different animals (of different breeds, sex and ages).

Canine skin samples were thawed in PBS, then cut in 2 x 2 x 0.1 cm sized sections, positioned in petri dishes filled with a sufficient amount of PBS to moisten the subcutaneous side (figure 3.3).

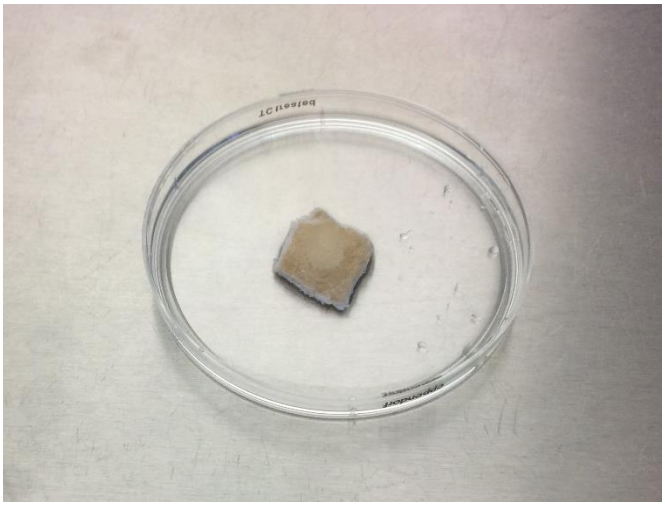

Figure 3.3 *Example of canine skin explant hydrated with PBS in a petri dish prior to Bleosome treatment.*

Subsequently, skin sections were treated with Bleosome 0.2% and for each experiment, a control sample (untreated) was used. Residual Bleosome cream was gently removed with a cotton swab at the indicated time point. Skin samples were processed according to section 2.9.1.1.4.

Four experimental settings were used in order to optimise the technique and validate the results:

1) Skin sections were treated with 0.1 ml of Bleosome 0.2%, dosed using an insulin syringe without needle and spread evenly with a gloved fingertip all over the free surface of the epidermis side of the skin section, without allowing the compound to be absorbed. Skin explants were treated for: 0 h (control, section kept hydrated by adding PBS, without Bleosome), 30 minutes (min), 2 h, 4 h, 6 h and 8 h. A variant of this experiment (including time points until 6 h) was performed twice.

2) Skin sections were treated with 0.1 ml of Bleosome 0.2% dosed using an insulin syringe without needle, positioning the drug on the top right corner of the skin section; from that corner, the compound was subsequently gently spread all over the free surface of the epidermis side. Time points used in this experiment were: 0h (untreated control), 30 min, 2h, 4h and 6h. This experiment was performed one time.

3) Skin sections were treated with 0.1 ml of Bleosome 0.2%, dosed using an insulin syringe without needle and spread evenly with a finger on the free surface of the epidermis side of the skin section, without letting the compound being absorbed. Skin sections were treated in this manner repeatedly, every 60 min. Time points for this experiment were set at: 0h (control, no Bleosome treatment, PBS only), 30 min (this section was treated one time), 2h (this section received two Bleosome treatments), and 4h (this section received four Bleosome treatments). This experiment was performed one time.

4) Skin sections used in this experiment were treated straight after the collection from the canine cadaver, without being frozen. Cutaneous explants were cut as in the previous experiments and treated with 0.1 ml of Bleosome 0.2%, dosed using an insulin syringe without needle and spread evenly with a finger all over the free surface of the epidermis side of the skin section, without letting the compound being absorbed. Lengths of treatment for this study were set at: 0h (control, no Bleosome treatment, but PBS), 30 min, 2h and 4h. This experiment was performed one time.

3.3.3.2 TEM visualisation

Skin samples were processed according to 2.9.1.1.4. Samples were visualised using a JEOL JEM-1400 Plus TEM. Representative images were collected on a GATAN OneView camera at a range of magnifications.

3.3.4. Coupling 120 mg of bleomycin sulphate (A2-B2) with the fluorophore Bodipy-FL

In order to visualise Bleosome and bleomycin activity within cells and skin tissues by microscopy, 120 mg of bleomycin sulphate (A2-B2) was coupled with a green fluorophore called Bodipy-FL. The efficiency of the reaction and the final product were assessed by High-Performance Liquid Chromatography/ Mass Spectrometry (HPLC/MS). The whole process was conducted in collaboration with the Division of Biochemistry at The Queen's Medical Research Institute (QMRI), the University of Edinburgh. The protocol is detailed in 2.8.

3.3.4.1 Viability assay using fluorescent Bleosome

The CellTiter-Glo® Luminescent Cell Viability Assay kit (Promega) was used to determine the viability of cells after treatment with several different doses of fluorescent Bleosome (F-Bleosome) and non-fluorescent Bleosome (Bleosome) as comparison. Detailed protocol can be found in 2.2.1. Briefly, 96-well plates were seeded with canine cancer cell lines: C2 (canine mast cell tumour) and CML10 (canine metastatic melanoma). Cells were treated with F-Bleosome 0.2% or Bleosome 0.2% using the flowing dose titration: 0, 0.1, 0.5, 1, 2, 3, 4, 5, 7, 10, 20 μM, to compare the efficacy of the fluorescent compound to the unlabelled one at 72 h post-treatment. The assay for each cell line was performed in duplicate. A prelinimanry experiment was performed treating cells with the concentrations of F-Bleosome indicated above and the luminometry was read after 10 min of treatment.

3.3.5. Multiphoton Microscopy (MP)

3.3.5.1 Processing canine and equine skin sections

Each experiment conducted with MP was performed using the skin withdrawn from a single dog and horse chosen randomly from the frozen skin library; hence, all the different penetration studies were conducted using canine and equine skin sections from different animals (including a range of breeds, sex and ages). At least two experiments were performed using canine skin and two using equine skin.

Equine and canine skin was processed in the same manner: skin was thawed in PBS and cut in 2 cm x 2 cm sections. The majority of the sections had a thickness of 1 mm (range from 0.5 to 1.5 mm), and was measured by an electronic caliper. Cutaneous explants were positioned in petri dishes (one for each sample) filled with enough PBS to prevent dehydration.

Each skin section, oriented with the epidermis side facing upward, was stained with Hoechst 33342 (ThermoFisher Scientific, Paisley, Uk) diluted in PBS at concentration of 0.02 mg/ml, spread with a syringe without needle on the epidermis side of the skin

explants and allowed to stain for 30 min in the dark at RT. The skin was then washed in PBS. Subsequently, skin explants were positioned with the subcutaneous surface facing upward and 0.5 ml of diluted (0.02 mg/ml) Hoechst stain was spread on this side of the sections, and incubated for 30 min in the dark at RT, and then washed with PBS.

For each experiment, 8 skin explants were used: 3 sections were treated with 0.1 ml of F-Bleosome 0.2% and the other 3 with 0.1 ml of aqueous F-bleomycin 0.2%. Both compounds were dosed and administered using an insulin syringe without a needle. One section was used as an untreated control and kept hydrated by adding PBS to the epidermal surface. The F-Bleosome cream was spread evenly over the epidermal surface, using a finger, preventing the compound from being absorbed. The F-bleomycin was administered by the syringe evenly on the epidermal surface of each section (figure 3.4). Particular attention was given to avoiding dropping of F-Bleosome and F-bleomycin on the side of the section, if this occurred, the explant was removed from the experiment and replaced with another skin section. Three time points for each treatment were set: 10 min, 4h and 6h. At the respective time point, the residual F-Bleosome cream was gently removed with a cotton swab, and the skin section rinsed with PBS; for the F-bleomycin treatment, sections were rinsed with PBS only.

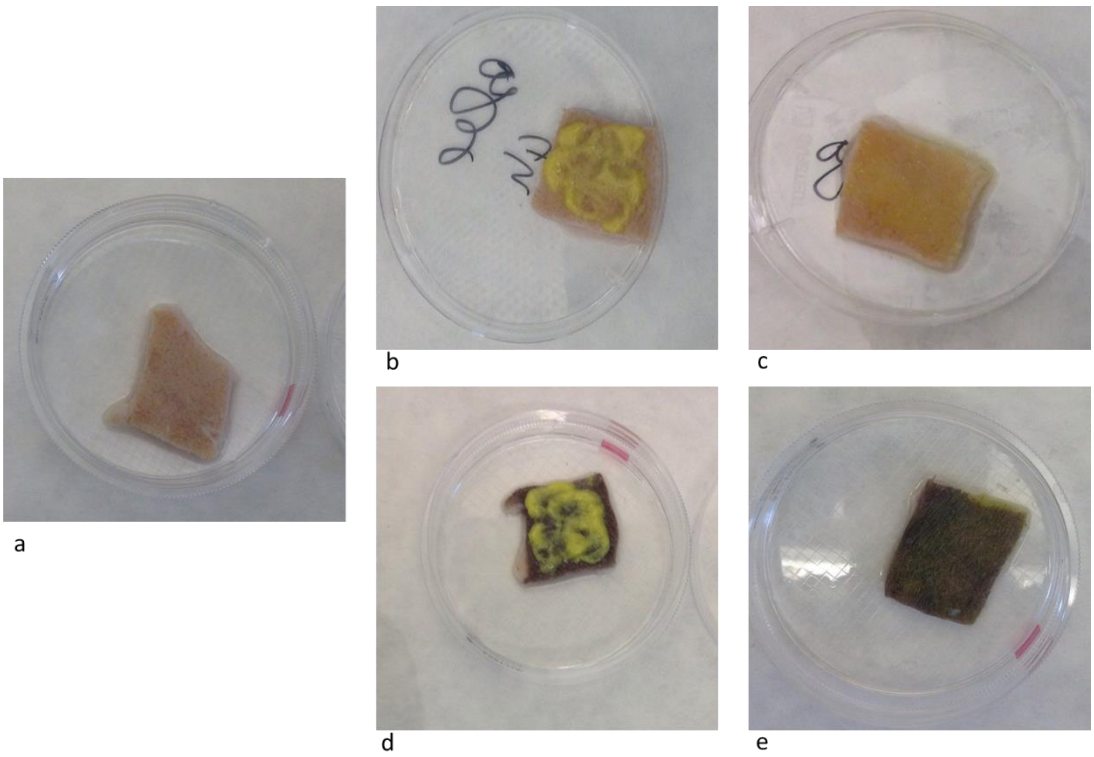

Figure 3.4 *Representative canine and equine skin sections treated with F-Bleosome and F-bleomycin. (a) is the untreated canine skin section (control), (b) and (d) are canine and equine skin explants treated with F-Bleosome respectively, (c) and (e) are canine and equine skin explants treated with F-bleomycin respectively.*

3.3.5.2 Processing human skin sections

Human skin used was collected from the breast of a healthy donor undergoing plastic reductive surgery. Skin was processed and treated following the same protocol detailed in section 3.3.5.1. The penetration experiment was performed once and the dimension of the skin explants used was 2 cm x 2 cm, with an average thickness of 0.5 mm (from 0.5 to 1 mm).

3.3.5.3 MP visualisation

All the samples were obsverved with a Zeiss LSM7 MP intravital. Skin explants were positioned in 35 x10 mm petri dishes, (gridded Nunclon™ Delta, Thermofisher) with the epidermis side anchored to the bottom of the dish by 4% agarose with the subcutaneous side facing upward, toward the microscope lens. The dish with the sample was filled with PBS and positioned in the visualising plate of the MP. The 20x upright lens was dipped in the PBS contained in the dish, avoiding the formation of air bubbles. Green (NDD R4 ET535/30) and blue (NDD R3 ET460/36) filters were used. Details of microscope settings are listed in 2.10.4.

3.3.5.4 3-D Image analysis with Imaris software

To analyse three-dimensional (3-D) images of skin, acquired using MP, we used Imaris 9.1.2 (Bitplane) software (complete protocol in Supplementary Data 8.2.4). In this study, two channels were used to detect green and blue fluorescence. However, the Imaris software is not capable of distinguishing between structures emitting low and high-intensity of the same fluorophore, detected in a single channel (e.g. green – NDD R4); similarly, structures emitting both green and blue fluorescence (e.g. cellular nuclei) are not considered as separate entities by the software, but they are categorised according to the higher fluorescent signal detected. Hence, a method aimed to distinguish between F-Bleosome and F-bleomycin particles from autofluorescent skin structure, was optimised. Briefly, structures labelled with Hoechst staining that did not emit or emitted a low green fluorescent signal (the majority of autofluorescent skin appendages, e.g. connective tissue and cellular elements) were considered as "surfaces" ("surfaces" had NDD R3-blue source channel); while all the elements emitting high level of green signal, either labelled with Hoechst (such as cellular nuclei) or not (F-Bleosome and F-bleomycin), were marked as "spots" ("spots" had NDD R4-green source channel). After this distinction, the program was asked to distinguish between the "spots far from surfaces" (green particles emitting high-intensity green fluorescence far from the particles emitting blue and low-intensity green fluorescence), from the "spots close to surfaces" (green particles emitting high-intensity green fluorescence, and blue fluorescence very close to autofluorescent skin

and cellular structures, emitting low-intensity green fluorescence), using a specific threshold (0.5). The aim was to target the green particles that were far from the autofluorescent skin structures and that were not stained with Hoechst (cellular nuclei were always close to intracellular autofluorescent elements and thus recognised as "spots close to surfaces"). This system enabled us to identify F-bleomycin and F-Bleosome particles within the examined skin section, recognised as green emitting particles far enough from autofluorescent structures ("spots far from surfaces").

3.4 Results

3.4.1 Fluorescent microscopy is not a suitable tool to evaluate the penetration potential of Bleosome through the skin

To assess the ability of Bleosome to penetrate through the skin we initially sought to take advantage of previously reported autofluorescence of the compound (Ranji et al. 2016) and fluorescent microscopy, as used in a similar study conducted using human skin explants treated with Bleosome 0.2% (personnel Communication, S. Chopra). Canine skin sections were treated with 0.1 ml of Bleosome (0.2%) for 0 (control), 2 and 4 h. We observed that the untreated skin section (0 h) is autofluresencent with hair follicles and glands within the outermost *stratum corneum* expressing the highest intensity (figures 3.5, 3.6 and 3.7). Nuclear staining with DAPI (blue) was successful, and all the underlying strata of the skin appeared with a bright green fluorescence signal. Furthermore, when compared to the treated sections, no significant differences were noted in the green intensity observed at 30 min, 2 h and 4 h time points. Initially, acetone was used as fixative for the cryosectioned slides (data not shown); however, this is a coagulative fixative that can cause the dissolution of lipidic particles. We then repeated the experiment fixing the slides with 10% NBF. Again, the background autofluorescence of canine skin was still too high to distinguish the autofluorescence of Bleosome and did not allow meaningful interpretation of the degree of skin penetration of Bleosome over time (figure 3.5).

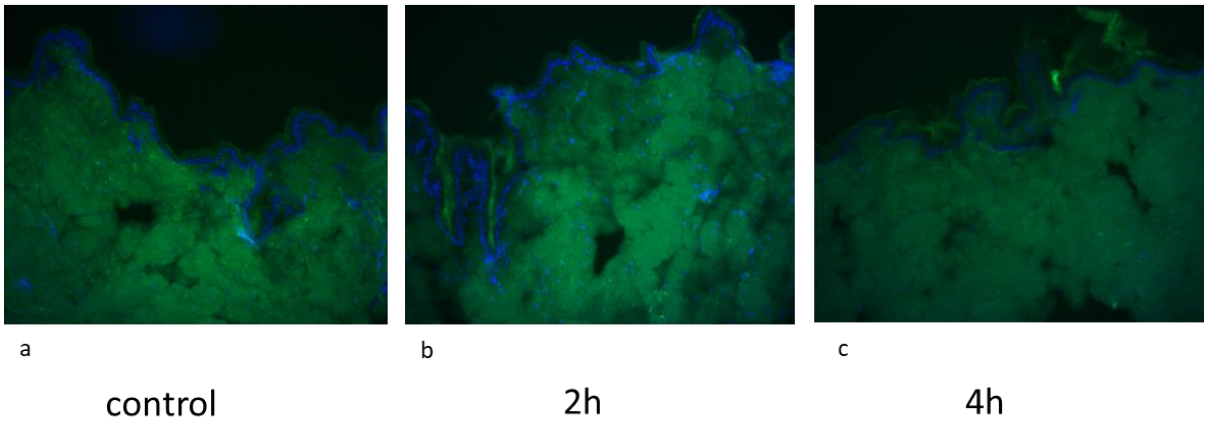

Figure 3.5 *Cryosectioned slides of canine skin explants fixed with 10% NBS. (a) is an image from a slide of the untreated section (0 h, control), (b) represents image from a slide of skin treated with Bleosome for 2h, (c) is a representative image from a slide of skin treated with Bleosome for 4 4h. In all the images, the outermost stratum coreum is visible, and the first cellular layer (the stratum spinosum) is highlighted by the presence of blue stained nuclei.*

To overcome the effect of autofluorescence of the skin we trialled fixing the slides with 10% NBS and using a quencher agent called TrueBlack®. TrueBlack® was added to half the examined slides, with the aim of extinguishing the inherent green fluorescent background signal of skin (figure 3.6). We found that the quencher agent had limited effect (figure 3.6).

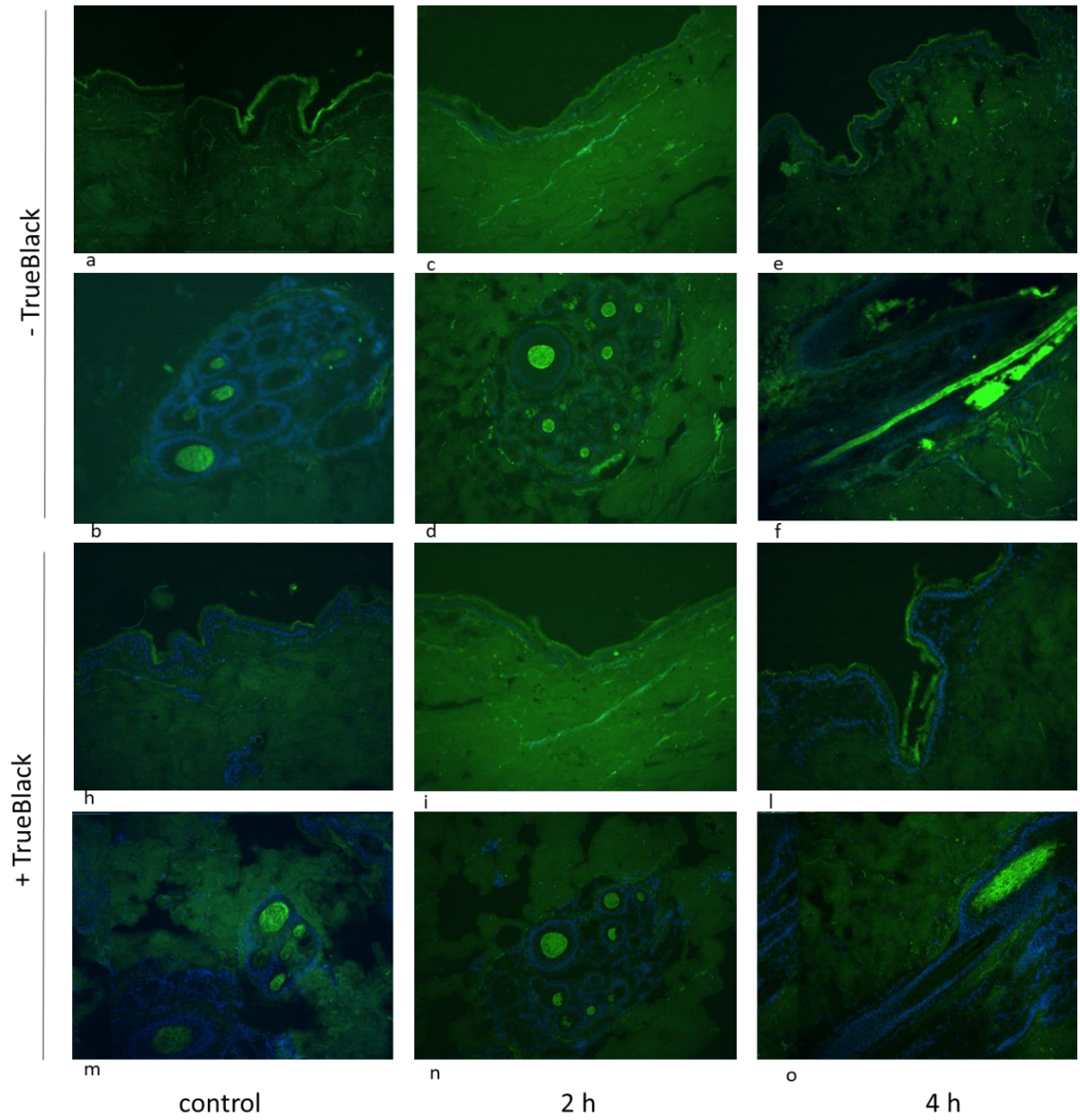

Figure 3.6 *The autofluorescence of skin is not extinguished by the quencher agent. Images from slides of skin sections without pre-treatment with TrueBlack® (from (a) to (f)) and pre-treted with TrueBlack® (from (h) to (o)). (a), (c) and (e) are the epidermis of the sections corresponded respectively to control, 2h and 4h of treatment, (b),(d) and (f) are details of hair follicles of sections corresponded respectively to control, 2h and 4h of treatment. (h), (i) and (l) are the epidermis of the sections corresponded respectively to control, 2h and 4h of treatment with Bleosome on slides pre-treated with TrueBlack®, (m),(n) and (o) are details of hair follicles of sections corresponded respectively to control, 2 h and 4 h of treatment.in slides pretreated with TrueBlack®*

All the images were captured using the same microscope settings and exposure time for the green and blue filter (section 2.10.1); they show how some cutaneous elements,

such as the *stratum corneum* and hair follicles, are intensely brightly fluorescent. Comparing the green intensity of the skin between each time points, some slight differences can be observed, however, this is not objectively quantifiable, and it can be due to a slight variation of the amount of autofluorescent skin structures rather than to the peak of penetration of the compound.

In order to confirm that liposomes did not hamper the autofluorescence and visulisation of bleomycin during the sample processing, we treated the skin sections with Bleosome, aqueous cream bleomycin and Bleovet ointment. Aqueous cream bleomycin and Bleovet ointment are two versions of non-encapsulated bleomycin (figure 3.7). We comfirmed that the inherent fluorescence of all of the compounds used did not exceed the autofluorescence emitted by skin (data not shown) and concluded that this technique was not suitable to visualise the penetration of Bleosome through the skin.

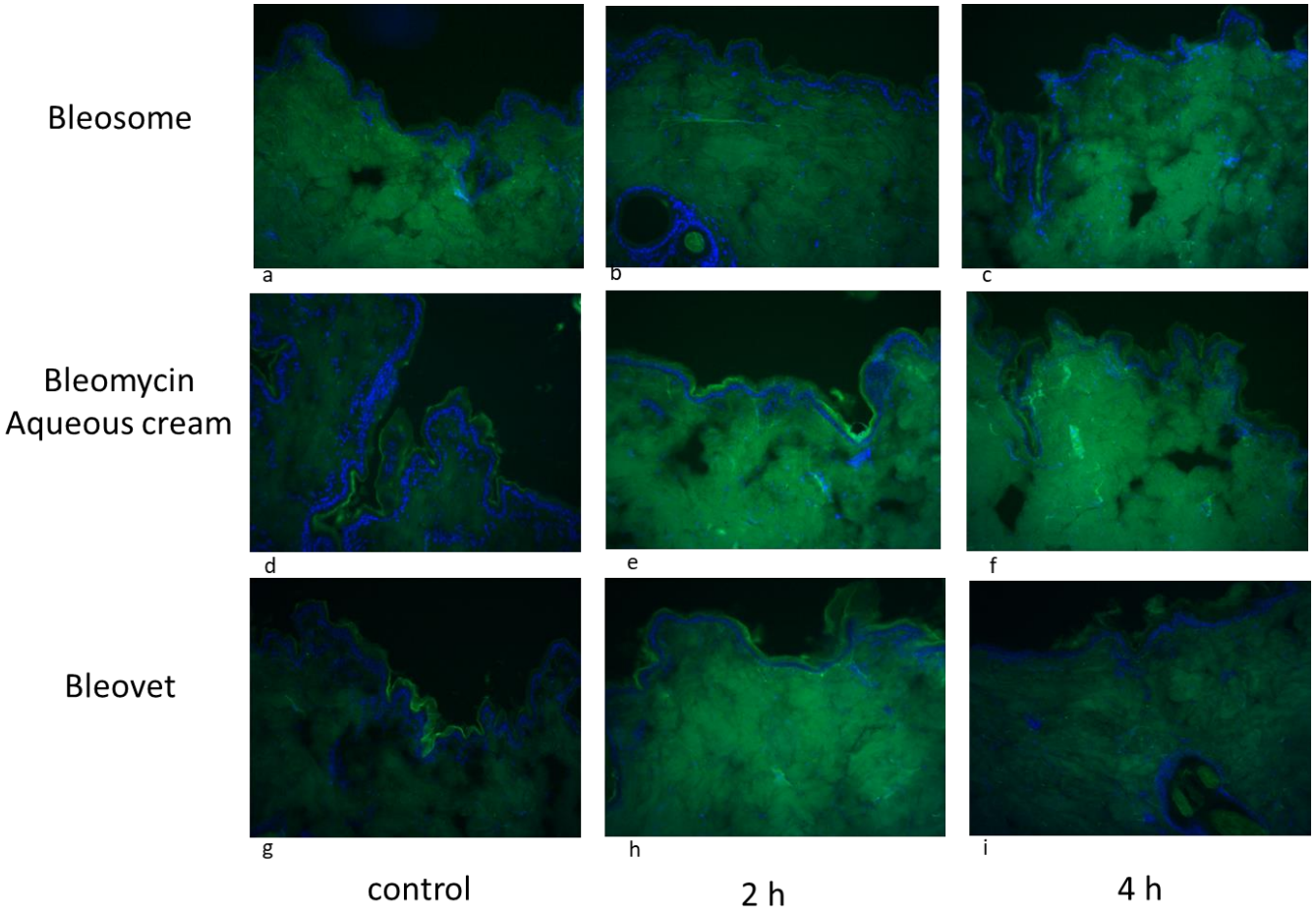

Figure 3.7 *Comparison of green fluorescence intensity of skin treated with encapsulated and free bleomycin. (a), (b) and (c) correspond to skin untreated (control), treated for 2 and 4 h respectively with Bleosome; (d), (e) and (f) correspond to skin untreated (control), treated for 2 and 4 h respectively with aqueous cream bleomycin; and (g), (h) and (i) correspond to skin untreated (control), treated for 2 and 4 h respectively with Bleovet*

3.4.2 Visualisation of liposome penetration through the skin by TEM

We have established a protocol for the visualization of liposomes within skin sections after treatent with Bleosome, in collaboration with the imaging unit at the King's Buildings (the University of Edinburgh). As a control, UD liposomes within Bleosome 0.2% cream were directly visualised using the TEM. The cream was sonicated, imaged, and liposomal nanoparticles appeared as electron-dense (black) round-shaped structures, with size varying between 150 to 250 nm (figure 3.8).

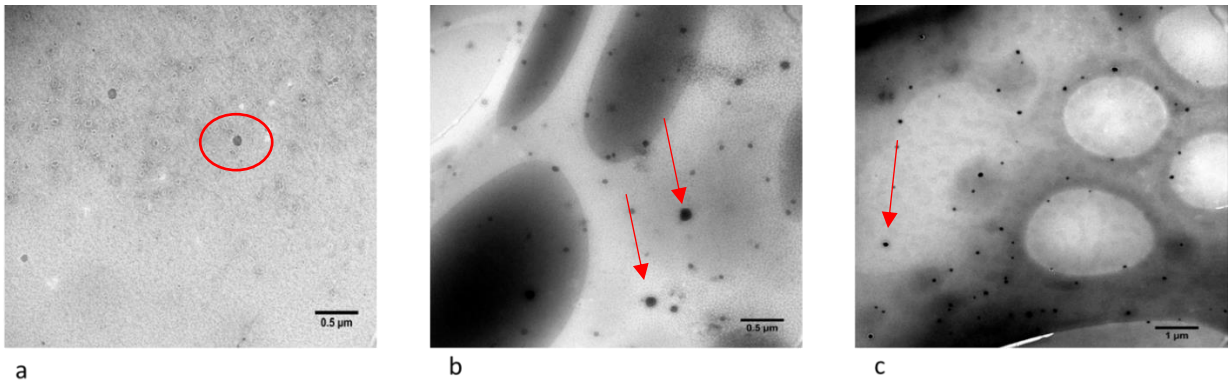

Figure 3.8 *Direct visualisation of UD liposomes included in the Bleosome cream after sonication, with TEM. (a) x1200, a liposomes is cirled in red, (b) x1200, relevant liposomes are indicated by red arrows, (c) x500, a nanoparticle is indicated by red arrow.*

To visualise liposomes within the skin, canine skin explants were treated with 0.1 ml of Bleosome 0.2% for 0 (PBS control), 0.5, 2, 4, 6 and 8 h. All the epidermal strata can be visualised with the TEM, from the outermost *stratum corneum,* and its layers of keratynocytes, to the cellular and extracellular matrix components of the innermost *strata spinosum* and *basale* (Figure 3.9). Within the untreated control skin section (0 h) liposomes were not observed in any of the epidermal structures visualised (figure 3.9 (a), (b) and (c)); whereas liposomal particles can be recognised in all the skin explants treated with Bleosome over the time course (figure 3.9 from (d) to (r)). At different magnifications, it is possible to see that the nanoparticles have penetrated through the corneocytes of the *stratum corneum*. Interestingly, liposomes did not penetrate deeper over time and were not found beyond the external keratynocytes layer. We also found in almost all the skin sections examined, including the control,

that external layers of corneocytes had a tendency of detaching from the innermost layers within the *stratum conreum*.

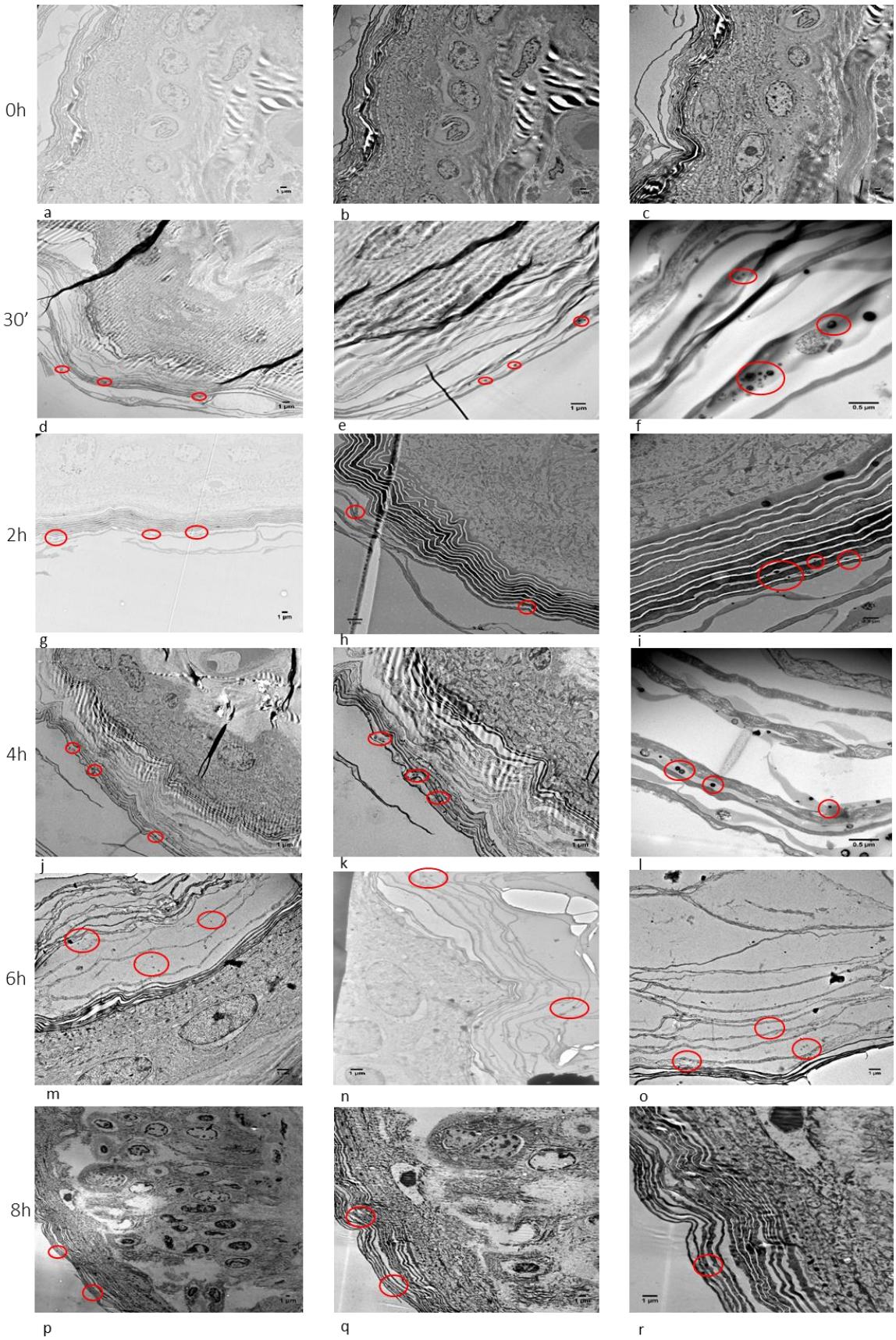

Figure 3.9 *Visualisation of liposomes through the skin at different time points after a single Bleosome administration at different magnifications. The line (0h) corresponds to the pictures of the untreated samples (control): (a) x500, (b) x1200, (c) x1200; the line (30') corresponds to the images of samples treated for 30 min with Bleosome: (d) x1200, (e) x2500, (f) x10K; line (2h) shows images taken from*

skin sections treated for 2 h: (g) x500, (h) x2500, (i) x5000, the line (4h) show images relative to skin sections treated for 4 h: (j) x 1200, (k) x2500K, (l) x10K. Line (6h) shows images relative to skin sections treated for 6 h: (m) x2500, (n) x1200, (o) x2500. Line (8h) includes pictures of the skin after 8 h of Bleosome treatment: (p) x500, (q) x1200), (r) x 2500. The (0h) line shows the whole epidermis layer without the precence of liposomes. Liposomal nanoparticles can be appreciated circled in red within the kerantynocyes of the stratum corneum only, in the pictures relative to every time points of treatmen. Detachemnt of the layers of corneocytes can be noted in all the pictures.

To confirm the hypothesis that there was no connection between the length of treatment and the depth of penetration of Bleosome through the skin, Bleosome was concentrated in one particular area of the section (data not shown). Moreover, in a further experiment, skin explants were subjected to repeated treatments, according to experimental setting number 3 in section 3.3.1. Here, skin sections were evaluated for 30 min, 2 and 4 h and the position of the liposomes within epidermal layers was found again within the keratynocytes of the *stratum corneum* only, and not deeper than this external stratum for each time point tested (figure 3.10).

Subsequently, to establish if artefacts due to the freezing and thawing of skin could be responsible for the detachment of layers of keratynocytes, the skin explants collected from a canine cadaver was immediately processed and treated, with a single administration of Bleosome, for 30 min, 2 and 4 h. These results were comparable to our previous findings, where nanoparticles were limited to the *stratum corneum* (data not shown), indicating that this is not due to freezing artefacts.

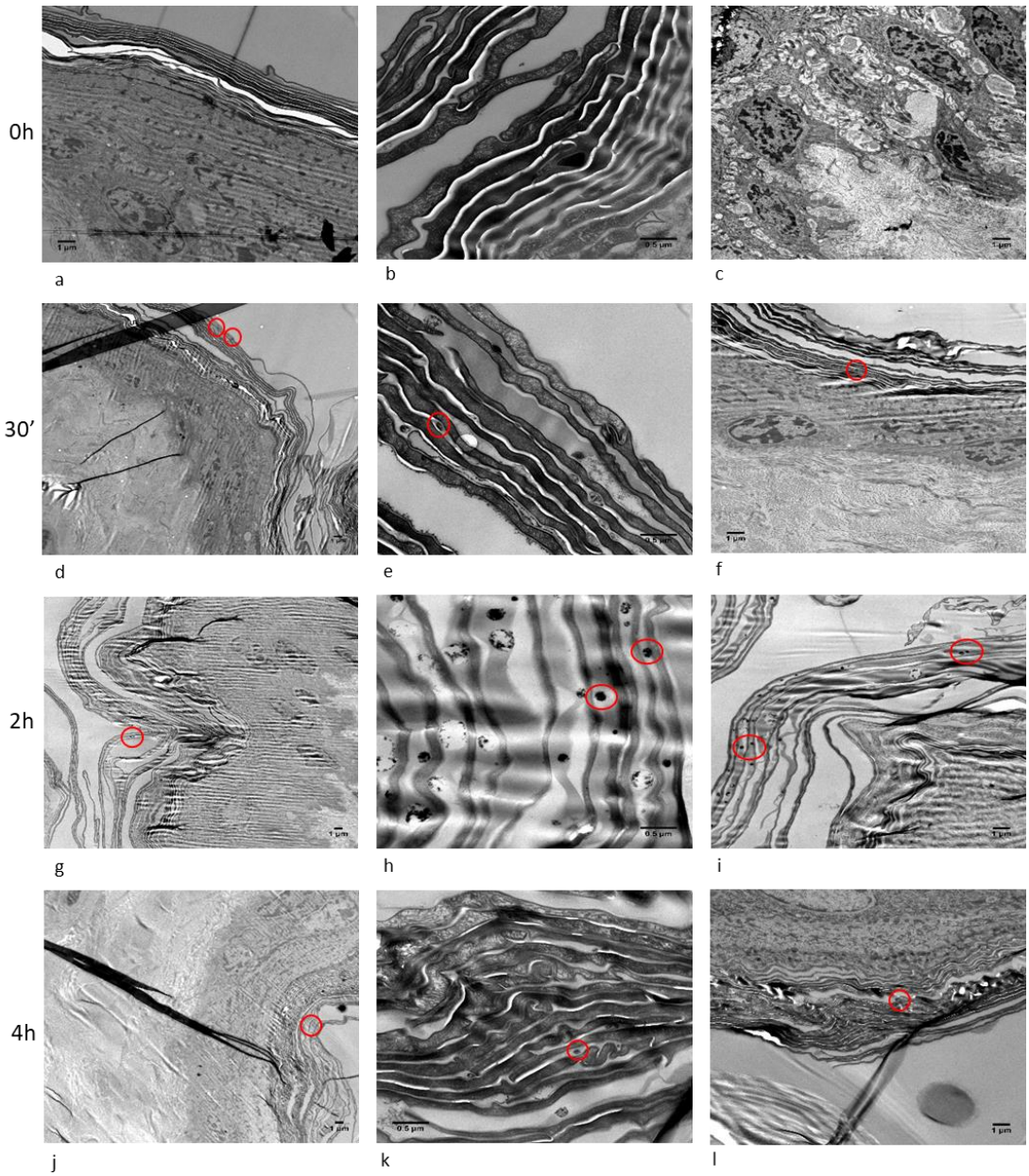

Figure 3.10 *Liposomes were found within the SC only after different time points and repeated Bleosome applications. The line (0h) corresponds to the pictures of the untreated samples (control): (a) x2500(b) x10K (c) x2500; the line (30') corresponds to the images of samples treated for 30 min with Bleosome: (d) x1200, (e) x10K, (f) x2500; line (2h) shows images taken from skin sections treated for 2 h: (g) x1200, (h) x10K, (i) x2500, the line (4h) show images relatives to skin sections treated for 4 h: (j) x 1200, (k) x10K, (l) x2500. (0h) line shows details of the whole epidermis (a), stratum conreum (b) and underlying cellular levels of the epidermis (c): liposomes are absent at every level of the examined skin.(b),(e),(h) and (k) show details of the keratynocytes of the outermost stratum corenum at high magnification: in the control (b) liposomes are absent, while in every other time points of treatment (30',2 and 4 h) the liposomal nanoparticles are present and visible between the corneocytes, relevant nanocarriers are circled in red. The other images shows details of the epidermis at lower magnification and confirmed the presence of liposomes only within the stratum conreum, nanoparticles are never found deeper that this layer. Detachemnt of the layers of corneocytes can be noted in all the pictures.*

3.4.3 Labelling of bleomycin with BODIPY-FL flurophore

To effectively observe Bleosome penentration though the skin we aimed to label bleomycin, prior to encapsulation into UD liposomes, with a fluorophore. In collaboration with Marc Vendrell's group at the QMRI, optimisation of the fluorescent labelling process was undertaken by trialling a range of fluorophore/bleomycin ratios (details in 2.8). Our main aim was to identify the optimal amount of fluorophore to use to produce a final compound containing the highest possible amount of mono-labelled bleomycin (bleomycin sulphate bound to one Bodipy unit), avoiding double and triple labelling of the drug (bleomycin sulphate bound to two or three Bodipy units). We also wanted to avoid residual unbounded fluorophore, as this could affect the imaging studies and generate unreliable data, while a small percentage of free bleomycin (less than 15%) was not likely to alter the efficacy of the final compound. Once we optimized the methodology with a small-scale trial, the reaction was scaled up and carried out in two larger batches. During the coupling process, the reaction was checked regularly by HPLC. Figure 3.11 shows the HPLC profile of the reaction after 30 min (Figure 3.11 (a) and (c)) of the first and the second batch respectively. The two reactions displayed a very similar HPLC profile at the end of the process (Figure 3.11 (b) and (d)): the major component of the reaction mixture was represented by mono-labelled bleomycin, while a small amount of free bleomycin and succinimide-OH were present before the purification process. Following the conjugation reaction between bleomycin and the fluorophore, the powders produced by the two experiments were combined, purified from succinimide-OH and other minor fluorescent impurities, and finally analysed by HPLC (Figure 3.11 (f) shows the components of the final fluorescently labelled bleomycin).

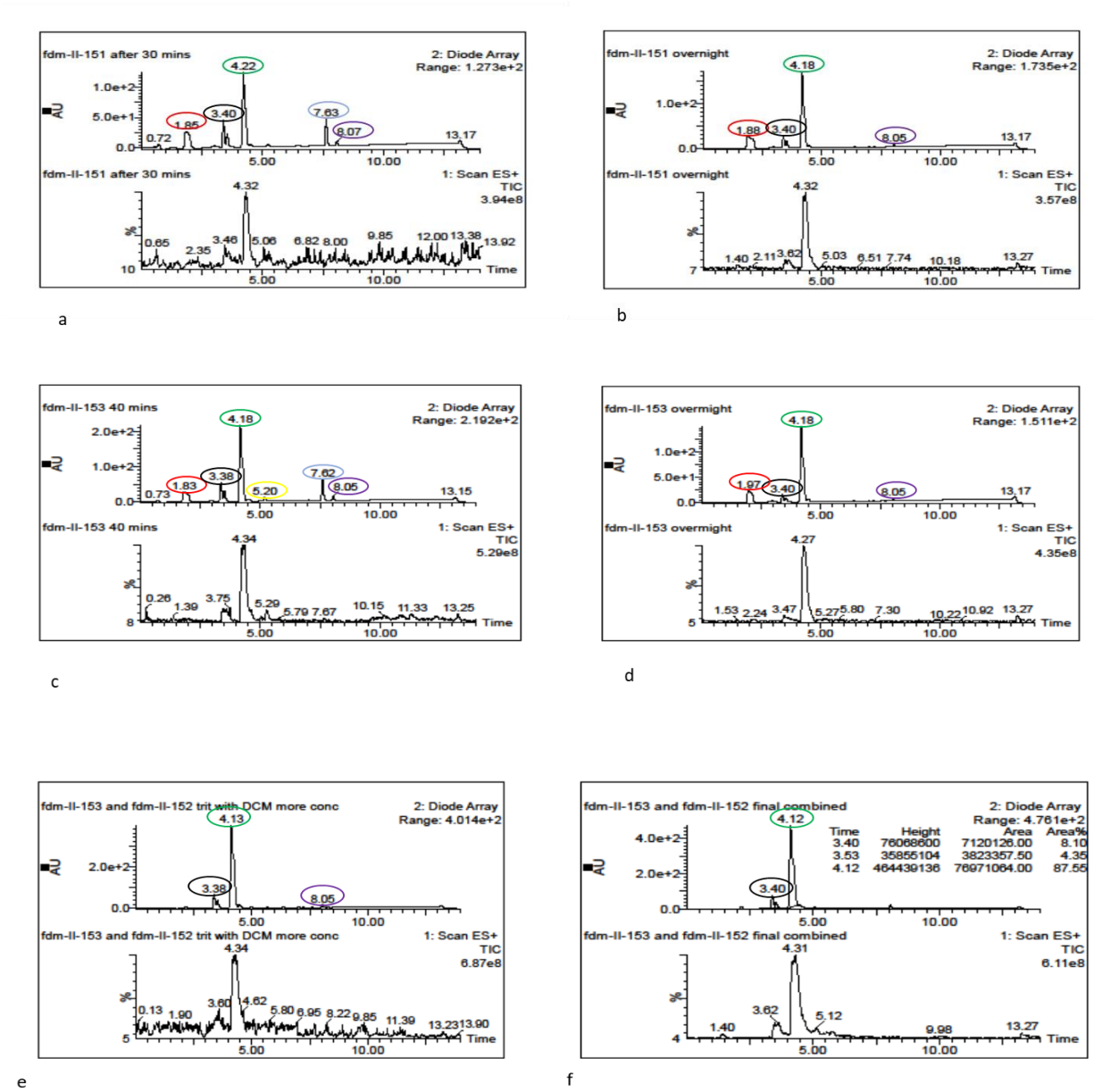

Figure 3.11 *Fluorescent labelling of bleomycin. (a) and (b) represent the HPLC profiles of the first coupling reaction between 45 mg of bleomycin and Bodipy-FL, after 30 min and overnight respectively; (c) and (d) represent the HPLC profiles of last coupling reaction between 81 mg of bleomycin and Bodipy-FL, after 30 min and overnight, respectively.(e) and (f) are the HPLC profiles of the combined labelled bleomycin batches before and after the final lyophilisation respectively. According to their absorbance profile and mass spectra: peak 1.83 (red circle) corresponds to succinimide-OH; peak 3.38 (black circle) to free bleomycin; peak 4.22-4.12 (green circle) corresponds to the mono-labelled bleomycin (bleomycin bound to the dye onto one amine group); 5.20 (yellow circle) corresponds to double-labelled bleomycin (bleomycin bound to the dye onto two amine groups); peak 7.63 (blue circle) corresponds to free (unbound) Bodipy-FL.; 8,05 (violet circle) corresponds to a minor impurity of the fluorophore. (f) shows quantification in percentage of the components of the final compound: 87.55% monolabelled bleomycin and 12.45% free bleomycin.*

The final powder contained 87% of mono-labelled compound and 13% of free bleomycin. This compound was sent, refrigerated and protected against direct light, to the *Ascot Laboratories Ltd* to be encapsulated into UD liposomes. A small amount

was saved to create the aqueous form of unencapsulated fluorescently labelled bleomycin (F-bleomycin), used as comparison with fluorescently labelled Bleosome (F-Bleosome).

Figure 3.12 *Final labelled bleomycin. (a) appearance of the final bleomycin powder coupled with Bodipy-FL; (b) appearance of the final bleomycin powder coupled with Bodipy-FL dissolved in PBS.*

3.4.4 F-Bleosome retains the same efficacy as unlabelled Bleosome

To determine if F-Bleosome retained comparable efficacy to unlabelled Bleosome, we utilised cell viability assays. A preliminary experiment confirmed that the fluorescence of the labelled compound did not affect the luminometer reading of the assay. Here, cells were treated with F-Bleosome for approximately 10 min before being analysed. The assumption was that these cells did not have time to be killed by the compound, and, for this reason, they would be detected as viable cells, and generate the same signal among different drug concentrations if the fluorescence did not interfere with the reading. We found that cells expressed approximately the same signal and level of viability, regardless of the concentration of the drug (Figure 3.13). For this reason, we concluded that this method was appropriate to assess the efficacy of F-Bleosome.

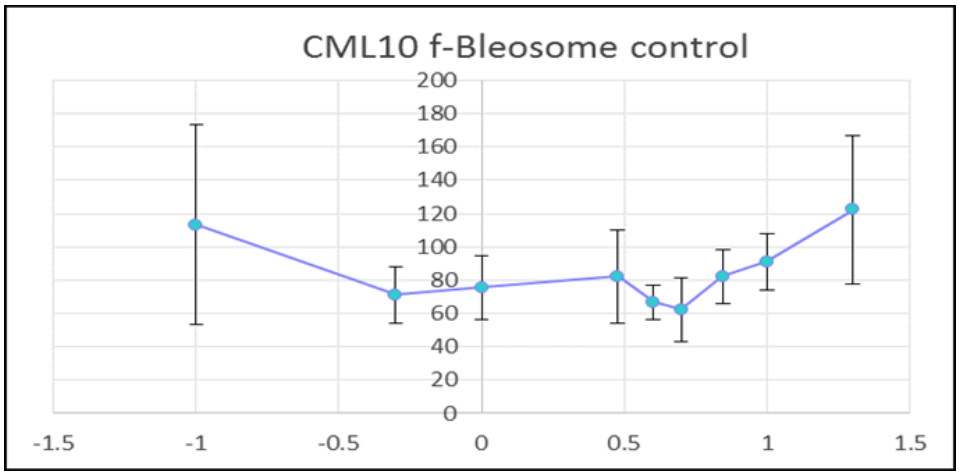

Figure 3.13 *Fluorescent label of F-Bleosome does not effect the reliability of the cell viability assay. F-Bleosome was added to cells 10 min prior to reading the assay and had no effect on the luminescence read-out.*

Hence, we performed the viability assay on two different canine cancer cell lines, using equivalent concentrations of Bleosome and F-Bleosome. Figure 3.14 shows that the mortality curve generated by both compounds followed the same trend: the percentage of viable cells decreased with increasing concentrations of the drug, and this was consistent in both cell lines tested. Therefore, we showed that there was no significant difference between the killing effect of F-Bleosome and Bleosome and concluded that the fluorescent dye coupled to bleomycin did not affect the cytotoxicity of the drug.

Confident that the biology of the drug was not impinged by the addition of the Bodipy-FL, we proceeded to utilise F-Bleosome in imaging studies.

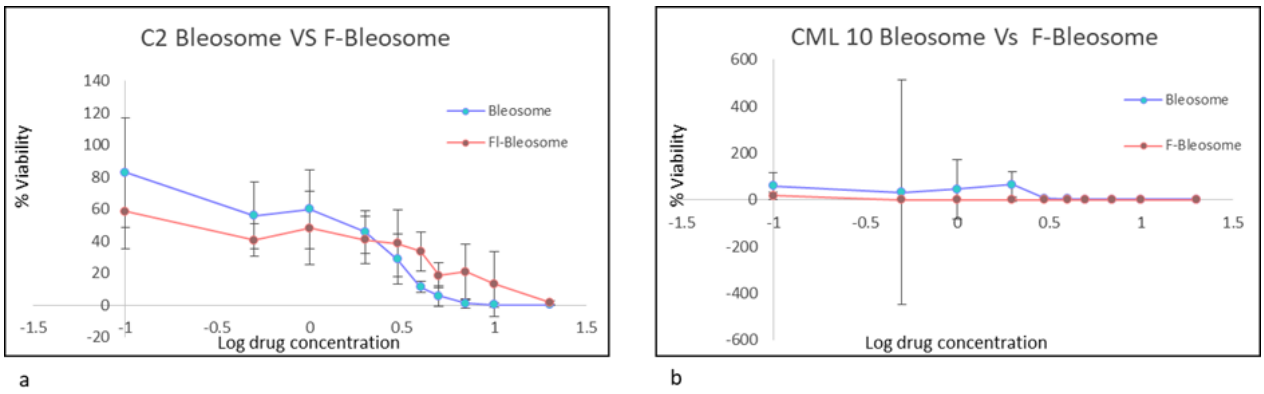

Figure 3.14 *Comparison of the viability of C2 (a) and CML10. (b) cells (y axis) treated with different concentrations of Bleosome and F-Bleosome (x axis) after 72 h.*

3.4.5 F-Bleosome is able to penetrate through skin better than F-bleomycin

Canine, equine and human skin sections were harvested and processed as before (3.3.5). Samples were counterstained with nuclear staining and treated with 0.1 ml of F-Bleosome or F-bleomycin for 10 min, 4 h and 6 h. Images were captured using a Zeiss LSM7 MP intravital and analysed with Imaris 9.1.2 (Bitplane) (protocol in Supplementary Data 8.2.4).

3.4.5.1. Canine skin

Several experiments were performed to confirm that F-Bleosome can efficiently penetrate through canine skin, and the results generated were always concordant; hence, here, representative results are shown.

The skin has several structures that are autofluorescent, including collagen, cellular nuclei and hair follicles. All images were compared to untreated control sections of skin to account for background fluorescence. The nuclear staining, performed by Hoechst, highlighted nuclei in all the sections examined. This was a novel finding, as this method for staining nuclei within the skin has not previously been reported. However, the intensity of the blue was very similar to the green of F-Bleosome (NDD

R4), and hence, we set the "blue" colour of Hoechst as "magenta" (NDD R3) during image acquisition, to have a better contrast in the image analysis. In merged pictures, when the two colours (magenta and green) are overlapping in one object, this object appears white (see cellular nuclei in figure 3.15 (c)). Hoechst does not stain liposomal particles or bleomycin, therefore objects appearing green in the merged pictures are considered as F-bleomycin and F-Bleosome. Control samples show structures that appear fluorescent in the untreated skin, by subtracting the fluorescence of these structures to the overall fluorescence of the treated samples (showed as white in the merged images), what appears as "green fluorescence" in merged may be considered as F-bleomycin and F-Bleosome (figure 3.15 (f)).

To provide a better understanding of the method and the appearance of F-Bleosome molecule on MP images using this technique, as an example, representative images are shown as z-projections in figure 3.15. Z –projections are images in which data from three dimensions are collapsed into two, putting all the pixel into a two-dimensional stack, that have the same x and y coordinate.

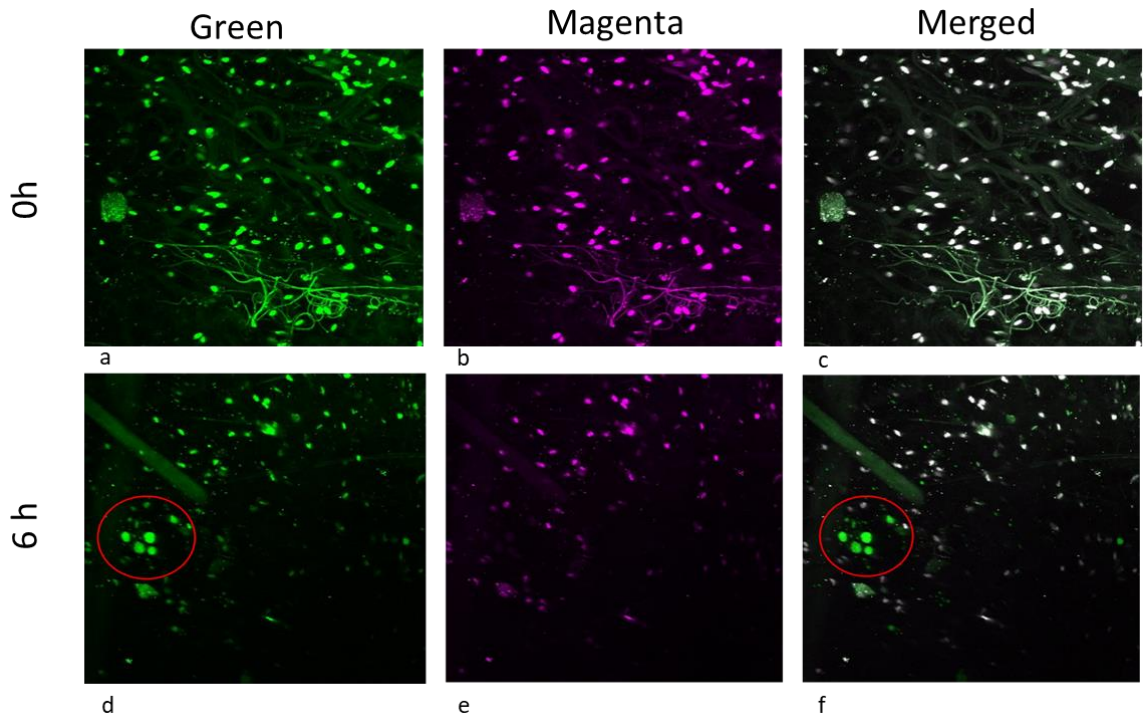

Figure 3.15 *Appearance of F-Bleosome particles with the MP images. Canine skin samples were treated with Blosome for 0h and 6h. (a - c) 0h line shows z-projections of the control (untreated skin section) in two different channels: the green channel (a); the magenta channel (Hoechst) (b) ; merged magenta + green channels (c). (d - f) 6h line shows z-projections corresponding to 6 h of Bleosome treatment in two different channels: the green channel (d); the magenta channel (Hoechst)(e) ; merged magenta + green channels (f).*

Three different areas of each sample were captured. All the images were analysed using Imaris. This software allowed us to visualize the skin section in 3-D and to inspect it from all possible perspectives. In figures 3.16 and 3.17 two sides of the 3-D skin sections of one representative image for each time point, plus the control, are shown.

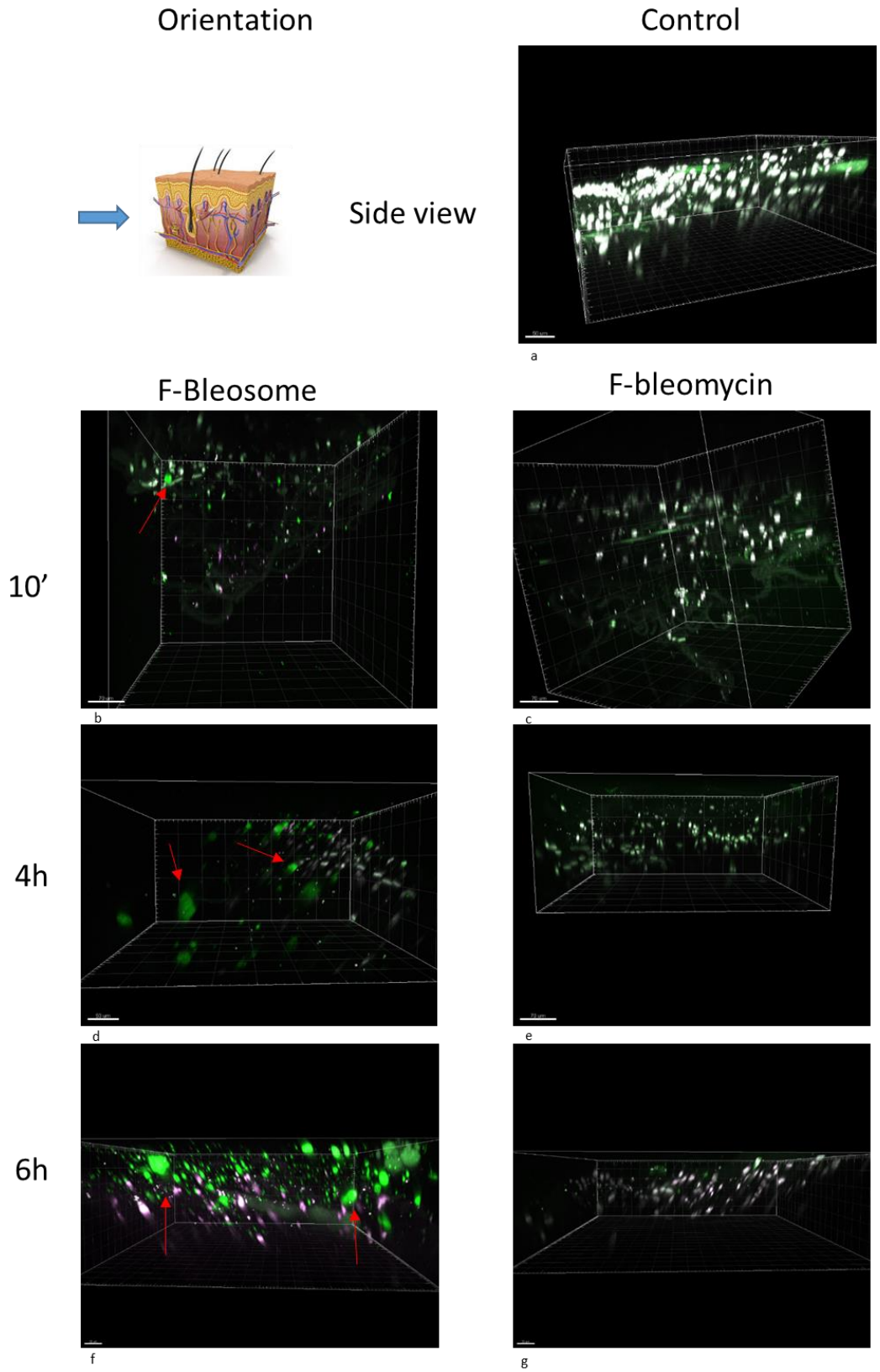

***Figure** 3.16 Side views of 3-D canine sections treated with F-Bleosome and F-bleomycin at each time point. (a) is the image of the control (untreated skin section); (b), (d) and (f) correspond to the 3-D images of the skin sections treated with F-Bleosome after 10’, 4 h and 6 h. Representative F-Bleosome molecules are indicated by red arrows. (c), (e) and (g) correspond to the side view of the 3-D sections after 10’, 4h and 6h of F-bleomycin treatment.*

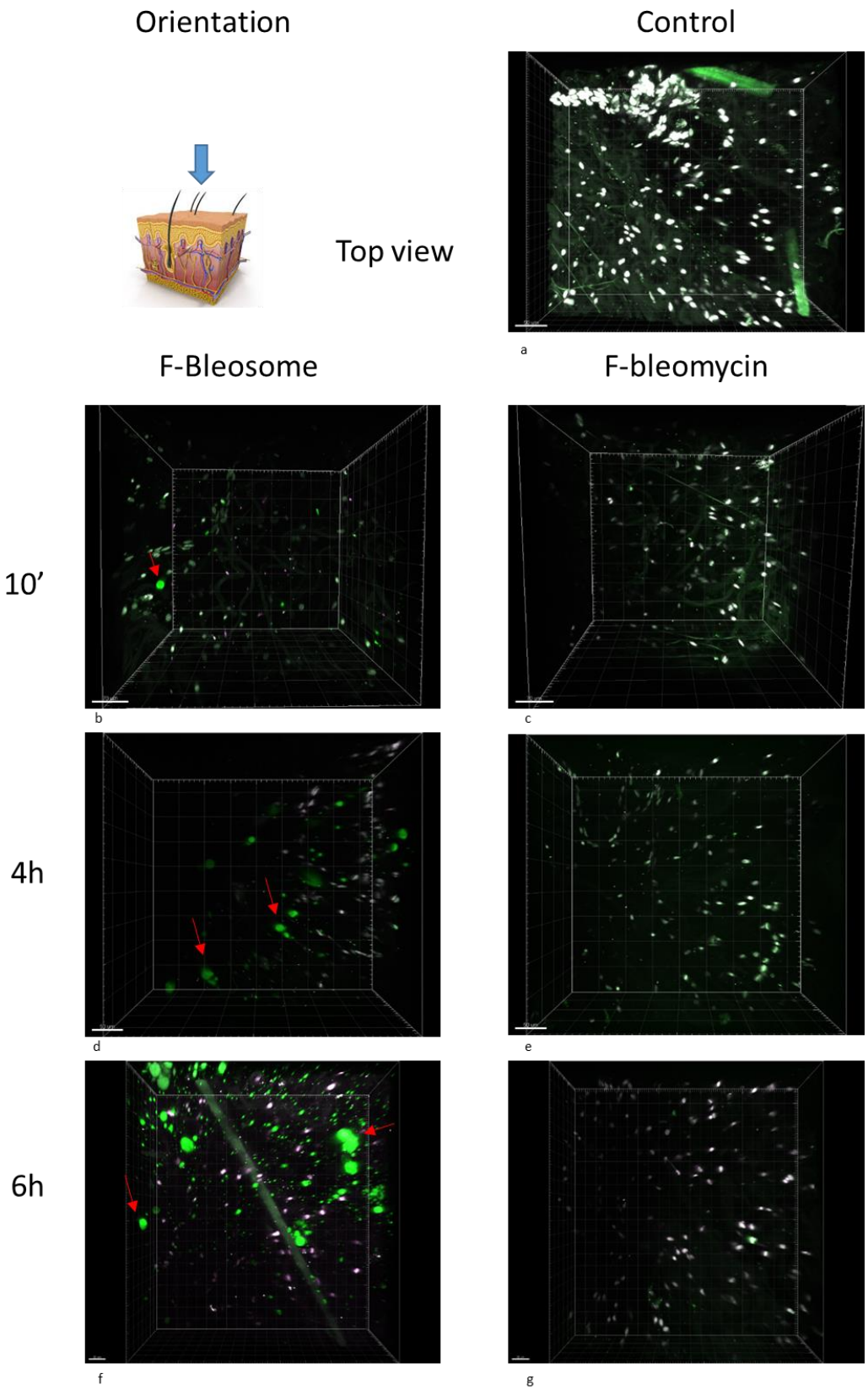

Figure 3.17 *Top view of the same 3-D canine sections treated with F-Bleosome and F-bleomycin showed in figure 3.16. (a) is the image of the control (untreated skin section); (b), (d) and (e) correspond to the 3-D images of the skin sections treated with F-Bleosome after 10', 4 h and 6 h. Representative F-Bleosome molecules are indicated by red arrows. (c), (e) and (g) correspond to the side view of the 3-D sections after 10', 4 and 6 h of F-bleomycin treatment.*

The untreated skin section did not show any distinct green particles, but displayed a high level of autofluorescence due mainly to cutaneous structures, such as the collagen associated with the extracellular matrix and the vascular wall, cellular nuclei and the hair follicles. These structures were also stained to some extent by Hoechst, and in the merged channel are shown as white (figues 3.16 and 3.17 (a)), whereas F-Bleosome and F-bleomycin molecules appear green in the merged picture (figures 3.16 and 3.17 (b); (d);(f)). Images in figures 3.16 and 3.17 show that the untreated section did not show any solid green fluorescent structures using this method, while in the skin sections treated with F- Bleosome, the presence of round green fluorescent particles is evident. These particles correspond to the fluorescently labelled bleomycin encapsulated in UD liposomes, and their presence can be detected at the earliest time point post-treatment. After 10 min, the F-Bleosome particles are located at a very superficial level through the skin explant, and have a defined small, round shape. However, over increasing time of treatment, F-Bleosome particles can be found at deeper levels through the skin section, at a higher overall number and also their dimensions appeared to increase compared to the early stage of the treatment with a less defined spheroid shape. As a comparison, we also treated additional skin sections in the same manner, with F-free bleomycin. Interestingly, F-bleomycin is rarely detected throughout the skin sections and when detected the particles are smaller in size compared to the same time-point of F-Bleosome treatment. Moreover, the number and the depth of F-bleomcyin particles does not seems to be affected by increasing the length of treatment.

All the images were analysed with Imaris software to quantify the data. However, Imaris is limited as it does not automatically subtract the objects expressing both magenta (Hoechst) and green from those that are generating only the green signal; hence, we have used an alternative system to identify the fluorescent drugs within the skin as detailed in 3.3.5.4. Figures 3.18 and 3.19 represent images after the Imaris software analysis: “surfaces” are yellow objects; while “spots” are oval objects. “Spots far from surfaces” (green spots in figures 3.18 and 3.19) are considered as F-Bleosome and F-bleomycin particles, and the “spots close to surfaces” (pink spots in figures 3.18 and figure 3.19) are recognised by the software as the cellular nuclei or other very bright skin structures. This system permitted us to identify a majority of F-bleomycin and F-Bleosome particles within the examined skin section. However, a limitation of

this method is that particles of drug located close to the autofluorescent skin structures are missed, thus producing an underestimation of the overall number of F-Bleosome molecules.

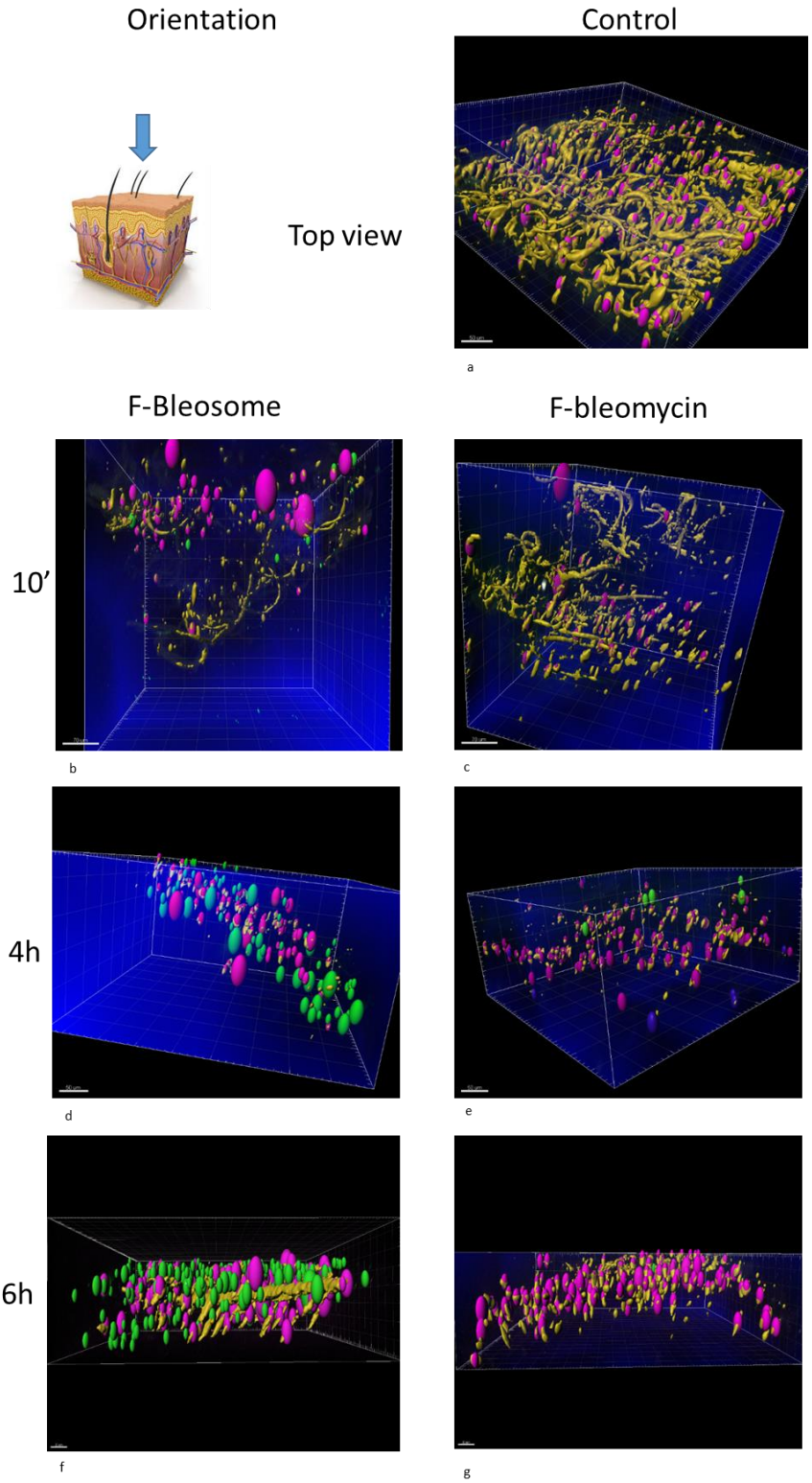

Figure 3.18 *Side view of the images shown in figure 3.16 following Imaris analysis. Yellow objects are "surfaces", corresponding to skin appendages stained with Hoechst and/or expressing a low level of green signal, oval objects are "spots", corresponding to the green-emitting structures (drug molecules) and the most autofluorescent skin structures stained also with Hoechst (cellular nuclei). After distance transformation, the pink spots are "spots close to surfaces" corresponding to cellular nuclei and green spots are "spots far from surfaces" corresponding to drug molecules. (a) Side view of the control, (b) analysis of skin section after 10' of F-Bleosome treatment, (c) 10' after F-bleomycin treatment, (d) the 4 h F-Bleosome treatment and (e) 4h F-bleomycin treatment,(f) 6h F-Bleosome treatment and (g) 6h F-bleomycin treatment.*

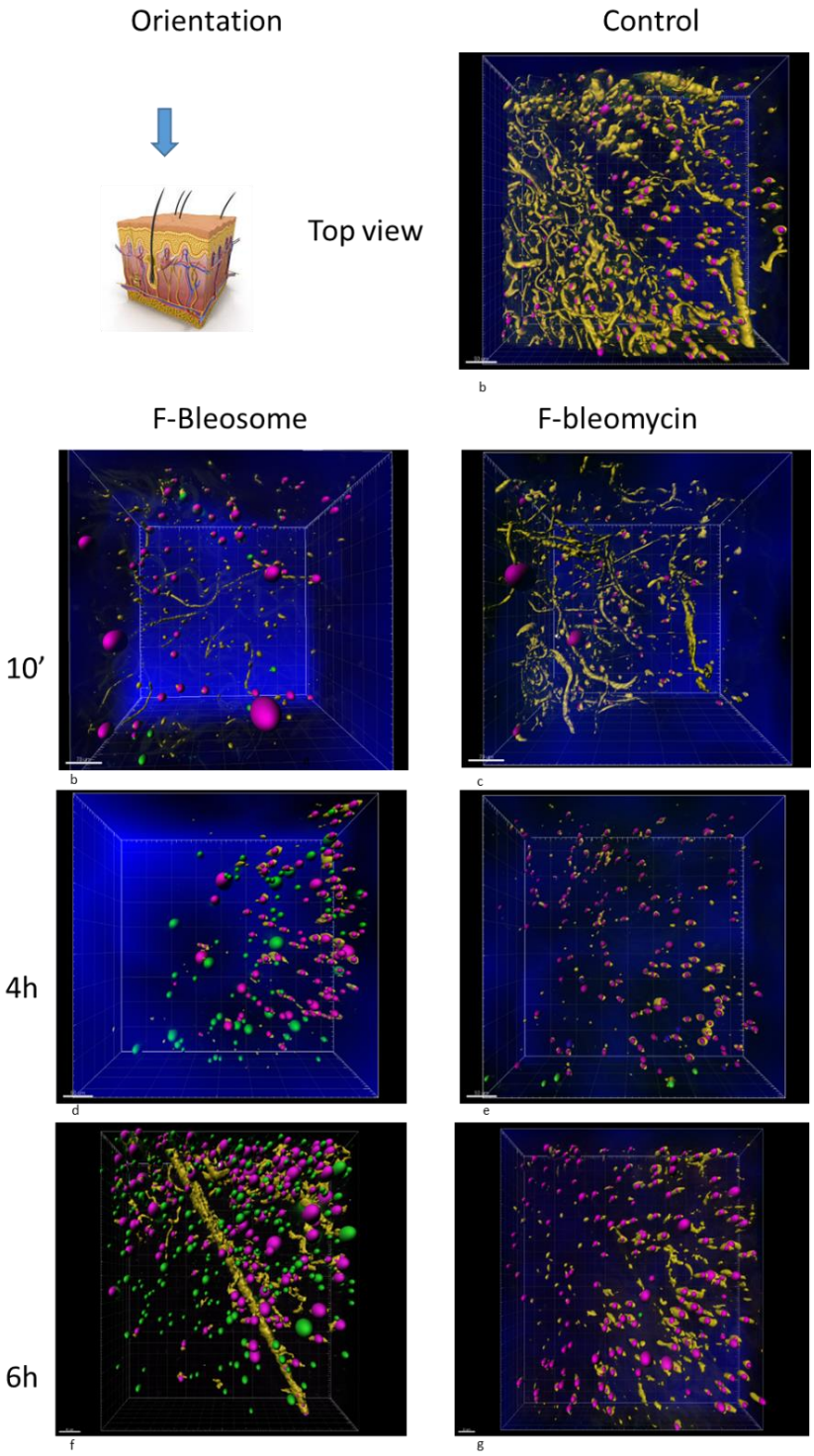

Figure 3.19 *Top view of the images shown in figure 3.17 after the Imaris analysis. Yellow objects are "surfaces", corresponding to skin appendages stained with Hoechst and/or expressing a low level of green signal, oval objects are "spots", corresponding to the green-emitting structures (drug molecules) and the most autofluorescent skin structures stained also with Hoechst (cellular nuclei). After distance transformation, the pink spots are "spots close to surfaces" corresponding to cellular nuclei and green spots are "spots far from surfaces" corresponding to drug molecules. (a) Top view of the control, (b) analysis of skin section after 10' of F-Bleosome treatment, (c) 10' after F-bleomycin treatment, (d) the 4 h F-Bleosome treatment and (e) 4h F-bleomycin treatment,(f) 6h F-Bleosome treatment and (g) 6h F-bleomycin treatment.*

The images analysed with Imaris generated data that weresstatistically analysed. The untreated skin section did not show any particles expressing the green signal alone, thus not producing any "spots far from surfaces"; all skin sections treated with F-Bleosome contained particles of drug, and they were always present in a greater number compared to the sections treated with F-bleomycin, as shown in table 3.1.

Time point	Treatment	N of particles	Treatment	N of particles
10'	f-Bleosome	17	f-Bleomycin	3
10'	f-Bleosome	68	f-Bleomycin	2
10	f-Bleosome	30	f-Bleomycin	0
4h	f-Bleosome	49	f-Bleomycin	0
4h	f-Bleosome	38	f-Bleomycin	3
4h	f-Bleosome	68	f-Bleomycin	5
6h	f-Bleosome	220	f-Bleomycin	0
6h	f-Bleosome	202	f-Bleomycin	2
6h	f-Bleosome	124	f-Bleomycin	3

Pearson Chi-Square = 12.211, DF = 2, P-Value = 0.002

Table 3.1 *Number of particles of drug detected within canine skin sections treated with F-Bleosome and F-bleomycin after 10', 4h and 6h. Overall number of drug particles detected between the two treatments were significantly different according to Pearson Chi-Square test (p-value: 0.002).*

The Imaris software was able to accurately localise every detected particle within the 3-D section examined. However, it was not possible to obtain the same accuracy in the measurement of the volume and of the area of the particles: the program estimated only an overall mean of the dimension of all the objects detected within an image. This threshold is applied in a pre-set mode to all the particles without the option to adjust for individual particles. For this reason, statistical analysis was focused on the position of the drug molecules, specifically on the depth (z-axis) of the particles within the skin section. Data were analysed using the general linear model (GLM): two-way ANOVA and Fisher's *post-hoc* test. Considering the location of every single particle of drug detected at every time point, the F-Bleosome molecules were found overall in a deeper position than the F-bleomycin ones. Significantly, we found that the depth of F-

bleomycin particles was unchanged over time (between 10 min and 6 h, p-value: 0.1) whereas the F-Bleosome particles penetrated deeper through the skin over time (p-value <0.001).

The two treatments were also compared at each time point, and F-Bleosome molecules were found at a significant deeper position within the skin than the free F-bleomycin after 4 and 6 h, while, after the 10 min of drug administration, both the entrapped and free bleomycin, were found at a similar superficial level within the skin (figure 3.20). Looking at the deepest position at which F-Bleosome molecule was found after 6 h, it was at approximately 800 µm and at more than 300 µm after 4 h of treatment, while the deepest particle of the free form of fluorescent bleomycin reached a depth of approximately 150 and 250 µm after 4 and 6 h of treatment, respectively.

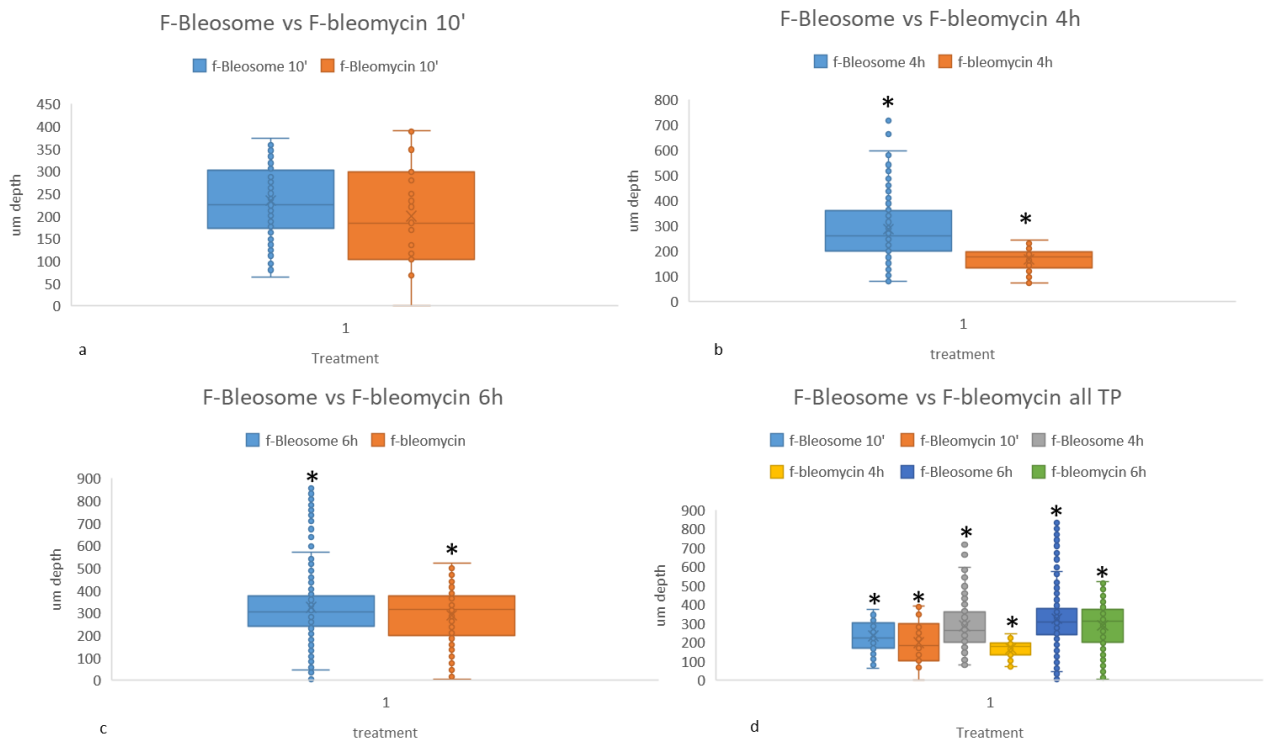

Figure 3.20 *Box plots comparing the depth of the drug molecules through the canine skin sections treated with F-Bleosome and F-bleomycin at each time point. (a) represents the different depth in µm of drug molecules in the skin sections treated with F-Bleosome (blue plot) and F-bleomycin (orange plot) after 10'. (b) Represents the different depth in µm of drug molecules in the skin sections treated with F-Bleosome (blue plot) and F-bleomycin (orange plot) after 4h and (c) represents the depth in µm of drug molecules in the skin sections treated with F-Bleosome (blue plot) and F-bleomycin (orange plot) after 6h. (d) compares the three time points. * indicates statistically significant difference (p-value <0.05, two-way ANOVA).*

3.4.5.2 Equine skin

The penetration study using equine skin sections was performed following the same procedure as used for the canine skin.

Skin explants were treated as previously explained and visualised by MP using the same microscope settings utilised for the visualisation of canine skin.

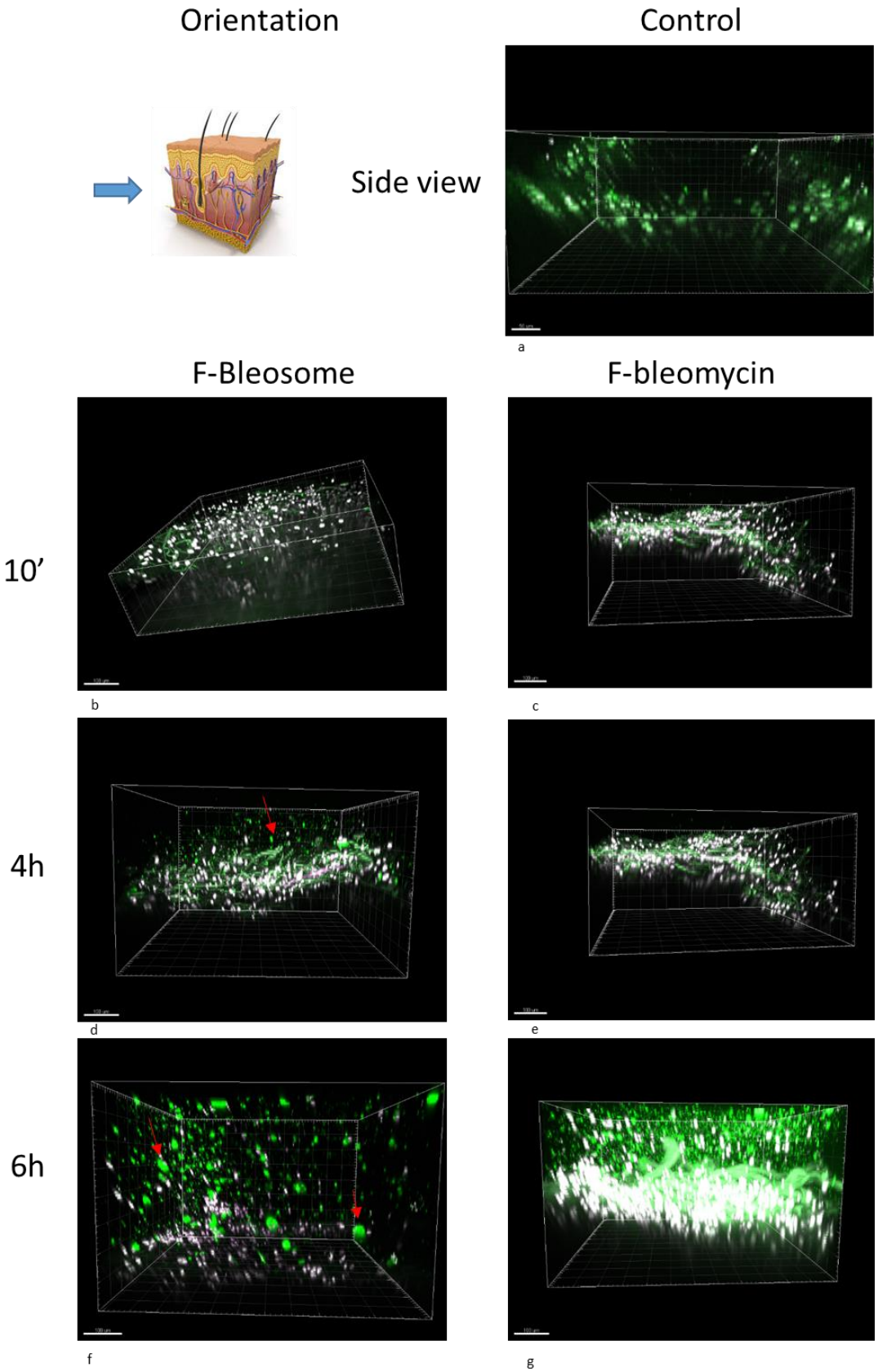

Figure 3.21 *Side view of 3-D equine sections treated with F-Bleosome and F-bleomycin at each time point. (a) is the image of the control (untreated skin section);(b), (d) and (f) correspond to the 3-D images of the skin sections treated with F-Bleosome after 10’, 4 h and 6 h. Representative F-Bleosome molecules are indicated by red arrows. (c), (e) and (g) correspond to the side view of the 3-D sections after 10’, 4 and 6 h of F-bleomycin treatment. Few particles of drug can be observed.*

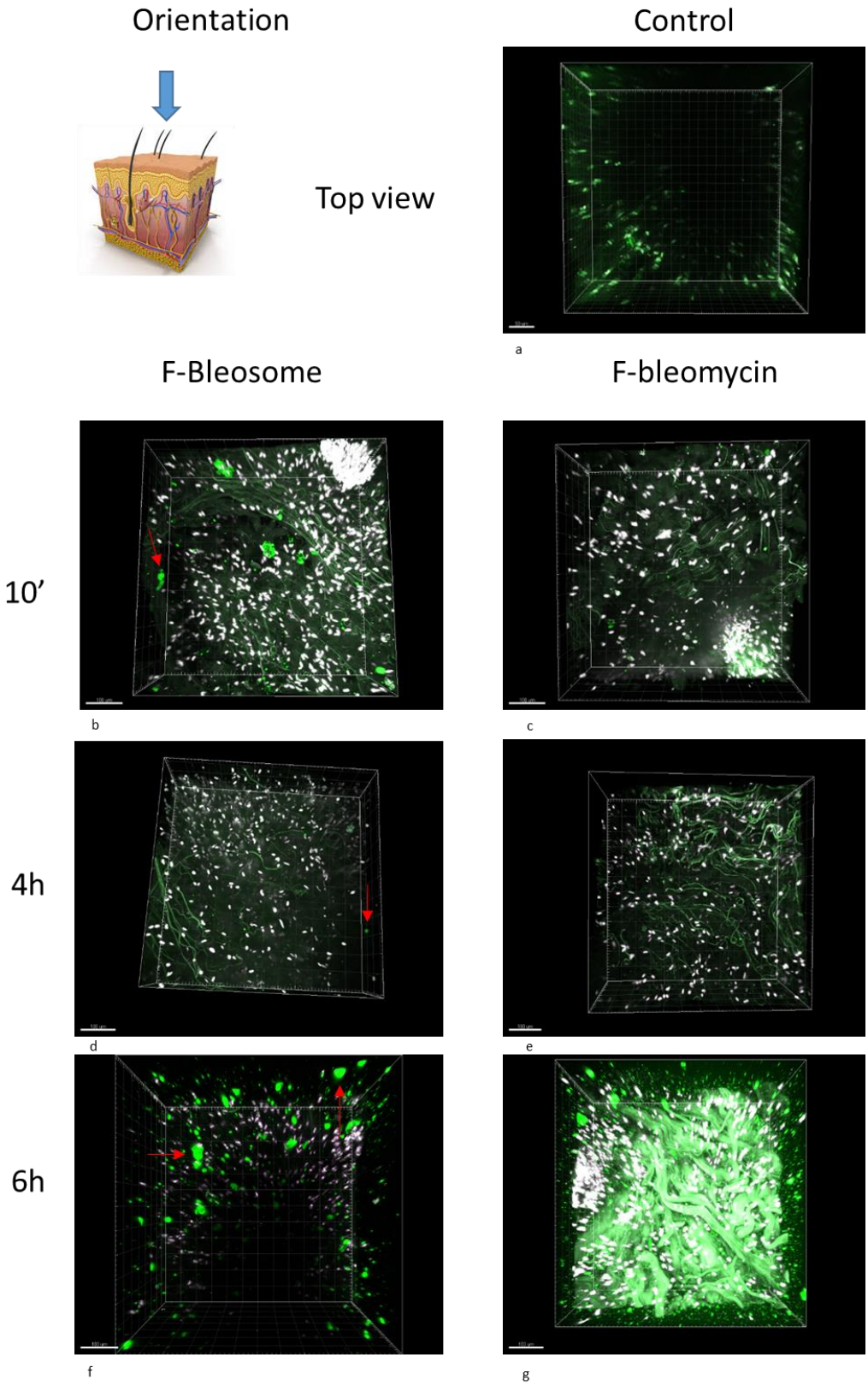

Figure 3.22 *Top view of the same 3-D equine sections treated with F-Bleosome and F-bleomycin of figure 3.21. (a) is the image of the control (untreated skin section);(b), (d) and (f) correspond to the 3-D images of the skin sections treated with F-Bleosome after 10', 4 h and 6 h. Representative F-Bleosome molecules are indicated by red arrows. (c), (e) and (g) correspond to the side view of the 3-D sections after 10', 4 and 6 h of F-bleomycin treatment. Few particles of drug can be observed.*

These images (figures 3.21 and 3.22) compare the penetration through equine skin F-Bleosome and F-bleomycin, according to the length of time of treatment. The results obtained from the skin penetration study using equine skin are comparable to the canine skin: the overall number of F-Bleosome particles was higher than the F-bleomycin at every time point, as well as their rate of penetration through the skin. Once again, in the F-bleomycin treatment, at 10 min, the drug particles are not as evident as the F-Bleosome ones. However, at the 6 h time point, the skin section treated with the free fluorescent drug here (figures 3.21 and 3.22(g)), showed a very high level of green background autofluorescence, and, without software analysis, F-Bleosome particles are more clearly visible compared to the canine skin treated for the same amount of time with free F-bleomycin.

Captured images were analysed by Imaris as previously described. An example of the distribution of green spots (F-Bleosome and F-bleomycin molecules) at indicated time points, as analysed by the software, is shown (figures 3.23 and 3.24).

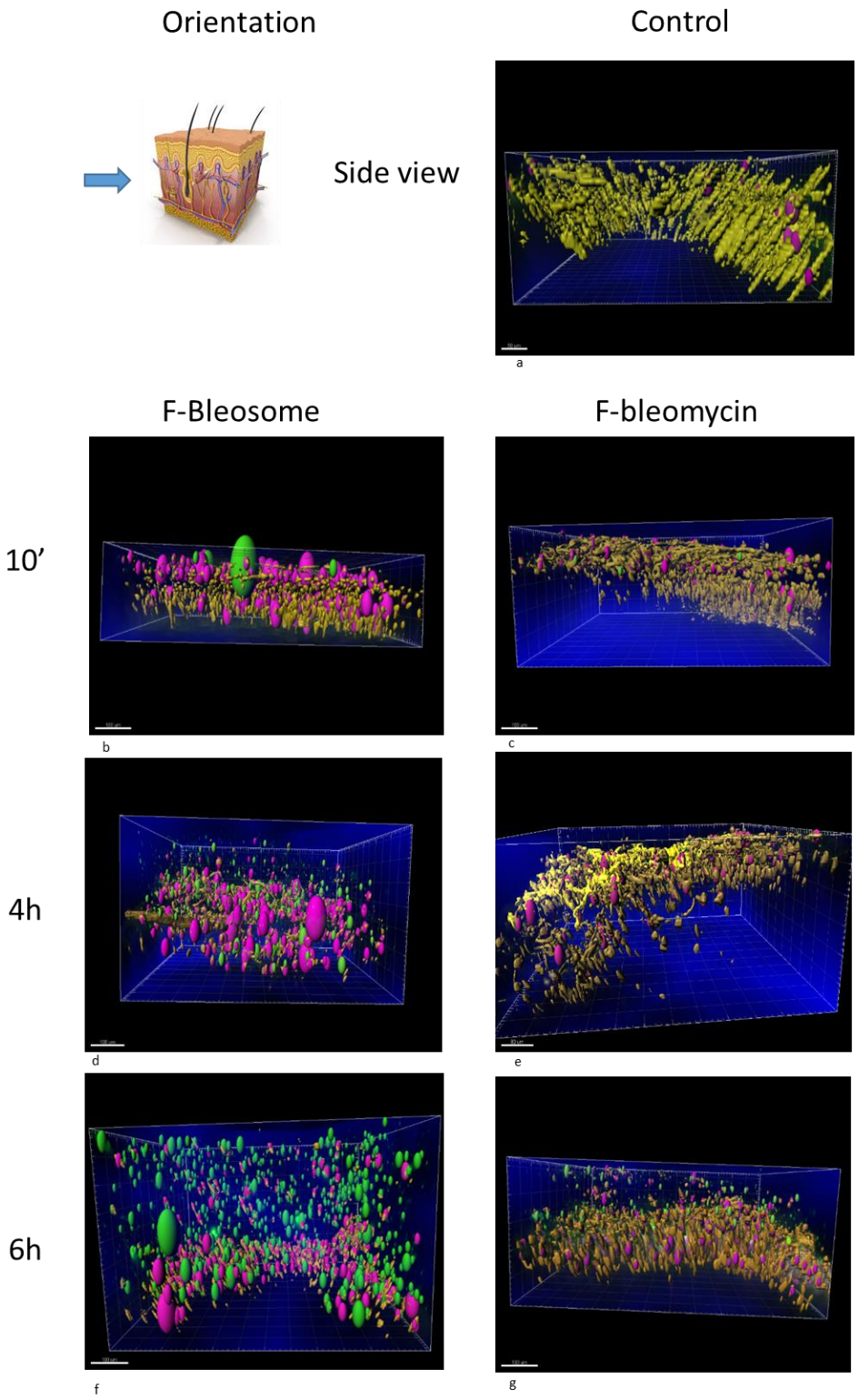

Figure 3.23 *Side view of the images shown in figure 3.21 following Imaris analysis. Yellow objects are "surfaces", corresponding to skin appendages stained with Hoechst and/or expressing a low level of green signal, oval objects are "spots", corresponding to the green-emitting structures (drug molecules) and the most autofluorescent skin structures stained also with Hoechst (cellular nuclei). After distance transformation, the pink spots are "spots close to surfaces" corresponding to cellular nuclei and green spots are "spots far from surfaces" corresponding to drug molecules. (a) Side view of the control, (b) analysis of skin section after 10' of F-Bleosome treatment, (c) 10' after F-bleomycin treatment, (d) the 4 h F-Bleosome treatment and (e) 4h F-bleomycin treatment,(f) 6h F-Bleosome treatment and (g) 6h F-bleomycin treatment.*

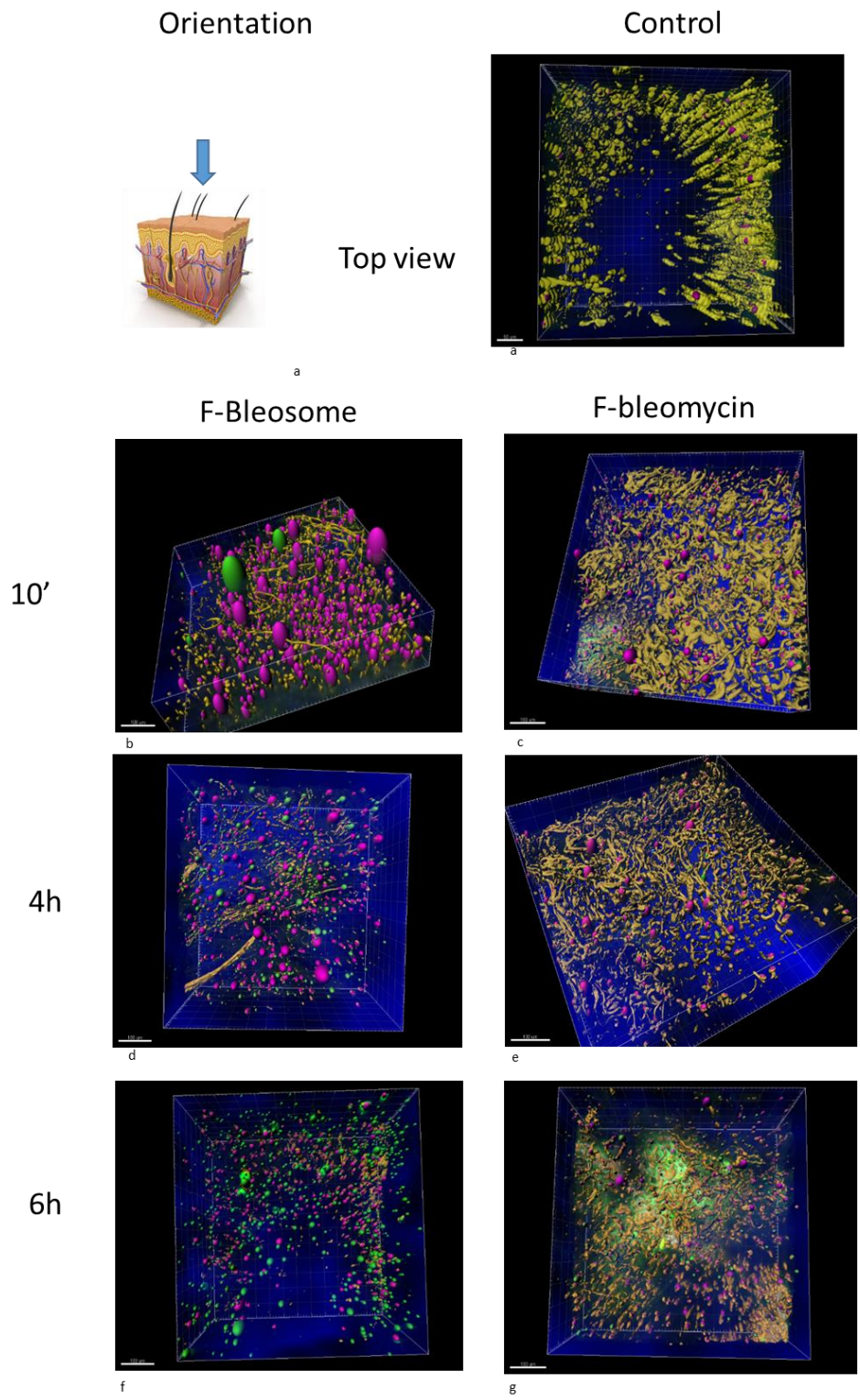

Figure 3.24 *Top view of the images shown in figure 3.22 after the Imaris analysis. Yellow objects are "surfaces", corresponding to skin appendages stained with Hoechst and/or expressing a low level of green signal, oval objects are "spots", corresponding to the green-emitting structures (drug molecules) and the most autofluorescent skin structures stained also with Hoechst (cellular nuclei). After distance transformation, the pink spots are "spots close to surfaces" corresponding to cellular nuclei and green spots are "spots far from surfaces" corresponding to drug molecules. (a) Side view of the control, (b) analysis of skin section after 10' of F-Bleosome treatment, (c) 10' after F-bleomycin treatment, (d) the 4 h F-Bleosome treatment and (e) 4h F-bleomycin treatment,(f) 6h F-Bleosome treatment and (g) 6h F-bleomycin treatment.*

Data gained from the image analysis supported our previous results in canine skin and revealed that the overall number of drug molecules was higher at every time point in the F-Bleosome-treated skin sections compared to those treated with the free F-bleomycin (table 3.2).

Time point	Treatment	N of particles	Treatment	N of particles
10’	f-Bleosome	5	f-Bleomycin	4
10’	f-Bleosome	87	f-Bleomycin	0
10	f-Bleosome	265	f-Bleomycin	7
4h	f-Bleosome	47	f-Bleomycin	77
4h	f-Bleosome	49	f-Bleomycin	14
4h	f-Bleosome	306	f-Bleomycin	19
6h	f-Bleosome	554	f-Bleomycin	70
6h	f-Bleosome	554	f-Bleomycin	157
6h	f-Bleosome	375	f-Bleomycin	567

Pearson Chi-Square = 173.136, DF = 2, P-Value = 0.000

Table 3.2 *Number of particles of drug detected within equine skin sections treated with F-Bleosome and F-bleomycin after 10’, 4h and 6h. Overall number of drug particles detected between the two treatments were significantly different according to Pearson Chi-Square test (p-value≤0.000).*

Statistical analysis was conducted on the z-position (depth) of particles of drug in all the skin sections (GLM: two-way ANOVA, Fisher’s *post hoc* test). Results were comparabe to the canine study. Position of F-Bleosome molecules was found to be significantly deeper and proportional to the length of treatment (10’ vs 4 h vs 6 h, p-value ≤0.000) compared to the F-bleomycin. Furthermore, comparing the position of all the particles of the drug detected, there was a statistically significant difference between the two treatments: F-Bleosome penetrated significantly deeper the F-bleomycin at 4h and 6h treament (p-value<0.001). However, there was no significant

difference after 10 min of treatment (figure 3.25). At 4 h, the deepest F-Bleosome particle was found at 271 µm of depth, and at 430 µm after 6 h of treatment, while the deepest molecule of the unencapsulated counterpart, was found at 108 and 222 µm after 4 and 6 h of treatment respectively.

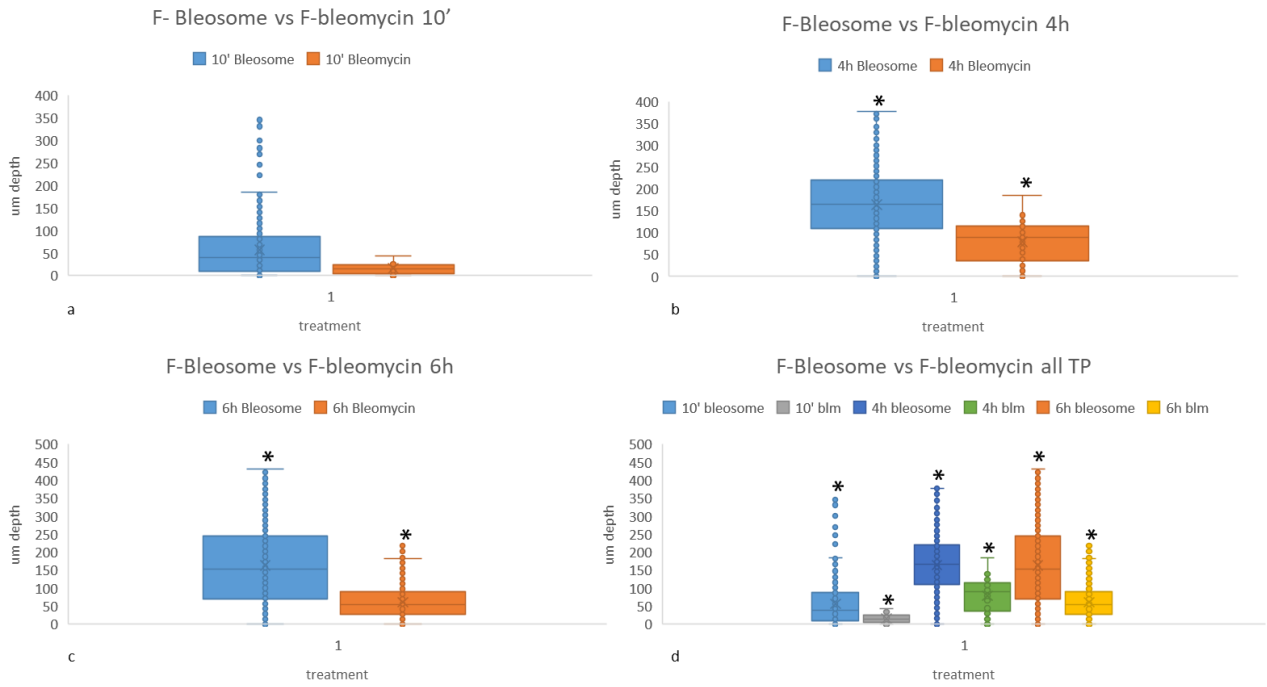

Figure 3.25 *Box plots comparing the depth of the drug molecules through the equine skin sections treated with F-Bleosome and F-bleomycin at each time point. (a) represents the different depth in µm of drug molecules in the skin sections treated with F-Bleosome (blue plot) and F-bleomycin (orange plot) after 10'. (b) Represents the different depth in µm of drug molecules in the skin sections treated with F-Bleosome (blue plot) and F-bleomycin (orange plot) after 4h and (c) represents the depth in µm of drug molecules in the skin sections treated with F-Bleosome (blue plot) and F-bleomycin (orange plot) after 6h. (d) compares the three time points. * indicates statistically significant difference (p-value <0.05, two-way ANOVA).*

3.4.5.3 Human skin

Human skin was kindly gifted to us by volunteers who agreed to take part in this study. To compare the penetration of Bleosome through human skin to our previous work in canine and equine skin we performed the skin penetration test on human samples following the same procedure and using same microscope settings as before. However, this experiment was only conducted once due to scarcity of human skin samples.

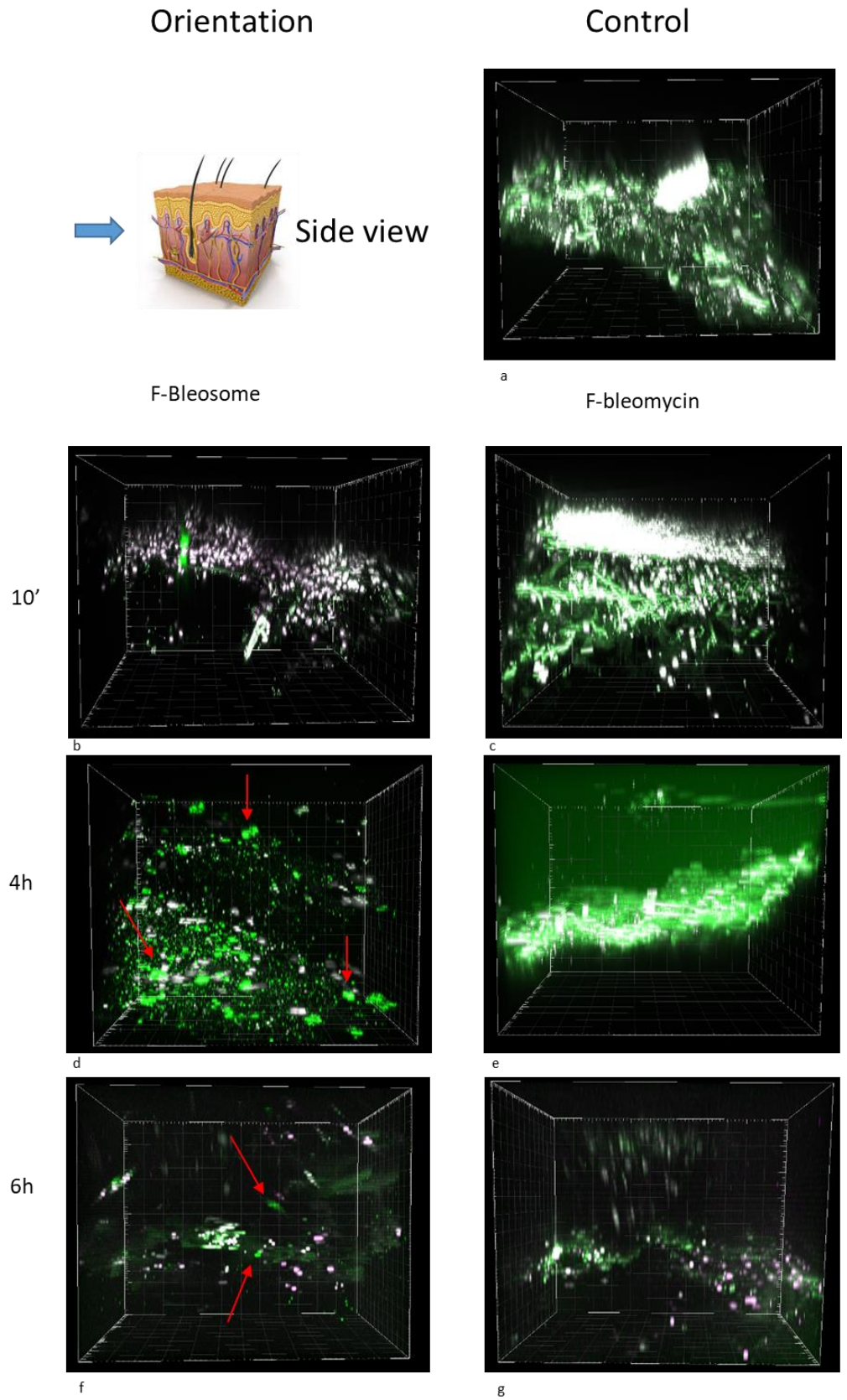

Figure 3.26 *Side view of 3-D human sections treated with F-Bleosome and F-bleomycin at each time point. (a) is the image of the control (untreated skin section);(b), (d) and (f) correspond to the 3-D images of the skin sections treated with F-Bleosome after 10', 4 h and 6 h. Representative F-Bleosome molecules are indicated by red arrows. (c), (e) and (g) correspond to the side view of the 3-D sections after 10', 4 and 6 h of F-bleomycin treatment.*

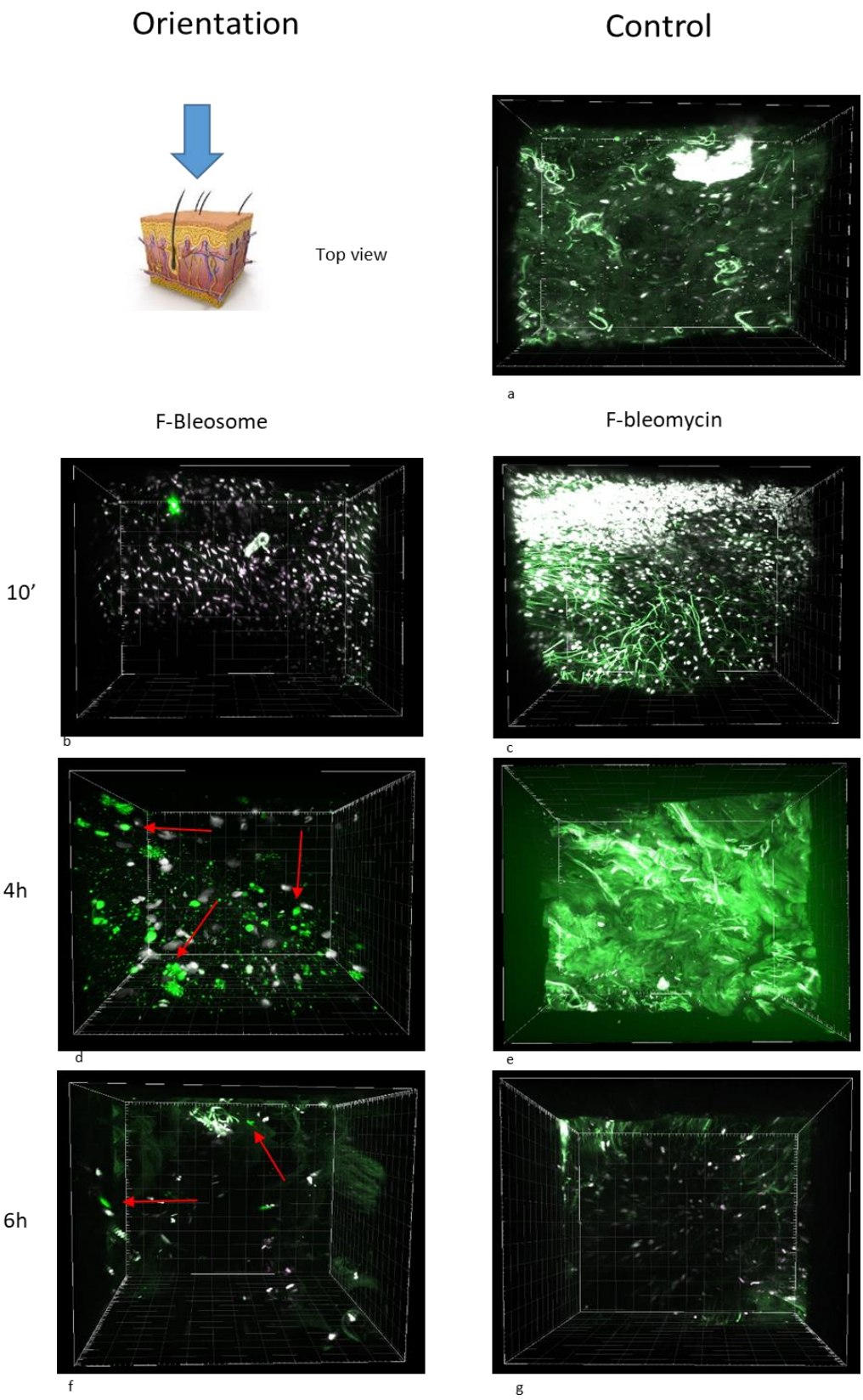

Figure 3.27 *Top view of the same 3-D human sections treated with F-Bleosome and F-bleomycin of figure 3.26. (a) is the image of the control (untreated skin section);(b), (d) and (f) correspond to the 3-D images of the skin sections treated with F-Bleosome after 10', 4 h and 6 h. Representative F-Bleosome molecules are indicated by red arrows. (c), (e) and (g) correspond to the side view of the 3-D sections after 10', 4 and 6 h of F-bleomycin treatment.*

As figures 3.26 and 3.27 show, after 10 min of treatment, particles of bleomycin from both compounds were not clearly detected, while, after 4 h, in the F-Bleosome treated section, several fluorescent molecules can be observed across the skin section (figures 3.26 and 3.27 (d)). Interestingly, at the same time point, in the sample treated with F-bleomycin, a stronger green background rather than proper fluorescent particles were observed (figures 3.26 and 3.27 (e)), and the intensity of the fluorescence was higher in the outermost layers of skin, without passing beyond the nuclear layer. After 6 h, fewer skin components were visible, resulting in ambigous images; this was probably due to photobleaching of the Hoechst staining over time. However, F-Bleosome particles can be still recognised in the deeper layers of the skin section (figures 3.26 and 3.27 (f)). Images were analysed with Imaris software as before.

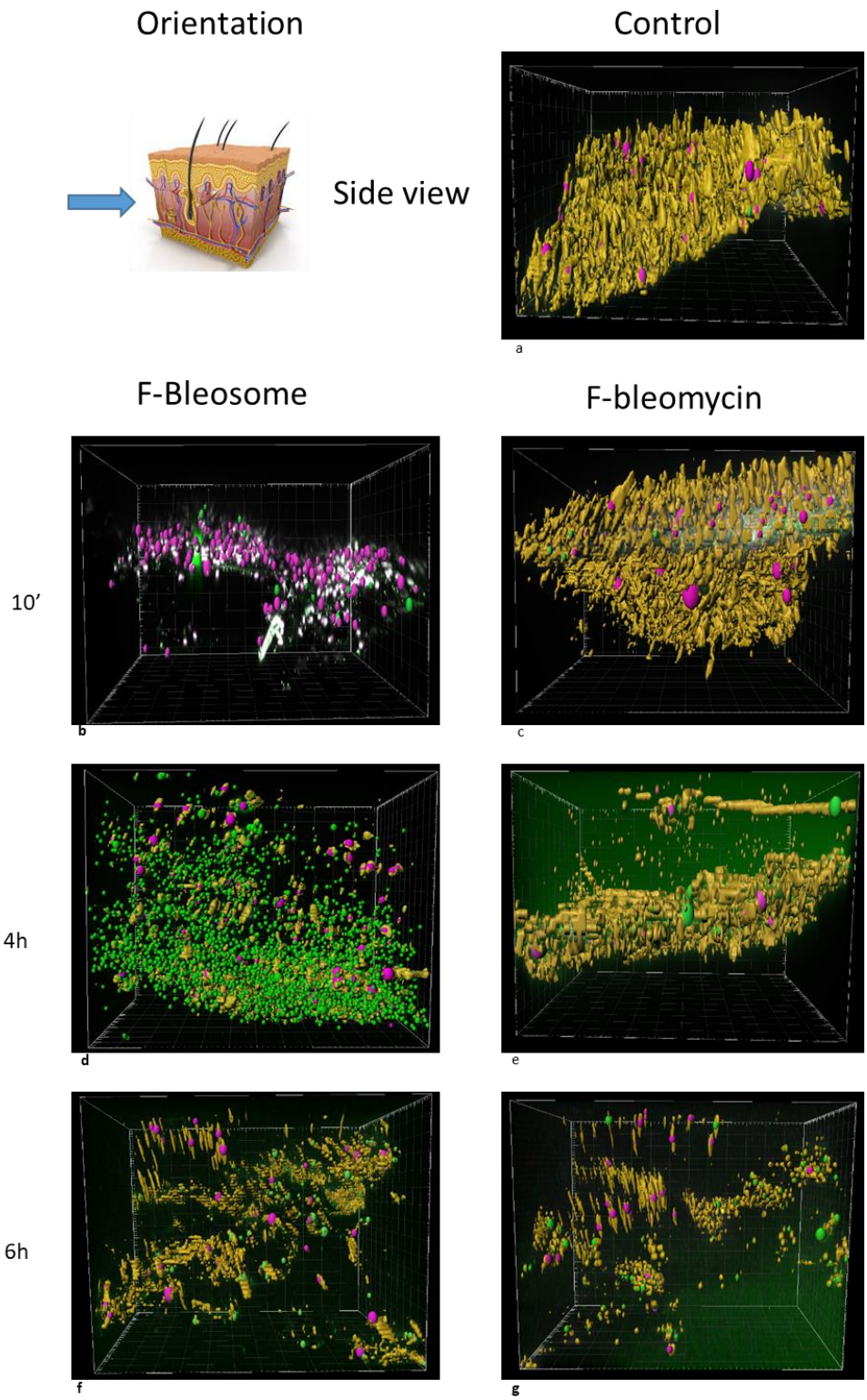

Figure 3.28 *Side view of the images shown in figure 3.26 following Imaris analysis. Yellow objects are "surfaces", corresponding to skin appendages stained with Hoechst and/or expressing a low level of green signal, oval objects are "spots", corresponding to the green-emitting structures (drug molecules) and the most autofluorescent skin structures stained also with Hoechst (cellular nuclei). After distance transformation, the pink spots are "spots close to surfaces" corresponding to cellular nuclei and green spots are "spots far from surfaces" corresponding to drug molecules. (a) Side view of the control, (b) analysis of skin section after 10' of F-Bleosome treatment, (c) 10' after F-bleomycin treatment, (d) the 4 h F-Bleosome treatment and (e) 4h F-bleomycin treatment,(f) 6h F-Bleosome treatment and (g) 6h F-bleomycin treatment..*

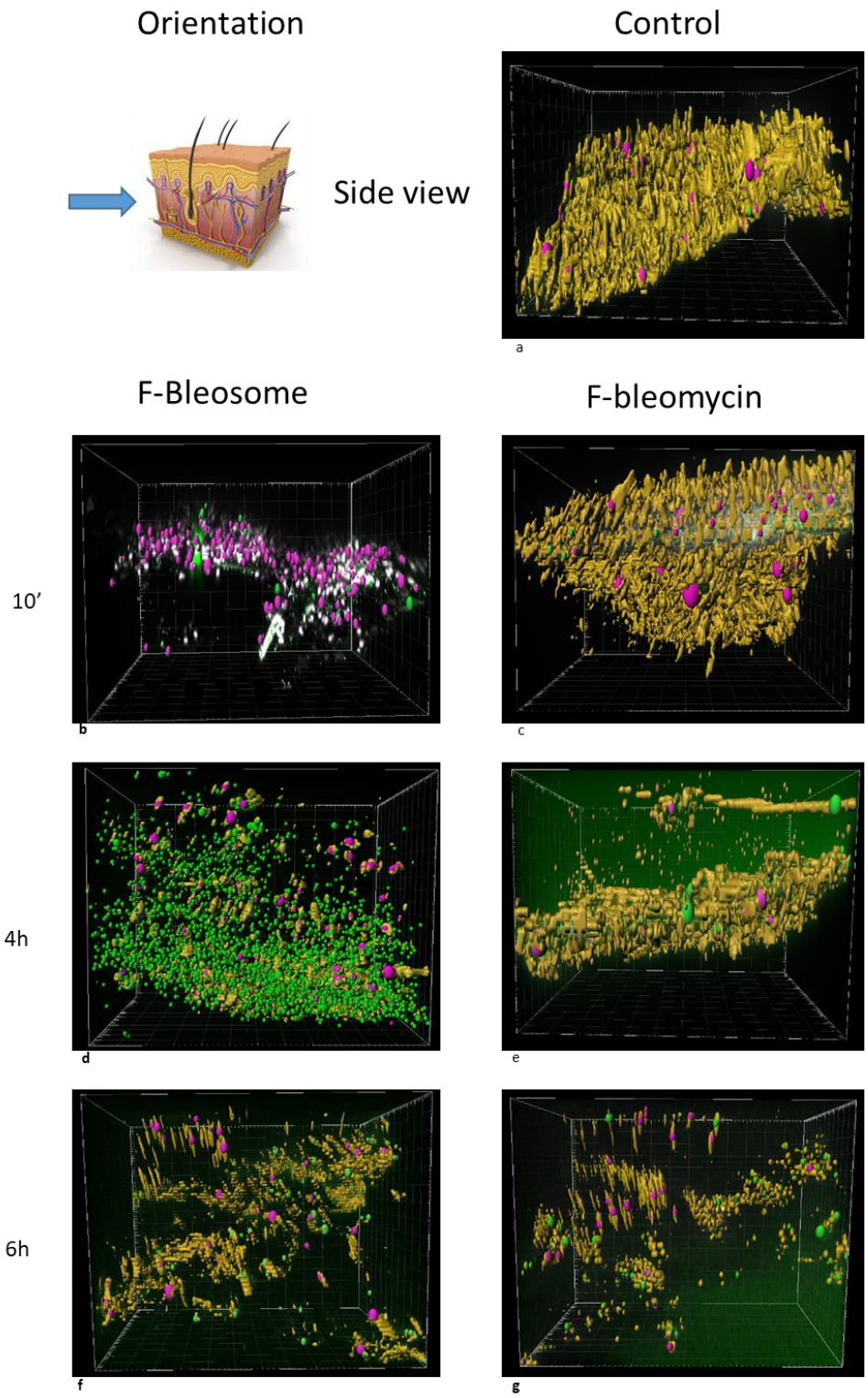

Figure 3.29 *Top view of the images shown in figure 3.27 after the Imaris analysis. Yellow objects are "surfaces", corresponding to skin appendages stained with Hoechst and/or expressing a low level of green signal, oval objects are "spots", corresponding to the green-emitting structures (drug molecules) and the most autofluorescent skin structures stained also with Hoechst (cellular nuclei). After distance transformation, the pink spots are "spots close to surfaces" corresponding to cellular nuclei and green spots are "spots far from surfaces" corresponding to drug molecules. (a) Side view of the control, (b) analysis of skin section after 10' of F-Bleosome treatment, (c) 10' after F-bleomycin treatment, (d) the 4 h F-Bleosome treatment and (e) 4h F-bleomycin treatment,(f) 6h F-Bleosome treatment and (g) 6h F-bleomycin treatment..*

We compared the z-position of F-Bleosome and F-bleomycin at each time point and confirmed that F-Bleosome can penetrate deeper through human skin, after 4 and 6 h of treatment, than free F-bleomycin. As previously reported in dogs and horses, after 10 min, both compounds appeared to be present at similar level in the outermost layers of the cutis (figure 3.30). Again, there was a significant difference in the rate of penetration of F-Bleosome through the skin compared to F-bleomycin (p-value ≤0.000) (GLM: two-way ANOVA, Fisher's *post hoc* test). In human skin, after 6 h, the deepest F-Bleosome particle was found at approximately 1 mm of depth, compared to F-bleomycin at 700 µm.

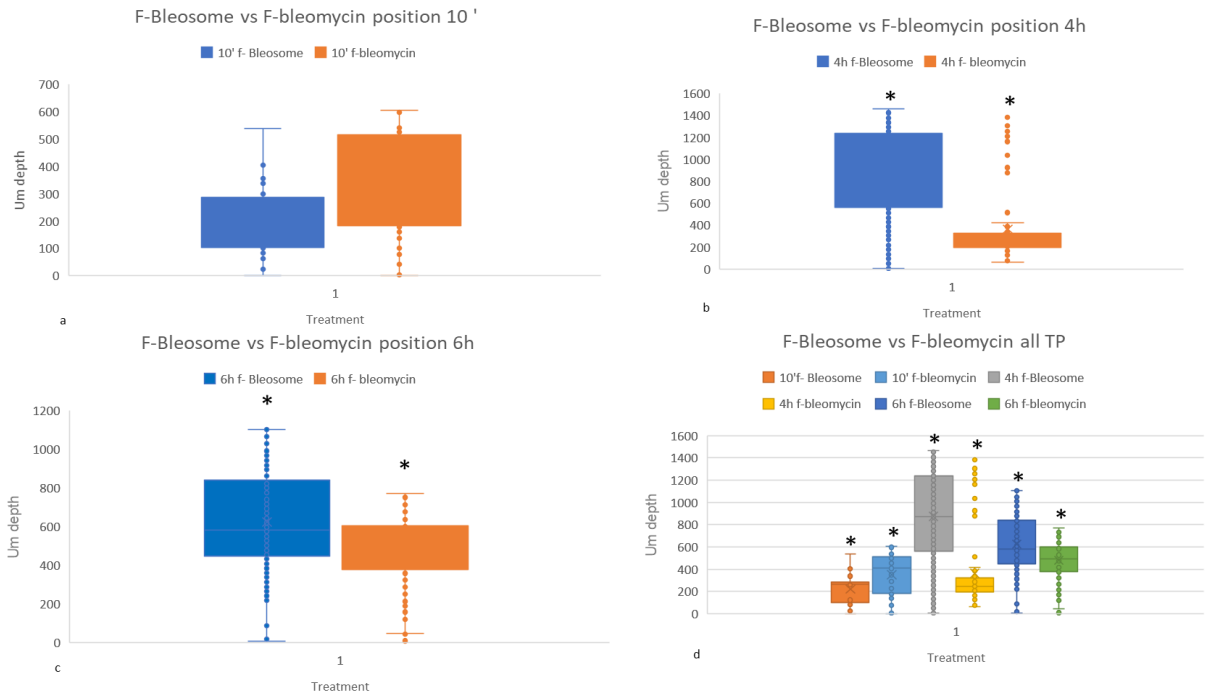

Figure 3.30 *Box plots comparing the depth of the drug molecules through the human skin sections treated with F-Bleosome and F-bleomycin at each time point. (a) represents the different depth in µm of drug molecules in the skin sections treated with F-Bleosome (blue plot) and F-bleomycin (orange plot) after 10'. (b) Represents the different depth in µm of drug molecules in the skin sections treated with F-Bleosome (blue plot) and F-bleomycin (orange plot) after 4h and (c) represents the depth in µm of drug molecules in the skin sections treated with F-Bleosome (blue plot) and F-bleomycin (orange plot) after 6h. (d) compares the three time points. * indicates statistically significant difference (p-value <0.05. two-way ANOVA)..*

3.5 Discussion

In this study, we optimised an imaging technique that enabled us to visualise both the UD liposomes and the entrapped bleomycin within layers of human and animal skin, after the Bleosome treatment. To this purpose, we took advantage of the TEM and the MP and we coupled the bleomcyin with the fluorophore Bodipy-FL to create a fluorescently labelled Bleosome and unencapsulated bleomycin, to the aim of visualising the drugs with the MP. The TEM visualisation revealed that the UD nanocarriers reside only within the outermost *stratum conreum* of the skin, after several length and modality of Bleosome treatment; while we obsverved a significantly improved penetration of the bleomycin, when encapsulated in UDs, within human and animal skin, compared to its free form. These results led us to conclude that UD liposomes enhance the transport of bleomycin through deep layers of animal and human skin. Furthermore, the double visualisation of liposomes and the entrapped drug through the skin allowed us to speculate that the nanocarriers might act as skin penetration enhncers, following the mechanism number 2 proposed by Verma et al (2003), when they transport bleomycin.

Several studies have reported that UD liposomes were able to penetrate through intact skin *in vivo*, transferring therapeutic amounts of drugs (Cevc and Blume 2001; Cevc and Blume 2003(A); Cevc and Blume 2004), including macromolecules, with efficiency comparable with subcutaneous administration (Paul, Cevc, and Bachhawat 1995; Cevc et al. 1998; Paul, Cevc, and Bachhawat 1995; Cevc and Gebauer 2003 (B)). Other *in vitro* skin permeation studies confirmed that deformable liposomes were able to improve skin delivery of various chemical entities. Although most of these results were indicative of improved transdermal delivery, *in vitro* transport rates were usually much lower than the exceptionally high transport rates reported *in vivo* (Elsayed et al. 2007). However, several comprehensive reviews suggest that there is still a scarcity of informative clinical data for the use of such carriers (Hussain et al. 2017). There are still many controversies regarding the actual mechanism of cutaneous penetration improvement of UD liposomes. Previous studies have investigated how UD vesicles could improve skin delivery of drugs and there are two main mechanisms proposed (Honeywell-Nguyen and Bouwstra 2003 (B)): the transappendageal and transepidermal pathways. The transappendageal routes are also known as the shunt

routes and include permeation through the sweat glands and across the hair follicles with their associated sebaceous glands (Honeywell-Nguyen and Bouwstra 2003 (B)). The transepidermal pathway can be defined as the pathway where compounds permeate across the intact, unbroken *stratum corneum*. This pathway contains two micropathways with two different mechanisms of skin penetration:

- Mechanism 1: The intercellular route, which is a continuous but tortuous way through the intercellular lipid domains (El Maghraby, Barry, and Williams 2008). Vesicles can act as drug carrier systems, whereby intact vesicles enter the *stratum corneum* carrying vesicle-bound drug molecules into the skin, passing through these tiny channels (Cevc, Schätzlein, and Richardsen 2002).

- Mechanism 2: The transcellular pathway through the keratinocytes, then across the intercellular lipids (Barry 1991). Here, vesicles can act as penetration enhancers, whereby vesicle bilayers enter the *stratum corneum* and subsequently modify the intercellular lipid lamellae. This will lead to the penetration of free drug molecules into and across the *stratum corneum* (Verma et al. 2003).

The first mechanism was put forward by Cevc et al. for deformable liposomes (G. Cevc and Blume 1992; Cevc, Schätzlein, and Richardsen 2002; Cevc and Blume 2001). They proposed that the driving force for the vesicles entering the skin is xerophobia (the tendency to avoid dry surroundings) (Cevc and Blume 1992). The important difference between deformable liposomes and traditional liposomes is the high and stress-dependent adaptability of such deformable vesicles, which enables them alone to squeeze between the cells in the *stratum corneum*, despite the large average vesicle size (Cevc, Schätzlein, and Richardsen 2002). Thus, they can trespass the intact skin spontaneously, under the influence of the naturally occurring *in vivo* transcutaneous hydration gradient (Cevc and Blume 2001), intact without permanent disintegration (Cevc, Schätzlein, and Richardsen 2002).

Several studies supported that deformable liposomes and surfactant-based elastic vesicles may act as carrier systems. In one study, pretreatment of skin membranes with empty deformable liposomes did not enhance oestradiol flux, while application of oestradiol entrapped in vesicles resulted in 14–17-fold increase in flux relative to control (El Maghraby, Williams, and Barry 1999). Interestingly, fluxes of oestradiol

from large and small vesicles were similar in this study, providing no evidence of intact vesicle penetration. Furthermore, (van den Bergh et al. 1999) showed that pre-treatment of hairless mouse skin with surfactant-based elastic vesicles increased the diffusion of $^{3}H_2O$ compared to pre-treatment with a buffer control, indicating a possible penetration enhancing mechanism. Based on results of previous studies, some authors support that both the intact vesicular permeation into the *stratum corneum* and the penetration enhancing effect play a role in the enhanced skin delivery of drugs by deformable liposomes under non-occlusive conditions, and suggest that one of the two mechanisms might predominate according to the physico-chemical properties of the drug. However, the rate and amount of released drug is a balance between two factors: (1) drug affinity to vesicles, and (2) drug solubility in lipids of the *stratum corneum* (Honeywell-Nguyen and Bouwstra 2003 (A)). As reported in a recent study, poor drug release resulted in retention of the drug within vesicles in the *stratum corneum* and elastic vesicles served as a slow release depot system (Honeywell-Nguyen and Bouwstra 2003 (A)). For hydrophilic drugs, such as bleomycin, the penetration enhancing effect seems to play a more important role in the enhanced skin delivery than in case of lipophilic drugs (as for many penetration enhancers), since permeation of hydrophilic molecules tends to be relatively slower and hence more enhanceable (Williams and Barry 1991). The intact vesicle penetration mechanism will also have an important role especially in improving skin deposition. However, as previously mentioned, drug release from vesicles in the *stratum corneum* is an important step that affects transdermal flux (Honeywell-Nguyen and Bouwstra 2003 (A)). For those reasons, the synergistic activity of liposomes and loaded drugs needs to be explored. In addition, research needs to be conducted to determine the final localisation of the entrapped drug after the skin penetration (Hussain et al. 2017). To the best of our knowledge, this is the first study to explore the mechanism of skin penetration of UD liposomes by direct visualisation of both the liposomal molecules and the entrapped drug through the skin using explants from dogs, horses and humans.

We initially attempted to visualise the penetration of Bleosome through the skin using fluorescent microscopy. Our collaborators (S. Chopra et al, unpublished) have previously shown in human skin explants the penetration of Bleosome over a time course (0 h – 6 h) using the intrinsic autofluorescence of Bleosome (Ranji et al. 2016). Their results showed a peak of overall fluorescence within the skin sections at 2 and 4

h, while the intensity of fluorescence decreased by 6 h, and they concluded that the peak of penetration of Bleosome is 2 - 4 h after the treatment. To reproduce these findings in animal skin, we conducted a similar experiment with canine skin excised from cadavers; however, the untreated (control) skin showed a high intrinsic autofluorescence (figure 3.5). Skin autofluorescence is a phenomenon likely due to flavoproteins (FAD) and NAD- related compounds, but also to elastin, collagen, and lipofuscin and redox state of the cells (Laiho et al. 2005). In our experiment, cryosectioned skin samples were evaluated, rather than formalin-fixed-paraffin-embedded (FFPE) tissues, as the latter are known to typically 'autofluoresce' when viewed under a fluorescent microscope (Laiho et al. 2005). However, even utilising the cryosectioning technique, the level of autofluorescence of canine skin was very high. To quench the autofluorescence we trialled multiple fixing techniques including pre-cooled acetone and organic solvents, and a quenching agent (TrueBlack®). However, the high autofluorescence of the skin was still higher than the intrinsic fluorescence of the drug (data not shown) and no significant difference was shown over the time course of treatment (figure 3.6). Interestingly, hair follicles appeared to be the most autofluorescent structures within the skin. One route by which liposome-encapsulated drugs are supposed to penetrate the skin is the transappendegeal mechanism (Scheuplein 1965), passing through the sweat glands and hair follicles. Thus, the high level of fluorescence emitted by those structure in the images of this study (figures 3.6), might be due to the passage of the Bleosome through these structures. However, it is important to note that in the untreated skin sections, hair follicles generated a level of green fluorescence, which is not significantly different from the green signal of the hair follicles in the treated skin.

To obtain more meaningful data and confirm that liposomal nanoparticles did not hindered the green fluorescence of the entrapped bleomycin, we compared the Bleosome treatment with other compounds containing free bleomycin without liposomes. Again, the results did not show a significant difference in the final emitted fluorescence between the control and all the time points of treatment (figure 3.7).

We therefore concluded that the penetration of the compound through the skin could not be observed by the intrinsic fluorescence of Bleosome.

Therefore, we aimed to explore the mechanism of skin penetration of Bleosome by visualising directly both the liposomes and the entrapped bleomycin. In order to

perform this study, TEM and MP were both used as complimentary techniques: the former allowed the direct visualisation of liposomes, the latter, the direct visualisation of encapsulated bleomycin particles within skin samples. Using TEM to compare untreated skin sections and skin sections treated with Bleosome at different time points, we found the presence of the UD nanoparticles through the *stratum corneum* in the treated samples only. The appearance of liposomes within skin layers in our images was consistent with the nanoparticles themselves visualised with TEM after sonication of Bleosome (figure 3.8) and with representative images in the literature (Subongkot et al. 2014; Rangsimawong et al. 2015). However, the quality of skin sections was variable: in the majority of the images, the layers of corneocytes were found detached from the underlying layers of the *stratum corneum* even in the untreated skin samples, which was considered during the evaluation of the rate of penetration over several time points. Similarly, Subongkot et al (2014) conducted a similar study on porcine skin and found that after the treatment with UD liposomal nanoparticles there was a detachment of the *stratum corneum*, while it was normal in untreated samples. Moreover, they observed that the broad shape and the fewer electron-dense keratin filaments of the corneocytes in the treated *stratum corneum* resulted from denaturation of keratin inside the corneocytes. The intercellular spaces of porcine skin treated with ULs were wider than those of intact skin, because the corneodesmosomes, that connected the corneocytes between each *stratum corneum* layer, were degraded. As a result of the degradation of corneodesmosomes, the *stratum corneum* layers of treated skin were detached (Subongkot et al. 2014). Observing our images, we could not reach the same conclusion, as the layers of the *stratum corneum* were found detached, in both treated and untreated skin sections, suggesting that this phenomenom could be due to slight damage of this outermost and fragile layer of the epidermis, during the sample processing. However, we do show that nanoparticles are able to penetrate through the *stratum corneum* and reside between corneocytes, but they could not be found deeper than this outermost layer, even after several hours of application of the compound (from 30 min to 8 h of treatment). The penetration experiment, using these experimental settings, was performed several times, and the resulting images were consistent, showing the presence of the liposomes in the *stratum corneum* only at every time point analysed. To explore the possibility that freezing procedures could affect the integrity of the *stratum corneum* by the formation of freezing crystals, we used ‘fresh’ skin samples, treated immediately after the

collection from cadavers, omitting the freeze storage and thawing of samples. The quality of 'fresh' skin sections was comparable to 'frozen skin' samples: all the layers of the skin could be visualised, there was still some degree of detachment of the keratinocyte layers, and the skin structures were recognisable. Moreover, UD liposomes within 'fresh' skin, after 2 and 4 h of treatment with Bleosome, resided in the outermost layers of the *stratum corneum*, and not deeper (data not shown), these results are in accordance with those using 'frozen' skin samples.

Our first penetration studies were based on a time course of administration of Bleosome, and demonstrated that the length of time of treatment did not affect the depth of penetration of liposomes through the skin. To explore the possibility that the quantity of compound played the main role in enhancing the penetration of liposomes deeper through the skin, we treated skin explants with repeated application of the compound every 60 min: applying from 0.1 ml to 0.4 ml of Bleosome per skin section. Again, we found that UDs were confined in the *stratum corneum* and were not in the deeper underlying cellular layers. This experiment was conducted multiple times, and we fully optimised the technique in terms of different length, quantity and modality of treatment; furthermore, each experiment was performed using skin explants derived from dogs of different breeds, sex and ages, and our results were always consistent. Therefore, we concluded that UD liposomes within Bleosome, are able to penetrate through the outermost layers of the skin, crossing and intercalating between the keratinocytes of the *stratum corneum*, but they cannot traverse beyond this layer. This finding is in accordance with a recent *in vivo* electron microscopy study, which demonstrated a fast (within 1 h of application) partitioning of intact surfactant-based elastic vesicles into the human *stratum corneum*, but no vesicles could be found in the deepest layers of the *stratum corneum* (Bouwstra et al. 2003). TEM and freeze-fracture electron microscopy demonstrated also major morphological changes in the intercellular lipid lamellar structure with no changes in the viable epidermis ultrastructure, after application of surfactant-based elastic vesicles (van den Bergh et al. 1999).

Given that our previous studies have highlighted that neither the autofluorescence of Bleosome or free bleomycin exceeds that of canine skin we determined that to effectively image the penetration through the skin of entrapped bleomycin molecules within UD liposomes we would need to effectively label Bleosome with a fluorescent

marker. In collaboration with Dr. Marc Vandrell's lab we successfully coupled bleomycin with Bodipy-FL prior to encapsulation within UD liposomes.

Bodipy was selected, from several different available dyes, as it is a relatively non-polar and non-charged chromophore. These properties tend to minimize dye-induced perturbation of the functional properties in the conjugate (Ulrich, Ziessel, and Harriman 2008). Bodipy dyes are therefore often the preferred choice for labelling nucleotides, amino acids and other low molecular weight ligands. In fact, the green-fluorescent Bodipy-FL fluorophore has several features that make it potentially superior to fluorescein in some applications (Strandberg et al. 1994). These include: high extinction coefficient and high fluorescence quantum yield; lack of ionic charge and a relative lack of sensitivity to solvent polarity and pH changes; narrow emission bandwidth resulting in a higher peak intensity than that of fluorescein; greater photostability than fluorescein in some environments and a large two-photon cross-section for multiphoton excitation (C. Xu et al. 1996). To the best of our knowledge, this is the first time that Bodipy-FL has been conjugated to bleomycin, and our main concern was that the reactive succinimidyl group of Bodipy-FL could have bound to all the three amine groups of the metal binding domain of the bleomycin molecule. The metal binding domain contains the ligands (nitrogen atoms) involved in octahedral complex formation with the transition metals. The N3- and N4-amino groups of the pyrimidine moiety of the metal binding domain of bleomycins are proposed to define the sequence specificity of DNA cleavage by binding to the N3- and N2-amino groups of the guanine 5' to the pyrimidine cleavage site. The pyrimidine moiety of bleomycin, interacting with the bithiazole tail, is responsible for DNA binding (Chen and Stubbe, 2005). Hence, during the coupling process, we wanted to prevent Bodipy-FL from binding to all the three amine groups of bleomycin, in order to avoid a diminished DNA binding and an overall decreased efficacy of the fluorescent compound. HPLC profile of the final labelled bleomycin confirmed that the fluorescent dye bound the bleomycin molecule on just one amine group. Moreover, cellular viability assays performed using two different canine cancer cell lines, confirmed that F-Bleosome is as cytotoxic as its unlabelled counterpart.

Confident in the functionality of F-Bleosome, we performed the last step of our study: the direct visualisation of the drug through skin explants of different species. Canine, equine and human skin sections were treated with fluorescently labelled Bleosome over a time course to assess the extent of penetration of bleomycin-encapsulated

liposomes within animal and human skin. Furthermore, we compared this innovative topical treatment with the standard unencapsulated bleomycin labelled with the same fluorophore. Our analysis showed that F-Bleosome penetrated significantly deeper through the skin than the free F-bleomycin, and that this was consistent for equine, canine and human skin sections. Furthermore, F-Bleosome penetrated significantly deeper through cutaneous layers with increasing time of treatment; indeed, after 4 and 6 h, the drug molecules were found at a significantly greater depth compared to the first 10 min of treatment in all the three species.

In all the three species examined, there was a significant difference in the position of F-Bleosome molecules within the skin at each time point of treatment, while this was not the case of the F-bleomycin particles, in which there was no significant difference in the position of the particles between 10 min, 4 h and 6 h of application. Interestingly, after the few min of treatment, the two compounds were found both in the superficial layers of the skin. However, after 4 and 6 h, F-Bleosome penetrated significantly deeper through skin compared to the free F-bleomycin. These findings indicate that the length of time of treatment is closely related to the ability of F-Bleosome in crossing several innermost cutaneous layers, rendering the time of treatment a crucial aspect to be considered when translating this therapy in the clinical application.

To confirm the superior ability of F-Bleosome in penetrating through the skin, the number of the Bleosome particles in canine and equine skin were analysed. We found significantly more drug molecules in skin sections, at each time point, treated with F-Bleosome compared to the free F-bleomycin, suggesting that liposomes are effective carriers for the passage of bleomycin through the skin.

The penetration experiment using human skin was conducted only once, and the number of particles of F-Bleosome and F-bleomcyin within skin was not analysed, as there was insufficient data to be statistically reliable. However, our initial results in human skin are comparable to those from canine and equine skin, indicating that F-Bleosome is more efficient at penetrating deeper into human skin that free F-bleomycin.

Our findings are compelling regarding the localisation of drug particles within the skin. Imaris calculated the position of the targeted drug particles in the canine skin treated with F-Bleosome: the maximum distance from the outermost cutaneous layer where the F-Bleosome molecule was found was ~300 μm after 4 h of treatment and

800 µm after 6 h. The canine skin sections used for this experiment were collected from the flank of canine cadavers. Theerawatanasirikul et al. (2012) found that the average thickness of the canine epidermis in this area is 40 µm, thus, F-Bleosome can cross the *stratum corneum* and penetrate deeper into the dermis, passing through the epidermis layers. In equine skin, after 4 h, the deepest Bleosome particle was found at 271 µm of depth and at 430 µm after 6 h of treatment. The skin sections used were collected from the abdomen of an equine cadaver. Although there is not a consensus on the exact thickness of the epidermis of horses, it is well recognised that this differs among different regions of the horse body, and Jorgensen et al. (2018), estimated an averaged epidermal thickness for this area of approximately 29.36 µm. Therefore, as for the canine experiment, F-Bleosome can reach deep regions within the dermis of equine skin, crossing the outermost layers of the skin and the epidermis. In human skin, we could not establish the exact depth of the F-Bleosome molecules due the limited availability of skin samples to conduct technical replicates. However, in the single experiment conducted, at 6 h of treatment F-Bleosome molecules were found at a depth of about 1 mm within skin explants, indicating that the fluorescent liposomal drug had the ability to penetrate through the whole skin section. The epidermal thickness of human breast is 76.9 µm (Ince et al. 2015) and thus, after 4 h of a single topical application, when encapsulated in liposomes, bleomycin seems to be able to penetrate into the dermal layer in human skin. However, these results are preliminary findings and an extended study using human skin should be considered.

In all three species tested F-Bleosome molecules, after 4 and 6 h of treatment, were found intercalated in skin structures at the same level of the cellular nuclei. The first nucleated layer of the skin, starting from the outermost *stratum corneum*, is the *stratum spinosum*, which, in human skin, has an approximative thickness of 100 µm (Horikoshi et al. 2005). Furthermore, the epidermis is an avascular component of the skin (Horikoshi et al. 2005), and in some 3-D images, it is possible to identify some F-Bleosome molecules located close to structures that appear similar to small blood vessels. This might reinforce the hypothesis that the encapsulated bleomycin is able to penetrate beyond not only the hard outermost corneocytes but also the epidermis.

However, a major issue in the evaluation of the exact z-position of the particles of drug was the overall depth of the skin explants themselves examined with MP. During the preparation of skin sections, care was taken to process samples with the same

dimension and thickness. However, to produce accurate and high-quality images, MP needs samples that are as flat as possible. Obviously, dealing with live, intact skin sections, rather than histological slides, leads to inherent variation in the final sample; however, in order to obtain an even surface, sections were anchored to the bottom of a petri dish, kept as flat as possible, embedded in agarose. Nonetheless, some areas of some sections were not clearly visible due to naturally occuring irregularity of the skin surface. Moreover, the cutaneous sections were visualised with the epidermis side facing the bottom of the petri dish and with the lens of the MP directed toward the subcutaneous side, because the epidermis is hairy and the keratynocytes themselves have a level of high autofluorescence and may prevent the visualisation of other structures within that section (data not shown). Hence, these additional factors were considered when establishing the exact z-position and depth of the skin section examined.

To gain quantifiable data from the images captured by MP, we used Imaris software; however, this program has several limitations and it was not always possible to accurately target all the F-Bleosome and F-Bleomycin particles. Hence, in limited situations, some particles recognised as cellular nuclei, were manually converted to F-Bleosome or F-bleomcyin molecules. Reasuringly, the consistency of the results between technical and biological replicates (including between different breeds and species), was a confirmation that, even with limitations, our methodology was a suitable and reliable first step towards accuratly visualising the fate and the mechanism of action of drug penetration through animal and human skin.

Unfortunately, it was not possible to have an accurate measurement of the size of the F-Bleosome and F-bleomycin particles, using the Imaris software. However, it is certainly possible to note, by the images gained with the MP, that the size of the F-Bleosome particles tends to increase at the increasing time points. Moreover, their shape, which is well demarcated and spheroidal in the early stage of treatment, changes at later time points of Bleosome application: molecules, after 6 h of treatment, appear without clear margins and with a wider variation among all the drug particles present. This is consistent across all the species compared in this study. These findings, together with the results of the TEM experiment, led us to hypothesise that Bleosome is able to reach the deeper strata of the epidermis and the underlying dermis, according the mechanism number 2 proposed by Verma et al (2003), acting as penetration

enhancer. In the electron microscope study, liposomes were found only in the *stratum corneum*, after treating skin explants for more than 6 h. However, having treated the skin explants in the same manner, and visualising with the MP, the F-bleomycin molecules reached the deeper layers of the skin after 4 h of treatment, and the dermal layer 6 h after one single application of Bleosome. Furthermore, the fact that F-Bleosome molecules tended to increase in size and have less defined margins at increasing time of treatment and thus, depth of penetration, it might be a further indication that liposomal nanocarriers interact with the hard keratynocytes, finding spaces between interlipidic lamellae and being therefore disrupted. Our hypothesis is that after 10 min, Bleosome consists of bleomycin still encapsulated in liposomes, and is found only at a superficial level. After 4 - 6 h, once Bleosome has passed beyond the *stratum corneum*, liposomes are damaged and the entrapped drug is released and free to expand, to aggregate with other molecules and to penetrate deeper into the cellular and vascular dermal layer.

To the best of our knowledge, this is the first study that has investigated the fate of bleomycin encapsulated liposomes after topical skin application, through direct visualisation of both UD liposomes and the entrapped drug. Our findings support the greater ability of Bleosome to penetrate through the skin, when compared to the free bleomycin, and explain that UD liposomes, when loaded with bleomycin, act as penetration enhancer, interacting with the *stratum corneum* and releasing the payload after 4 h of treatment.

3.6 Conclusions, limitations and future directions

In this study, we sought to assess if and how Bleosome was able to penetrate through animal and human skin. To this extent, we optimised an innovative imaging technique to directly visualise both the liposomes and the entrapped bleomycin in *ex-vivo* viable skin explants. Firstly, we attempted the direct visualisation of the drug using the fluorescent microscope, confident of the intrinsic fluorescence of bleomcyin. However, the high level of the autofluorescence of skin structures hampered a clear visualisation of the drug; hence, we performed a penetration study using canine skin sections treated with Bleosome over several time points. After the treatment, sections

were analysed with the TEM. This technology does not allow direct visualisation of bleomycin particles, however, liposomes were observed and recognised and they were consistently found within the *stratum corneum*, but were not detected in any of the deeper layers of the epidermis after 30 min, 2, 4, 6 and 8 h of treatment. Subsequently, we coupled the bleomycin with a fluorophore, Bodipy-FL, to detect F-bleomycin using the MP. We successfully visualised F-bleomycin inside liposomes, and detected their localisation after different times of treatment. After 6 h of treatment, the deepest particle was found at 800 µm in the canine skin, at 430 µm in the equine skin, and at approximately 1 mm in human skin. This is significantly deeper than the average thickness of the *stratum corneum* (15/20 µm) (Theerawetanasirikul, et al 2012), and the average thickness of the epidermis (40 µm). We therefore propose that liposomes allow and improve the penetration of encapsulated bleomycin through animal and human skin, acting as penetration enhancers, following the mechanism number 2 proposed by Verma et al (2003): liposomal vesicles might interact with outermost keratinocytes, disrupting intercellular lipid lamellae and allowing the release and consequently the penetration of the entrapped bleomcyin through the skin.

This study has several limitations: The TEM and the MP provided integrative data, however, even if the experimental settings used were the same, the studies were performed under different conditions and this might cause some variability in the outcome. We did not visualise equine and human skin with the TEM, to prove that liposomes behave in the same manner in the skin of these species. Images gained with MP were analysed with using Imaris software. However, the program did not allow us to compensate for variability in depth of single skin explant imaged (which might explain the different position of the particles after 4 and 6 h of treatment among the different species), nor the exact dimension and size of the drug particles. Furthermore, our Imaris protocol generated some controversies in distinguishing exactly all the F-Bleosome particles from the autofluorescent skin structures, generating the need to manually adjust the count in limited circumstances.

The skin samples used for this study were collected from abdomen and flank of dogs and horses, and from breast tissue in human. These anatomical regions were chosen as they are easy accessibility from cadavers and we wished to remove the skin promptly after the euthanasia of the animals. Moreover, withrowing skin from a large, even surface of the body allowed us to perform our study on the penetration of

Bleosome through the skin, using samples from the same animal and from the same anatomical region, hence, with similar characteristic and thickness. This was an important factor in order to assure the reproducibility and consistency of the study and allowed us to locate the position of the drug particles according to the depth of epidermis of that particular body area.

The skin explants used for this study were withdrown from cadavers, immediately frozen and thawed at the time of the relative experiment. This methodology was used according to the OECD guidelines for assessing the permeability and penetration of compounds through the skin. These guidelines state that the features of the skin processed according to the procedure illustrated within the document and used in our study, resemble to a good extent the ones of skin in a living organism. However, several studies also claim that the fluxes of transdermal permeation of compounds *in vitro* are generally lower than what found *in vivo*; this might be due to the dermal vasculature and to the hydration gradient present in the skin of living body, which is diffuclt to reproduce in the laboratory (Nakadate 1991; Davies, Ward, and Heylings 2004). Hence, although with some limitations, this type of studies is considered a suitable metodology in order to assess the ability of a substance to penetrate through the skin (Nakadate 1991; Davies, Ward, and Heylings 2004).

The next step would be to repeat the TEM study using equine and human skin explants; to have at least a duplicate of the MP study using human skin and to improve the protocol used with Imaris, designing a bioinformatics script, made *ad-hoc* for this purpose. Furthermore, longer time points and repeated treatment can be employed to perform the penetration study with MP. We established a method to fluorescently label the bleomycin prior to encapsulation within liposomes, and it would be exciting to expand this experiment to include labelling of the liposomal nanoparticles with a contrasting fluorescent probe, this would enable a direct comparison of the position of the liposomes and the entrapped bleomycin within the skin after treatment with Bleosome.

Chapter 4 Cellular uptake and molecular signalling in cancer cell lines in response to Bleosome treatment

4.1 Abstract

Bleomycin is a chemotherapy agent that induces cancer cell death mainly by producing double- and single-strand (DSB and SSB) DNA breaks. However, the action of bleomcyin is proposed to be cell type dependent and more efficient in certain types of tumours indicating that there may be different mechanisms of cellular uptake and of cellular resistance to the treatment. To date, these processes are still undefined. We are interested in studying the cellular effects of Bleosome, a form of bleomycin encapsulated in ultra-deformable (UD) liposomes and aim to determine if liposome-encapsulation can improve the cellular uptake of the entrapped drug and to elucidate the mechanism of resistance to the treatment.

Here, we showed that Bleosome kills canine, feline and human cancer cell lines, and compared its efficacy with free bleomycin. From our data, Bleosome is taken up by cells and stored in the cytoplasm more efficiently than free bleomycin. Furthermore, a preliminary investigation within two different types of canine cancer cell lines revealed that the response to Bleosome treatment is cell type dependent. Focusing on canine melanoma cancer cell line (CML10), we found that these cells were unable to repair the DNA lesions, produced by Bleosome treatment, through the activation of DNA repair pathways and cell cycle checkpoints, while, after initial Bleosome treatment, CML10 cells may stimulate the promotion of the tumour microenvironment.

We also investigated the effect of Bleosome on bleomycin hydrolase (BLMH) levels, an enzyme previously shown to be induced by bleomycin treatment and to mediate inactivation of the drug. We speculated that BLMH may drive cellular resistance to bleomycin but found no evidence of a link between the treatment and the level of BLMH within cells and tumours.

Overall, our findings provide novel and compelling information about both the mechanism of cellular interaction of liposomal encapsulated bleomycin and the molecular response to the Bleosome treatment in a canine cancer cell line.

4.2 Introduction

Bleomycin (BLM) is a chemotherapeutic drug belonging to the class of glycopeptidic antibiotics; it exerts its function against cancer cells by producing DNA single and double-strand breaks (SSB and DSB), and, to some extent, RNA damage as well (Chen and Stubbe, 2005). Depending on the presence of oxygen, this mechanism generates radical intermediates, which can be rearranged to produce different types of DNA lesions, closely related to the ones produced by ionizing radiation (Ramotar and Wang 2003). However, bleomycin is considered more efficient against some types of cancer than others, and this may be related to the efficiency of drug uptake and to the mechanism of action in specific cancer cell types.

Bleomycin is a large (molecular weight of 1.5 kDa), hydrophilic molecule that is unable to efficiently diffuse across cell membranes. The mechanism of cellular uptake has been the focus of several investigations (Roy and Horwitz 1984; Lyman et al. 1986). However, there is no general consensus regarding the mechanism of uptake, efficiency of translocation into the nucleus or annotation of the domains of the bleomycin molecule. Some studies using bleomycin labelled with radioactive cobalt have identified a potential cellular binding partner on the surface of Chinese hamster fibroblasts and human head and neck carcinoma cells. These studies indicated that bleomycin binds to a receptor protein on the plasma membrane that is then transferred into intracellular endocytotic vesicles by receptor-mediated endocytosis. Furthermore, A253 cells are inherently resistant to bleomycin because they have reduced bleomycin-membrane binding sites (Pron et al. 1999). The mechanism of transport of bleomycin from the endocytotic vesicles to the cytosol has not yet been elucidated. No further characterisation of this putative binding protein or the endocytosis pathway has been reported. Identification of the plasma-membrane binding protein and its expression in different tissues could be the key to the differential toxicity of bleomycin to tumour cells and lung cells. (Chen and Stubbe 2005).

Bleosome is a form of bleomycin encapsulated in ultra-deformable (UD) liposomes. This formulation has been created with the aim to enable the passage of bleomycin molecules through the skin. However, to what extent liposomes can improve the cellular uptake of the entrapped drug is still under investigation.

Liposomes have been developed as versatile nanocarriers for various pharmacological agents. The effect of surface charges on the cellular uptake of the liposomes has been

studied by various methods. However, due to limitations of techniques used, the exact mechanism of cellular uptake of the liposomal nanocarriers is still poorly understood (Kang, Jang, and Ko 2017). Types of liposomal nanocarrier, entrapped drug and target cells all contribute to the different pathway of cellular internalisation of liposomes, however, endocytosis appears to be the most likely mechanism of cellular penetration used by liposomes (Alshehri, Grabowska, and Stolnik 2018). In addition, the mechanistic effects at cellular level of bleomycin are not fully understood. Early studies in cultured cells indicated that bleomycin did not directly inhibit DNA replication, RNA synthesis or protein synthesis. Instead, numerous studies on a range of cell lines demonstrated that bleomycin induced global changes in chromosome morphology, including chromosome breaks, gaps, and deletion (Hecht 2000; Schroeder et al. 2014). More quantitative and molecular analysis of DNA from cells treated with bleomycin demonstrated that both SS and DS DNA cleavage resulted. Furthermore, the extent of the DNA cleavage was dependent on the bleomycin concentration and time of incubation (Chen and Stubbe, 2005).

Studies in cell culture have given further insight into which stages in DNA biology are most susceptible to bleomycin damage. Actively transcribed genes, for example, were shown to be more susceptible to bleomycin than silenced genes. Kuo (1981) examined the DNA cleavage of the globin and ovalbumin genes by bleomycin in different tissues (Kuo 1981). The globin gene is actively transcribed in erythrocytes and inactive in ovocytes, while the ovalbumin gene is actively transcribed in ovocytes and inactive in erythrocytes. Kuo (1981) showed that, in both cases, the actively transcribed chromatin was more sensitive to bleomycin-induced DNA damage.

Cell culture studies further revealed that bleomycin-induced DNA damage is cell-cycle dependent. In synchronized Chinese hamster lung fibroblasts, DNA DSBs induced by bleomycin at different stages in the cell cycle were examined. Bleomycin caused 2–3 times fewer DNA DSB in S-phase cells than in G1 or G2/M phase cells. This observation is consistent with previous studies claiming that bleomycin does not directly interfere with DNA replication (Kunimoto, Hori, and Umezawa 1967).

In summary, in a wide range of experimental cell-culture systems, using numerous methods for analysis of DNA cleavage, there is mounting evidence that DNA damage is a likely contributor, if not the major contributor, to the cytotoxicity of bleomycin. These studies further show that proteins interacting with DNA affect cleavage susceptibility in ways that remain to be elucidated (Chen and Stubbe 2005;.Tounekti

et al. 2001; Mekid et al. 2003). Further studies where the concentration of bleomycin inside the cell was controlled by electric pulses, which temporarily altered cell permeability (also known as electroporation), showed that bleomycin induced two distinct types of tumour cell death, which were dependent on the bleomycin concentration within the cell and consequently, different amounts of DNA DSBs. At a low therapeutic dose of bleomycin, cells accumulated in G2/M phase and a slow, mitotic cell death was observed. At high doses of bleomycin, the drug itself acted as a micro-nuclease, causing extensive DSBs in DNA and rapidly initiating an apoptotic-like process. The operative pathway was related to the number of DSBs mediated by activated bleomycin (Chen and Stubbe 2015). However, there is evidence that the cell death pathway induced by bleomycin is cell type dependent (Fulda et al. 2001). The reason why this drug seems to be more efficient against some malignancies rather than others is currently unknown. A possible reason could reside in the mechanism of drug resistance and in the different mechanisms of cellular uptakes (Chen and Stubbe 2005; Pron et al. 1999). The DNA-repair pathway is part of a bigger cellular response network that has evolved to deal with DNA damage generated by bleomycin, ionising radiation and other DNA-damaging agents. Cells detect DNA damage and trigger various signal-transduction cascades that ultimately lead to different fates, including cell-cycle arrest, DNA repair, mitotic cell death and apoptosis. (Chen and Stubbe 2005). Bleomycin causes mutational lesions; it is likely that the normal cells of a cancer patient exposed to bleomycin rely on mechanisms that lead to repair of the drug-induced lesions (Ramotar and Wang 2003). Several studies have identified some repair pathways involved in repair of bleomycin-induced lesions; among these, Xu et al. (1998) claimed that the single-strand lesions of DNA could be rescued by the base excision repair pathway (BER). Moreover, as bleomycin is capable of producing DNA DSB, it is likely that specific DS-lesion repair pathways are involved in this process, such as non-homologous end joining (NHEJ) and homologous recombination repair (HRR) (Chen and Stubbe 2005). Lu et al. (2017) performed a microarray analysis on gene expression in response to bleomycin treatment in human fibroblasts. They found that fibroblasts respond to Bleomycin-induced DNA damage mainly by activating the p53 pathway, but that ATM, cell cycle checkpoint and NHEJ were also implicated in the cellular signalling cascade generated by the treatment (Lu et al. 2017). Moreover, Forrester et al. (2012) found that lymphoblastoid cells responded to IR in a different manner compared to fibroblasts, and that nucleotide excision repair (NER, another

DNA repair mechanism), rather that HRR and NHEJ, was the most representative activated pathway.

However, major targets of bleomycin toxicity are lungs and skin; these two tissues have a low level of an enzyme called Bleomycin hydrolase (BLMH). This enzyme plays a role in the degradation of the bleomycin molecules, rendering the drug inactive and unable to exert its function, hence, BLMH might play a key role in the bleomycin resistance, although the current literature remains controversial (Chen and Stubbe 2005).

In this chapter, our aim was to provide an insight into the molecular mechanisms exploited by Bleosome (bleomycin encapsulated within liposomes) to kill different types of cancer cells, in comparison with free bleomycin. Here, we investigated the cellular uptake of the fluorescently labelled Bleosome by live-cell imaging and FACS to quantify the amount of drug taken up over a time course of treatment, and compared it with the free bleomycin. Furthermore, we explored the molecular signalling cascades activated by Bleosome in two different types of canine cancer cells at the cellular level and used RNA Seq to identify global differences in transcriptomic profiles after Bleosome treatment. Lastly, we evaluated the role of BLMH in response to Bleosome treatment at the cellular and tumour level.

4.3 Material and Methods

4.3.1 Cell culture

For routine cell culture, all cell lines used for the experiments (MCF7, REM134, C2, CML10, SMG, SCCF1) were grown using appropriate media (section 2.1) in an incubator at 37^{o}C, in a humidified atmosphere with 5 % CO_2 under mycoplasma-free conditions.

4.3.2 Cell viability assay

Cells were trypsinised into single cells and seeded at a density of $5x10^2$ cells in the media, in triplicate, in opaque 96-well plates (Corning, CA, USA). Serial dilutions of Bleosome and free (aqueous cream) bleomycin (containing bleomycin non-encapsulated within liposomes) (table 4.1) were added to the appropriate cells the following day. The control was represented by media and bleomycin dilutions. Dose-response curves were generated 48 hours after exposure. Cytotoxicity was measured using the CellTiterGlo® Luminescent Cell Viability Assay (Promega, Madison, USA), which quantifies the number of viable cells in culture based on quantification of ATP present. Luminescence was recorded by luminometer (Viktor3, PerkinElmer, Massachusetts, USA). Data was averaged and normalized against the average signal of untreated/vehicle control treated samples (details in section 2.2). Each experiment was performed at least twice: in the first Cell Viability Assay, drug titration showed in table 4.1 (A) was used, while the second experiment was performed with the concentrations showed in table 4.1 (B), adapted according to the results of the first experiment, in order to gain more precise data for establishing IC_{50}.
For each cell line, two 96 well plates were used at the same time: one with cells treated with Bleosome and the other with cells treated with bleomycin aqueous cream. Each drug concentration and control was performed in triplicate.

A
D1: 100 µM, D2: 60 µM, D3: 30 µM, D4: 10 µM, D5: 1 µM, D6: 0.5 µM, D7: 0.25 µM, D8: 0.1 µM, D9: 0.05 µM, D10: 0.025 µM
B
D1: 20 µM, D2: 10 µM, D3: 7 µM, D4: 5 µM, D5: 4 µM, D6: 3 µM, D7: 2 µM, D8: 1 µM, D9: 0.5 µM, D 10: 0.1 µM

***Table** 4.1 Drug titrations. (A) dilutions (D) of Bleosome and aqueous cream bleomycin used for treating cells during the first experiment, while (B) shows dilutions (D) of Bleosome and aqueous free bleomycin used for treating cells during the second experiment*

IC_{50} values were obtained using GraphPad Prism7 software, with non-linear regression equation. Final IC_{50} for each cell line was calculated as the average of the results of the two viability experiments.

4.3.3 Colony formation assay

Cells were trypsinised into single cells and seeded at 1000 cells/10 cm plate (CML10) and at 500 cells/10 cm plate (REM134). Experiments were performed twice. During the first experiment, cells were treated with doses of Bleosome and aqueous cream bleomycin indicated in table 4.2. The second experiment was conducted with drug concentrations showed in table 4.3. Each drug titration was performed in triplicate. Plates were incubated at 37ºC in humidified CO_2 incubator within 10-14 days, until colonies were visible. Growth media was changed once a week. The colonies were fixed by incubating with ice-cold methanol for 5 minutes at room temperature. Colonies were stained with Giemsa stain (Invitrogen, Paisley, UK) according to the manufacturer's instruction. The total number of colonies was counted and the average number of colonies for each condition calculated.

A **REM 134**	Drug concentration **Bleosome**	C **CML 10**	Drug concentration **Bleosome**
IC_{50}	5.06 µM	IC_{50}	3.81 µM
½ IC_{50}	2.53 µM	½ IC_{50}	1.90 µM
¼ IC_{50}	1.26 µM	¼ IC_{50}	0.95 µM
B **REM 134**	**Free bleomycin (aqueous solution)**	D **CML 10**	**Free bleomycin (aqueous solution)**
IC_{50}	0.23 µM	IC_{50}	0.68 µM
½ IC_{50}	0.115 µM	½ IC_{50}	0.34 µM
¼ IC_{50}	0.057 µM	¼ IC_{50}	0.17 µM

Table 4.2 *Concentrations of drug corresponding to the relative titrations of Bleosome and free bleomycin (aqueous cream solution) IC_{50} in REM134 cell lines, (A) and (B) respectively, and in CML10 cells, (C) and (D) respectively.*

Bleosome: 0 µM, 0.25 µM, 0.5 µM, 1 µM
Aqueous cream bleomycin (free form): 0 µM, 0.25 µM, 0.5 µM, 1 µM

Table 4.3 *Titrations of Bleosome and aqueous cream bleomycin used to treat the plates for the second experiment in both C2 and CMl10 cells.*

4.3.4 Immunoblotting

To analyse the protein levels, immunoblotting, using a list of primary antibodies, was performed, according to section 2.3. Cell lysates were obtained from MCF7, SMG, CML10 and C2 cells. Cells were treated for 4 hours with several dilutions of Bleosome, or aqueous cream bleomycin for comparison, as following: 0 µM, 0.25 µM, 0.5 µM, 1 µM, 4 µM, 8 µM, 16 µM. A further immunoblotting was conducted using CML10 cells treated with the relative IC_{50} of Bleosome (3.81 µM) or free bleomcyin (0.68 µM), and the double of the IC_{50} value of Bleosome (7.62 µM) or free bleomycin (1.36 µM), over a time course of 2, 4 and 6 hours for each treatment. Untreated cells were used as control.

4.3.5 Quantitative Real Time (qRT) PCR

4.3.5.1 Treatment of cells

C2 and CML10 cells were treated in 100 x 17 mm petri dishes (Nunclon™ Delta, ThermoFisher), with the relative IC_{50} concentrations of Bleosome: 1.56 µM and 3.81 µM respectively over a time-course including 2, 4, 8 and 24 hours of treatment. Untreated cells were used as control. At the relative time point of treatment, cells were washed with 2X PBS, harvested and lysates were prepared as detailed in section 2.4.

4.3.5.2 RNA extraction and quantitative Real Time PCR

Basic methods for RNA extraction and qRT-PCR are described in section 2.4. Briefly, total cellular RNA was extracted using RNeasy® kit (Qiagen, CA, USA) and RNA quality was determined by A260 measurement. Total RNA was reverse transcribed using the Omniscript TM RT Kit (Qiagen, CA, USA) according to the manufacturer's instruction. Primers were designed using *Ensembl.org* and *Primer3Plus* online software and tested as detailed in section 2.4. qRT-PCR was performed using the Roche LightCycler® 480 instrument with LightCycler® 480 Multiwell Plate 96 according to the manufacturers protocol. The reactions were performed with QuantiNova™ Sybr® Green (Qiagen) master mix.

All measurements were performed at least in triplicates. Normalisation was made using GAPDH gene expression. Relative gene expression levels were obtained by normalisation to the expression levels of housekeeping gene (*GAPDH).* Comparative quantification was made using the Delta Delta Ct Method for calculating fold-changes in the gene of interest normalised to the untreated samples. Results were statistically analysed using MINITAB, fitting data in a general linear model (GLM): two-way ANOVA and Tukey's *post-hoc* test.

4.3.6 RNA sequencing

4.3.6.1. Samples

C2 and CML10 cells were treated with the respective IC_{50} of Bleosome as detailed in 4.3.5.1. For this experiment, cells were treated for 8 and 24 hours and cells untreated were used as control. For each time point of treatment, three biological replicates were used: they corresponded to the same cancer cells treated at a different passage numbers. In details, CML10 cells were treated at passages (P) 37, 38 and 40, whereas C2 cells were treated at passages (P) 29, 35 and 37, as illustrated in table 4.4.

External	Number	Group	Time	Passage	Cell
CML_P37_UT	1	CML_UT	UT	37	CML
CML_P37_8H	2	CML_8H	8H	37	CML
CML_P37_24H	3	CML_24H	24H	37	CML
CML_P38_UT	4	CML_UT	UT	38	CML
CML_P38_8H	5	CML_8H	8H	38	CML
CML_P38_24H	6	CML_24H	24H	38	CML
CML_P40_UT	7	CML_UT	UT	40	CML
CML_P40_8H	8	CML_8H	8H	40	CML
CML_P40_24H	9	CML_24H	24H	40	CML
C2_P29_UT	10	C2_UT	UT	29	C2
C2_P29_8H	11	C2_8H	8H	29	C2
C2_P29_24H	12	C2_24H	24H	29	C2
C2_P35_UT	13	C2_UT	UT	35	C2
C2_P35_2_8H	14	C2_8H	8H	35	C2
C2_P35_24H	15	C2_24H	24H	35	C2
C2_P37_UT	16	C2_UT	UT	37	C2
C2_P37_8H	17	C2_8H	8H	37	C2
C2_P37_24H	18	C2_24H	24H	37	C2

Table 4.4 *Samples with sample-associated variables*

RNA isolation, quality control and mRNA sequencing are detailed in section 2.5.

4.3.6.2 Exploratory analysis

Exploratory analysis was conducted by Edinburgh Genomics (Edinburgh, UK). A principal component analysis (PCA) was undertaken on normalised and filtered expression data to explore observed patterns with respect to experimental factors. The cumulative proportion of variance associated with each factor was used to study the level of structure in the data, while associations between continuous value ranges in principal components and categorical experimental factors was assessed with an ANOVA test.

4.3.6.3 Differential gene expression

Differential analysis was performed by Edinburgh Genomics (Edinburgh, UK). Briefly, analysis was carried out with edgeR (version 3.20.9). edgeR was chosen for this study as it is the only software that can account for biological variability with only few replicates per sample. (Robinson *et al.*, 2010). edgeR software was used for the identification of differences in gene expression of pairwise comparisons organised as follows: (1) CML10 cells treated with Bleosome for 8 hours against CML10 cells

untreated; (2) CML10 cells treated for 24 hours with Bleosome against CML10 cells untreated; (3) CML10 cells treated with Bleosome for 24 hours against CML10 cells treated with Bleosome for 8 hours. Fold changes were estimated as per the default behaviour of edgeR, to avoid artefacts, which occur with empirical calculation. Specifically, a small prior count is added to each observation before fitting a model, in proportion to the library size. Log fold-changes are shrunk towards 0, to a greater degree with genes of low count, and infinite fold changes are avoided. Statistical assessment of differential expression was carried out with the quasi-likelihood (QL) F-test using the contrasts shown in table 4.5. Where specified in this table, confounding covariates (for example sample pairing, batch effects) were adjusted for by incorporating them as a blocking factor in an additive model. Where comparisons were to be compared, comparisons instead of individual sample groups are specified in the 'Group' columns of Table 4.5 with notation like (Treatment-Control).

Variable	Group 1	Group 2	Blocking
Group	CML_UT	CML_8H	Passage
Group	CML_UT	CML_24H	Passage
Group	CML_8H	CML_24H	Passage

Table 4.5. *Contrasts specified for differential analysis. Any variable specified under 'blocking' was used as part of an additive model, and accounted for in differential analysis of that contrast.*

Genes were considered differentially expressed only at a p-value <0.05 and at FDR < 0.05. Genes with log2-fold changes of more than 2 or less than 2 were then selected to ensure that only robust changes were considered. Differentially expressed genes were identified by hierarchical clustering analysis. In hierarchical clustering, each cluster is subdivided into smaller clusters, forming a tree-shaped data structure or dendrogram. Agglomerative hierarchical clustering starts with the single-gene clusters and successively joins the closest clusters until all genes have been joined into the supercluster (D'haeseleer, 2005). Heatmaps were generated using the package called "pheatmap" in R.

4.3.6.4 Functional Annotation

To examine whether certain pathways are over- or under-represented in the gene list,

all genes significantly differentially expressed between the three comparisons were introduced into GSEA (GSEA version 4.0.1). GSEA employs the (weighted) Kolmogorov-Smirnov (K-S) statistic to test whether genes contributing to the phenotype are 'enriched' in each gene-set (Boerkamp et al, 2013). Thereby, GSEA evaluates how genes in queried pathways are distributed in the fold change ordered list generated by the data. This distribution is quantified by using the Enrichment Score (ES) that evaluates if the members of the pathway are randomly distributed or found at the extremes (top or bottom) of the list (Boerkamp et al, 2013). For each gene set, GSEA looks if differentially expressed genes in a pathway rank are enriched at the top fold change list (up-regulated genes), then the ES will be close to 1. Conversely, if the ES = −1, then genes are enriched at the bottom of our fold change data (down-regulated genes) (Lowes et al, 2010). Pathways and biological processes with an FDR value <0.05 were considered as significantly over- or under-represented. Also, Reactome (http://www.reactome.org) and Ingenuity Pathway Analysis (IPA, Qiagen Bioniformatics) were performed based on the dysregulated genes that were identified in the RNA-seq datasets (data not shown).

4.3.7 Immunohistochemistry (IHC)

Equine sarcoids and equine skin were collected according to section 2.9.2. For this study, three sarcoids from patients that underwent surgery, and skin from an equine cadaver without any known cutaneous disease were used. All the samples were withdrawn from different animals. Sarcoids used derived from patients that were presented to the Equine Hospital of the R(D)SVS for the surgical excision of cutaneous sarcoids as part of their planned treatment. Due to limited number of sarcoids available for our research, all the samples collected at the time of the experiment were used (3 sarcoids). The first sample was a mixed fibroblastic sarcoid collected from the elbow, the second one was a nodular sarcoid excised from the region close to the umbilicus and the third mixed sarcoid was excised from the shoulder area. Skin was collected from the abdomen. Each sarcoid was cut in two parts: one part was left untreated and considered as the control, and cut in small pieces of approximately 0.5 x 0.5 x 0.5 cm, and fixed individually in 10% NBF. The second part was treated with Bleosome for 6 hours, spreading the compound all over the free surfaces of the tumour/skin. At the

time point, the sample was cut in small pieces of approximately 0.5 x 0.5 x 0.5 cm and fixed individually in 10% NFB. Each sample was processed by the Pathology Unit of the Royal (Dick) Veterinary School of the University of Edinburgh, as detailed in section 2.6. At least three histological slides were examined from each sample (from both treated and untreated part), one from each 0.5 x 0.5 x 0.5 cm section, and positive staining was evaluated for each slide. Endogenous negative controls were represented by slides of the treated and untreated part of the sample, not stained with the antibody. Absolute positive and negative controls was represented by an equine melanoma stained and unstained with anti-BLMH antibody ab204584 (Abcam), respectively. Each slide was scanned with the slide scanner Nanozoomer XR **(**Hamamatsu) according to the manufacturer's protocol. Quantitative comparison of immunohistochemical staining was measured by image analysis performed by QuPath software. QuPath is designed for digital pathology and whole slide images for bioimaging analysis. Briefly three areas of 35000 μm^2, visualised at 40X magnification, were analysed for each slide. Using the appropriate thresholds and settings the software was able to detect the positive stained cells within the area and indicated the overall positivity as a percentage. Positivity of the three areas, examined within the same slide, were averaged and final value for each sample (treated and untreated) was obtained comparing the means of the three slides.

4.3.8 Bleosome cellular up-take evaluation

4.3.8.1 Visualisation by live-cell imaging study

4.3.8.1.1 *Sample preparation*

C2 and CML10 cells were seeded in 2-well chamber slides (Nunc Lab-Tek II Chambered Coverglass, 1.5 borosilicate glass, ThermoFisher) at a density of $3x10^7$ cells per well, immersed in DMEMs without phenol red (details in table 4.6) When near confluency, cells were stained with Hoechst 33342 (ThermoScientific) as per manufacturer's protocol. Subsequently, cells of both cell lines, were treated with the

relative IC_{50} of F-Bleosome (3.81 µM for CML10 and 1.56 µM for C2) and F-free bleomycin (0.68 µM for CML10 and 0.28 µM for C2) for 2 and for 24 hours. Untreated CML10 and C2 cells were used as control. At the relative time points, drugs were removed and chamber slides were rinsed with 3X PBS, filled with new media and visualised under the Zeiss LSM 880 Confocal microscope Airyscan/Fastscan with 32 sensitive GaAsP detectors, equipped with an incubation chamber, which is maintained at 37 °C with controlled CO_2 flow, as detailed in section 2.10.3.2.

Cell Line	Media	Supplements
C2	Eagles Dulbecco's Modified Eagle Media(DMEM) low glucose, pyruvate, no glutamine, no phenol red (11880028) (Gibco®, Life Technologies, Invitrogen, UK)	5% Foetal bovine serum 0.1 mg/ml; 1x Non-essential amino acid; 1% Glutamax: 25 mg Gentamicin
CML	Dulbecco's Modified Eagle Media (DMEM) low glucose, pyruvate, no glutamine, no phenol red (11054020) (TermoScientific)	10% Foetal bovine serum 0.1 mg/ml; Penicillin/Streptomycin, 1% Glutamax

Table 4.6. *Media used to grown C2 and CML10 cells for live-cell imaging*

.

4.3.8.2 Quantification by fluorescence activated cell sorting (FACS)

4.3.8.2.1 Sample treatment

C2 and CML10 cells were seeded in 6-well cell culture plates (ThermoScientific) at a density of $3x10^7$ cells per well and let them attaching to the bottom of the wells overnight. The day after, cells were stained with Hoechst 33342 (ThermoScientific) as per manufacturer's protocol. Subsequently, cells of both cell lines, were treated with the relative IC_{50} of F-Bleosome (3.81 µM for CML10 and 1.56 µM for C2) and F-free bleomycin (0.68 µM for CML10 and 0.28 µM for C2) for 2 and for 24 hours. Untreated CML10 and C2 cells were used as control. Contemporarily, other two 6-well plates were used as compensation for the FACS analysis. Briefly, two 6-well plates were seeded respectively with C2 and CML10 cells and stained as following: in one well,

cells were stained with Hoechst 33342, the second well included cells treated for two hours with F-Bleosome, the third well included cells treated for two hours with F-free bleomycin, another well included cells stained with Zombie Yellow dead cell marker (BioLegend Inc., USA) and the last well included cells left untreated and unstained.

4.3.8.2.2 FACS

At the relative time points, C2 and CML 10 cells were detached by trypsinisation, washed with PBS and stained with Zombie Yellow Fixable Viability Kit (BioLegend Inc., USA) to detect dead cells. Next, cells were washed again with PBS, re-suspended in PBS and analysed using the cytometer BD Fortessa (BD Biosciences, USA) with a throughput detection set at 30000 events/second. Analysis post-acquisition were performed according to section 2.7

4.4 Results

4.4.1 Bleosome decreases cell viability and colony forming ability in a dose dependent manner in a panel of cancer cell lines

The aim of the experiment was to determine the effectiveness of Bleosome (bleomycin encapsulated within liposomes) to reduce the cell viability of a panel of cancer cell lines, to establish the IC_{50} of Bleosome for each cell line, and to compare its efficacy with non-encapsulated free bleomycin (bleomycin aqueous cream). The following graphs, shown in figure 4.1, illustrate the effect of Bleosome on the viability of the indicated cell line, and comparison with the free bleomycin. After each assay, IC_{50} values were calculated using GraphPad Prism software, with the non-linear regression equation, the results are shown in table 4.7

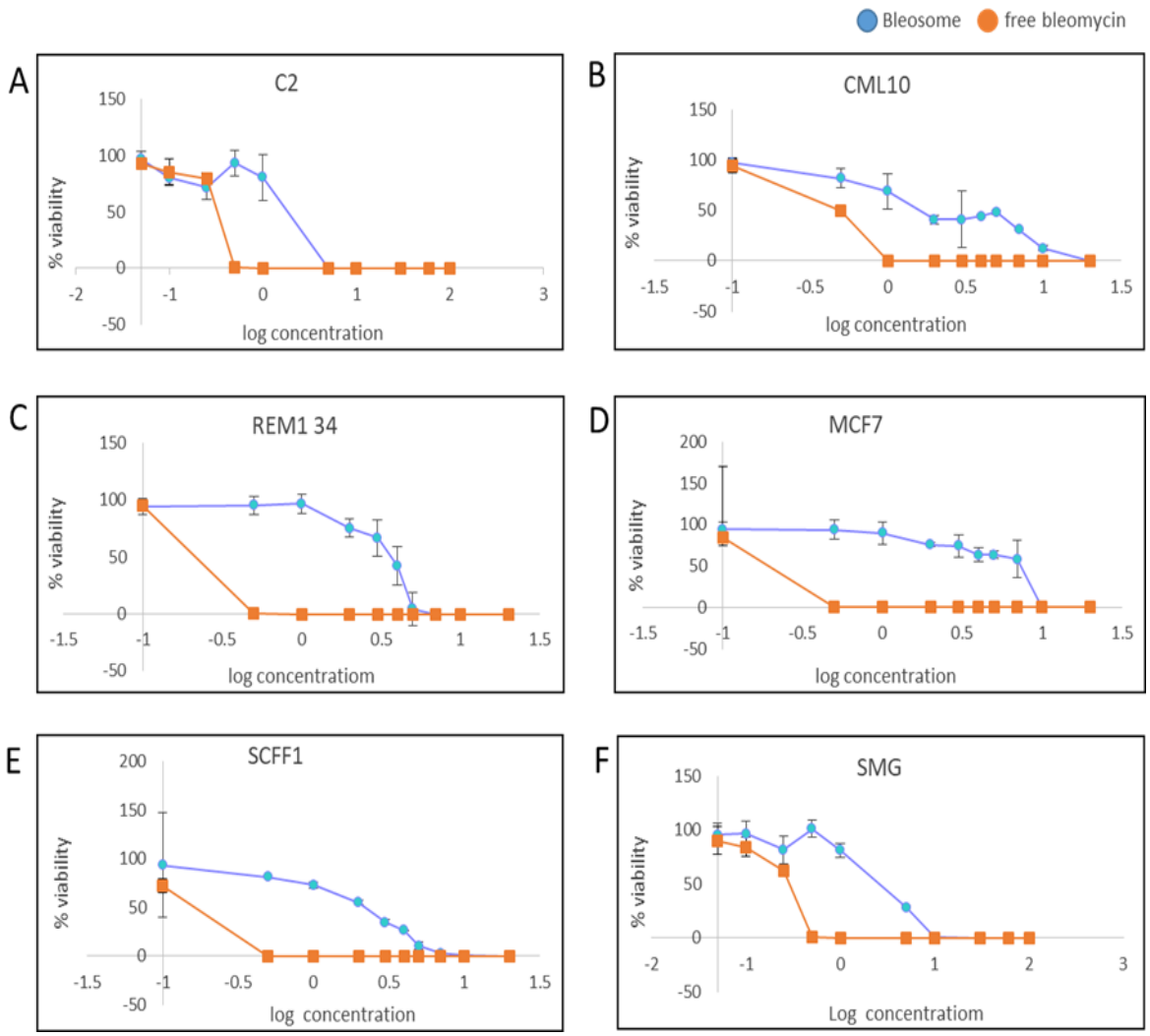

Figure 4.1 *Viability curves produced by dose titrations of Bleosome and free bleomycin. The effect of Bleosome (blue line) compared with free bleomycin (orange line) 72 hours post-treatment, on cell viability of C2 (A), CML10 (B), REM134 (C), MCF7 (D),SCFF1 (E), and SMG (F) cell lines.*

In canine mammary carcinoma (REM134) and in canine mast cell tumour (C2) cell lines, the free bleomycin produced a steep decrease in cell viability, while Bleosome caused a dose-dependent reduction in viability. In canine melanoma cells (CML10), the two curves looked similar, but the drug concentration needed to kill all the cells was lower for the free bleomycin than Bleosome. In human mammary carcinoma (MCF7) and in feline laryngeal squamous cell carcinoma (SCC) (SCCF1) cell lines, the free bleomycin produced a steep decrease in cell viability, while Bleosome caused a steady fall in viability. In feline oral SCC (SMG) cells, the two curves generated by the two treatment had the same trend, but the concentration of Bleosome necessary to cause 100% of cell death was higher than the free form.

Cell line	IC_{50} Bleosome µM	IC_{50} free bleomycin µM
C2	1.56	0.28
CML10	3.81	0.68
MCF7	8.96	0.16
REM134	5.06	0.23
SCFF1	1.68	0.09
SMG	3.26	0.12

Table 4.7 *IC_{50} of Bleosome and aqueous cream bleomycin in different cancer cell lines. These values were made by the mean of the IC_{50} obtained by each viability assay per cell line and calculated using the GraphPad software.*

Both Bleosome and free bleomycin produced a 100% of mortality in all the treated cancer cell lines. However, the drug concentration of the aqueous cream with free bleomycin, needed to cause cell death, was consistently several-fold lower compared to the IC_{50} of Bleosome as illustrated by the IC_{50} values in table 4.7. Importantly, these results do show that Bleosome is able to kill a range of canine cancer cell lines.

To substantiate the cell viability data, we assessed the effect of Bleosome on colony forming ability, focusing on two canine cell lines: REM134 and CML10 cells.
Cells were treated with a titration of previously calculate IC_{50} values (table 4.7), and the number of colonies assessed after 10 days. In the REM134, Bleosome inhibited the formation of all the colonies even at a quarter of IC_{50} drug concentration, while the free form allowed the formation of a small number of colonies at the half and a quarter of the respective IC_{50} value. In the melanoma cell line, CML10, both the compounds prevented the formation of colonies at the respective IC_{50} values, while free bleomycin yielded the formation of more colonies at the lower titrations compared to the encapsulated drug (figure 4.2).

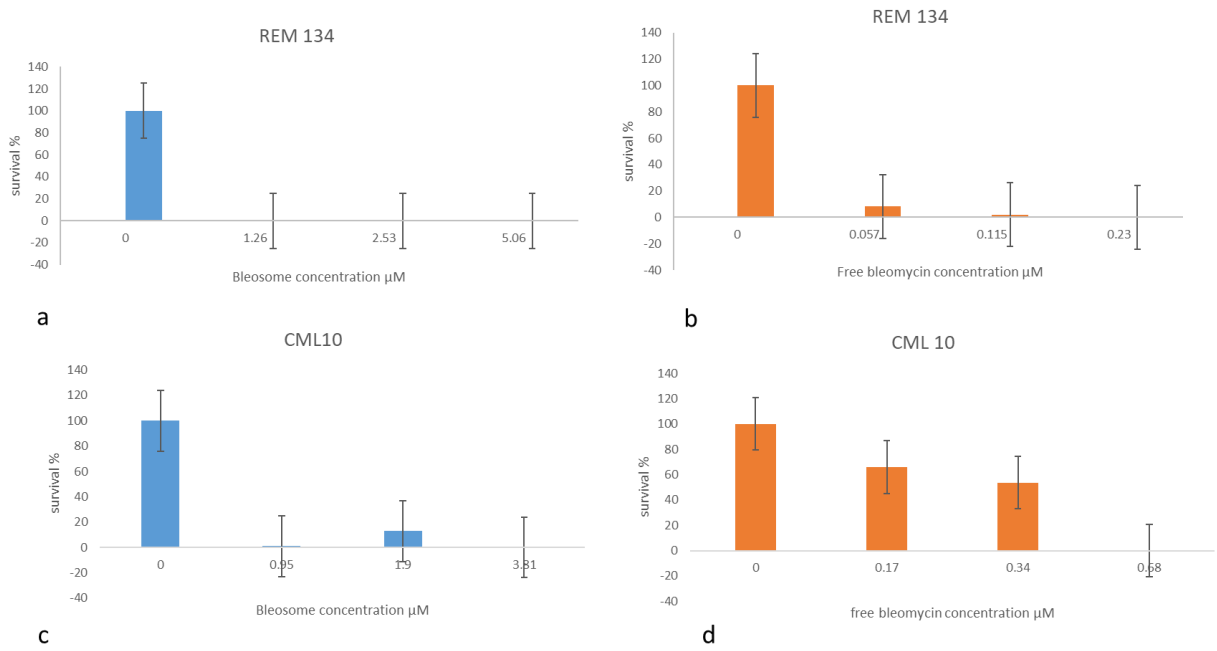

Figure 4.2 *Colonies formed after IC_{50} – based assay in CML10 and REM134 cells treated with Bleosome or free bleomycin.. (a) shows the percentage of colonies found in REM 134 plates after titrations of Bleosome (blue) (0, 1.26, 2.53 and 5.06 µM), (b) shows the percentage of colonies found in REM 134 after titration of free bleomycin (orange) (0, 0.057, 0.115, 0.23). (c) shows the percentage of colonies found In CML10 plates after titrations of Bleosome (blue) (0, 0.95, 1.9 and 3.81 µM) and (d) after free bleomycin (orange) (0, 0.17, 0.34 and 0.68 µM). The treatments lasted 10 days*

To directly compare the effect of Bleosome and free bleomycin on colony forming ability, both cell lines were treated with titrations showed in table 4.3. Figure 4.3 reveals that free bleomycin was able to inhibit the formation of colonies at each concentration used, while Bleosome produced a dose-dependent decrease in the formation of colonies.

The results of the first assay suggest that at the previously calculated IC_{50} value Bleosome is more efficient in inhibiting the growth of cancer cells compared to free bleomycin compound. However, using the same titrations for both the compounds, aqueous cream bleomycin was more effective at killing cells than Bleosome. Although of note, Bleosome was effective at inhibiting colony-forming ability in a dose-dependent manner.

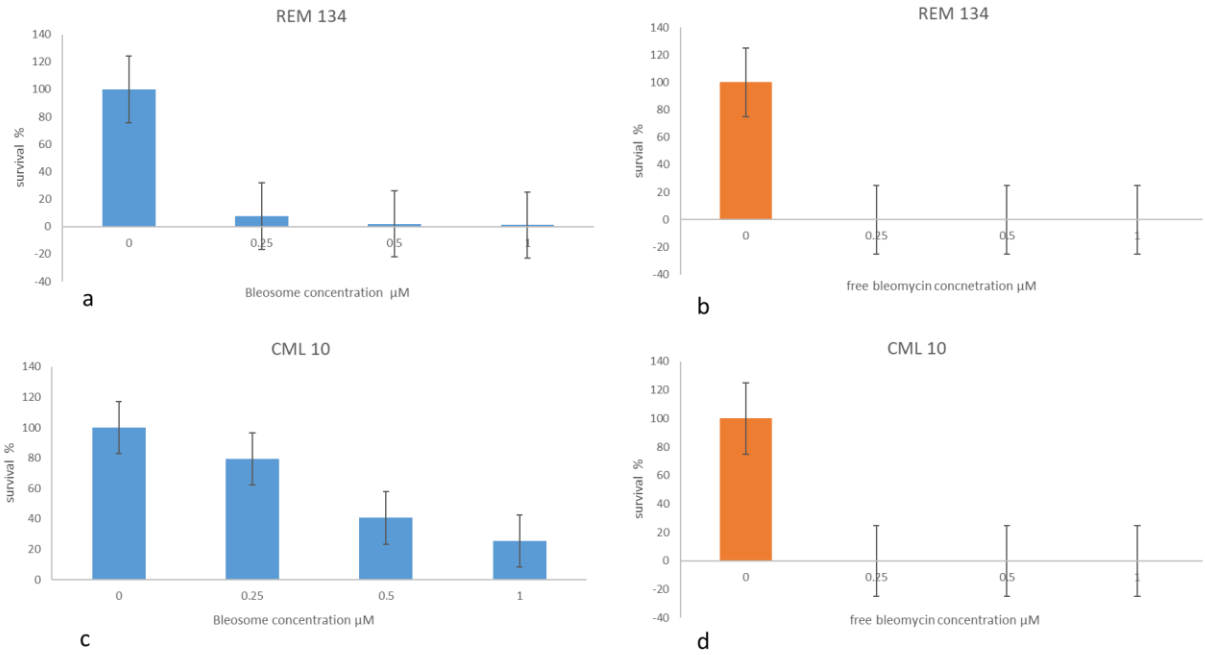

Figure 4.3 *Bleosome inhibits the colony forming ability of canine cancer cells in a dose-dependent manner. The colony-forming ability of (a) REM 134 cells after 0, 0.25, 0.5 and 1 µM of Bleosome (blue columns) and (b) after 0, 0.25, 0.5 and 1 µM of free bleomycin treatment (orange coloumns). Percentage of colonies found in (c) CML10 cells after 0, 0.25, 0.5 and 1 µM of Bleosome (blue columns) and (d) after 0, 0.25, 0.5 and 1 µM of free bleomycin treatment (orange coloumns) Colonies were counted after 10 days of incubation with treatments.*

4.4.2 Bleosome is taken up by cancer cells more efficiently than free bleomycin

To evaluate the mechanism of Bleosome cellular uptake and to compare it with the free bleomycin, we treated two types of different canine cancer cell lines with their respective Bleosome IC_{50}. C2 cells and CML10 cells were treated with 1.56 µM and 3.81 µM of F-Bleosome and F-bleomycin (preparation of fluorescent drugs is detailed in section 2.8) respectively, and both compounds were applied for 2 and for 24 hours. Untreated cells were used as a control. Cells were visualised using the confocal airyscan/fastscan microscope (Figures 4.4 and 4.5).

In the untreated cells, no green particles were observed within the cytoplasm or the nuclear compartment. Whereas, after 2 hours post-treatment with both fluorescent compounds, the presence of drug molecules was located within the cytoplasm. In particular, there are more F-Bleosome particles within cells, compared to the F-bleomycin. However, the position of both compounds is evenly distributed within cell

cytoplasm, but not within the nucleus, as confirmed also from videos made in time-lapse, related to this time-points (supplementary data 8.2.5). Interestingly, after 24 hours of treatment, drug molecules were strongly evident within cells, and the overall amount of green particles appeared to be increased compared to the earlier time-point, in both C2 and CML10 lines treated with F-Bleosome and F-bleomycin. However, some key differences between the two treatments can be observed. In the F-Bleosome treatment, the shape of F-Bleosome molecule is spherical and the dimension varied from very small particles to larger oval structures (figures 4.4 and 4.5 (b), (c), (d), (e)). This finding was consistent between the two different types of cells and can be interpreted as the aggregation of liposomal carriers, which fuse together after several hours following their cellular uptake, or as the results of the storage of the drug by cellular organelles (e.g. lysosomes). Of note, this pattern of fluorescence is typical of F-Bleosome treatment, as, in C2 and CML10 cells treated with F-bleomycin after 24 hours, an overall green background and uniform presence of very small particles could be observed within cytoplasm, but without the presence of large spheroid green structures or spherical molecules (figures 4.4. and 4.5 (i), (j)). Moreover, in the case of F-Bleosome only, few green fluorescent objects were appreciated overlapped to cellular nuclei (figures 4.4 and 4.5 and supplementary data 8.2.5).

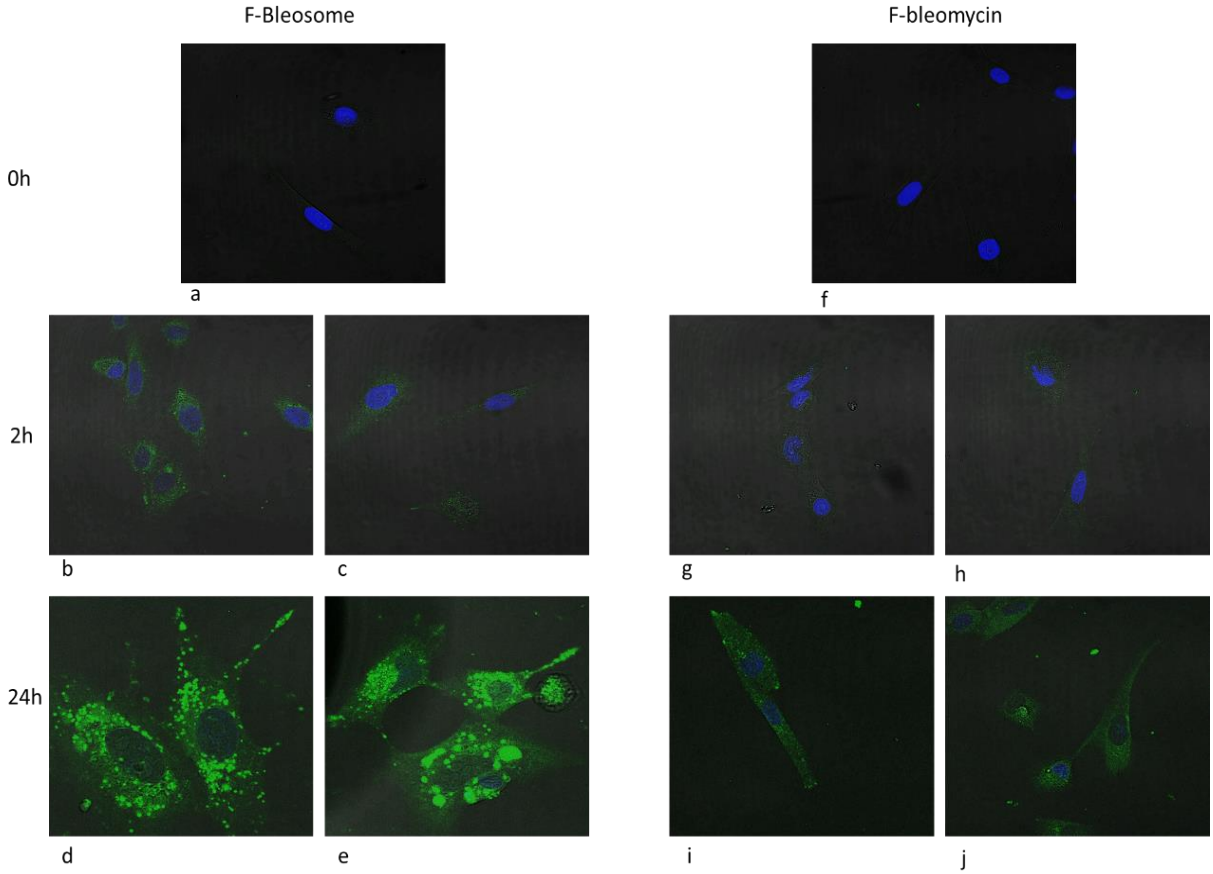

Figure 4.4 *CLSM appearance of C2 cells treated with F-Bleosome and F-bleomycin. (a) are cells untreated and represent the control. (b) and (c) indicate cells treated with F-Bleosome for 2 hours, (d) and (e) represents cells treated F-Bleosome for 24 hours. (f) are cells untreated and represent the control, (g) and (h) represent cells after 2 hours of F-bleomycin treatment, while (i) and (j) illustrate cells treated for 24 hours with F-bleomycin.*

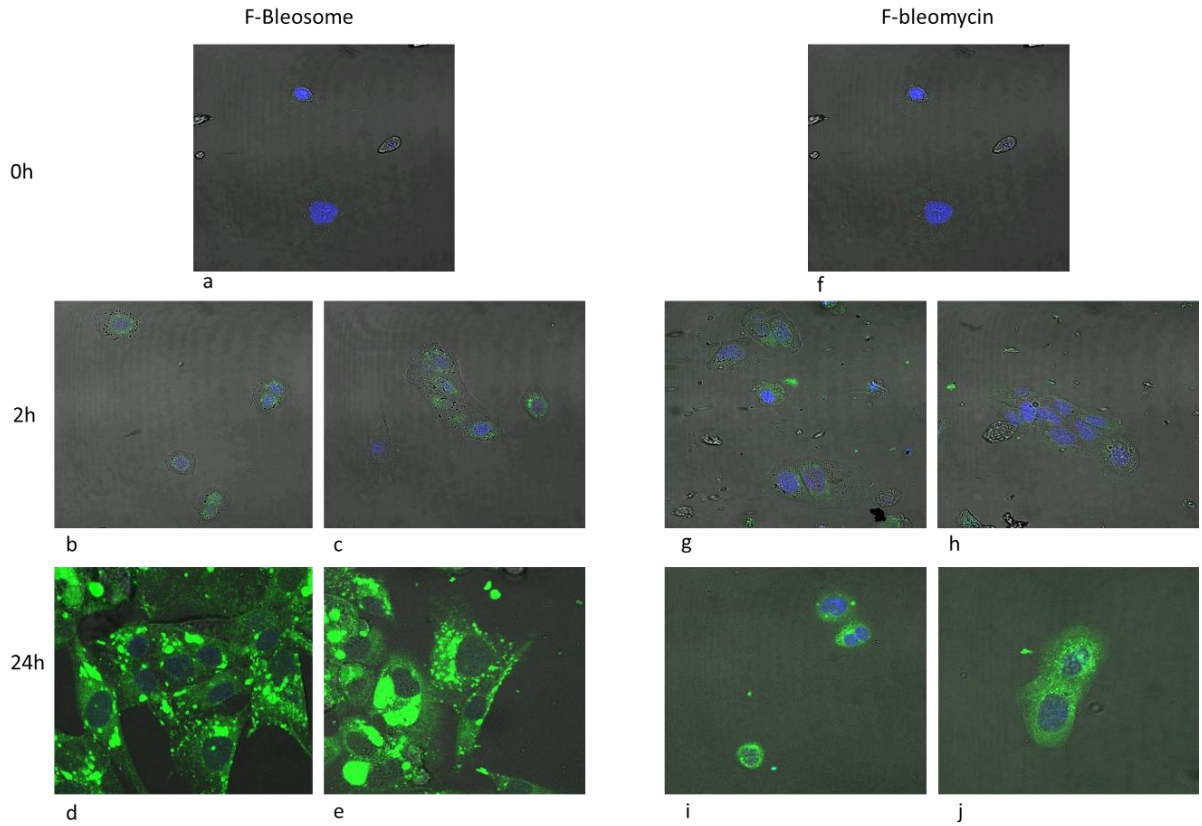

Figure 4.5 *CLSM appearance of CML10 cells treated with F-Bleosome and F-bleomycin.(a) are cells untreated and represent the control. (b) and (c) indicate cells treated with F-Bleosome for 2 hours, (d) and (e) represents cells treated F-Bleosome for 24 hours. (f) are cells untreated and represent the control, (g) and (h) represent cells after 2 hours of F-bleomycin treatment, while (i) and (j) illustrate cells treated for 24 hours with F-bleomycin.*

Fluorescence-activated cell sorting (FACS) was performed to quantify the green fluorescence intensity corresponding to the amount of F-Bleosome and F-bleomycin taken up by cells at the indicated time points. Results of cell sorting revealed that the level of green intensity within cells treated with F-Bleosome was consistently higher compared to the F-bleomycin-treated cells, indicating the greater cellular uptake of Bleosome, compared to the free bleomycin, after 2 and 24 hours of treatment in both cell types. Figures 4.6 and 4.7 show the results of imaging in tandem with the relative FACS quantification of drug included within cells. Confocal images and cell sorting analysis were concordant, indicating that the overall cellular uptake of F-Bleosome was higher than free F-bleomycin in both C2 and CML10 cell lines. This finding was consistent at both 2 and 24 hours post-treatment.

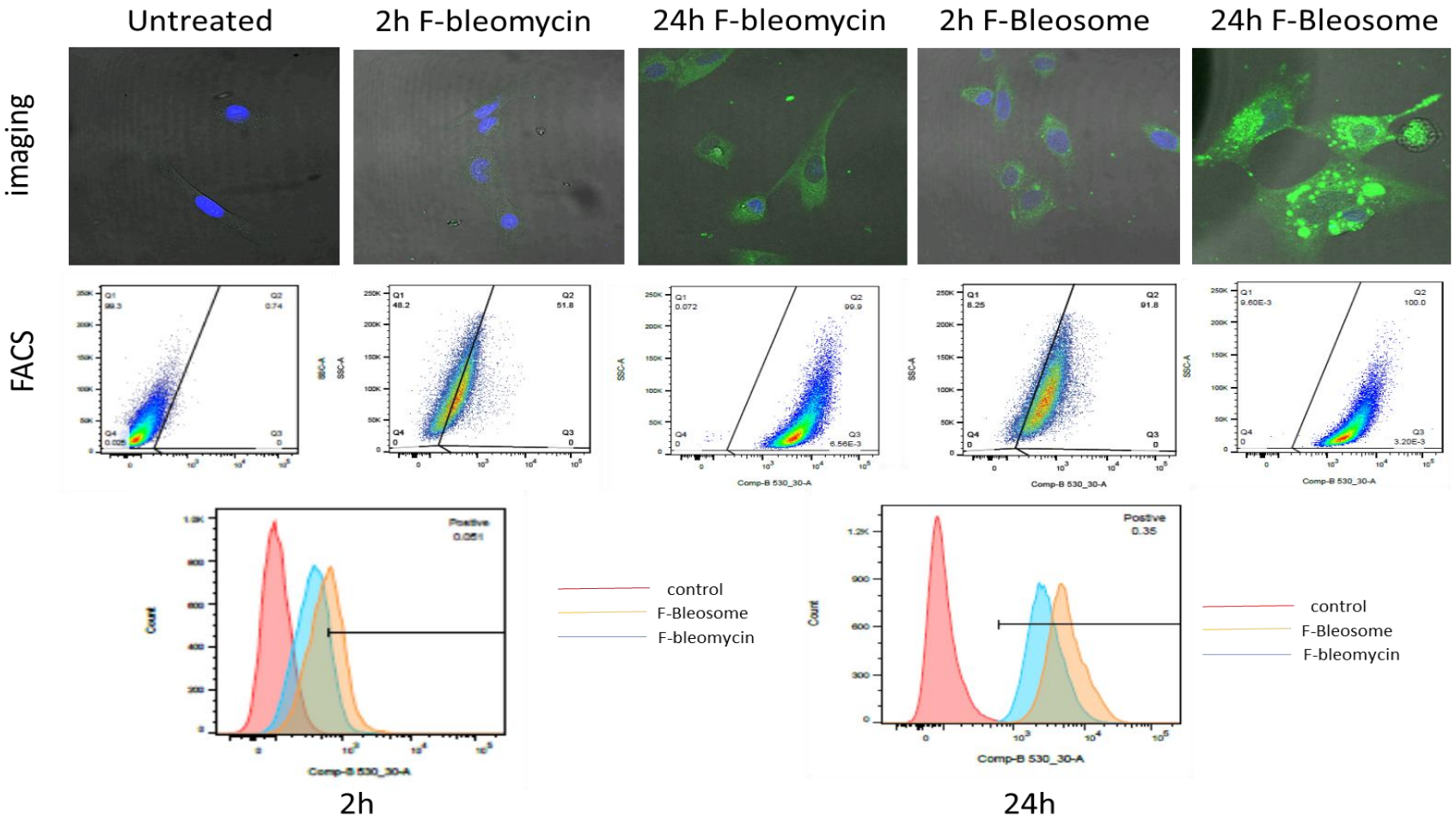

Figure 4.6 *Bleosome is taken up more than free bleomycin in C2 cells. Confocal laser scanning images and respective FACS analysis of C2 cells treated with F-Bleosome and F-bleomycin for 2 and 24 hours. Pictures of C2 cells captured with the confocal airyscan/fastscan microscope with their respective green fluorescence quantification through FACS*

are shown. "Untreated" represents C2 cells not treated with drugs (control), "2h and 24h F-bleomycin" indicates cells treated for 2 and 24 h with F-bleomycin, while "2h Bleosome and 24h F-Bleosome" represents C2 cells treated with fluorescent Bleosome for 2 and 24 hours. Graphs represents the level of green fluorescent within control cells (pink), cells treated with F-Bleosome (orange) and F-bloemycin (blue) after 2 and 24 hours.

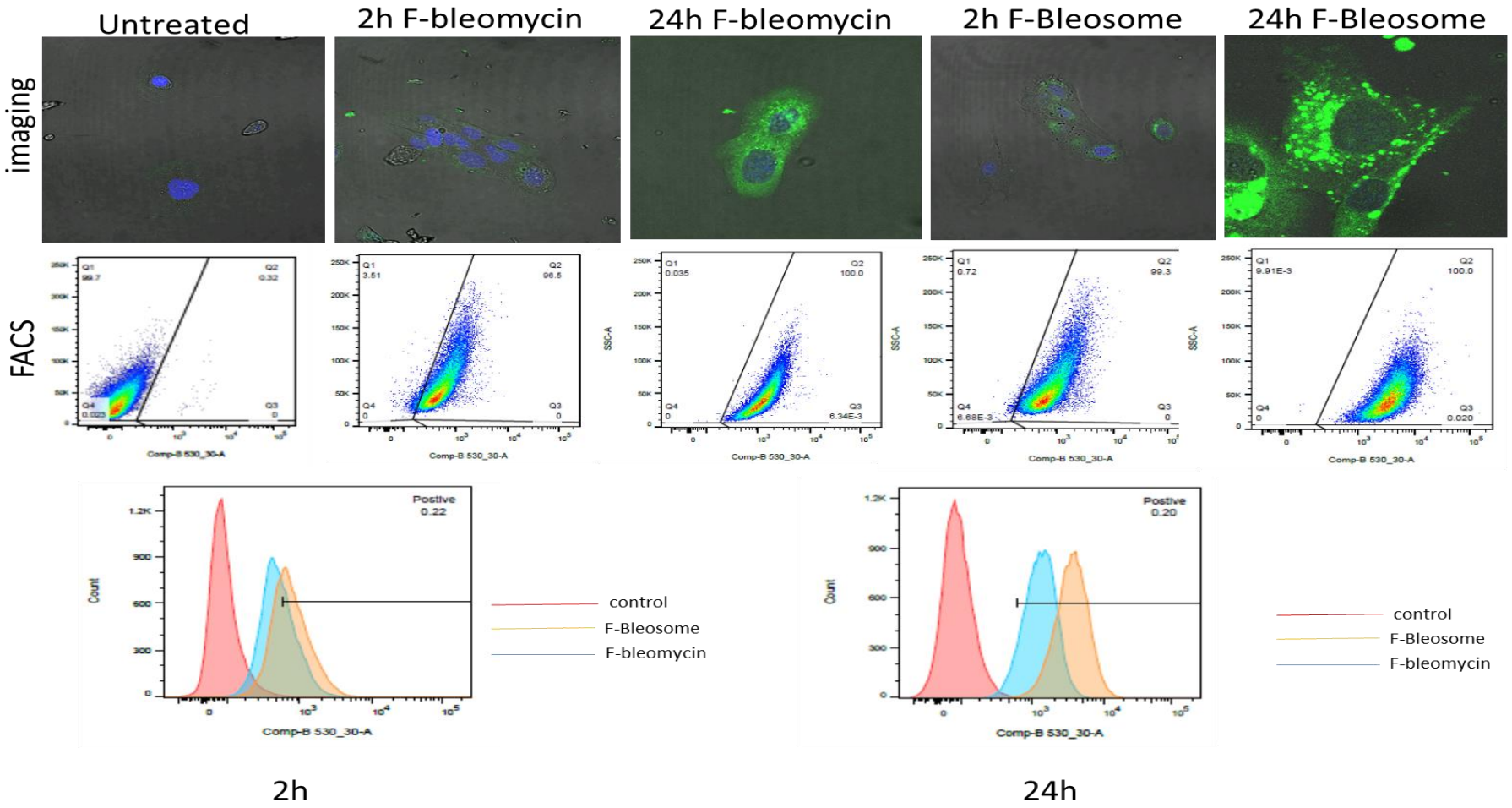

Figure 4.7 *Bleosome is taken up more than free bleomycin by CML10 cells. Confocal laser scanning images and respective FACS analysis of CML 10 cells treated with F-Bleosome and F-bleomycin for 2 and 24 hours. Pictures of CML10 cells captured with the confocal airyscan/fastscan microscope with their respective green fluorescence*

quantification through FACS are shown. "Untreated" represents CML10 cells not treated with drugs (control), "2h and 24h F-bleomycin" indicates cells treated for 2 and 24 hours with F-bleomycin, while "2h Bleosome and 24h F-Bleosome" represents C2 cells treated with fluorescent Bleosome for 2 and 24 hours. Graphs represent the level of green fluorescent within control cells (pink), cells treated with F-Bleosome (orange) and F-bleomycin (blue) after 2 and

Furthermore, the rate of both free and encapsulated drug up-taken by cells increases over time. Figure 4.8 shows that the amount of green fluorescence detected within the two canine cancer cell lines is much higher after 24 hours of treatment than after 2 hours, in both F-Bleosome and F-bleomycin treatment, yet confirming the greater level of F-Bleosome found within both cell lines, compared to the one of F-bleomycin.

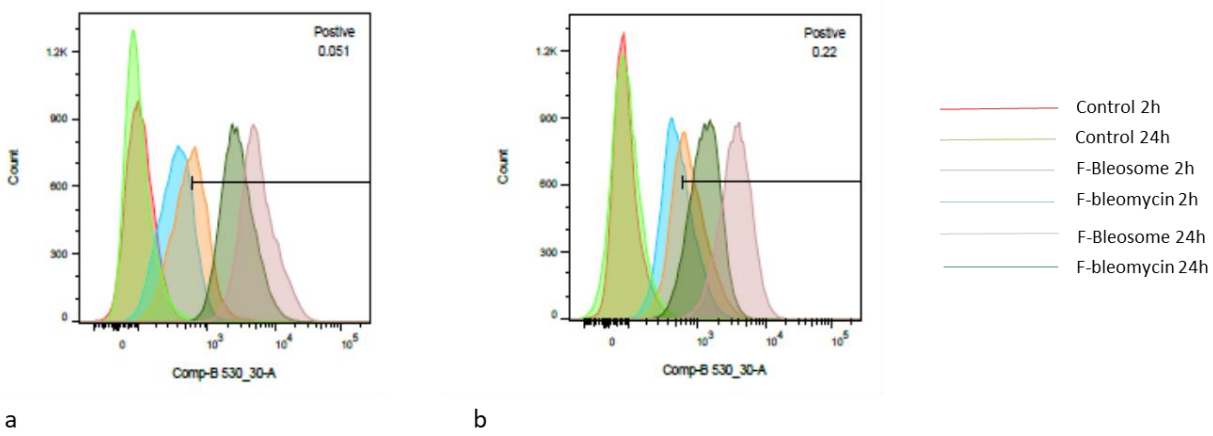

Figure 4.8 *Comparison of green fluorescence intensity detected through FACS between treatments and time points in C2 and CML10 cell lines. (a) represents areas of green fluorescence intensity detected within each time points and treatment in C2 cells: pale green and red areas are the green intensity of the untreated cells. Blue and dark green areas corresapond to F-bleomycin treated cells after 2 and 24 hours respectively; orange and pink areas correspond to F-Bleosome treated cells for 2 and 24 hours respectively. (b) shows areas of green fluorescence intensity detected within each time points and treatment in CML 10 cells: pale green and red areas are the green intensity of the untreated cells. Blue and dark green areas corresapond to F-bleomycin treated cells after 2 and 24 hours respectively; orange and pink areas correspondo to F-Bleosome treated cells for 2 and 24 hours respectively.*

4.4.3 Investigation of the cellular response to Bleosome: exploring the role of DNA DSB and repair mechanisms

We have previously shown that Bleosome is effectively taken up by cancer cells. To further elucidate the cellular response to Bleosome treatment and to investigate the hypothesis of a cell type dependent effect of Bleosome, we evaluated the activation the DNA damage pathways in several cancer cell lines after Bleosome treatment.

Canine, feline and human cell lines were treated with a drug titration of either Bleosome or free bleomycin, and harvested after 4 hours. Firstly, the level of phosphorylation of the histone H2AX (ɣH2AX), which is a marker of DNA DSB, was

evaluated. In all cell lines tested, both Bleosome and free-bleomycin, induced a dose-dependent increase in ɣH2AX and therefore of DNA DSBs (Figure 4.9)

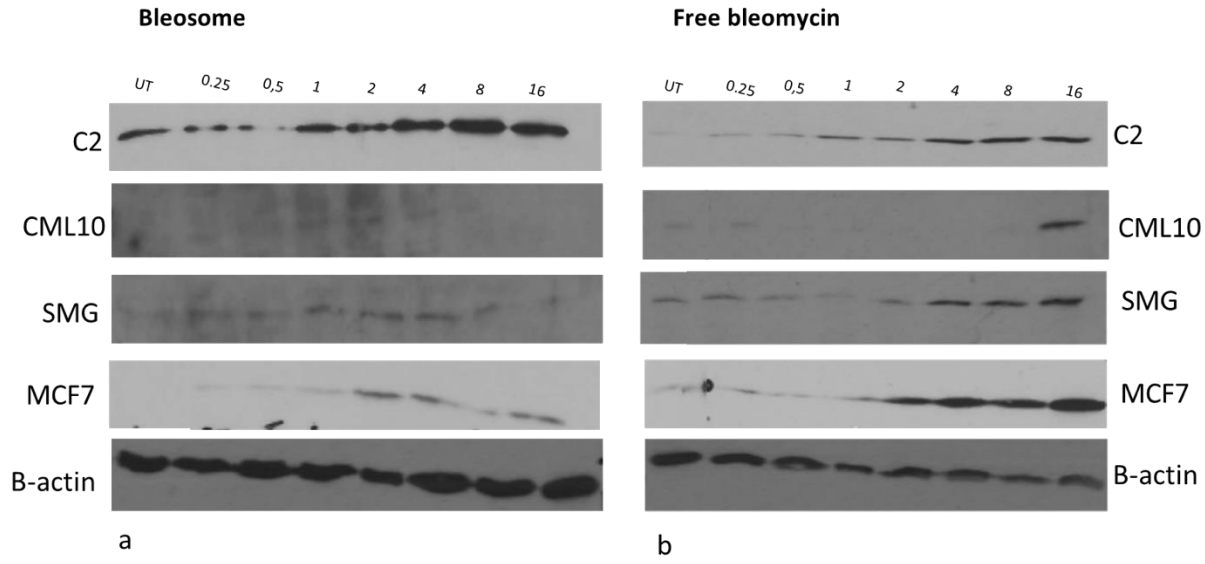

Figure 4.9 *Bleosome and free bleomycin induce DNA DSBs in a dose-dependent manner. Bands relate to the level of Histone ɣH2AX as marker of DNA DSBs Four cancer cell lines: C2 (canine mast cell tumour), CML 10 (canine melanoma),, SMG (feline squamous cell carcinoma), MCF7 (human breast tumour), were treated for 4 hours with the following concentrations: 0.25 µM, 0.5 µM, 1 µM, 2 µM, 4 µM, 8 µM, 16 µM of Bleosome (a) and aqueous form free bleomycin (b). UT represents the untreated control cells. Beta actin band is shown as control.*

We focused on the evaluation of C2 and CML10 canine cells by probing for markers of key pathways involved in the DNA DSB repair machinery including NHEJ and HRR signalling. Key elements in HRR and NHEJ were evaluated at genomic and proteomic level. In the qRT PCR study, we treated C2 and CML10 cells with their respective IC_{50} concentrations of Bleosome (1.56 µM and 3.81 µM) for 2, 4, 8 and 24 hours. Untreated cells were used as control. All the genes, when compared together in statistical analysis, showed a significant difference in their relative expression during the time-course, in both C2 and CML10 ($p \leq 0.000$, two-way ANOVA). Interestingly, figure 4.10 (c) and (d) shows the activation of the HRR pathway in C2, with a peak of expression after 8 hours for Rad51 and after 2 hours for BRCA1; at subsequent time-points, the expression of both genes appeared to slightly decrease. However, the fold changes in the expression level of these two genes in CML10 cells is relatively low and decreased with the time after treatment, indicating that this pathway is not active within canine melanoma cells.

The NHEJ pathways was also differentially activated between the two cell lines tested. After an initial increase and a slight decrease at 8 hours post-treatment, PRKDC level rose in C2 after 24 hours of treatment, while it tended to remain steady in CML10. In contrast, expression of XRCC4 was elevated after 8 hours of treatment but reduced back to basal level by 24 hours post-treatment in the CML10 cell line, whereas in the C2 cell line XRCC4 expression was always low (Figure 4.10 (a) and (b)). Of note, we found interesting differences in the activation of these two DNA-damage repair signalling between the two different canine cancer cell lines tested, suggesting that the mechanism of cellular response to the Bleosome treatment may be cell type-dependent.

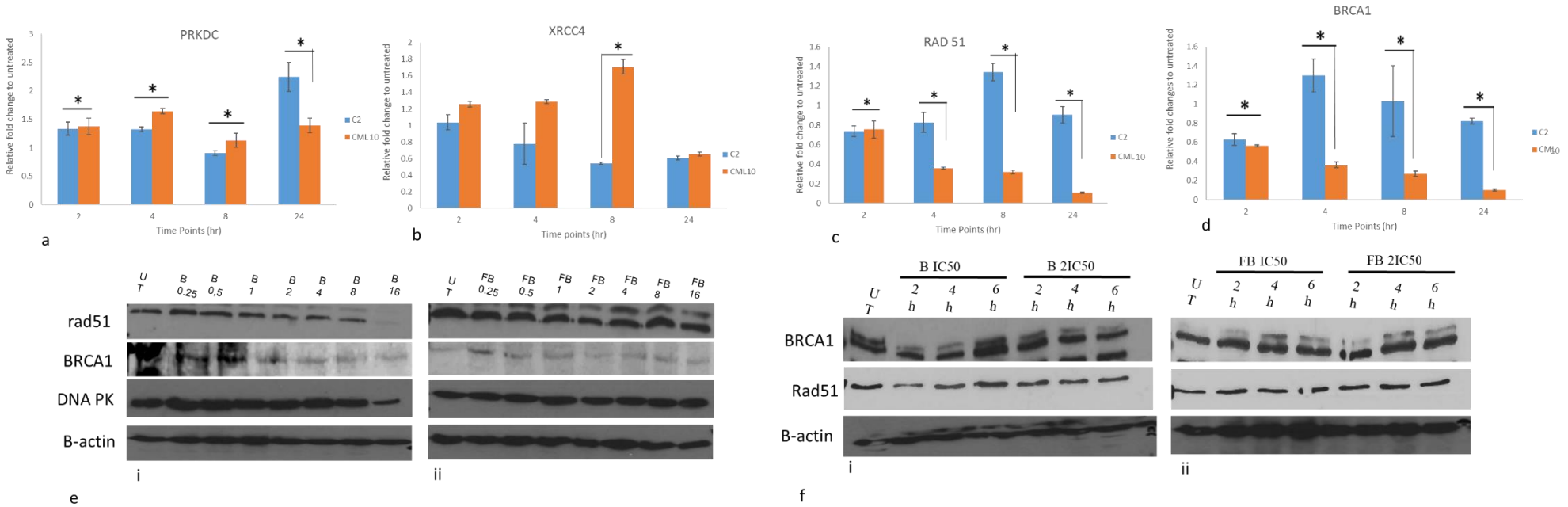

Figure 4.10 *Cell-type dependent activation of DNA damage repair is affected more by the length rather than by the dose of Bleosome treatment. Differences in gene expression of components of NHEJ and HRR evaluated by mean of qRT PCR (a), (b),(c) and (d) and by immunoblotting (e) and (f). (a) and (b) represent graphs of the relative expression of PRKDC and XRCC4 (elements of NHEJ pathways) in C2 (blue) and CML10 (orange) at 2, 4, 8 and 24 hours of Bleosome treatment. (c) and (d) represent graphs of the relative expression of Rad51 and BRCA1 (elements of HR pathways) at 2, 4, 8 and 24 hours. in C2 (blue) and CML10 (orange). Statistical analysis was performed by GLM: two-way ANOVA and Tukey's post-hoc test * represent significant differences ($p<0.05$). (e) Evaluation of activation of HR pathway at protein level in canine mast cell tumour cell line (C2) in response to Bleosome (i) and free bleomycin treatment (ii). Cells were treated with seven growing concentration of Bleosome (B) or free bleomycin (FB): 0.25;0.5;1;2;8 and 16 µM and compared to the untreated cells (UT) as control. BRCA1 indicates the bands corresponding to the BRCA1 protein, Rad51 indicates bands corresponding to Rad51 protein. (f) Evaluation of activation of HR pathway at the protein level in canine melanoma cell line (CML10) in response to Bleosome (B) or free bleomycin (FB). Cells were treated with Bleosome (i) at two different concentration: IC_{50} (B IC_{50}):3.81 µM and the double of the IC_{50} (B $2IC_{50}$): 7.62 µM, for 2, 4 and 6 hours respectively (2h, 4h, 6h); UT represent the untreated control. Column (ii) shows the treatment with free bleomycin aqueous form (FB) at the IC_{50} concentration (FB IC50) (0.68 µM) and the double dose (FB 2IC50) (1.36 µM), for 2, 4, and 6 hours (2h, 4h, 6h). UT represent the untreated control. BRCA1 indicates the bands corresponding to the BRCA1 protein, while Rad51 indicates bands corresponding to Rad51 protein. Beta actin bands are shown as control in (e) and (f).*

To validate our findings, to explore the role of drug concentration and to compare Bleosome treatment with the free bleomycin, we treated C2 cells with a drug titration of Bleosome or free bleomcyin for a total length of treatment of 4 hours, and immunoblotted for key players in the HRR signalling. From PCR analysis, this pathway resulted activated in mast cell tumour cell lines but not in the melanoma ones (figure 4.10 (a), (b), (c), (d)). For this reason, the protein levels of RAD51and BRCA1 were evaluated over different concentration of both chemotherapeutics, and C2 cells revealed that these proteins were not much affected by the increase of concentration of both encapsulated and free bleomycin. Figure 4.10 (e) illustrates how the intensity of the bands from RAD51 and BRCA1 slightly increased at the increase of bleomycin and Bleosome dose to slightly decrease at higher doses; however, the variation of the intensity of the relative bands are minimal, indicating that the timing rather than the concentration of treatment is crucial for the activation of the pathway.

Moreover, to further confirm the non involvement of the HRR pathway in the cellular response of CML10 cells to the Bleosome treatment, we treated the canine melanoma cell line with two doses of Bleosome corresponding to the IC_{50} (3.81 µM) and twice the IC_{50} (7.62 µM) as previously determined, or the equivalent of bleomycin (0.68 and 1.36 µM respectively) and harvested over a time course of 2,4 and 6 hours. This allowed assessment of the levels of RAD51 and BRCA1 proteins at both increasing of doses and time points of treatment. Figure 4.10 (f) shows that the basal level of both proteins was unchanged compared to the untreated cells and over time, irrespective of dose or form of the drug. These findings suggest that the overall level of components of HRR and NHEJ are not strictly dependent on Bleosome concentration, but rather on the timing of treatment and that the cellular response to Bleosome is likely cell-type dependent.

4.4.4 Exploring the molecular response to Bleosome in CML10 cells by RNA sequencing over a time-course

We showed that the DNA repair pathways were differentially activated in two different canine cancer cell lines and that the level of proteins was affected more by the time of treatment rather than the concentration of the drug. Hence, after having

focused on the main pathways underlying DNA repair, our further aim was to have a more comprehensive understanding of the molecular mechanisms triggered by the Bleosome treatment within these cancer cell lines, to find out whether other signalling could play a key role in the treatment response. To this extent, we treated CML10 and C2 cell lines with the respective Bleosome IC_{50} for 8 and 24 hours, and performed next generation sequencing (NGS) comparing the relative gene expressions to the untreated cells of both cancer cell lines.

4.4.4.1 Quality analysis of RNA-sequencing data

RNA-Sequencing generated a total reads pairs, after trimming, between 74 and 104.3 million paired-end reads and around 80% of the reads were mapped to the canine genome.

Principal Component Analysis (PCA) was used as a type of clustering to check the quality of RNA-seq data in the three pairwise comparisons. PCA represents a plot of the RNA samples in which distances correspond to leading log-fold-changes between each pair of RNA samples, and it is considered, therefore, the clustering algorithm of choice to predict the relatedness of samples based solely on differential gene expression (Gerst and Hölzer 2018). PCA analysis of the expression profiles of C2 cells (untreated vs treated for 8 hours vs treated for 24 hours) revealed that the biological replicates did not cluster together according to the time point of treatment, but were randomly allocated within the PCA plot (data not shown). This finding indicated that C2 cells treated with Bleosome over a time course of treatment were highly heterogeneous and not optimal for drowning significant conclusion with this genetic study. For this reason, C2 cells were excluded from the analysis. Figure 4.11 illustrates how the three biological replicates for each group of CML10 cells (untreated, cells treated for 8 hours and cells treated for 24 hours) formed a homogeneous cluster and were clearly separated from each other in all the three components of the PCA plot. For these reasons, following analysis were performed on CML10 cells only.

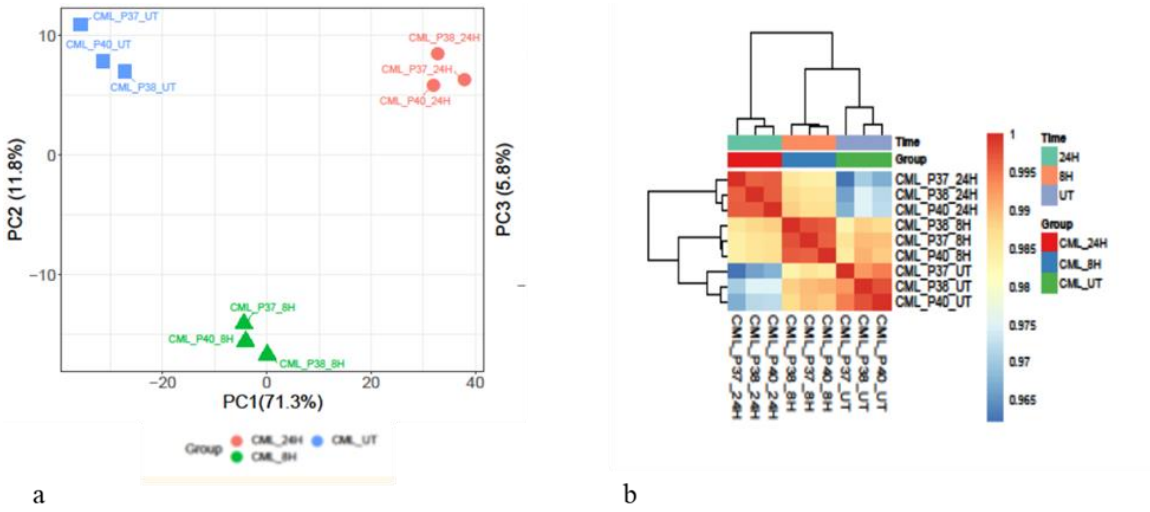

Figure 4.11 *Exploratory analysis of CML10 cells. (a) Plots of the first, second and third components from principal components analysis (PCA) using all CML10 samples. (b) Heatmap and hierarchical clustering dendograms illustrating clustering of samples by filtered and normalised expression values for all CML10 samples. Figures were generated with the 'pheatmap' package.*

4.4.4.2 Differential expression gene analysis

In the differential expression gene analysis, genes above a minimum 2-fold change difference and below the maximum level of false discovery rate (FDR) of 0.05 were considered. These thresholds were set to give statistical robustness to the data and to produce significant results. Within the analysis, three contrasts were considered: 1) comparison between CML10 cells treated for 8 hours with Bleosome and CML10 cells untreated (CML_8H vs CML_UT), here 365 genes were found differentially expressed, 221 of which were upregulated and 144 downregulated. 2) Comparison between CML10 cells treated with Bleosome for 24 hours and CML10 cells untreated (CML_24H vs CML_UT), where the majority of differentially expressed genes were found. In this contrast, 766 genes showed to be upregulated, against 1025 genes downregulated, for a total of 1791 genes. 3) Comparison between CML10 cells treated with Bleosome for 24 hours and 8 hours (CML_24H vs CML_8H), in this group there were 345 genes upregulated and 488 genes downregulated (table 4.8 and figure 4.12).

Contrast name	Up	Down
Group: CML_8H vs CML_UT	221	144
Group: CML_24H vs CML_UT	766	1,025
Group: CML_24H vs CML_8H	345	488

Table 4.8 *Table of statistics showing numbers of differentially expressed genes in each contrast according to the threshold on minimum fold-change (2) and maximum FDR (0.05).*

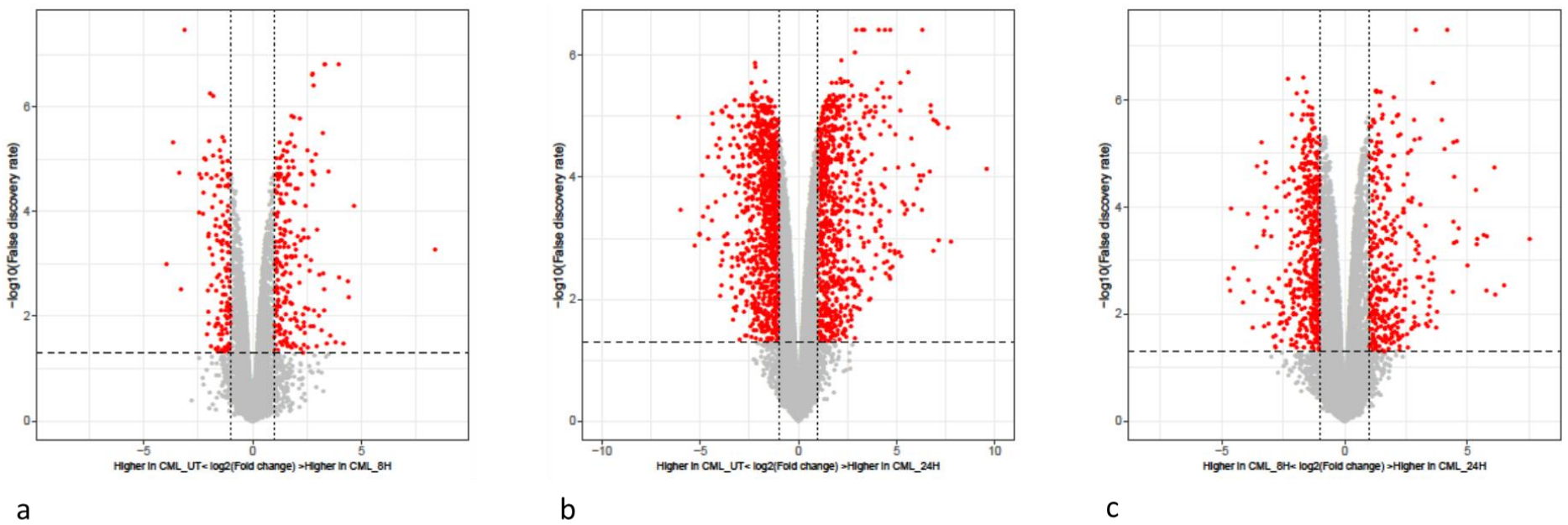

Figure 4.12 *Differential plots for specified contrasts. Volcano plots illustrate log(2) fold change vs –log(10) false discovery rate (FDR) between groups, with FDR calculation adjusted for passage. The horizontal dashed line represents the specified FDR threshold for significance (0.05), dotted lines represent the specified fold change threshold (2) in both the positive and negative directions. Point passing both thresholds are colored red. (a) represents volcano plot related to the comparison between cells untreated and treated with Bleosome for 8 hours, (b) is the comparison between CML10 cells untreated and treated for 24 hours, (c) is the volcano plot related to the comparison between CML10 cells treated for 8 and 24 hours.*

4.4.4.2.1 Different gene expression profile of CML10 cells treated with Bleosome for 8 hours compared to untreated cells

Within the group including the comparison between cells treated with Bleosome for 8 hours and untreated cells, a heatmap was generated including the top 50 most differential genes according to FDR value (figure 4.13). Hierarchical clustering analysis confirmed the distinction in gene profiles between cells treated for 8 hours with Bleosome compared to untreated cells. Of note, the heatmap shows that among the 50 most differentially expressed genes, 33 genes were upregulated and 17 downregulated in the melanoma cells treated for 8 hours. Interestingly, when we interrogated the details of the differentially expressed genes, many of the genes upregulated following the Bleosome treatment, were involved in cellular growth and proliferation signalling (RAB20, FOSL1, PLIN2, TNFAIP3, EGR2, JUN, ATF3). Moreover, we found also key players in inflammatory response, such as TNFα induced protein (TNFAIP3) and the early growth response protein 4 (EGR4), which is supposed to play a role in the downstream signalling in naïve CD8+ T-cells, or the interferon regulatory factor 5 (IRF5). However, we also found genes involved in anti-proliferative processes, such as BTG2 or DUSP5, which block the activation of MAP kinase pathway, indicating that, after 8 hours of treatment, cells, that survived the treatment, may trigger anti-mitotic cellular signalling. Looking at the genes that were downregulated following the chemotherapeutic treatment, most of them are involved in metabolic (LIPG, MSMO1, INSIG1) and endocytosis processes (LDLR), highlighting the metabolic activity of untreated cancer cells.

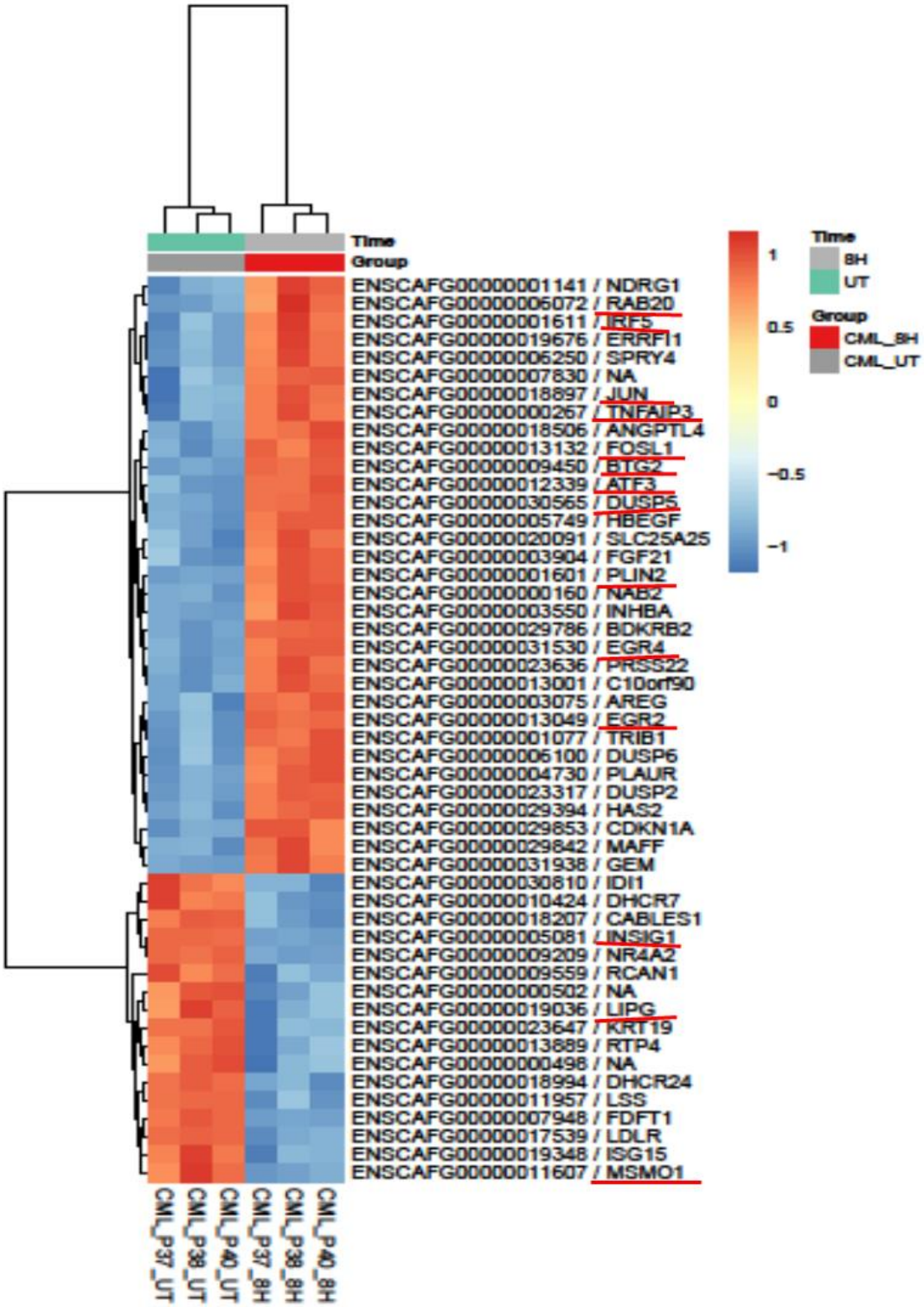

Figure 4.13 *Heatmap showing the top 50 most differential genes by false discovery rate (FDR) between CML10 cells treated with Bleosome for 8 hours and the untreated cells, with the FDR calculation adjusting for passage. Figure was generated with the 'pheatmap' package. Factor variables from the experiments are highlighted above each plots and key genes discussed in the text are highlighted in red.*

4.4.4.2.2 Different gene expression profile of CML10 cells treated with Bleosome for 24 hours compared to untreated cells

The heatmap related to the contrast between cells treated for 24 hours and the untreated, including the 50 most differentially expressed genes, revealed again two distinct clusters formed by melanoma cells treated for 24 hours and by the untreated cells (figure 4.14). 24 hours of Bleosome treatment triggered the upregulation of many genes involved in inhibition of cell growth and angiogenesis (DUSP5, DUSP2, SPRY2, THBS2), to a greater extent than the 8 hour time point, suggesting that, after 24 hours of treatment, cells are no longer able to proliferate and divide properly. This finding was confirmed also by the overexpression, in the same cluster, of CDKN1A, which is supposed to play a main role as a cell cycle inhibitor. Similarly, to the earlier time point, in 24 hours-treated cells signals of inflammatory response, such as interferon regulatory factor 5 (IRF5), were also found, along with genes responsible of remodelling the extracellular matrix (PLAUR), indicating a key role of the tumour microenvironment. Interestingly, when the downregulated cluster of genes within the treated cells group was interrogated, many regulators of cell cycles and chromosome stability were present. NUF2 and ASPM are involved in regulation of cell cycle and normal function of mitotic spindle formation, suggesting that Bleosome treatment affects the ability of the cells in undergoing mitotic division.

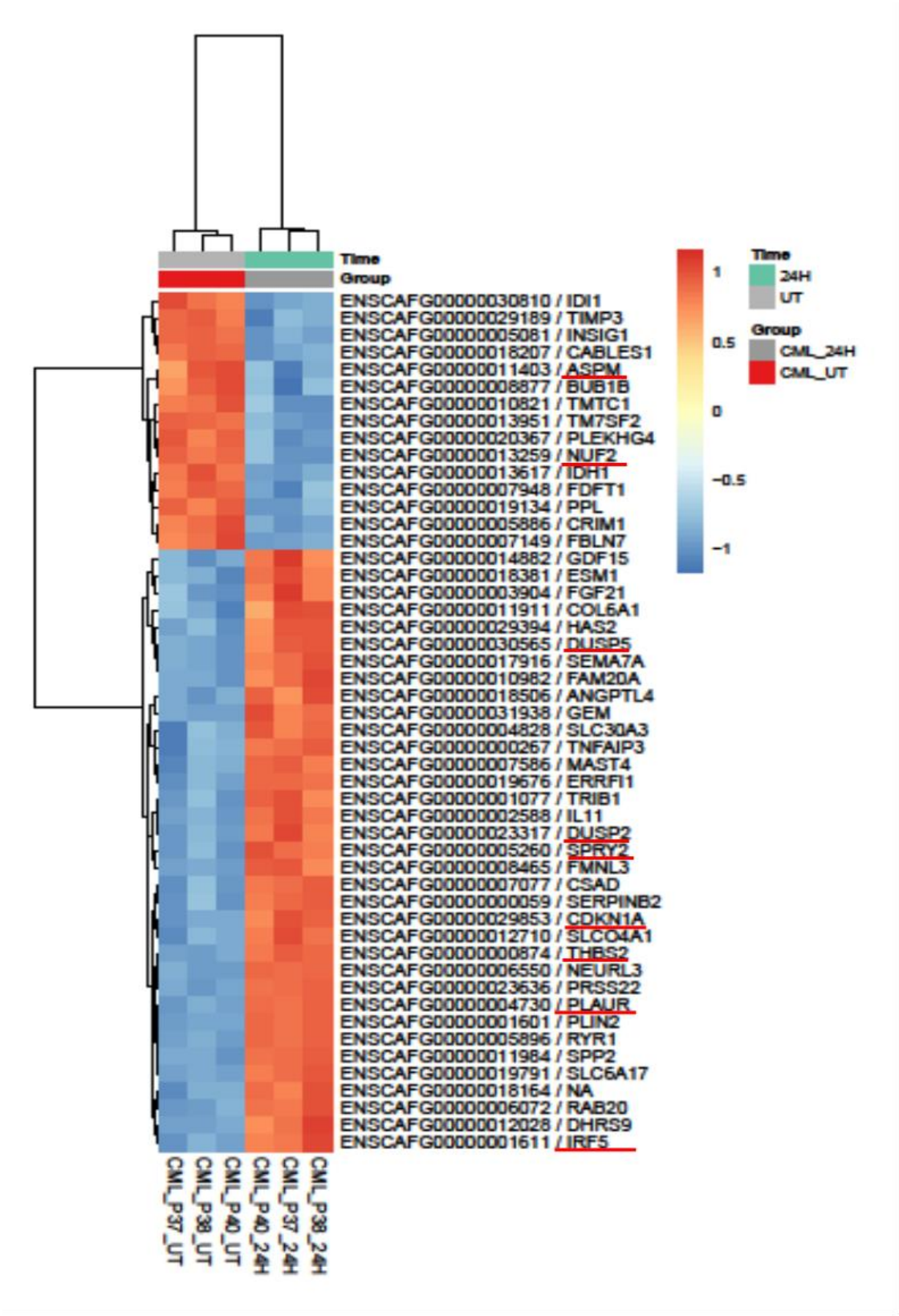

Figure 4.14 *Heatmap showing the top 50 most differential genes by false discovery rate (FDR) between CML10 cells treated with Bleosome for 24 hours and untreated cells, with the FDR calculation adjusting for passage. Figure was generated with the 'pheatmap' package. Factor variables from the experiments are highlighted above each plots and key genes discussed in the text are highlighted in red.*

4.4.4.2.3 Different gene expression profile of CML10 cells treated with Bleosome for 24 hours compared to cells treated for 8 hours

.

Figure 4.15 relates to the heatmap generated by the 50 most differentially expressed genes in the contrast made by cells treated for 24 and 8 hours. There was a distinct separation of genetic profiling between the two time points of treatment, as confirmed by the hierarchical clustering analysis. Again, when the fold-change expression was evaluated, genes were subdivided in two clusters: one included 22 genes upregulated in cells treated with Bleosome for 24 hours compared to the earlier time point of treatment, while the second cluster contained 28 genes downregulated in cells following 24 hours of treatment compared to 8 hours post-treatment. In the longer time point of treatment, signal of chromosome stability (CENPE) and regulator of cellular mitosis (NUF2), still present after 8 hours of treatment, were downregulated. Genes related to inhibition of cellular proliferation and migration (HYAL1 and ARNT2) and transport of cations (SLC6A17, SLC30A3) were upregulated after 24 hours of treatment, compared to earlier time point, suggesting that the duration of treatment may play a role in regulating cell cycle arrest following the Bleosome treatment.

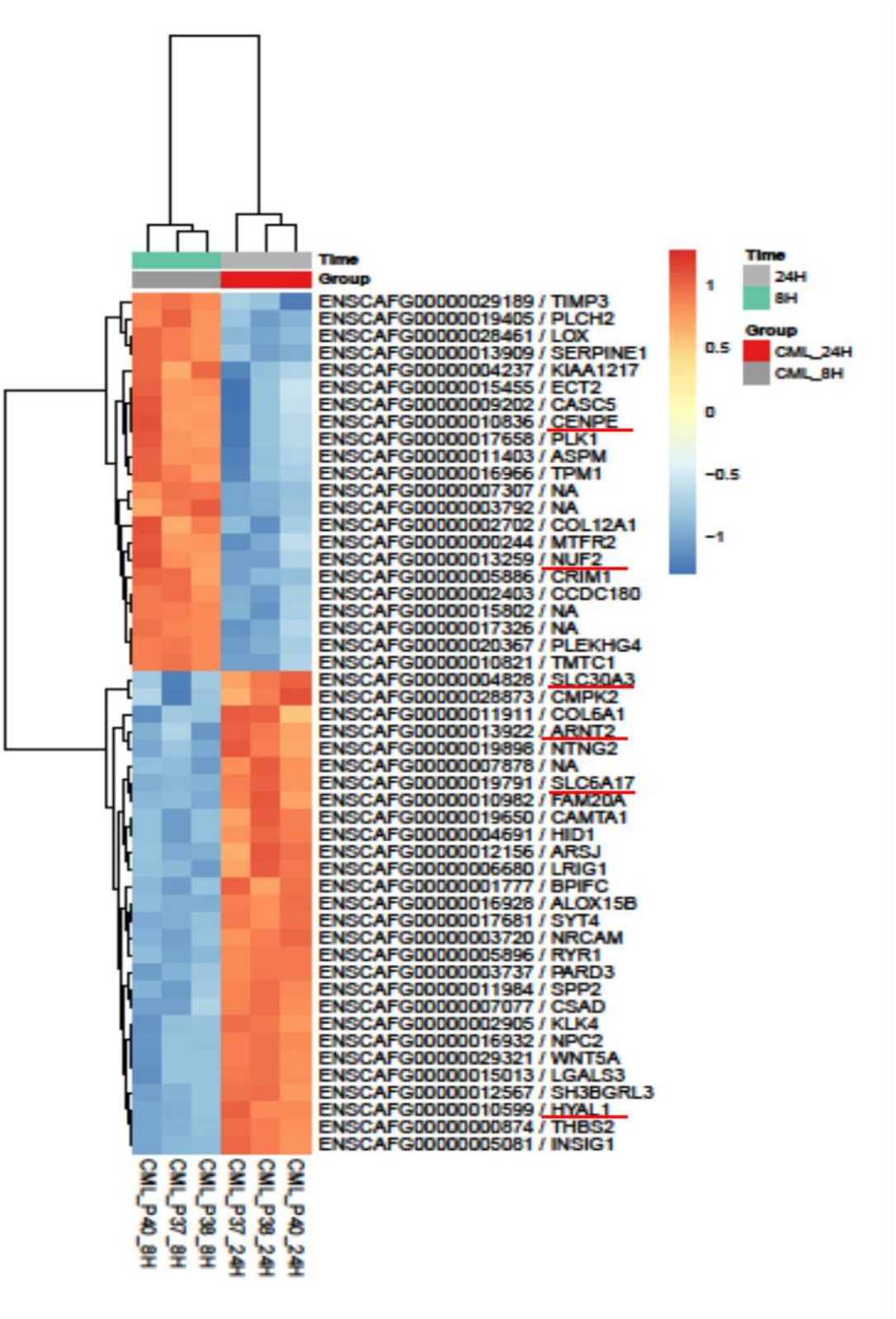

Figure 4.15 *Heatmap showing the top 50 most differential genes by false discovery rate (FDR) between CML10 cells treated with Bleosome for 24 and 8 hours., with the FDR calculation adjusting for passage. Figure was generated with the 'pheatmap' package. Factor variables from the experiments are highlighted above each plots and key genes discussed in the text are highlighted in red.*

4.4.4.3 Functional annotation

To further consider the biological significance of these data, GSEA was used to identify upregulated and downregulated pathways correlating to the three comparisons: CML10 cells treated with Bleosome for 8 hours and CML10 untreated; CML10 treated for 24 hours and untreated cells; CML10 cells treated for 24 hours and for 8 hours. For accuracy and reproducibility, analysis was repeated using also Reactome tool and Ingenuity Pathway Analysis (IPA) (data not shown). Results from the three software programs were consistent. Furthermore, GSEA was also used to highlight biological processes involved within the differential expressed genes between the comparisons. Pathways and biological processes with FDR<0.05 were considered as significant.

4.4.4.3.1 Dysregulated pathways between CML10 treated with Bleosome for 8 hours compared to untreated control

GSEA revealed 47 upregulated and 81 downregulated pathways in cells treated with Bleosome for 8 hours when compared to the untreated cells. Of note, Bleosome treatment triggered various immune response signalling within melanoma cancer cells. Figure 4.16 (a) illustrates the plethora of toll-like receptors cascade, along with the activation of myeloid differentiation primary response pathway (MyD88), which activates the transcription factor NF-κB and is involved in signalling within immune cells. Moreover, mechanisms of recruitment of cytokines and interleukins were also upregulated. Interestingly, in cells treated for 8 hours, mitogen activated protein kinase (MAPK) and the phosphoinositide 3-kinase (PI3K) signalling were still active. Considering the upregulated biological processes, GSEA found 17 upregulated processes (supplementary data 8.2.6, figure 8.1), all involved in the inflammatory and immune responses, cellular growth and migration. Interestingly, following the Bleosome treatment, there was a downregulation of chromosome maintenance and of several mechanisms involved in the mitotic process (including cell cycle checkpoint, mitotic prometaphase and anaphase, separation of sister chromatids). However, within the downregulated pathways, an interesting finding was the presence of mechanisms implicated in the arrest of DNA synthesis and replication and in the downregulation

of various DNA DSB repair signalling. Moreover, pathways involved in metabolism of lipids were also downregulated, suggesting the progressive arrest of cellular activity and of their metabolism. Twenty-four biological processes were found downregulated in this contrast and confirmed the results of the pathway analysis (supplementary data 8.2.6, figure 8).

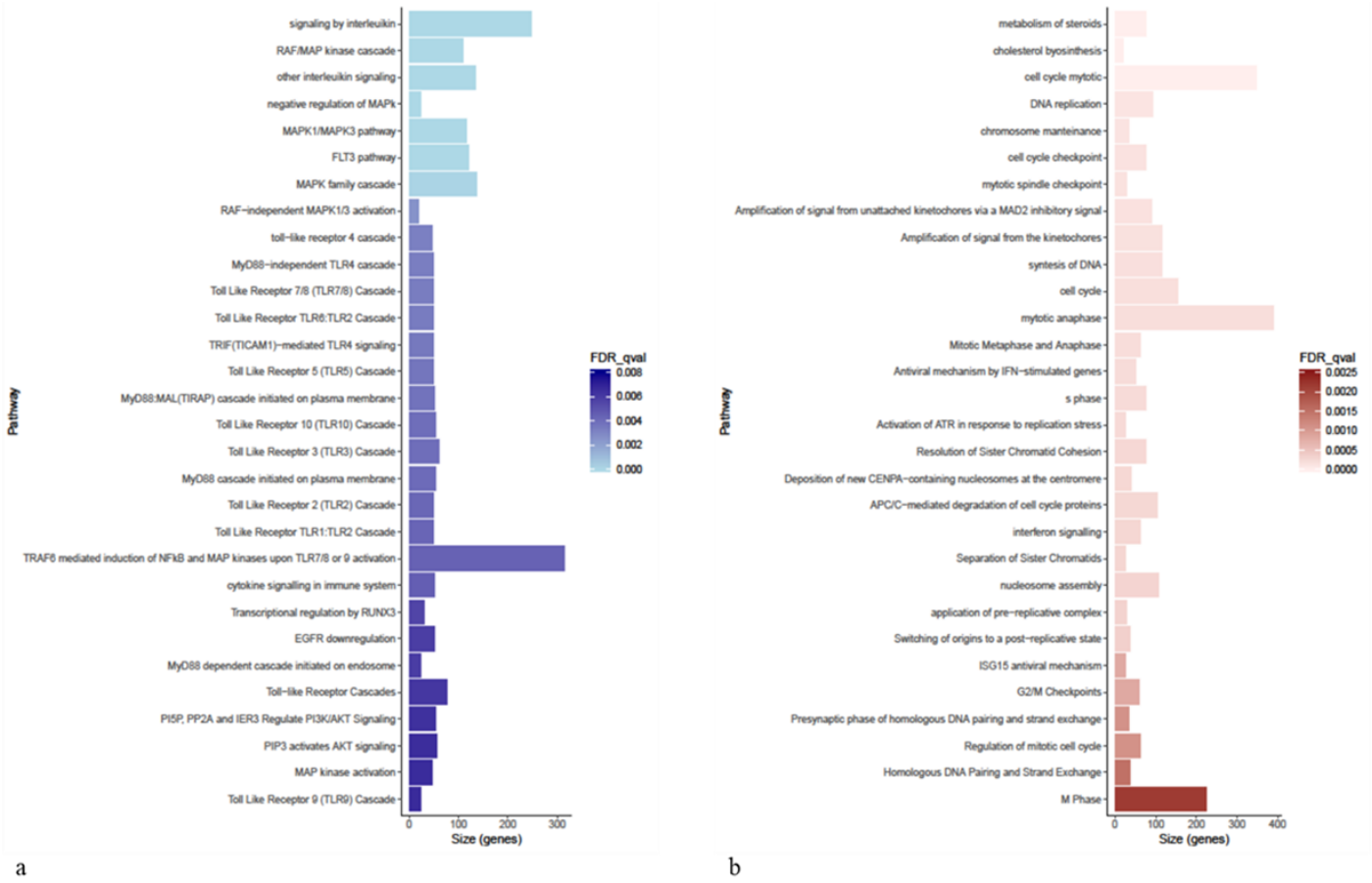

Figure 4.16 *Top 30 most significant (according to FDR<0.05) upregulated (a) and downregulated (b) pathways between CML10 cells treated with Bleosome for 8 hours and CML10 cells untreated. Analysis were performed using gene set enrichment analysis (GSEA) software.*

4.4.4.3.2 Dysregulated pathways between CML10 treated for with Bleosome for 24 hours compared to untreated control

Pathway analysis of the contrast between CML10 cells treated for 24 hours and untreated highlighted 52 upregulated and 117 downregulated pathways (figure 4.17). Incubation of CML10 cells for 24 hours with Bleosome triggered the upregulation of signalling pathways similar to the earlier time point. Of note, immune response mechanisms were highly represented, with the activation of several types of Toll-Like receptor cascades, MyD88 pathway, recruitment of interleukin and cytokines and, interestingly, also with the dysregulation of B-cell receptors. As reported in the previous comparison, MAPK pathway was also activated in melanoma cells after 24 hours of treatment. Here, the expression of genes associated with the autophagy process are upregulated, suggesting that autophagy is a potential mechanism of cell-death induced by the Bleosome treatment. When considering biological processes, GSEA found only two positive regulated functions, according to the FDR threshold (<0.05). However, ranking the first 30 most significant biological processes according to crescent FDR, it was interesting to note how, other than the same signalling pathways indicated in the initial pathway analysis, transport of different types of ions was a recurrent mechanism, along with the regulation of intracellular pH and the response to amyloid beta. These pathways are related to the promotion of tumour microenvironment, which appear to have a key role within this type of cancer, especially during stress condition caused by the treatment with Bleosome. Interestingly, along with the downregulated pathways, gene set enrichment analysis revealed also 117 negatively regulated biological processes (supplementary data 8.2.6, figure 8.2). According with what found in the earlier time point, also here, both pathways and biological processes were concordant and identified the arrest of cell division, with the affection of mitotic processes, DNA synthesis and chromosome stability, as major elements. Furthermore, from the data, it appeared that cells were unable to repair the damaged DNA by DNA DSB-repair mechanisms

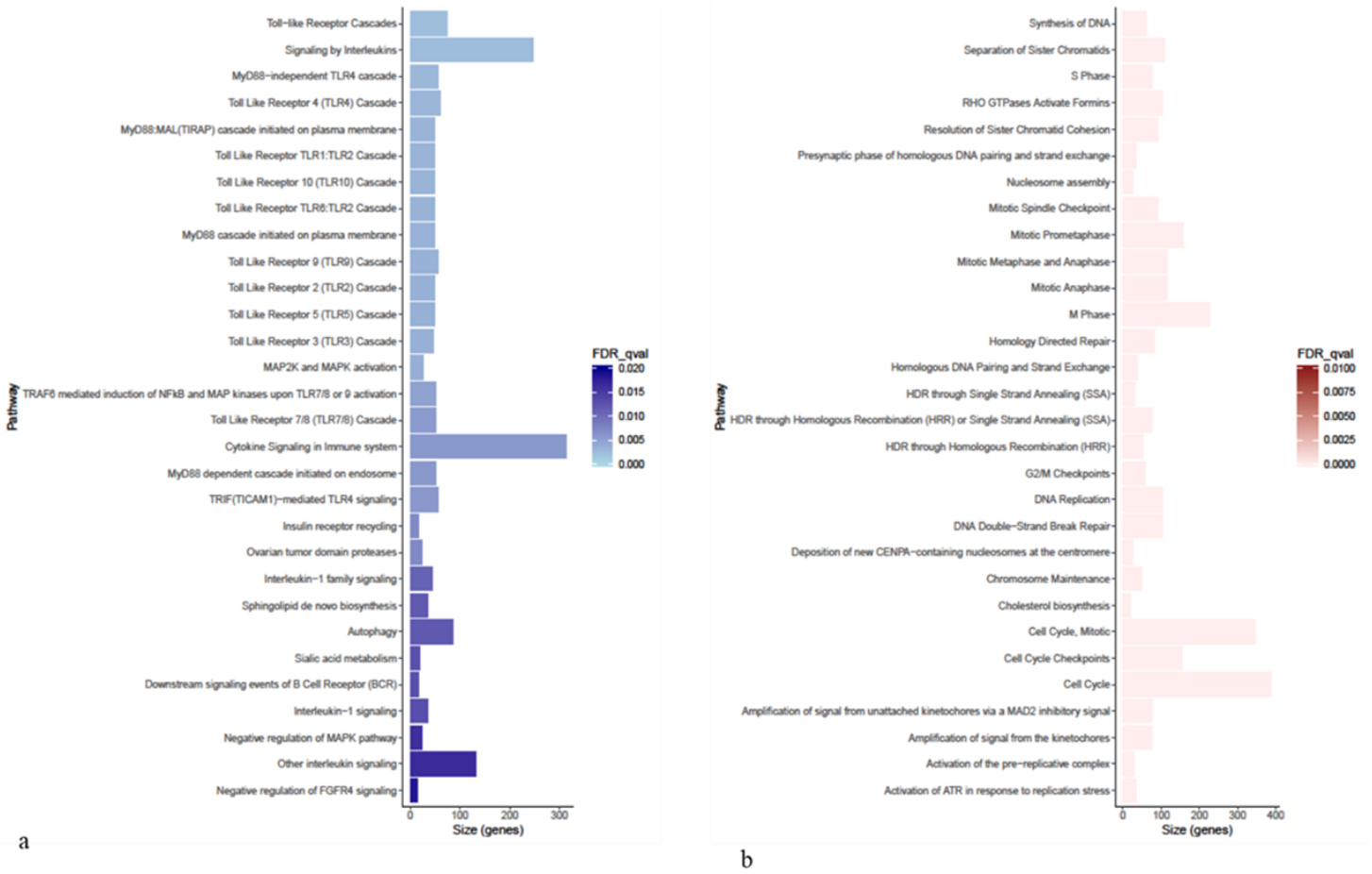

Figure 4.17 *Top 30 most significant (according to FDR<0.05) upregulated (a) and downregulated (b) pathways between CML10 cells treated with Bleosome for 24 hours and CML10 cells untreated, Analysis were performed using gene set enrichment analysis (GSEA) software*

4.4.4.3.3 Dysregulated pathways between CML10 treated with Bleosome for 24 hours compared to cells treated for 8 hours

Here we compared CML10 cells treated with Bleosome for 24 hours to cells treated with Bleosome for 8 hours. Differences in gene expression profiles were investigated with GSEA and showed that 35 pathways were upregulated and 117 downregulated after 24 hours' time point, compared to the 8 hours' time point (figure 4.18). Interestingly, after 24 hours, cells upregulated mechanisms involved in translational initiation and protein phosphorylation (Cap-dependent translation initiation, formation of a pool of free 40S subunits, ribosomal scanning and start codon recognition). Signals of cell growth and migration were still present (MAPK, m-TORc, EPHB), along with upregulation of transport of ions and small molecules. Interestingly, after 24 hours of treatment, pathways associated with autophagy (microautophagy and macroautophagy) were upregulated, similarly to what was observed in the previous comparisons (section 4.4.4.3.2). Moreover, pathways associated with the production of ROS and RNS were upregulated as a consequence of the Bleosome effect. Just one upregulated biological process was found below the FDR threshold (0.05), however, if considering the 29 following biological processes, according to FDR values, results were concordant with pathway analysis, highlighting also the recruitment of macrophages and the involvement of interferon-gamma as part of cellular response to the treatment (supplementary data 8.2.6, figure 8.3). The study of the most significantly downregulated pathways suggested, according to results of previously analysed contrasts (4.4.4.3.1 and 4.4.4.3.2), that cells had impaired cell cycle functions after 24 hours of Bleosome treatment. Moreover, again, several mechanisms of DNA DSB repair were downregulated, indicating how it is unlikely that cells are able to repair the DNA damage produced by the Bleosome treatment. The evaluation of thirty-one significantly downregulated biological processes revealed results consistent with pathway analysis (supplementary data 8.2.6, figure 8.3).

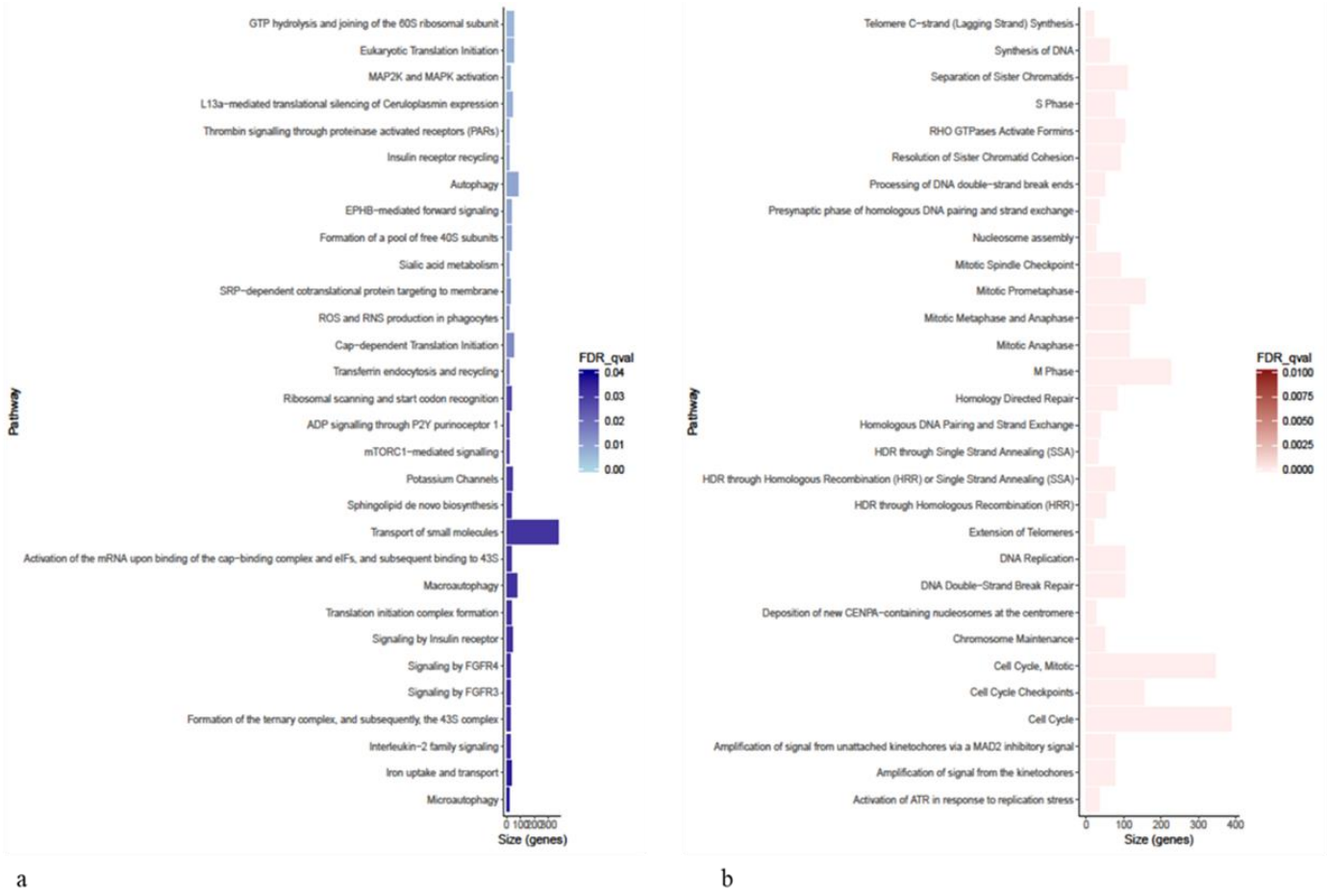

Figure 4.18 *Top 30 most significant (according to FDR<0.05) upregulated (a) and downregulated (b) pathways between CML10 cells treated with Bleosome for 24 hours and CML10 cells treated with Bleosome for 8 hours, Analysis were performed using gene set enrichment analysis (GSEA) software*

4.4.5 Investigating the role of bleomycin hydrolase (BLMH) after Bleosome treatment

A further aim was to focus in particular on the investigation of the role of bleomycin hydrolase (BLMH) in response to Bleosome treatment. To this extent, we evaluated the presence of the enzyme at the cellular level, treating several cancer cells with either Bleosome or free bleomycin and compared results to the untreated cells. Furthermore, we explored the role of the enzyme also at the tumour level, analysing immunohistochemical slides from equine sarcoids and equine healthy skin treated with Bleosome, and we compared them to their respective untreated counterparts.

4.4.5.1 Evaluation of the role of BLMH in the response to Bleosome treatment at the cellular level

Canine cancer cells (C2 and CML10), feline squamous cell carcinoma (SMG) and human breast cancer cells (MCF7) were treated with either a drug titration of Bleosome or free bleomcyin for 4 hours and immunoblotted for BLMH antibody (figure 4.19 (a) and (b)). The total basal protein level of the enzyme was comparable among the four cancer cell lines from three different species. The band corresponded to BLMH, after treatment with either Bleosome or bleomycin, had a steady intensity over the drug titrations and when compared to relative untreated cells of each cell lines, indicating that the enzyme might not be affected by the drug treatment. Only in CML10 cells, there was a slight decrease in the intensity of the relative band, at increasing drug dose. However, it is interesting to note that a second close paler band was always present at a slightly higher molecular weight of the BLMH protein. We speculate that this represents a post-translationally modified version of BLMH, which may be biologically active.

We explored the BLMH gene expression by quantitative real-time PCR over a time course of Bleosome treatment of 2, 4, 8 and 24 hours. C2 and CML10 canine cancer cells were treated with respective IC_{50} concentrations of Bleosome (1.56 µM and 3.81 µM). Again, BLMH expression was consistent during the indicated time course and there was no significant change in expression compared to the untreated cells.

Moreover, statistical analysis (two-way ANOVA and *Fishers's post-hoc* test) revealed no significant difference in the gene expression between the C2 and CML10 cell lines (Fig 4.19 (c)).

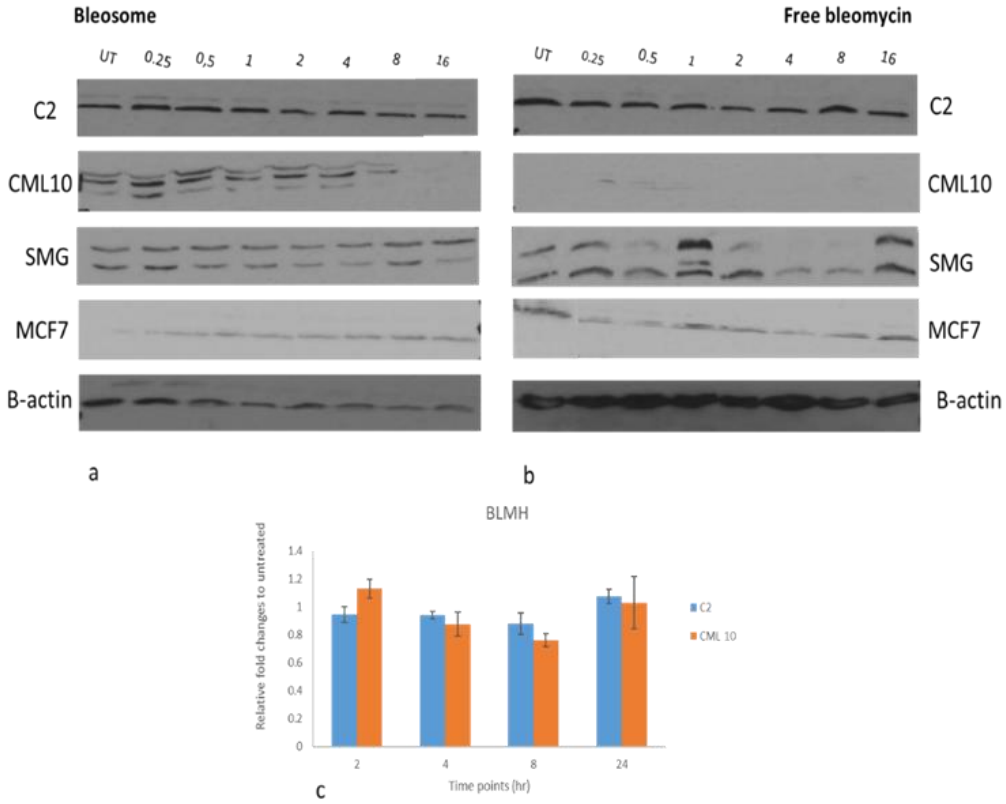

Figure 4.19 *Evaluation of bleomycin hydrolase (BLMH) protein after Bleosome (a) and free bleomycin (b) treatments and comparison of BLMH gene expression in C2 and CML10 cells after Bleosome treatment (c). C2, CMl10, SMG, MCF7 cells were treated with 0.25, 0.5,1, 2, 4, 8, 16 µM of Bleosome (a) and free bleomycin (b) for 4 hours and relative levels of BLMH protein are shown. UT represents cells untreated and beta actin bands are shown as control. (c) illustrates the relative expression of BLMH gene in C2 (blue columns) and in CML10 (orange columns) after 2, 4, 8 and 24 hours of treatment with relative Bleosome IC_{50s} (3.81 and 1.56 µM).Statistical analysis were performed with GLM: 2-way ANOVA and post-hoc Fisher's test.*

4.4.5.2 Evaluation of the role of BLMH in the response to Bleosome treatment at the tumour level

To further investigate if Bleosome treatment increases the protein level of BLMH within the context of a tumour, we performed an immunohistochemistry (IHC) study, using an antibody to BLMH on three different types of equine sarcoids and on healthy equine skin sections. They aim was to evaluate whether Bleosome treatment induces BLMH within tumour models and skin, using live samples. Each sarcoid and skin

section were treated with Bleosome for 6 hours and compared to their respective untreated counterpart. Evaluation of each tumour/ skin was made averaging three technical replicates for statistical robustness and results validation.

An endogenous negative control for each sample was used and represented by a slide of the lesion or the skin not stained with the antibody anti-BLMH. Furthermore, an equine melanoma was used as positive control for the antibody staining (supplementary data 8.2.7, figure 8.4). This latter was particularly important not only to assess the efficacy of the antibody, but it also highlighted the difficulty in distinguishing between the melanin pigments and the colour of the antibody staining. For this reason, a Vector Red chromogen (Impact Nova Red Vector SK-4805) was used to visualise positive antibody-staining in red, rather than in brown, to differentiate it clearly from melanin pigments. Histological slides were visualised and processed using *QuPath* software. The intensity of the staining was weak in each slide examined, and slightly weaker compared to the positive control, suggesting either that the overall presence of BLMH was not abundant in any of the lesions or that the cross-reaction of the antibody was not optimal within samples.

However, the antibody staining was visible in all the sarcoids examined, either whether untreated or treated with Bleosome, and easily distinguishable from melanin. The distribution of the staining within single sections did not followed a specific pattern and, in some areas, stained structures were over-represented compared to others, without a specific tropism for particular features of tumour. However, the staining positivity was always found within the cytoplasm of fibroblasts. Of note, first layers of epidermis did not express any positivity to the staining, and this might be due to the lack of fibroblasts within this outermost stratum. Figure 4.20 illustrates the lack of a link between treatment and pattern or presence of antibody staining. In each treated sarcoid and in the respective untreated counterpart, the feature of histological slides appeared very similar and the software analysis confirmed that there was no significant difference in the amount of BLMH within sarcoids treated with Bleosome compared to their respective untreated counterparts (figure 4.21). Interestingly, the BLMH was not present in healthy skin (either treated with Bleosome or untreated). This finding, together with the preliminary molecular data, indicate that the level of bleomycin hydrolase is not affected by the Bleosome treatment.

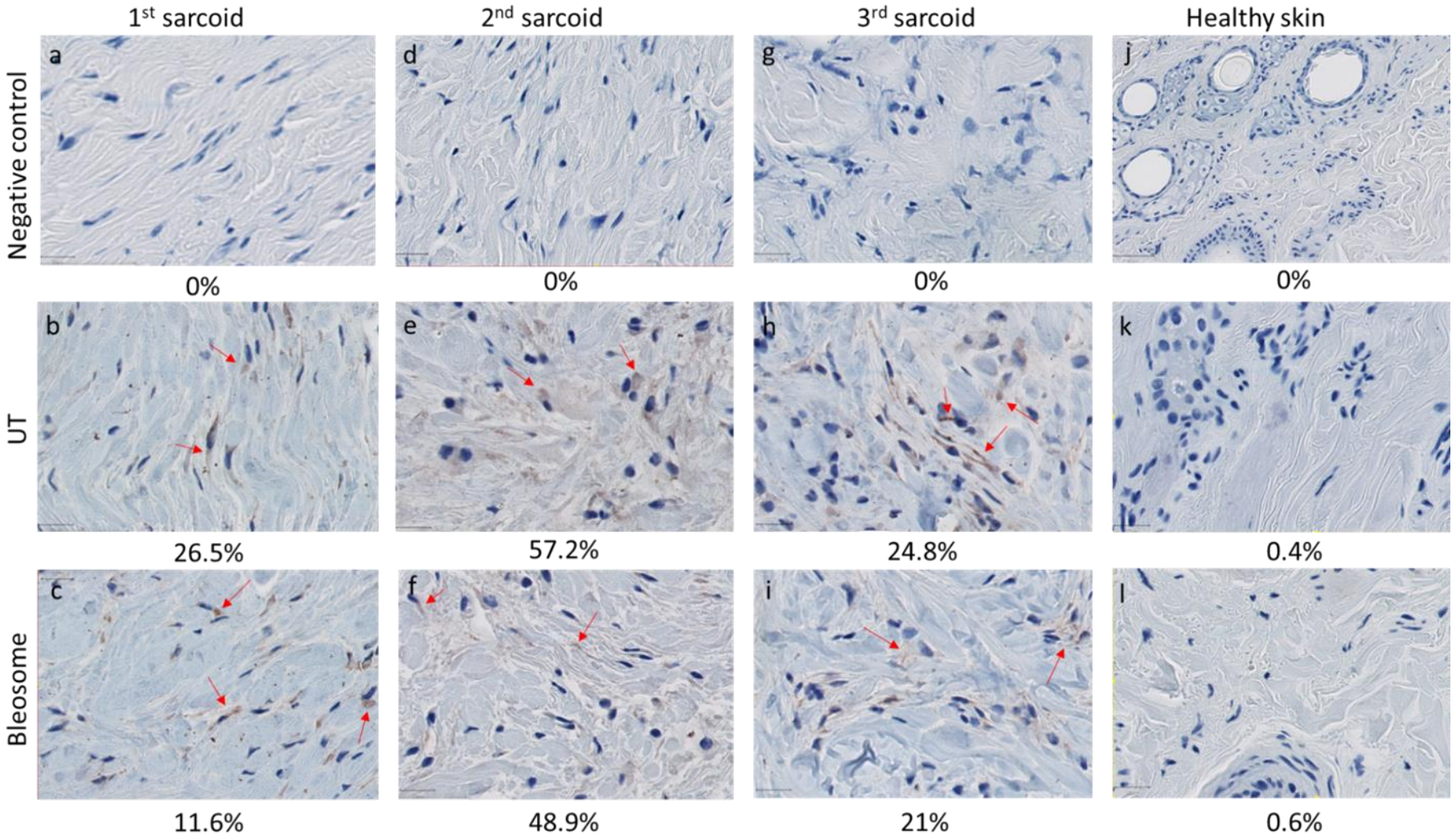
1st sarcoid
2nd sarcoid
3rd sarcoid
Healthy skin
Negative control
UT
Bleosome
a
d
g
j
0%
0%
0%
0%
b
e
h
k
26.5%
57.2%
24.8%
0.4%
c
f
i
l
11.6%
48.9%
21%
0.6%

Figure 4.20 *Level of BLMH is not affected by Bleosome treatment at the tumour level. Histological slides stained with the antibody anti-BLMH of three different equine sarcoids and healthy skin untreated and treated with Bleosome. Slides were stained with anti-BLMH antibody ab204584 (Abcam), processed and scanned. QuPath software was used to detect positivity of stained cells. The showed percentage value of the positivity is the mean values of the positivity detected in nine areas analysed for each lesion (three areas for each slide of the same lesion, as described in 4.3.7). (a), (d), (g), (j) represents slides of relative samples not stained with the BLMH antibody and used as negative control. (b), (e), (h), (k) represents slides of the first, second, third sarcoid and healthy skin untreated, while (c), (f), (i) and (l) represent their counterpart treated with Bleosome. Red arrows indicate selected positive antibody staining.*

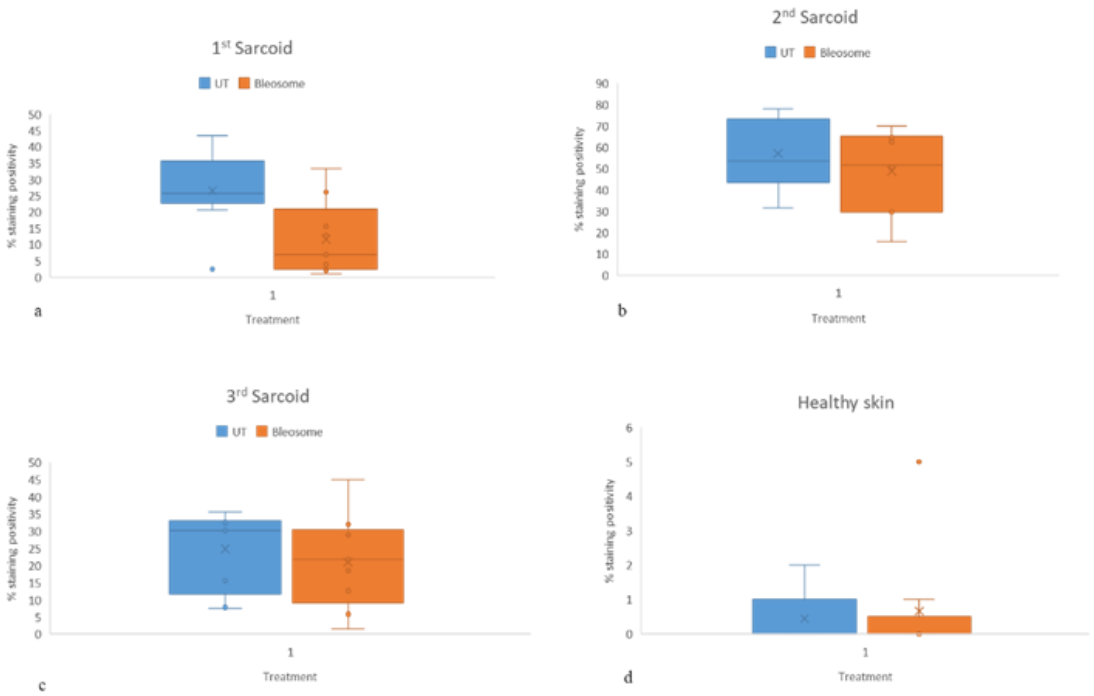

Figure 4.21 *Box plots related to staining positivity of immunohistochemistry (IHC) confirm the lack of connection between Bleosome treatment and levels of BLMH. (a) refers to the untreated (blue) and Bleosome treated parts of the firs sarcoid, (b) illustrates the level of antibody staining of the untreated part (blue) and Bleosome treated counterpart (orange) of the second sarcoid, (c) shows the positivity of staining of the third sarcoid in its untreated (blue) and treated (orange) portion and (d) shows the presence of BLMH antibody in the untreated (blue) and Bleosome treated (orange) healthy skin. Statistical analysis were performed using GLM: 2-way ANOVA, and Tuckey post-hoc test. * indicates statistically significant differences ($p \leq 0.05$).*

4.5 Discussion

4.5.1 Bleosome is efficient in killing a panel of human, canine and feline cancer cell lines *in vitro*

The efficacy of Bleosome in inhibiting the viability of cancer cells has been tested using a panel of canine, feline and human cancer cells. However, not all the cell lines used in this study derived from cutaneous cancers. The main reason resides in the limited access to cell lines derived from skin cancers for all the species tested, due to technical and financial restrictions; however, cell lines derived from cancers of interest in this study has been used when possible.

Our further experiments using cell lines were performed using a canine mast cell tumour (C2) and a canine melanoma (CML10) cell lines. The rationale behind this

choise was to compare the effect of the treatment on a melanoma and a non-melanoma tumour, in order to highlight the possible different, cell-type dependent effects of the Bleosome treatment at the molecular level, and have a better understanding of its mechanism of action within the class of tumours of our interest.

The results of cytotoxicity assays confirmed that Bleosome, the encapsulated form of bleomycin, is able to kill different types of cancer cell lines *in vitro* at different drug concentrations. However, it is less potent than free bleomycin. These findings were confirmed when Bleosome was tested for inhibiting cells growth and reproducibility using a colony formation assay. Encapsulating bleomycin molecules inside vesicles naturally partitions them away from and hinders their presentation to cells. This compartmentalisation of the cytotoxin most likely limits the immediate amount of drug available to the cells *in vitro*. This finding is in accordance with the study by Lau et al (2005), which compared the efficacy of encapsulated bleomycin with the free form *in vitro,* to target human keratinocytes and a human squamous cell carcinoma (SCC) cell line. The authors concluded that IC_{50} values for immortalised keratinocytes (NEB-1) were found to be 30µg/ml for Bleosome and 1µg/ml for free bleomycin solution, while the estimated IC_{50} values for SCC cells were found to be 9 µg/ml for Bleosome and 3 µg/ml for free bleomycin solution (Lau et al 2005). These results are comparable to our data derived from different types of human, canine and feline cancer cells. In particular, in two feline squamous cell carcinoma cell lines, SCFF1 and SMG (table 4.1), the free bleomycin showed a stronger cytotoxicity as compared to Bleosome, of 19 and 27-fold respectively. The greatest difference in efficacy between the two compounds was found in MCF7 cells, where the free bleomycin was 56-fold more efficient at killing cancer cells than Bleosome, whereas C2 and CML10 cells had the smallest difference of 5.6-fold.

4.5.2. UD liposomes improve the cellular uptake of bleomycin

To better evaluate whether this difference in IC_{50} values between encapsulated and free drug was due to the hindrance of cellular uptake, we treated two canine cancer cell lines, at two time points (2 and 24 hours), with either Bleosome or free bleomycin,

and compared the rate of cellular uptake using live-cell microscopy in conjunction with FACS analysis.

Previous studies have utilised confocal laser scanning microscopy (CLSM) and flow cytometry, in particular FACS, to determine the cellular uptake of liposomal drug delivery systems. These techniques provide the potential to localize carriers in cells and quantify the amount of liposomal uptake, leading to essential information on the interaction between the formulation of the drug and the target cells (Ducat et al. 2011). Mechanisms of liposome-cell interaction vary as a consequence of the type and composition of the formulation used but also as a function of the type of cell and stage of the cell cycle (Ducat et al. 2011). According to the types of liposomal nanocarrier, entrapped drug and target cells, several mechanisms of cellular uptake have been implicated in the literature, however, endocytosis pathway seems to be the predominant one for internalisation of liposome-entrapped compounds. For instance, clathrin-mediated endocytosis, macropinocytosis, and cell membrane cholesterol dependent processes were all shown to play a role in the internalisation of siRNA-liposomes (Alshehri, Grabowska, and Stolnik 2018). In another study, the cationic and anionic liposomes were mainly taken up via macropinocytosis, while the neutral liposomes mainly via caveolae-mediated endocytosis (Kang, Jang, and Ko 2017).
Our results showed that bleomycin encapsulated in UD liposomes was internalised by cells more efficiently than the free bleomycin after 2 hours of treatment, in both types of canine cancer cells treated. Moreover, after 24 hours of treatment, imaging and FACS analysis confirmed that the gap between the concentration of Bleosome and free bleomycin inside cells was even greater compared to earlier time point of treatment, with Bleosome being taken up more than free bleomycin. Therefore, the length of treatment influences the rate of cellular uptake in both free and encapsulated bleomycin. This was confirmed by microscopy and FACS showing a significantly higher level of green fluorescence within cells after 24 hours of treatment compared to the earlier time point in C2 and CML10 cells treated with both compounds. This finding is in accordance with literature; Kang et al. (2017), indeed demonstrated that cationic, neutral and anionic liposomes showed time-dependent cellular uptake through specific endocytic pathways. Interestingly, we found also a different pattern of fluorescence expression within cells between treatments. After 2 hours and, more evidently, after 24 hours of treatment, F-Bleosome was found in cell cytoplasm within well-defined, round shaped structures of different dimensions, while the fluorescence

of free bleomycin was evenly present within cell cytoplasm. This might indicate that liposomal bleomycin particles fuse together in particular cytoplasmic area, especially after several hours of treatment, or that liposomes accumulate within cellular organelles, likely lysosomes, as part of the endocytic pathway for the cellular internalisation. To explore this latter hypothesis, during our previous live-cell experiment (data not shown), we used a red lysosomal staining (Lysotracker Deep Red). However, as this dye has an affinity for the inside of the lysosomal particles rather than for their membrane, after the staining procedure, we noticed a marked reduction of the presence of the green drug particles and the red lysosomal staining, when combined together. We assumed that this phenomenon was due to a possible competitive mechanism between F-Bleosome molecule and the red staining to be stored inside lysosomes. For this reason, we tried to use another type of lysosomal dye, which has a greater affinity for the lysosomal membrane (CellLight Lysosomes RFP, BacMam 2.0). However, this dye was previously untested on canine cell lines and, after several attempts with the support of the manufacturer, we concluded that this product was not suitable for canine samples (data not shown). For these reasons, it is difficult to draw definitive conclusions about the molecular mechanism of Bleosome cellular uptake. However, our previous live-cell imaging experiment using the red lysosomal staining (Lysotracker Deep Red), showed some degree of co-localisation between the green fluorescence of F-bleomycin and the red staining of the lysosomal dye (figure 4.22), suggesting the involvement of the endocytic pathway in the storage of bleomycin within cells.

Overall, our results showed that bleomycin, when encapsulated in UD liposomes passes through plasma membrane and is internalised by cancer cells more efficiently than free bleomycin, in the two different cancer cell lines tested. However, we confirmed the presence of the drug inside the cytoplasm of the cell but we could not confirm its location within the nucleus. Also taking into account the results of the viability study and the reduced efficacy of the encapsulated drug compared with the free form, we speculate that, after the initial passage through plasma membrane, liposomes are stored within lysosomal compartments and this might hamper or delay the passage of the drug into the nucleus after its release from the liposomes. This is consistent with a similar study conducted on Doxil (liposomal encapsulated doxorubicin). Here, the authors found that 8 hours after administration of free

doxorubicin 26% of the drug translocated to the nucleus and, when reaching a specific concentration, killed the cell, whereas only 0.4% of the doxorubicin encapsulated in liposomal formulation entered the nucleus and had a cytotoxic effect. Kinetically, they observed a build-up of nuclear doxorubicin within minutes of adding free doxorubicin whereas translocation of Doxil to the nucleus was slow and accumulated in the cytoplasm. The authors concluded that liposomal doxorubicin was sequestered in the lysosomal compartment and resulted in limited delivery to the nucleus, therefore the bioavailable concentration of Doxil-delivered doxorubicin is significantly lower than free doxorubicin (Seynhaeve et al. 2013).

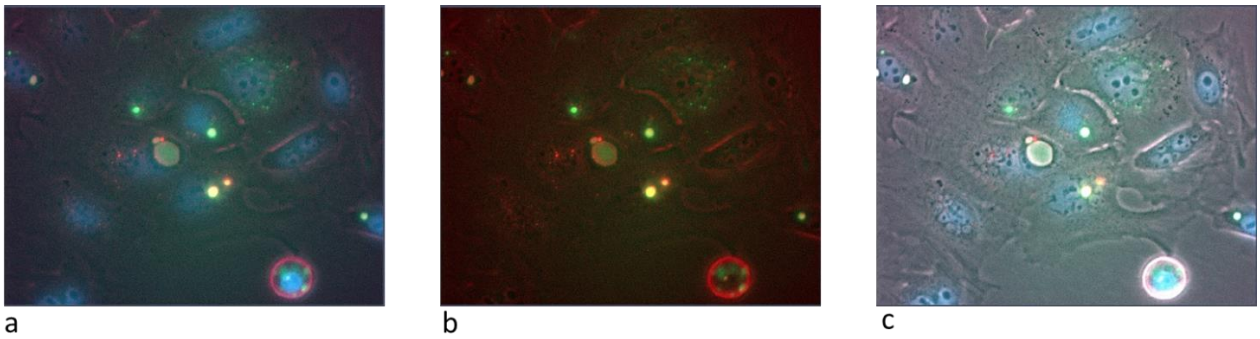

Figure 4.22 *Co-localisation of F-bleomycin and lysosomes. (a) shows blue (Hoechst, nuclear staining), red (Lysotracker Deep red lysosomal staining) and green (F-bleomycin) channel, (b) shows the same picture highlighting only the red and the green channel, (c) is the same picture including blue, red, green and phase contrast channel.*

4.5.3 Bleosome treatment triggers alternative DNA-repair pathways in two different canine cancer cell lines

We established that Bleosome was able to kill several types of human, canine and feline cancer cell lines, and provided an insight into its cellular uptake. We subsequently aimed to gain a better understanding of the molecular effects underlying the mechanism of action of Bleosome at cellular level.

Bleomycin produces DNA SSB and DSB (Chen and Stubbe 2005). This mechanism generates free-radical intermediates, it is dependent on the presence of oxygen, and can produce a range of different types of DNA lesions, comparable to those produced by ionising radiation (Ramotar and Wang 2003). The sensitivity of cancer cells to bleomycin it is reported to be variable and tumour type dependent (Chen and Stubbe

2005). It is currently unknown why this drug is more efficient against some malignancies rather than others. Studies propose that this variability is related to upregulation of alternative DNA damage and repair signalling pathways (Chen and Stubbe 2005; Pron, Mahrour et al. 1999). As bleomycin is capable also to produce DNA DSB, it is likely that specific DS-lesion repair pathways are involved in this sense, such NHEJ and HRR (Chen and Stubbe 2005). Moreover, major targets of bleomycin toxicity are lungs and skin, two tissues that have a low level of an enzyme called bleomycin hydrolase (BLMH). This enzyme might play a role in the degradation of the bleomycin molecules, rendering the drug inactive and unable to exert its function; hence, BLMH might play a key role in the bleomycin resistance (Chen and Stubbe 2005). For these reasons, our aim was to gain insight into the molecular cascades activated by cancer cell lines treated with Bleosome, focusing on the HRR and NHEJ as possible pathways affecting its therapeutic efficacy. Furthermore, we compared the liposome-encapsulated bleomycin with the free bleomycin, treating canine cancer cells with both forms of the drug, to the purpose of understanding whether liposomal formulation might modulate the activation of specific signalling pathways following the treatment. Canine mast cell tumour (C2) and canine melanoma (CML10) cell lines were chosen to prove the cell-type response of Bleosome treatment and to compare the efficacy of the compound on cellular model of NMSC with a malignant melanoma one. A very early step in the response of mammalian cells to DNA DSBs is the phosphorylation of histone H2AX at serine 139 at the sites of DNA damage (Burma et al. 2001). This newly phosphorylated protein, γ-H2AX, is a marker of DNA DSB foci (Kuo and Yang 2008). Firstly, we assessed the efficacy of Bleosome in producing DNA DSBs in different species, by treating canine, feline and human cell lines with a dose titration of the drug, and compared its effects with those generated by the same dose titration of free bleomycin. Both encapsulated and free drugs increased the level of the protein γ-H2AX in a dose-dependent manner, suggesting that Bleosome retains the efficacy of the free bleomycin in causing DNA lesions according to the increase of the dose (figure 4.9).

The DNA damage produced by bleomycin can be considered as radiomimetic; several studies claim that the most representative repair pathways for this class of chemotherapeutic agent include NHEJ and HRR (Helleday et al. 2008) (figure 4.23). Therefore, we have focused our analysis on these two pathways, using CML10 and C2 cells.

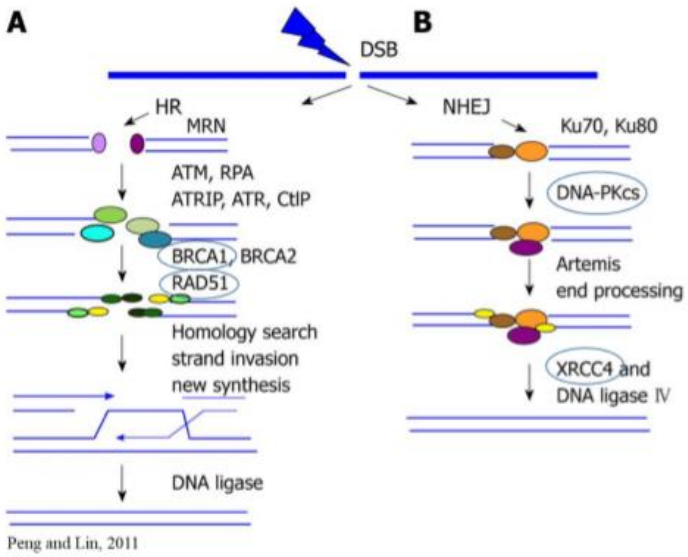

Figure 4.23 *DNA DSB repair pathways. (a): Homologous recombination (HR) repair. MRE11-RAD50-NBS1 (MRN) complex recognizes and senses DSBs. This complex activates ATM kinase, which in turn initiates the full DNA damage response. Then Rad51 nucleoprotein filament is assembled, which, performs homology sequence searching, and mediates strand invasion. DSBs are restored by branch migration of this joint DNA molecule, DNA synthesis, ligation, and resolution of Holliday junctions; B: Non-homologous end joining (NHEJ) repair. The two broken ends are processed and ligated directly by the action of the end-binding KU70/80 complex and DNA-PKcs, followed by XRCC4-ligase4. Thus, NHEJ is an intrinsically error-prone pathway while HR results in accurate repair (Peng and Lin 2011). Elements circled in blue were investigated in this study.*

Considering the NHEJ and HRR pathways, our qRT-PCR results indicated that the two cell lines responded to the treatment in differently (figure 4.10 (a),(b),(c),(d)). Components of HRR following Bleosome treatment, Rad 51 and BRCA1 were differently expressed between the two cancer cell lines during every time point of treatment, showing increasing expression and peaking at 8 hours post-treatment in C2. In contrast, in CML10 cells, Rad 51 and BRCA1 showed a consistently low level of expression and a decreasing trend over the time course. These findings suggest that the HRR pathway might be activate in mast cell tumour (C2) cells after Bleosome treatment but not in canine melanoma cells (CML10). Interestingly, XRCC4 which is associated with NHEJ, was only differentially expressed in the two cancer cell lines after 8 hours of Bleosome treatment, peaking at this time-point in CML10 cells. XRCC4 is a key player in the repair of DNA DSB in mammalian cells, as part of the NHEJ signalling. XRCC4 is also an integral part of the DNA end-joining in V(D)J recombination, the mechanism that assembles coding regions for the variable domains of immunoglobulin and T cell receptors in developing lymphocytes (Grawunder et al.

1998). Level of expression of PRKDC, the gene coding for DNA-PK, a protein involved in NHEJ, was slightly, yet significantly, higher in CML10 cells until 8 hours of treatment, while, after 24 hours, there was an upregulation of this gene in C2 and a downregulation in CML10. However, it is important to say that DNA-PK also cooperates with ATR and ATM to phosphorylate proteins involved in the DNA damage checkpoint (Arlander et al. 2008) and thus, its activation can be unrelated to the NHEJ. These findings exclude the activation of the NHEJ pathway in C2 cells and limit the evidence of its involvement in CML10 cellular response to Bleosome.

To confirm the different role of HRR in the two cell lines, and to explore the possibility that drug concentration also affected the activation of this DNA repair signalling, we immunoblotted for the Rad51 and BRCA1 proteins in canine cancer cell lines (figure 4.10 (e) and (f)). To rule out the activation of the pathway in CML10 cells, we used two different concentrations of Bleosome or free bleomycin, and evaluated cells after 0, 2, 4 and 6 hours of treatment. Protein levels of Rad51 and BRCA1 were found steady when compared to the untreated cells, regardless of type, dosage and timing of treatment, confirming that HRR is not the route of DNA repair in CML10 canine melanoma cells. C2 cells were treated with Bleosome and free bleomcyin for 4 hours, using a drug titration. The dose kinetics of the DNA repair proteins showed slightly increased level at the lower doses, but commonly reached a maximum level before reaching the maximal dose, to decrease at the highest drug concetration, indicating a plateau effect. This is an interesting finding, especially if compared to the parallel study conducted by Forrester et al. (2012), where they treated lymphoblastoid cell lines and primary fibroblasts with increasing dose of ionising radiation (IR). Authors tested the expression of the major DNA damage repair pathways genes, and they reached similar conclusion on the plateau effect happening at increasing doses. In the same study, a subsequent time-course experiment showed, similarly to our results, that the expression of most genes associated with DNA damage repair peaked at 8 hours after treatment. In our qRT PCR data all the genes tested, resulted in differential expression levels between C2 and CML10 cells, 8 hours after treatment indicating that signalling pathways are initially activated at this time point.

These findings confirm the hypothesis of a cell-type dependent response to bleomycin, in its free and encapsulated form. Interestingly, HRR seems to be activated in C2 but not in CML10 cell line. However, CML10 has a higher IC_{50} than C2; this might

indicate that there are some other mechanisms implicated in the drug resistance, and that more than one pathway might be activated within the same cell line.

4.5.4 Bleosome treatment of CML10 cells may produce unrepairable DNA damage and increase the expression of factors that stimulate the tumour microenvironment

Subsequently, we aimed to have a better understanding of the cellular mechanisms triggered by Bleosome treatment, by performing NGS on C2 and CML10 cells that have been treated with either Bleosome or free bleomycin at the respective Bleosome IC_{50} concentration at 0 hr, 8 hr and 24 hours. These time points were chosen based on our previous qRT PCR data, showing that the most significant variations in gene expression were found at 8 and 24 hours post-treatment. Exploratory analysis of the data generated by RNA seq revealed that C2 cells did not form homogeneous groups according to the time points of treatment; moreover, when considering cell passages, we found a significant variation of gene expression in samples derived from cells from different passages. This finding suggested that this cancer cell line is highly heterogeneous, hampering, functional analysis and the production of significant results. The transcriptomic analysis therefore, focused on CML10 cells only. PCA clustering of the RNA seq data separated the CML10 cells according to time point of treatment (CML10_UT vs CML_8H vs CML10_24H) thus suggesting a good quality of our data. Using edgeR, we (with the help of Edinburgh Genomics) evaluated the expression levels of genes in the different pairwise comparisons. edgeR was used as it has the advantage of implementing the method based on negative binominal distribution, and model over dispersion for digital gene expression data even with small replicates (Robinson, McCarthy, and Smyth 2010).

Our data showed that the majority of differentially expressed genes (1791 genes) ($|\log(FC)| > 2$ and FDR <0.05) were found in the comparison between the 24 hour and 0 hr time point, suggesting that the majority of changes in gene expression occurred after 24 hours of treatment compared to 8 hours.

We generated heatmaps containing the top 50 most significantly differentially expressed, according to the FDR value (<0.05), genes for each contrast, in order to highlight the genes underlying the most representative molecular variations. Of note, in each of the pairwise comparison, time points of treatment were grouped in two

distinct hierarchical clusters, with opposite trend of gene expression, highlighting the different gene signatures produced by the treatment.

When cells were treated with Bleosome for 8 hours, a plethora of growth factors and oncogenes were found overexpressed. Notably, among them, RAB20 was present and similarly upregulated after 24 hours of treatment. This gene is a member of RAS oncogene family; it is well-established in literature that activated RAS pathway, anchored by oncogenic BRAF, appears to be the central motor driving melanoma proliferation (Ji, Flaherty, and Tsao 2013). When treated for 8 hours, cells overexpressed JUN, the gene encoding for the c-Jun protein, which is reported to plays a crucial role in the development and progression of malignant melanoma via direct regulation of cancer-relevant target genes (Schummer et al. 2016). EGR4 was also overexpressed after 8 hours of treatment, and, of note, it was found that the early growth factor 4 (EGR4), a DNA-binding, zinc-finger transcription factor, plays a critical role in cell proliferation and metastasis in small cell lung cancer (Matsuo et al. 2014). Interestingly, after 24 hours of treatment with Bleosome, the most representative upregulated genes compared with untreated cells, were involved in the regulation of extracellular matrix and maintenance of tumour microenvironment, such as IRF5 and PLAUR, rather than proper transcription factors directly related to cell division and motility. Indeed, we also found the upregulation of ARNT2, which is the gene encoding for the hydrocarbon receptor nuclear translocator 2. This gene is associated with inhibition of proliferation and tumour aggressiveness in gastric carcinoma and in non-small cell lung cancer (Yang et al. 2015; Jia et al. 2019)

This is an interesting finding as it may indicate that after prolonged time of treatment, melanoma cancer cells are no longer able to rapidly divide and grown; however, to sustain their vitality, they could stimulate the tumour microenvironment, which could play a major role in the cellular response to Bleosome, and may represent a valuable target to consider for combined treatments. In further support of this hypothesis, when we compared differentially expressed genes between cells treated for 24 and 8 hours, we found that after 24 hours hyaluronidase-1 (HYAL1) was overexpressed. Hyaluronidases intracellularly degrade hyaluronan, one of the major glycosaminoglycans of the extracellular matrix and involved in cell proliferation, migration and differentiation (Weber et al. 2019). Thus HYAL1 is considered as a tumour suppressor (Lokeshwar et al. 2005).

When compared the two time points of treatment to the untreated canine melanoma cells**,** another important finding was that the cells, after both 8 and 24 hours overexpressed genes responsible for inflammation and modulation of immune response. Experimental evidence links inflammatory and immune cells to cancer development. Tumour infiltrating myeloid and lymphoid cells can either promote or inhibit cancer development, depending on the nature of the immune-cancer interaction (Tang and Wang 2016). Through the production of cytokines, chemokines and extracellular enzymes, tumour infiltrating immune cells may serve as tumour promoter by supporting tumour cell proliferation and inhibiting programmed cell death. In addition to the direct tumour-immune interaction, different branches of immune cells also crosstalk within the tumour microenvironment and regulate their counterparts' recruitment and activity, regulating, for instance, also oxygen and nutrient supply to tumour cells (Tang and Wang 2016). The eventual outcome of this complicated network of regulation is the formation of a unique tumour microenvironment that has profound impacts on the development, progression, and metastatic spread of cancers (Tang and Wang 2016)

Furthermore, in the cells treated for 8 hours, TNFAIP3 was found upregulated. This gene encodes for the A20 protein and was identified as a gene whose expression is rapidly induced by the tumour necrosis factor (TNF). The encoded protein, which has both ubiquitin ligase and de-ubiquitinase activities, is involved in the cytokine-mediated immune and inflammatory responses (Yu et al. 2019). However, interestingly, a recent study identifies the ubiquitin-editing enzyme A20 as a key factor in mediating cancer cell resistance to DNA-damaging therapy (Yang et al. 2018). Hence, further studies aimed to target this gene are needed to observe whether the response to Bleosome could be improved.

Interestingly, in cells treated with Bleosome for 24 hours there is an increase in the expression of IL11 and IRF5 compared to untreated control. These genes are associated with inflammation. IRF5 is a member of the interferon regulatory factor (IRF) family, a group of transcription factors with diverse roles, including virus-mediated activation of interferon, and modulation of cell growth, differentiation, apoptosis, and immune system activity. IRF5 acts as a molecular switch that controls whether macrophages will promote or inhibit inflammation. We speculate that in this context, IRF5 can play an important role in the stimulating tumour associated macrophages, contributing to the promotion of tumour microenvironment (Thompson,

Matta, and Barnes 2018). However, after 8 and 24 hours of Bleosome treatment, cells expressed also genetic elements regulating tumour suppression. Among those, DUSP2, DUSP5 and DUSP6 were present. In particular, dual-specificity phosphatase 5 (DUSP5) is one of four mammalian inducible, nuclear mitogen-activated protein kinase (MAPK) phosphatases (MKPs). However, DUSP5 is unique within this group, targeting only the classical extracellular signal-regulated kinases 1 and 2 (referred to hereafter as ERK). This, coupled with the finding that ERK activation is required for inducible DUSP5 expression, indicates that it acts as a negative feedback regulator of nuclear Ras/ERK signaling (Rushworth et al. 2014). Ectopic expression of DUSP5 in lung and colon cancer cells lowers ERK activity and suppresses growth. Furthermore, in stomach cancer, low DUSP5 expression correlates with poor prognosis and its re-expression reduces both cell growth and colony-forming ability in vitro. Taken together, these observations suggest that DUSP5 may act as a tumour suppressor (Rushworth et al. 2014). This finding might confirm the impaired cellular growth and division and the activation of tumour suppressive elements triggered by Bleosome treatment in CML10 cells.

Considering the downregulated elements after Bleosome administration at 8 hours post-treatment, the majority of genes were involved in cellular metabolism of lipoprotein and endocytosis (LIPG, LDLR, MSMO1), while after 24 hours, key regulator of mitosis and chromosome stability were lost. Notably, NUF2 is responsible for the attachment of mitotic spindle microtubules to kinetochore, cell division, kinetochore organization, meiotic chromosome segregation and mitotic spindle organization (Xu et al. 2019). We speculate that its downregulation may contribute to the arrest of mitotic division after 24 hours of Bleosome treatment.

Interestingly, the ASPM gene was also found downregulated. The ASPM gene provides instructions for making a protein that is involved in cell division. ASPM is upregulated in several types of cancer. In particular, upregulation of the ASPM gene has been studied in brain tumours and liver tumours. Studies suggest that unusually high activity of the ASPM gene is related to cancer progression, spread to other parts of the body (metastasis), and recurrence (Pai et al. 2019). Its downregulation following Bleosome treatment, therefore, confirms the compelling role of the drug in hampering cell division and growth in the treated cells. When looking at the genes downregulated after 24 hours compared with earlier time of treatment, we found key elements for cellular division, as CENPE and NUF2. CENPE encodes for a kinesin-like motor

protein that accumulates in the G2 phase of the cell cycle. This protein is required for stable spindle microtubule capture at kinetochores, which is a necessary step in chromosome alignment during prometaphase. Hence, we speculate that its downregulation can affect the cell mitosis and replication. Furthermore, recently, a study found that its overexpression was a negative prognostic indicator for overall survival in oesophageal carcinoma (Zhu et al. 2019).

These findings indicate that the Bleosome treatment triggers the activation of tumour suppressor elements and signals that block mitosis and cell cycle progression following the DNA damage caused by the treatment.

Genome analysis provides a large quantity of information concerning molecules that are involved in disease pathogenesis and may be used to interpret health disorders (Soneson and Delorenzi 2013). While it is not difficult to obtain the gene expression profiles, the extraction of biological insight from such information remains a major challenge.

Pathway analysis is a frequently used analytical tool for a better detection of biological processes related to a wide distribution throughout the whole network of genes (Suarez-Farinas et al. 2010). GSEA compared to single-gene methods gives a better overview of the complex biological altered hubs such as metabolic pathways and transcriptional programmes. GSEA can capture the subtle but coordinated changes in a gene-set and has been commonly used to find important pathways or functions in various diseases (Yoon, Kim, and Nam 2016). Reactome is a peer-reviewed pathway database of human pathways that have additional types of annotations to support pathway curation including a variety of biological processes such as signalling, metabolism, transcriptional regulation, apoptosis and synaptic transmission (Croft et al. 2011). Ingenuity pathway analysis (IPA) is a web-based software application for the analysis, integration, and interpretation of data derived from ‘omics’ experiments, such as RNA seq, small RNA seq and microarrays. Data analysis and interpretation with IPA builds on the comprehensive, manually curated content of the Ingenuity Knowledge Base. Powerful algorithms identify regulators, relationships, mechanisms, functions, and pathways relevant to changes observed in an analyzed dataset.

In this project, combined analysis with GSEA, Reactome and IPA tools revealed a set of mechanisms dysregulated in untreated and CML10 cells treated for 8 and 24 hours with Bleosome. For instance, when cells treated with Bleosome in both considered time points where compared to the untreated, we identified that the majority of the

upregulated pathways were involved in inflammation, immune response and growth factor. Among those, a plethora of toll-like receptor (TLR) signalling were found to be upregulated. TLRs serve as signalling molecules that are usually expressed on sentinel cells, such as macrophages and dendritic cells, and recognise pathogen-associated molecular patterns (PAMPs) as well as damage-associated molecular patterns (DAMPs) (Burns and Yusuf 2014). However, studies argued that several kinds of toll-like receptors, such as TLR3 and TLR4, are strongly expressed on cells isolated from human cutaneous melanoma biopsies. Chronic inflammation is a risk factor for the development and progression of cancer. Infiltration of tumours with specific T-cell subsets can be beneficial to control the tumour; however, overabundant innate immune cells and chronic inflammation can also relate to angiogenesis and poor prognosis (Goto et al. 2008). Activation of TLR triggers a cascade of intracellular events, including innate immune responses, through NF-κB–dependent and interferon regulating factor (IRF)-dependent signalling pathways. This is known to recruit and activate leukocytes to sites. Moreover, MyD88 pathway (also found upregulated in our pathway analysis), which is the canonical adaptor for inflammatory signalling pathways, was found significantly stimulated by activation of TLR2, TLR3, and TLR4 in melanoma cells, similarly to our study. MyD88 is considered a central node in inflammation and can cause also chemo resistance (Deguine and Barton 2014). NF-κB plays a key role in regulating the immune response and controls many genes involved in inflammation, such as growth factors, cytokines, and chemokines. Moreover, activation of the NF-κB and IRF family members may play a significant role in regulating cytokine and chemokine production and recruiting immune cells in the tumour microenvironment. TLR activation of tumour cells has been suggested to be a factor promoting tumour progression in carcinomas (Goto et al. 2008).

The molecular pathogenesis of cutaneous melanoma is strongly correlated with a constitutive activation of the mitogen-activated protein kinase (MAPK) signalling pathway (Acosta and Kadkol 2016), which, together with PI3K, was found as upregulated pathway after Bleosome treatment. The MAPK pathway plays a key role in modulating melanoma survival, proliferation, invasion and angiogenesis. In normal cells, this pathway is tightly regulated by extracellular signals from the cell membrane to the nucleus, mediated by a cascade of phosphorylation events. Frequent somatic point mutations have been found in the BRAF (66%) and N-RAS (15%) genes, two key elements of this pathway. The activity of the PI3K pathway is also increased in

melanomas, due to the loss of function of the phosphatase and tensin homolog (PTEN), either through mutation, deletion or methylation (Daphu et al. 2014). Interestingly, when interrogating the pathways differentially regulated after 24 hours of treatment compared to the earlier time point, we found that autophagy was upregulated. Autophagy is induced by starvation to capture and degrade intracellular proteins and organelles in lysosomes, which recycles intracellular components to sustain metabolism and survival. Autophagy also plays a major homeostatic role in controlling protein and organelle quality and quantity. The role of autophagy in cancer is still controversial; it can be neutral, tumour-suppressive, or tumour promoting in different contexts (Amaravadi, Kimmelman, and White 2016). Moreover, autophagy influences the interaction between the tumour and the host by promoting stress adaptation and suppressing activation of innate and adaptive immune responses. Additionally, autophagy can promote a cross-talk between the tumour and the stroma, which can support tumour growth, particularly in a nutrient-limited microenvironment. Thus, the role of autophagy in cancer is determined by nutrient availability, microenvironment stress, and the presence of an immune system (Amaravadi, Kimmelman, and White 2016). Recent studies revealed that the consequence of defective autophagy in the context of melanoma is fundamentally contingent upon the stage of cancer development (Ndoye and Weeraratna 2016).

Notably, a number of downregulated pathways were mostly related to DNA synthesis, DNA damage repair and mitotic checkpoints. DSBs are extremely hazardous lesions for all DNA-bearing organisms and the mechanisms of DSB repair are highly conserved. The DSBs are mainly repaired by HRR, which utilises an intact DNA molecule as the repair template. Mitotic HRR is managed by checkpoints that inhibit cell division until DSB repair is complete. The mitotic cycle is managed by a checkpoint mechanism that acts to delay cell division when DSBs are present at the end of G2, during the G2/M checkpoint (Burgoyne, Mahadevaiah, and Turner 2007). Although the exact fate of the cell cycle following the DNA damage is still poorly elucidated (Thompson, Gatenby, and Sidi 2019), some authors consider the process of HRR as having three components: (1) the process of HRR itself that achieves the re-joining of the broken DNA duplex, (2) the process by which the cycle is prevented from proceeding to cell division, and (3) the management and coordination of these two processes, such that only when DSB repair is completed, the cell division occur (Burgoyne, Mahadevaiah, and Turner 2007). The latter two components are strictly

dependent on mitotic checkpoints, while, among other factor, ATR plays a key role in the third one. Interestingly, in our pathway analysis, G2/M checkpoint, ATR, mitosis, the cell cycle and HRR were all downregulated in cells treated for 8 and 24 hours, indicating that cells after Bleosome treatment are not able to repair the impaired genetic material. This is a compelling finding as it can open novel perspectives on the putative mechanism of resistance to the treatment, which, to date, is still lacking of consensus.

So far, it has been reported that extended cell-cycle arrest/senescence, apoptosis and mitotic cell death are the most common cellular responses to bleomycin treatment and that bleomycin was found to induce G2/M cell cycle arrest in cancer cell lines (Wang et al. 2013). Previously, it has been speculated that this may be because of a G2/M checkpoint response to DNA damage. The G2/M checkpoint is important for genomic stability; it ensures that chromosomes are intact and ready for separation before cells enter mitosis. Thus, authors of the study concluded that although the mechanism of bleomycin-resistance is unclear, the ability for bleomycin-induced DNA damage to be repaired is the most likely one (Wang et al. 2013).

Our results open novel perspectives on the putative mechanism of action and of resistance to bleomycin treatment, as we have evidence that the DSBs induced by Bleosome are not repaired in canine melanoma cells, by activating cell cycle checkpoint, and HRR. Taken together, we speculate that after Bleosome treatment melanoma cancer cells are still metabolically active and produce signals of cell growth. However, importantly, the DNA damage produced by Bleosome is not repaired in CML10 cells, as the cell cycle progression is arrested, cell cycle and mitotic checkpoints are inhibited along with DNA synthesis and DNA DSB repair mechanisms. We also speculate that cells can respond to the stress of the Bleosome treatment by undergoing autophagy. We assessed by viability assays the efficacy of Bleosome in killing CML10 cells, however, in this study, we did not identify clear markers of cellular apoptosis or other processes directly related to cellular death; thus we hypothesise that autophagy might be the mechanism leading to cellular death after Bleosome treatment. Moreover, in order to survive after the treatment, cells may rely on tumour microenvironment, by triggering inflammatory processes and dysregulating immune system, and thus, creating a protective environment that might represent a key factor in the resistance to the Bleosome treatment in this cell line.

4.5.5 BLMH is not a key player in the response to the Bleosome treatment

In regards to the possible mechanism of resistance to Bleosome treatment, results of RNA sequencing did not reveal any significant variation in the expression of BLMH after the Bleosome treatment.

Several papers identified BLMH, a neutral cysteine protease, as another key factor in bleomycin resistance. It is supposed to inactivate bleomycin in normal and cancer tissues (Umezawa et al. 1974). It also plays an important role in antigen presentation, hydrolysis of homocysteine-thiolactone, and breakdown of deaminated filaggrin into amino acids N-terminal proteolysis of huntingtin (Y. Chen et al. 2013). To better understand the role of BLMH, using a specific thiol protease inhibitor (E64) that blocks BLMH activity, it was shown that mammalian cells exposed to E64 become more sensitive to bleomycin (Sebti et al. 1991). However, a more recent study in the yeast orthologue gene, BLH1, showed that this enzyme does not affect cytotoxicity of bleomycin in the organism when deleted or overexpressed. Thus, the role of BLMH in producing tumour resistance is controversial (Ramotar and Wang 2003). On the basis of the foregoing studies, it would appear that BLMH has a more general role in cells to degrade proteins, or perhaps to regulate gene expression by degrading certain transcription factors (Koldamova et al. 1999). In the scenario of bleomycin cellular response, we aimed to investigate the role of this enzyme at cellular and tumour level. We treated canine (C2 and CML10), feline (SMG) and human (MCF7) cancer cell lines for 4 hours with crescent doses of Bleosome or free bleomycin as comparison, and immunoblotted for the BLMH protein. Band intensities in C2 and in SMG did not show significant differences between increasing doses of the drug. In CML10 cells treated with Bleosome, the level of BLMH appeared to decrease with increasing doses of the drug, while it was overall very low at every drug dose of the free bleomycin. Human breast cancer cells, when treated with Bleosome, revealed a slight increase in the intensity of the BLMH related bands at the increase of the drug concentration, suggesting a possible activation of the enzyme within this cell line, after the Bleosome treatment. However, the intensity of this variation is very weak, without giving sufficient evidences about its modification following the treatment. Furthermore, our results on the BLMH gene, by mean of qRT PCR, did not show significant changes in

the expression of the enzyme in response to a time-course of Bleosome treatment in two canine cell lines (figure 4.19).

However, the western blot analysis revealed the constant presence of a second band at a slightly higher molecular weight of the BLMH protein. This might indicate that BLMH is activated post-translationally after the Bleosome treatment. Further studies are needed to better investigate these possibilities. To validate these results and explore further the possible involvement of BLMH in response to Bleosome treatment, we decided to use also a tumour model, treating cutaneous sarcoids excised from equine patients. As control, we used also healthy equine skin. Three different pathological types of sarcoids, excised from different patients, were cut in two parts, one was left untreated and represented the control, and the other part was treated with Bleosome for 6 hours, spreading the cream on all over the free surfaces of the lesions. We choose 6 hours as length of treatment because from our previous skin penetration studies (section 3) we observed that Bleosome penetrates deeper in the skin after 6 hours than earlier times of treatment. Moreover, according to our qRT PCR findings in this chapter (section 4.4.5), we observed that the activation of pathways implicated in DNA damage repair might occur after 6\8 hours of bleomycin administration.

Subsequently, histological slides generated from each sample were stained with an antibody anti-BLMH, to observe whether the level of the enzyme in sarcoids and healthy skin was affected by the Bleosome treatment. Equine melanoma was used as control, to assess the efficacy of the antibody in staining cell cytoplasm (supplementary data 8.2.7). Moreover, the adding of Vector red enabled clear distinction between the melanin pigment and area of positive antibody staining. As reported in figure 4.20, the presence of BLMH was constantly low in all the sarcoids examined; this might be due to the small amount of the enzyme present within the slides or to the poor efficacy of this particular antibody in equine samples. Due to technical and financial restrictions, it was not possible to test further the quality of the antibody; however, an accurate optimisation of the staining procedure was performed by the pathology unit of the R(D)SVS to the best of their possibility, in light of the described limitations. The staining appeared in the cytoplasm of fibroblastic cells, without a specific tropism for elements or layers of the cancer lesion. However, as statistical analysis confirmed, the amount of BLMH within sarcoids was not affected by Bleosome treatment, as there was no difference in the amount of staining, in the treated and the untreated portion of every lesion considered. We are confident in the

reliability of these results as the starting samples (excised sarcoids) were processed and treated according to OECD guidelines (Davies, Ward, and Heylings 2004) to maintain them vital over the chemotherapeutic treatment. Importantly, we analysed every portion of each considered sarcoid, obtaining at least three histological slides withdrawn from every area of the lesions. Moreover, we performed at least three technical replicates, to produce statistically significant results. Of note, the use of NanoZoomer XR **(**Hamamatsu) to scan single histological slides enabled us to analyse the whole section, avoiding the possibility of missing area of BLMH accumulation. Interestingly, the enzyme was not present in equine healthy skin, regardless of whether it was treated with Bleosome or not. This finding is in accordance with literature as skin is one of the targets of bleomycin toxicity and several authors claim that this is due to its lack or low level of BLMH, which exert in other organs, protection against the effect of the drug (Reinert et al. 2013). It is interesting however, that equine sarcoids of different pathological types and excised from different patients manifested the presence of the enzyme. The involvement of BLMH in cutaneous disorder is preliminary investigated in some studies, although there is still a lack of consensus in literature about its role in different cutaneous pathologies (Kamata et al. 2011; Kamata et al. 2007). However, our finding might open novel routes to explore the actual role of BLMH, not only in response to the bleomycin treatment, but also in pathological and cancerous skin conditions.

These results, together with the molecular data, suggest that the level of bleomycin hydrolase is not increased or affected in response to Bleosome treatment.

4.6 Conclusions

In this study, we found that Bleomycin encapsulated in UD liposomes can kill several types of human, canine and feline cancer cell lines, although its efficacy is slightly reduced compared to the free form of drug, *in vitro*. We determined that the cellular uptake of Bleosome is time-dependent and that it can more effectively cross the plasma membrane and penetrate into cells than the free drug. Given these counterintuitive findings we determined that the encapsulated form of bleomycin is less efficient at killing cancer cells than the free form because the drug is sequestered in the cytoplasm

and unable to penetrate the nucleus and cause DNA damage. Further live-cell imaging studies, including optimising the labelling of cellular organelles within canine cells, could further elucidate the mechanism of cellular uptake of Bleosome. This was the first study to examine the global changes in gene expression induced by Bleosome treatment. We found that Bleosome treatment generated DNA DSBs and that, interestingly, canine CML10 melanoma cells were unable to repair the DNA damage through cell cycle arrest and HRR. Interestingly, CML10 cells overexpressed genes responsible of inflammation and organisation of extracellular matrix, suggesting that Bleosome treated cancer cells stimulate the tumour microenvironment and that cellular components of the tumour microenvironment may mediate the patient's response to treatment. Further work is required to establish if the cytotoxic effects of Bleosome can be enhanced by dual targeting of components of the tumour microenvironment, potentially with specific anti-inflammatory and/or immunomodulatory agents.

Chapter 5 Evaluation of Bleosome as part of a therapeutic protocol for the management of equine sarcoids

5.1 Abstract

In veterinary medicine, sarcoids are neoplasms belonging to the non-melanoma skin cancer (NMSC) class of tumours and are the most common skin tumours in equids. This class of tumours are not fatal in most cases, in both human and veterinary patients, but their treatment still represents a challenge as it includes disfiguring and highly invasive treatments in both species. For this reason, there is growing interest in Bleosome, a topical compound made by encapsulating the bleomycin in ultra-deformable (UD) liposomes, as a novel, non-invasive treatment option. To date, there have been limited pilot studies conducted on the safety and efficacy of Bleosome as a topical treatment in the management of NMSCs, including one study using Bleosome alone to treat human NMSC, and a second study in horses using Bleosome in combination protocol to treat equine sarcoids. Both studies showed promising results and highlighted the non-invasive nature and lack of side effects of the treatment.

Here, we aimed to assess the ability of Bleosome to penetrate through equine cutaneous sarcoids *in vitro*, and to conduct a preliminary investigation of the clinical application of Bleosome administered topically to equine patients bearing sarcoids.

To this extent, we treated patient-derived sarcoids with F-Bleosome for 6 hours and visualised the living-samples by using the CLSM. We found the presence of drug particles within the whole depth of the lesion and concluded that Bleosome is able to penetrate through sarcoids, accumulating within the superficial layers, but also to reach inner parts of the lesions, until the bottom of the tumour model after a 6-hour long single application of the compound.

Subsequently, we treated 12 horses bearing different types of cutaneous sarcoids with Bleosome, following CO_2 laser excision, at the Dick Vet Equine Hospital of the University of Edinburgh. To date, we found that 5 patients (41.6%) were in complete remission, 4 patients (33.3%) experienced relapsed lesion(s), and 3 (25%) were failed

to follow-up. Sarcoids that recurred were previously reported to be at higher risk of relapse because of their pathological types, multiple lesions or location in anatomical areas where it is difficult to achieve clean margins by surgery. Overall, Bleosome treatment was well tolerated and no established adverse reactions were reported.

5.2 Introduction

Sarcoids are the most common type of equine skin neoplasm on a worldwide basis (Bergvall 2013). Approximately 1% to 11.5% of all horses have sarcoids, and this type of tumour is reported to account for up to 90% (35%–90%) of all skin neoplasms in horses (Bergvall 2013). Sarcoids are non-metastatic, fibroblastic neoplasms that rarely regress spontaneously; they can remain static or become very aggressive locally. Although the condition is not lethal itself, size and distribution of the tumour can severely compromise the use and value of the horse, and lead to a decision of euthanasia (Bergvall 2013).

Equine sarcoids are proposed to have a multifactorial aetiology. An association with infectious agents in the form of bovine papillomavirus (BPV) types 1 and 2, as well as genetic risk factors, have been documented (Angelos et al. 1991). Sarcoids are generally first noticed in horses aged 1 to 7 years old and there is no reported colour or gender predisposition (Brostrom 1995).

The macroscopic presentation of sarcoids can be highly variable. A clinically based classification of sarcoids has been suggested by Knottenbelt (2005), which includes occult, verrucous, nodular, fibroblastic, mixed, and malignant/malevolent types of tumours.

Occult sarcoids are focal areas with alopecia, scaling, skin thickening, hyperkeratosis, and hyperpigmentation. Common locations include the neck, face, sheath, medial thigh, and shoulder (Knottenbelt 2005).

Verrucous sarcoids have a rough, alopecic, raised surface, which can be verrucous and irregular. This type is usually found on the head and neck and in the axillae and groin.

Nodular sarcoids can be divided into types A and B, whereby type A are spherical subcutaneous masses and type B have dermal involvement, which precludes the independent movement of the overlying skin. The overlying skin is often haired, but

can become alopecic and ulcerated. These types are often seen in the eyelid region and groin, and on the prepuce. Fibroblastic sarcoids are fleshy, ulcerated masses; type 1 is pedunculated and type 2 has a broad, locally invasive base. Common locations include the axillae, groin, legs, and the periocular region. Tumours can resemble granulation tissue or infectious processes, such as habronemiasis. Another differential is squamous cell carcinoma. Non-fibroblastic tumours can become fibroblastic after being traumatised. Mixed forms (two or more types) of tumours are common. Malignant/malevolent sarcoids are aggressive and locally invasive. These tumours extend widely into adjacent skin and subcutis, are invasive, and infiltrate lymphatic vessels. The occult and verrucous type can remain static for years if not traumatised. Nodular tumours can also remain unchanged, although less often. Any type of sarcoid lesions can develop into an aggressive fibroblastic or malignant/malevolent tumour if traumatised (Knottenbelt 2005; Bergvall 2013).

A high proportion of affected horses (14%–84%) have multiple tumours, and all types of sarcoids can be present in the same horse. Sarcoids often develop at the site of previous trauma or where the skin is thin. Exposure to trauma can induce a worsening of the lesion and a more aggressive development of the tumour (Knottenbelt 2005). An early age of onset, time, and number of lesions are associated with larger tumour size (Bergvall 2013).

Sarcoids are diagnosed based on clinical signs and histopathology, as other conditions can macroscopically be difficult to differentiate from sarcoids (Bergvall 2013). For instance, alopecia areata, bacterial folliculitis, and dermatophytosis can mimic occult sarcoids. Moreover, all types of nodular conditions (eosinophilic granulomas, melanomas, schwannomas, and so forth) can be mistaken for nodular sarcoids. One important differential diagnosis for fibroblastic sarcoids is exuberant granulation tissue. A biopsy should include deep dermal tissue and be at least 6 mm in diameter if a biopsy punch is used to harvest the sample (Bergvall 2013). Before verifying the diagnosis by biopsy, serious consideration should be given to the fact that traumatised sarcoids can potentially transform into a more aggressive type of tumour. It has been recommended that traumatic intervention should not be performed on a presumed sarcoid unless a treatment plan has been established after the diagnosis is confirmed.

Fine-needle aspiration (FNA) for cytology is usually unrewarding and carries the same risk of exacerbating tumour growth. FNA is not recommended for the diagnosis of sarcoids (Bergvall 2013).

Despite being so widespread, there is no a universal consensus of treatment for sarcoids, which has been suggested to be related to their diverse phenotypic appearance (Compston et al. 2016). A range of treatment modalities, including various topical applications, immunotherapy, radiation therapy, chemotherapy, cryosurgery, 'traditional' sharp surgery and laser surgery, have all been reported in the veterinary literature and an even wider variety of non-prescription treatments are used by the horse-owning public (Compston et al. 2016). Success rates with respect to recurrence vary widely; however, no single treatment has been shown to be suitable for all sarcoids in all locations (Compston et al. 2016).

If complete surgical removal with wide margins is achievable, it may be an optimal choice for therapy. The presence of BPV DNA has been demonstrated up to 16 mm outside the macroscopic lesion, and local recurrence has been correlated to DNA-positive surgical margins (Martens et al. 2001). The probability of local recurrence after sharp surgery or carbon dioxide laser is significantly higher for large sarcoids and sarcoids that had previously failed to respond to treatment (Martens et al. 2001).

Sharp surgery has been reported to result in 50% to 64% recurrence of the tumour within six months. With non-touch techniques that avoid autoinoculation and wide surgical margins, the result improved to 82% complete remission without recurrence (Martens et al. 2001). In a retrospective study of 28 periorbital verrucous and nodular sarcoids without extensive involvement of the eyelid, 23 had recurrence (82%) and 39% grew additional tumours after surgery (Knottenbelt and Kelly 2000). Furthermore, recurrence was associated with a more aggressive behaviour. Combination of sharp surgery and other therapies, for example, cisplatin injection, has been reported to improve success rates. In one case report, surgery was combined with photodynamic treatment in a horse with multiple lesions, some, but not all sarcoids, went into remission (Reschke 2012).

Carbon dioxide laser treatment was reported by Carstanjen et al. (1997) to result in remission without recurrence in 62% of sarcoids from 60 equids, of which 45 were horses. Follow-up was longer than 6 months. Animals with multiple sarcoids had a higher risk of recurrence. In another study, 20 of 28 sarcoids (71%) resolved after laser treatment (Martens et al. 2001), while in the study by Compston et al. (2016), 82 (83%) out of 99 horses treated with CO2 laser surgery had no recurrence of the sarcoid removed. Advantages over conventional surgery are reduced risks of postoperative swelling, pain, and hypergranulation.

Cryotherapy has achieved up to 42% to 100% success with no recurrence, with an average healing time of 2 to 4 months (Taylor and Haldorson 2013). A successful outcome was obtained in 11 of 14 (79%) horses treated by cryosurgery (Martens et al. 2001). However, when small (<2 cm2), occult, or verrucous periocular sarcoids were treated with liquid nitrogen, 91% had aggressive, rapid-growing relapses within 12 weeks of treatment (Knottenbelt and Kelly 2000). Side-effects reported included post-treatment alopecia or regrowth of white hair and, if used on the face or periocular area, facial nerve paralysis and loss of the upper eyelid function. Caution is also warranted when lesions are located close to joints, as septic arthritis has also been reported.

Hyperthermia through heating the sarcoid with a thermo-probe has been used alone or in combination with chemotherapy, radiotherapy, or immune modulation. Only a small number of cases resolved and stayed in remission for 6 months to 1 year (Knottenbelt and Kelly 2000).

Radiotherapy, also known as interstitial brachytherapy (implants of, eg, iridium-192, cobalt-60, radium-226, radon-222, or gold-198) was effective in 50% to 100% of cases, with a low (5%) recurrence rate. By use of ionizing-radiation brachytherapy (iridium-192), 8 of 8 and 13 of 15 periocular and non ocular sarcoids, respectively, went into remission (Theon and Pascoe 1995). In another study, 66 nodular, fibroblastic, and mixed tumours were treated with brachytherapy with platinum-sheathed iridium. Of the 53 cases that were followed up, 98% were resolved (Knottenbelt and Kelly 2000).

Chemotherapy can be effective, either by intralesional injections (cisplatin powder emulsion in sesame oil or almond oil, or aqueous formulation of fluorouracil) or topical application (fluorouracil, thiouracil). Mixing cisplatin with oil increases the local concentration and prolongs the retention time of the drug, and reduces the risk of cisplatin-induced nephrotoxicity and hepatotoxicity. Cisplatin is usually recommended at a dose of 1 mg/cm^3 and is deposited intralesionally using sedation and analgesia 4 times at 2-week intervals. The treatment can be combined with debulking surgery (Bergvall 2013).

The intralesional administration of 5-fluorouracil (5-FU) into 13 sarcoids at the dose of 50 mg/cm^3 given every 2 weeks for up to 7 treatments resulted in complete regression in 61.5% of cases. Follow-up time was 3 years. Lesions larger than 13.5 cm^3 responded less favourably (Stewart, Rush, and Davis 2006). Topical 5% 5-FU was used twice daily for 5 days then once daily for 5 days, followed by 5 applications

on an every-other-day schedule in 9 periocular, occult, and verrucous lesions. Six sarcoids resolved, and 3 improved but later developed into fibroblastic tumours (Knottenbelt and Kelly 2000).

AW4(5)-LUDES, a combination of topical fluorouracil, thiouracil, and heavy metals, has been reported to result in 35% to 80% complete regression (Knottenbelt and Kelly 2000). When used in 159 periocular small occult or verrucous sarcoids, 35% resolved. Significant scarring and a detrimental effect on eyelid function were recorded in 6 cases. Because of the risk of side effects, this treatment is not recommended for periocular regions, distal limbs, and coronary bands (Knottenbelt and Kelly 2000).

With all chemotherapy protocols, consideration must be given to the risk of exposing health care personnel, owners, and others who handle the treated horses.

Despite the implementation of safety precautions (eg, double gloves, mask, safety bench), surface contamination with antineoplastic drugs including 5-FU was detected in 65% to 75% of samples taken from 6 cancer treatment centres in the United States and Canada (Connor et al. 1999). Furthermore, one study detected cytotoxic drugs or metabolites in urine samples from nurses not directly involved in drug preparation or administration (Sessink et al. 1992). These findings stress the importance of establishing strict safety precautions for both health care workers and owners who handle the horses.

Other reported treatments for equine sarcoids include the use of antiviral agents.

Acyclovir, used in human herpesvirus infections, is metabolised to the active form acyclovir triphosphate in virally infected cells. It inhibits viral DNA replication, but is not known to eradicate latent virus (Bergvall 2013). Topical daily application of acyclovir 5% was used in 47 sarcoids, in a few of which after surgical debulking. 32 of 47 (68%) lesions went into remission, whereas incomplete resolution was observed in the remaining 15 (32%). Tumour thickness was associated with a less favourable response (Stadler et al. 2011). Other antiviral agents, such as Cidofovir and Xanthates have been reported as treatments for sarcoids, although the reported outcomes achieved were doubtful (Scagliarini et al. 2012).

As BPV might be one of the key players involved in the aetiology of sarcoids, few immune-modulating agents have been experimented as possible therapeutic strategy. Among them, bacillus Calmette-Guerin (BCG) from Mycobacterium bovis is an immune modulator that stimulates host lymphocytes and natural-killer cells. With this therapy, only sarcoid cells undergo necrosis, as has been shown histologically.

Inflammatory reactions to BCG frequently require nonsteroidal anti-inflammatory (eg, flunixin) and/ or corticosteroid treatment. The best results have been seen with periocular sarcoids, where, in one study, 18 of 27 (67%) lesions treated with BCG vaccination resolved (Knottelbelt and Kelly 2000).

Imiquimod is an immune-modulating agent used to treat human genital warts, actinic keratosis, and superficial basaliomas. Imiquimod has potent antiviral and antitumor activity. It stimulates both the innate and acquired immune system via toll-like receptor 7, thereby inducing a T-helper–1 cytokine response as well as an increase of TNF-a, IL-1, IL-6, and IL-8 (Bergvall 2013). A 5% cream (Aldara) was used in one study, applied topically 3 times weekly for up to 32 weeks. 56 % of treated sarcoids went into complete remission and 20% had partial remission. Overall, 80% had a greater than 75% reduction in tumour size (Pettersson, Bergvall, and Humblot 2011). However, few side effects were reported within this therapy. Pain, erythema, exudation, and erosion of the area of the application were reported following Aldara treatment (Pettersson, Bergvall, and Humblot 2011).

Retinoid drugs such as tazarotene have been trialled on over 500 cases. It could be considered a useful adjunctive treatment in some forms of sarcoids (especially verrucous and occult lesions) but it seldom results in a cure. Furthermore, in one study, treatment with a retinoid (0.1% tazarotene gel) resulted in high recurrence (60%) and variable outcomes (Knottenbelt et al. 2018).

In conclusion, although there is a plethora of therapeutic options, there is a lack of consensus on the best treatment option for equine sarcoids; furthermore, most of these treatments produce several side effects. Therefore, our aim was to test the efficacy of Bleosome as topical non-invasive treatment for equine sarcoids in an adjuvant setting. Bleosome has previously been applied, in a preliminary study, on human patients bearing NMSC, showing promising outcomes without adverse reactions reported (Chopra, S. unpublished data). Furthermore, a pilot study on the efficacy of Bleosome in combination with other topical agents, as a treatment for equine sarcoids, was conducted by Knottenbelt et al. (2018). The authors showed that when applied alone, tazarotene and 5-FU achieved only 17% and 27% of completely resolved sarcoids respectively, by 12 months, whereas the combinations of either 5-FU and Bleosome, or tazarotene and Bleosome, resulted in resolution of 77% and 78% of the lesions, respectively. Combination treatment was significantly superior to sole treatments with

tazarotene or 5-FU, however, this study was limited by the number of horses treated with Bleosome alone to reach a meaningful conclusion regarding the synergy of Bleosome and other treatment options.
Moreover, in that study, all horses treated using tazarotene showed pain and skin exudation. Pain and discomfort were also noted with application of 5-FU. Throughout the duration of treatment with Bleosome, no pain or discomfort, or any overt inflammatory effects, were noted and no apparent systemic effects of the treatment were encountered in any of the horses (Knottenbelt et al. 2018).

In this study, we conducted a preliminary experiment to test the ability of Bleosome to penetrate through sarcoids *in vitro*. We used sarcoids surgically excised from patients as part of their standard therapeutic protocol, we treated them with Bleosome and assessed the degree of Bleosome penetration, using the confocal laser scanning microscope. To the best of our knowledge, this was the first study that explored the ability of penetration of a chemotherapeutic through a tumour by directly visualising with microscopy the Bleosome particles within a living sarcoid tissue, following its topical application.
Subsequently, we treated equine patients, presented to the Dick Vet Equine Hospital (The University of Edinburgh), bearing single or multiple cutaneous sarcoids, with topical application of Bleosome to the tumour excision site, following surgical excision with a CO_2 laser. Our aim was to observe whether the topical compound improved the outcome of the surgical treatment, lessening the rate of re-occurrence of the neoplasms, compared to previously reported case studies. Furthermore, we aimed to confirm, in a wider cohort of patients, the safety and lack of side effects of the treatment. This study was still on going at the time of the writing and therefore, data shown should be considered as preliminary results.

5.3 Materials and Methods

5.3.1 Evaluation of Bleosome penetration through equine sarcoids *in vitro*

Two sarcoids, excised from two different equine patients, were used in this study. They were of different clinical type and located in different anatomical regions: one was a fibroblastic sarcoid excised from the elbow of a patient and the other lesion was a mixed sarcoid excised from the neck of a different horse.

Pathological samples were provided by the surgical team of the Equine Veterinary Hospital at the Royal (Dick) Veterinary School of the University of Edinburgh, as part of the study on the Bleosome efficacy on equines sarcoids (VERC reference number 6.19.). Straight after the collection, sarcoids were wrapped in aluminium foil, stored in sealed plastic bags and snap frozen in dry-ice, and stored at -70◦C or -20◦C.

At the time of the experiment, each sarcoid was thawed in 3x PBS at RT and then cut into two sections: one section was used as the untreated control, and the other was treated with F-Bleosome. Both sections were stained with Hoechst 33342 (ThermoFisher Scientific) diluted in PBS at concentration of 0.02 mg/ml, for 1 hour at RT. Subsequently, F-Bleosome was applied to the outermost surface of the tumour, in an amount sufficient to completely cover the external area of the lesion, and incubated for 6 hours at RT.

At the indicated time point, F-Bleosome was gently removed and the sarcoid was washed with PBS; subsequently, the tumour (both treated and untreated parts) was cut into 1 mm thick slices including the whole thickness of the lesion, using an acrylic mouse brain matrix (RBMA 600C, repeatable sections, coronal slices, 1 mm spacing, World Precision Instruments). The section was oriented with the outermost surface (the part where F-Bleosome was applied), facing the right of the glass slide and the innermost part of the sarcoid facing left (figure 5.1).

Figure 5.1 *Orientation of the sample on the slide**.** The section is cut horizontally, from the outermost to the innermost part of the lesion. The blue arrow indicates the outermost surface of the sarcoid, where F-Bleosome was applied.*

Three sections from the F-Bleosome treated part of the sarcoid and three from the untreated control were analysed. Slices were put on a glass slide and kept flat by positioning another glass on the top. Slides were visualised using the Zeiss LSM 710 AxioObserver Confocal Microscope equipped with EC Plan-Neofluar 20x/0.50 M27 objective lens (details on microscope settings in section 2.10.3.1).

5.3.1.1 Image analysis

Images captured with the confocal laser scanning microscope (CLSM) were analysed using the software Zen lite 3.0 (Blue edition, Zeiss). This software has dedicated tools that allowed the measurement of the fluorescence intensity of the green (F-Bleosome) and blue (Hoechst) channel. Thanks to this software, we were able to assess the overall fluorescence intensity of a selected slide as well as the fluorescence intensity level for every pixel detected within the whole slide analysed. The fluorescence intensities relative to the length of the section were plotted (from the outermost surface, where F-Bleosome was applied, to the opposite innermost surface), in order to obtain information about the level of fluorescence relative to every distance (in µm) from the outermost external surface of the sarcoid (depth). The relative graphs were generated using the software 'R', with the help of Dr Gianluigi Rossi (The Roslin Institute). The position of F-Bleosome molecules (green objects) were calculated by Zen lite, in relation to their distance from the outermost surface of the sarcoid.

Statistical analysis was performed using the 'Minitab' software.

5.3.2 Preliminary evaluation of the efficacy of Bleosome on equine sarcoids *in vivo*

This study was conducted in collaboration with the staff of the Dick Vet Equine Hospital of the University of Edinburgh (in particular with Dr Richard Reardon) and was considered as a preliminary case-observation study. It was conducted to gain

information about the efficacy *in vivo* of the Bleosome, as an adjuvant treatment for horses bearing cutaneous sarcoids. The study was on-going at the time of writing and preliminary results achieved to date are reported.

5.3.2.1 Patients

This was a prospective study using clinical cases presented to the Royal (Dick) Veterinary Equine Hospital of The University of Edinburgh between 2018 and 2020. Owners were informed of all the procedures and provided with a dedicated information leaflet (supplementary data 8.2.8) before consenting to include their horses in this study by signing a consent form. This study received the approval of the Veterinary Ethical Review Committee (VERC) with the VERC reference number 6.19.

Horses with different clinical type (fibroblastic, nodular, verrucous, occult and mixed according to clinical classification; Knottenbelt 2005), size, number and location of cutaneous sarcoids were treated. Cases in which previous therapy had been unsuccessful were included, with these tumours classified as recurrent. Twelve animals met the criteria for inclusion in the study (Table 5.1). There were four Irish Sports Horses, one Welsh Cob, one Appaloosa, one Warmblood, one Clydesdale, one Icelandic Horse, and three Racehorses. The cases ranged in age from 3- to 16-years-old with a mean of 7.7 years. There were seven geldings and five mares, in the study. Sarcoids were measured and evaluated by clinicians prior to therapy. Serial photographs were obtained and clinical records were kept of the sarcoid(s) size on presentation, location, and previous treatments. Owners were asked to provide photographic, telephonic and/or written updates of the lesions every two weeks and feedbacks about the general health status of their animals. Over serial evaluations, the response to treatment, side effects and the length of Bleosome treatment were recorded.

5.3.2.2 Procedure of treatment

In all but two patients, Bleosome was administered in an adjuvant setting, after the surgical excision of the sarcoid(s) by means of CO_2 laser. Among the two exceptions: one patient received cisplatin beads implant concomitant to CO_2 laser excision, followed by Bleosome treatment, and the other one received combined Bleosome and tazarotene as the only treatment, without surgical excision. Prior to surgical excision, each patient received anti-inflammatory (1.1 mg/kg flunixin meglumine intravenously) and antibacterial (20 mg/kg penicillin procaine intramuscularly) treatments. Some of the cases underwent the surgical procedure under standing sedation and local anaesthesia, while other patients received general anaesthesia according to clinician preference (predominantly based on lesion location). Procedures for proper handling and disposal of Bleosome followed the Occupational Safety and Health Administration guidelines.

Following surgical procedures, owners were given guidelines for safely and correctly applying Bleosome. Briefly, they were asked to wear two pairs of nitrile gloves before coming into contact with the Bleosome, to clean the lesion, removing any loose scale and crust. Subsequently, they were advised to apply Bleosome cream, wearing gloves, in an amount sufficient to cover the whole surface of the lesion, and to massage it gently over the target area, until the lesion dried out, and to repeat the procedure every 12 hours (twice per day). The overall length of treatment suggested ranged between 4 and 6 weeks, according to the response to the treatment, side effects and tolerance of the patient. Owners were asked to bring their horses to the Equine Hospital of the R(D)SVS for regular post-operative checks every 2 weeks, or, where not possible, to provide photographic and/or telephonic updates. Particular emphasis was put in requesting description of the surgical site and in reporting any signs of bleeding, inflammation, swelling or poor healing of the scar. Owners were also asked to provide accurate information about any signs of stress, discomfort, pain or behavioural abnormalities of their horses during the course of application of Bleosome.

5.3.2.3 Classification of response

The responses to treatment were classified according to the following outcomes. A case was classified as ‘resolved’ if the tumour was not visible at the time of evaluation by clinicians or by owners after the course of Bleosome treatment. A case was

considered to be ‘persistent’ if the tumour was grossly visible at inspection following the treatment. A case was considered to be ‘recurrent’ if the tumour had disappeared at inspection at any point during Bleosome therapy, but was reported to be present in the same site any time after the completion of the Bleosome therapy or after the initial resolution (if any) during the treatment.

5.4 Results

5.4.1 Bleosome penetrates through equine sarcoids *in vitro*

We used patient excised sarcoids as a model to test the efficacy of Bleosome to penetrate through cutaneous neoplastic lesions. Sarcoids were treated with Bleosome for 6 hours, observed at the CLSM and compared to their untreated counterparts. The same experiment was performed twice, using two different types of sarcoids excised from two different patients (section 5.3). We obtained comparable results and will focus on the results from one experiment in more detail.

Three sections from the F-Bleosome treated part of the sarcoid and three sections from the untreated control were visualised using the CLSM. This type of visualisation allowed us to explore the whole depth of the sarcoid section and to detect the position of the drug particles within this area using the Zen lite software. As shown in section 3, Hoechst staining highlighted cellular nuclei and other background skin structures containing DNA. As skin has intrinsic autofluorescence, when the image was analysed with Zen lite, in the control section a very low level of green background was detected, as shown in figure 5.2 (c).

The section of the sarcoid treated with F-Bleosome showed an overall high level of green fluorescence. When the fluorescence level was plotted against the length of the section, the maximum intensity of the green fluorescence was detected within 0.4 cm depth, indicating that the majority of the F-Bleosome compound is in the superficial layers of the tumour. However, some F-Bleosome molecules were observed at a much greater depth, up to 1.6 cm from the top surface of the sample (figure 5.3 (b)),

suggesting that after 6 hours of treatment, with a single application, F-Bleosome is able to penetrate through almost the whole of the tumour section.

We compared the overall green (F-Bleosome) fluorescence intensity within the treated and untreated sections and we found that this was significantly higher ($p < 0.05$) in the F-Bleosome treated part than the very low green fluorescence detected within the control, confirming the abundant presence of the fluorescent drug within the treated slides (figure 5.4).

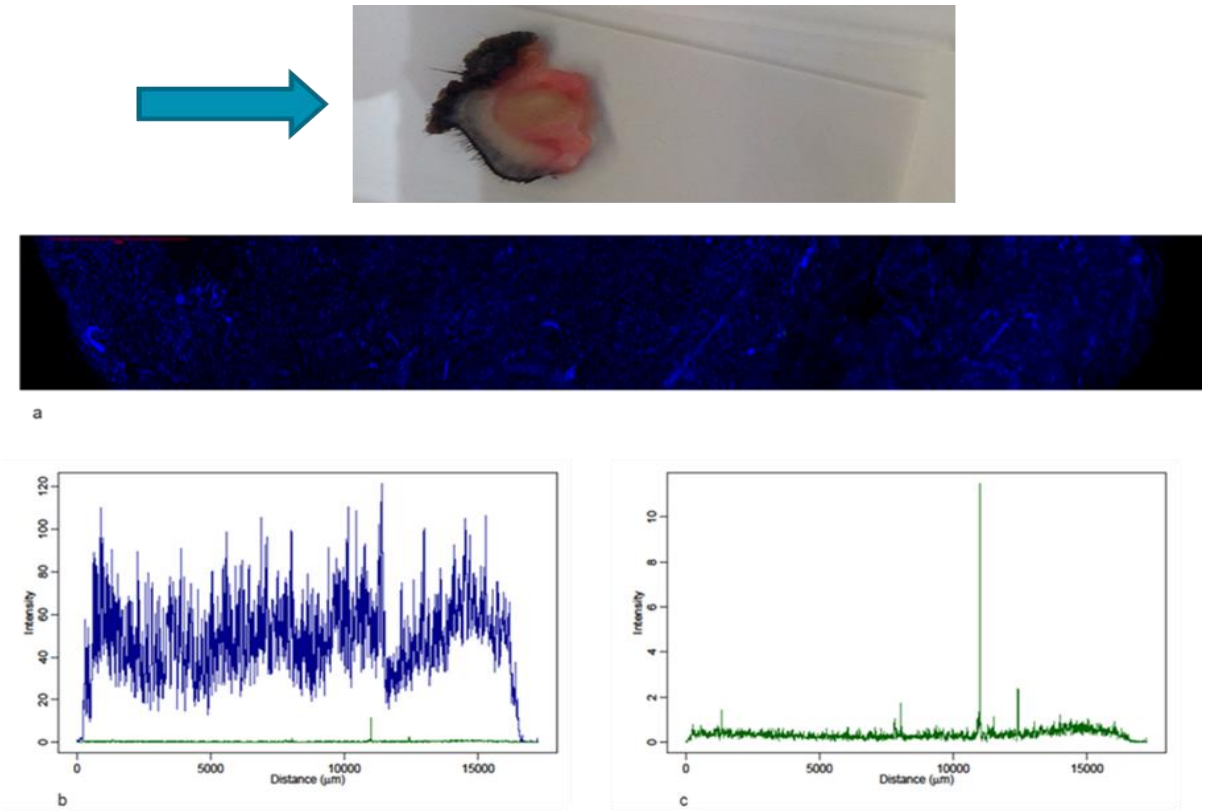

Figure 5.2 *Image and fluorescence intensity plots of the untreated sarcoid (control). (a) Image of the whole depth of the untreated section of the sarcoid captured with the CLSM, the outermost surface is facing left (as indicated by the blue arrow). (b) Represents the intensity of Hoechst blue fluorescence (blue lines) compared to green fluorescence (green lines) detected along the whole section. "Distance" in the histogram indicates the position related to the outermost surface (0 - 16000 µm). (c) Indicates the green fluorescence intensity only, detected along the whole section.*

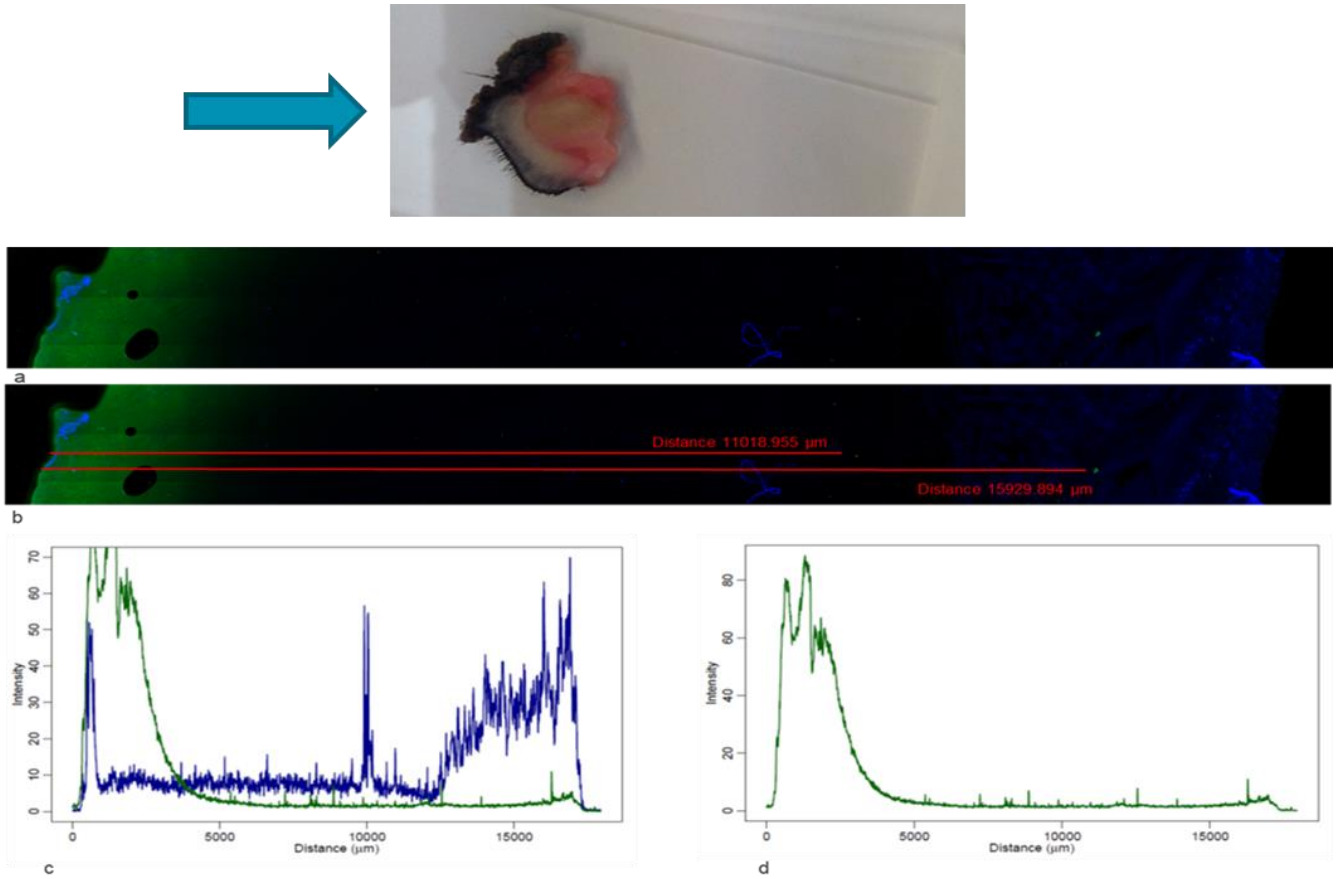

Figure 5.3 *Images and fluorescence intensity of the F-Bleosome treated sarcoid. (a) Image of the whole depth of the F-Bleosome treated section of the sarcoid captured with the CLSM, the outermost surface is facing left (as indicated by the blue arrow). (b) Highlights the indicated position (distance from the top surface) of selected F-Bleosome particles (11018.995 and 15929.894 µm depth). (c) Represents the intensity of Hoechst blue fluorescence (blue lines) compared to green fluorescence (green lines) detected along the whole section. "Distance" in the histogram indicates the position related to the outermost surface (0 - 16000 µm). (d) Indicates the green fluorescence intensity only, detected along the whole section.*

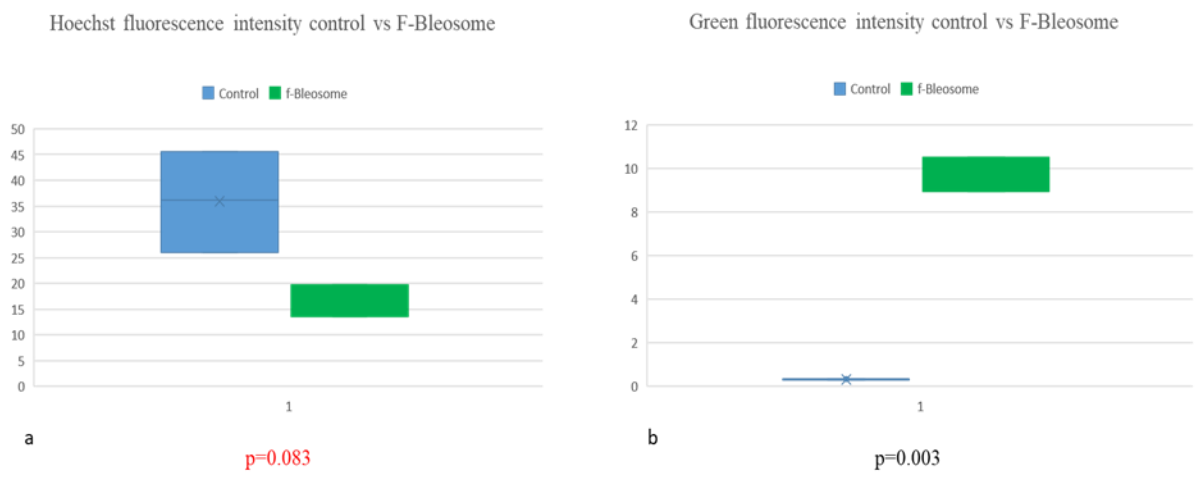

Figure 5.4 *Box-plots comparing the blue and the green fluorescence intensity between the treated and untreated part of the sarcoid. (a) Hoechst blue fluorescence intensity of the control (untreated sample, blue plot) and the F-Bleosome treated portion of sarcoid (green plot). The difference between the two is not statistically significant (p: 0.083, Student T-test). (b) Comparison of the green fluorescent intensity of the control (untreated sample, blue plot) and the F-Bleosome treated portion of the sarcoid (green plot); they are statistically different (p<0.05), as the treated sarcoid has a significantly higher green fluorescence intensity (p: 0.003, Student T-Test).*

Subsequently, we compared the overall green fluorescent intensity, detected along the whole depth of the section, of each of the three examined slides of the F-Bleosome treated part of the sarcoid, and the untreated control. All of the F-Bleosome-treated sections showed a high intensity of green fluorescence up to 0.4 cm distance from the outermost surface of the sarcoid (figure 5.5 (b)). Deeper than 0.5 cm, the green fluorescence gradually decreased and followed a steady pattern, remaining close to the average green intensity of the three sections; however, there were some notable peaks at deeper depth. As confirmed from imaging, these peaks indicate single F-Bleosome particles detected in the innermost part of the sarcoid. Whereas the green intensity of the untreated sections was consistently very low and evenly close to the average (figure 5.5 (a)). This indicates that the green fluorescence detected in the control represents the autofluorescence background of the skin, a feature already confirmed in section 3, with the experiments on penetration of F-Bleosome on healthy animal and human skin using the MP. Rare peaks noted in the histogram (figure 5.5 (a)) probably represent cutaneous structures, such as hair follicles, which naturally auto-fluoresce more intensely than other structures (section 3).

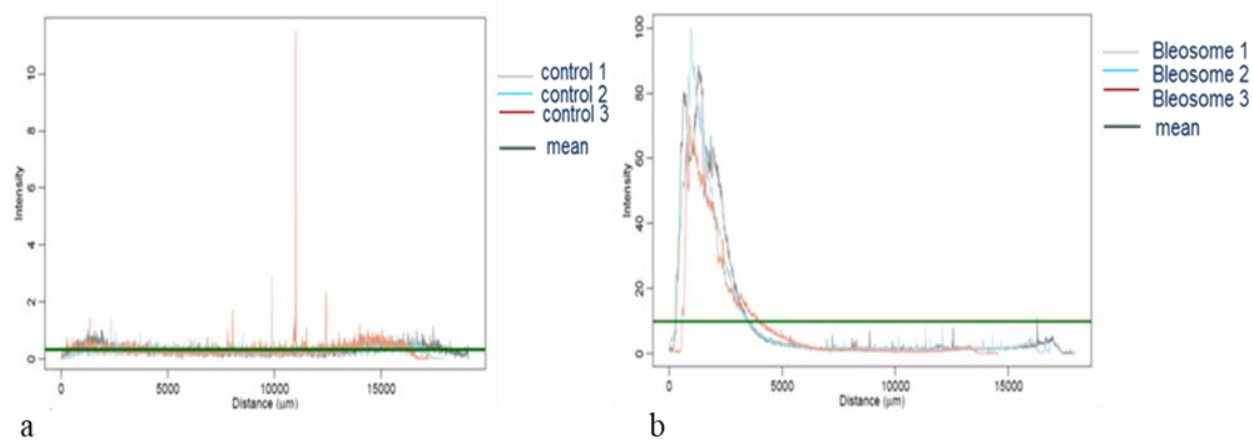

Figure 5.5 *Histograms of green fluorescence intensity of the three slides of the treated and untreated part of the sarcoid.(a) compares the green fluorescence intensity of the three slides analysed of the untreated part of the sarcoid (control). Profile of the first slide is the grey line, profile of the second slide is the blue line and the third slide has red line. The green line represents the mean value of the green fluorescence intensity within the three slides (b) compares the green fluorescence intensity of the three slides analysed for the F-Bleosome treated part of the sarcoid. Profile of the first slide is the grey line, profile of the second slide is the blue line and the third slide has red line. The green line represents the mean value of the green fluorescence intensity within the three slides.*

These significant findings demonstrate that F-Bleosome can penetrate through cutaneous sarcoids and reach some of the innermost structures of the lesion with a single administration *in vitro,* and that after 6 hours, F-Bleosome mainly concentrates at a depth of 0.4 cm but can penetrate as far as 1.6 cm.

5.4.2 Bleosome shows potential as an adjuvant therapy in the treatment of equine sarcoids *in vivo*

To date, 12 horses fulfilled the inclusion criteria for this study (table 5.1). There were 7 males and 5 females, and the mean age was 7.7 years. To date, 5 patients were in remission (41.6%), 4 experienced recurrences (33.3%), and 3 failed to follow up (25%). Overall mean of follow-up was 12 months.

Within the horses in remission, 3 horses had sarcoids in multiple sites and some of them were recurrent lesions at the time of the initial presentation at the Dick Vet Equine Hospital. The remaining 2 patients had 1 primary lesion each: 1 had a

verrucous sarcoid on the neck and the other one had a fibroblastic sarcoid on the abdomen. The mean follow up for this group was 14.8 months.

The relapse group includes 1 horse with multiple lesions classified as recurrent at the time of the initial presentation; in particular, this patient had multiple nodular, mixed and occult sarcoids in the abdomen, legs and chest areas. This horse experienced recurrent lesions (reappearance of a nodular lesion on the left radius and 2 occult plaques in the left inguinal area) after 5 months from the laser surgery, however, due to initial intolerance to the treatment Bleosome was applied only for 2 weeks. At the re-check, another course of Bleosome was prescribed to cure the recurrent sarcoid, the compound was applied for 4 weeks, it was well tolerated, and after 3 months from the end of the treatment, the horse experienced a remission, however after 7 months from the end of the second course of Bleosome, clinicians noted another single recurrent lesion, which is currently being treated with Bleosome. Of the other 3 patients experiencing recurrence following the treatment, 2 had multiple verrucous, nodular and occult sarcoids in the face and abdomen, and in multiple locations respectively. The first horse experienced a recurrence of the verrucous lesion close to medial cantus of the eye. Neither of the patients had any previous treatments. However, the latter received cisplatin beads within the laser surgery as part of the treatment and experienced a recurrence 4 months following surgery. The last horse within this group had a primary fibroblastic sarcoid in the abdominal area, which recurred after 1 year post-surgery. The mean time of recurrence was 9.25 months after surgery.

At the time of writing, 3 patients failed to follow up; 1 of them had multiple recurrent occult and nodular sarcoids on the thighs and on the penile sheath, and was reported to be free from disease 3 months after the surgery. The other 2 had multiple nodular, ulcerated, and nodular and occult primary sarcoids. The first was reported to be free from disease 6 months after the surgery. Owners of this horse reported a minor swelling and bleeding on one of the surgery sites at the time of Bleosome administration, however it was unclear whether this was due to delayed healing of the surgical wound or to the Bleosome treatment. The other surgical sites treated with Bleosome did not manifested any of these side-effects and, after some topical symptomatic medications, the swollen site recovered and the Bleosome course was completed. The second horse had an occult and a nodular primary sarcoids in the groin area and was treated with Bleosome and Tazarotene, without surgical excision. 6

months following the topical application of both medications, the owner reported that the horse was in remission; subsequently, the animal was sold and failed to be followed up.

Overall, follow-ups ranged from 3 to 20 months after surgical excision, the treatment was well tolerated, and none of the horses experienced topical and systemic side-effects, except for one and the cause was doubtful.

Fig. 5.6 and 5.7 show as an example, the appearance of three excised sarcoids on the same patient, immediately after the surgery (fig. 5.6) and two months after the end of Bleosome treatment (fig 5.7).

Figure 5.6 *Appearance of three sarcoids after surgical excision prior to Bleosome application. (a) The scar of a lesion on the left thigh, (b) a lesion removed in the left axilla and (c) the scar of the inguinal region.*

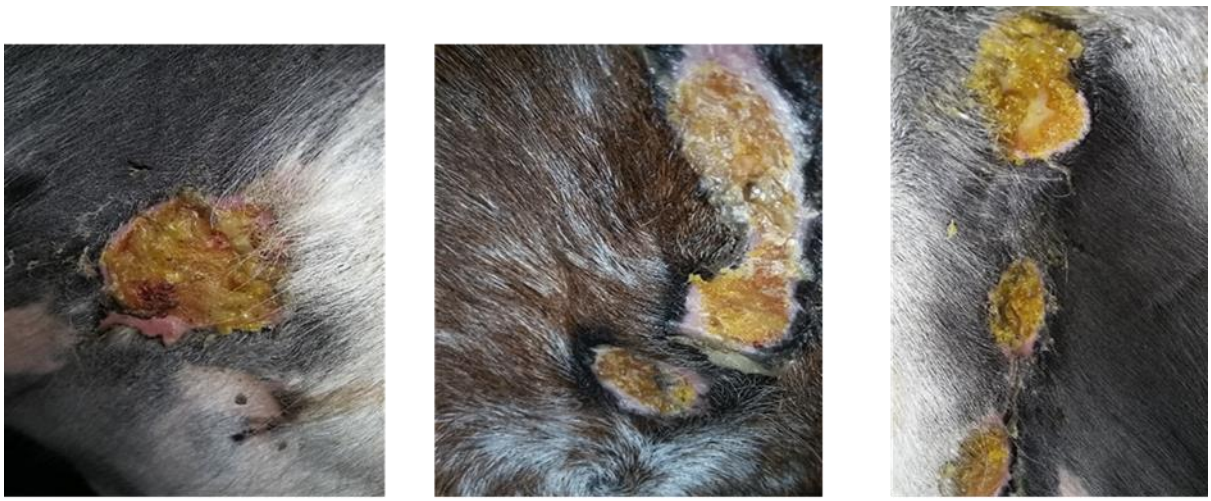

Figure 5.7 *Appearance of scars 2 months after the Bleosome application. There is no evidence of recurrence, inflammation or adverse skin reaction. (a) is the scar on the left thigh, (b) in the axilla and (c) is the inguinal region.*

Case No	Breed	Age (years, months) and sex	Type(s)	Site(s)	Previous tx.	Treatment	Length of Bleosome application (weeks)	Complications	Modality of follow up	Time (months) of follow-up	Recurrence
1	Skewbald Irish Sports Horse	8, CM	Verrucous	Neck	No	CO2 surgical excision + Bleosome	4	No	E-mail	20	No
2	Chestnut Irish Sports Horse	7.11; CM	Verrucous, Mixed fibroblastic	Pinna, penile sheath	Yes	CO2 surgical excision + Bleosome	4	No	Photos	20	No
3	Race Horse	7.3; CM	Fibroblastic	Head, Axilla	Yes	CO2 surgical excision + Bleosome	4	No	Photos, Phone	8	No
4	Race Horse	5.8; F	Fibroblastic	Abdomen	No	CO2 surgical excision + Bleosome	4	No	Photos, Phone	19	Yes
5	Piebald Irish Sports Horse	10.2; F	Nodular, Mixed nodular/occult, Occult	Axilla L+R inguinal	Yes Yes	CO2 surgical excision + Bleosome	2 – intolerant 6 - tolerant	No No	Photos Photos	5 17	Yes Yes
6	Race Horse	9; CM	Occult, Nodular, Occult Occult (multi)	Inner thigh, Sheath, Sheath, Inner thigh	Yes	CO2 surgical excision + Bleosome	4	No	Photos Physical exam	3	LF
7	Clydesdale	10; F	Fibroblastic (+ multi nodular), Multi verrucous/nodular, Nodular (multi), Nodular	Inner thigh, Inguinal, Axilla, Abdomen	Yes	CO2 surgical excision + Bleosome	6.5	No	Photos, E-mail	17	No
8	Appaloosa	16.4; CM	Nodular, Ulcerated, Nodular, Nodular	Inguinal, Abdomen, Pinna	No	CO2 surgical excision + Bleosome; Abdomen and pinna: Bleosome only	6	swelling / bleeding	Photos	6	LF
9	Dark Bay Irish Sports Horse	4.8; F	Verrucous, Nodular	Face, Abdomen	No	CO2 surgical excision + Bleosome	4	No	Phone Photos	12	Yes
10	Welsh Cob	3; F	Fibroblastic	Abdomen	No	CO2 surgical excision + Bleosome	4	No	Photos	9	No
11	Warmblood	5.8; CM	Occult, Verrucous, nodular	Elbow, Axilla, Sternum, Sheath, Inner thigh	No	CO2 surgical excision /cisplatin + Bleosome cream	4	No	Emailed	7	Yes
12	Icelandic Horse	5; CM	Occult, Nodules	Sheath	No	Bleosome + Tazarotene	4	No	Phone	6	LF

Table 5.1 *List of patients enrolled in the study. Signalment including breed, age and sex (F: female, CM: castrated male), is reported. Types of sarcoids, location and whether they were primary or recurrent lesions at the time of the first presentation at the Dick Vet Equine Hospital is given. Type of treatment, length of Bleosome application, type and length of follow-up are illustrated. Outcome is showed: 'yes' represents the presence of recurrent lesion after the treatment; 'no' represents the absence of recurrent lesions after the treatment; 'LF' represents the failed to follow-up.*

5.5 Discussion

In this section, we aimed to investigate the ability of Bleosome in penetrating through equine cutaneous sarcoids and its efficacy as non-invasive treatment in the management of the disease. We addressed our aims by assessing the penetration of Bleosome through excised, living sarcoid tissues and by applying the compound on equine patients bearing sarcoids, as adjuvant treatment.

Skin is the external barrier of the body and its main function is to provide protection against the surrounding environment, and to limit the absorption of exogenous molecules (Fleury and Vianna Lopez 2011). UD liposomes are nanocarriers designed to carry entrapped drugs through the hardest layers of the skin and delivery their payload directly to the target lesion. However, the mechanism exploited by UDs to penetrate through the skin is still poorly elucidated (Romero and Morilla 2013). In section 3, we proposed that UD liposomes allow the penetration of encapsulated bleomycin through animal and human skin, acting as penetration enhancers, following the mechanism number 2 proposed by Verma et al. (2003): liposomal vesicles might interact with outermost keratinocytes, disrupting intercellular lipid lamellae and allowing the release and consequently the penetration of the entrapped bleomycin through the skin. Furthermore, we showed that after 6 hours of skin treatment, F-Bleosome particles can be found at 430 μm of depth within healthy equine skin. This depth is significantly greater than the average thickness of the *stratum corneum* (Theerawatanasirikul et al. 2012), and the average thickness of the epidermis. Hence, we concluded that, with a single administration on healthy equine skin, Bleosome penetrates through the skin and enables the encapsulated bleomycin to reach the deeper cutaneous structures after only 6 hours of topical application. These findings were reproducible in a tumour model, where we interrogated the penetration of F-Bleosome through equine sarcoids *in vitro.* In this study, we treated patient-derived equine sarcoids with Bleosome for 6 hours. We choose this length of treatment as, in our previous experiment on the efficacy of Bleosome in passing across healthy equine skin (section 3), we observed the deepest penetration of F-Bleosome molecules at 6 hours post application. In the previous penetration study (section 3), we used the MP to visually explore the position of F-Bleosome within the live cutaneous tissue. Here, we cut the sarcoid into thin slices (1 mm) after the application of the chemotherapy,

and we visualised the treated lesion by means of CLSM. MP holds inherent advantages for imaging living tissues by improving depth penetration and reducing photodamage (Larson 2011). However, its imaging penetration power does not exceed 700-800 μm depth (Durr et al. 2011). As the thickness of the sarcoid lesions was greater than 1.5 cm, we concluded that it was not optimal to visualise a whole section of the sarcoid with the MP, as performed previously with healthy equine skin. Furthermore, MP does not produce images with higher resolution than CLSM (Jonkman and Brown 2015). The illumination in a CLSM is achieved by a collimated laser beam across the specimen (Jonkman and Brown 2015); just the light in-focus can pass through the pinhole, reach the detector, and then form the image with more details because the blurring from out-of-focus has vanished. By using CLSM, it is possible to obtain high-resolution images from the samples, which increase to accuracy of the microscopic images (Rossetti 2013).

As performed for healthy skin, we still aimed to visualise the treated sarcoids without fixing them, in order to avoid possible artefacts and alteration of the structure and position of F-Bleosome molecules within the lesion. For these reasons, we cut the sarcoids horizontally, including the whole depth of the lesion, in order to investigate the penetration of F-Bleosome throughout the entire neoplasm. To this extent, after having tried several techniques for cutting live sarcoids in even and thin slices without damaging the tissue, a mouse brain matrix was used. This tool, thanks to repeated grooves with 1 mm distance gaps, enabled the sarcoid to be sectioned in thin and homogeneous slices, suitable for evaluation with the CLSM. Analysis of obtained images revealed, in the F-Bleosome treated section of the sarcoid, an abundant presence of the fluorescence compound within the first 0.4 cm from the outermost surface of the lesion, indicating that the majority of the applied compound, after a single application, resides within the superficial layers of the neoplasm. However, it was interesting to observe the presence of several F-Bleosome particles within the whole depth of each section examined of the treated sarcoid, with the deepest drug particle found very close to the bottom of the lesion (1.6 cm depth). This is a compelling finding that further confirms our previous data on the efficacy of Bleosome in penetrating through healthy animal and human skin. Moreover, it provides evidence on how just a single application of Bleosome in a tumour model leads the chemotherapy to pass the superficial layers of the neoplasm and to reach the bottom of the lesion. This information might have important repercussions in the

application of the Bleosome on equine patients in clinics, not only because it supports the penetration power of the chemotherapy compound, but also because it suggests that multiple topical applications could be of a great benefit, as Bleosome may spread within the area of the target lesion. Furthermore, this is an optimised, novel technique to directly visualise the fate of Bleosome through living tumour explants and can open innovative ways of exploring the concentration and the pattern of accumulation of a chemotherapeutic drug within target tumours.

We confirmed that the green fluorescence detected was due to the presence of F-Bleosome particles rather than background autofluorescence of skin structures by comparing to the untreated control. Within the control section some peaks could be observed and likely correspond to some specific structures of the skin, such as hair follicles, with a higher basal level of autofluorescence as previously discussed (section 3). The overall level of the green fluorescence was significantly higher in the F-Bleosome-treated sarcoid compared to the control. However, there was no statistically significant difference between the level of Hoechst signal indicating that the intensity of the nuclear staining was comparable between the F-Bleosome treated and control. These findings indicate that Bleosome can effectively penetrate through sarcoids after a single topical application.

NMSC are a group of cutaneous tumours, which include basal cell carcinoma (BCC) and squamous cell carcinoma (SCC) in men, dogs and cats (Simonetti et al. 2009). Within this class of neoplasms, in horses, sarcoids are locally invasive, fibroblastic skin tumours and represent the most common tumours in equids worldwide (Bergvall 2013). Despite the high frequency of this class of malignancies, their therapeutic management it is still challenging in both human and veterinary medicine. Therefore, the topical administration of Bleosome has begun to be investigated. This is an interesting alternative for reducing side effects and for increasing drug targeting. In a preliminary study conducted on human patients, 0.1% liposome-encapsulated bleomycin was used successfully in named patient to treat a variety of skin malignancies including BCC, SCC, actinic keratosis and keratoacanthoma, as well as benign growths such as warts and verrucae (S. Chopra, personal communication). Standard care for these conditions included localised tissue ablation through cryotherapy, chemical ablation or surgical excision, all aggressive and potentially disfiguring treatments, particularly if the lesion involve the facial area. The face is

one of the most common locations for BCC and actinic keratosis in people. In the study of Dr Chopra, involving 60 named patients, Bleosome gave 100% responses and 97% clearance rates, including large, deep or multiple BCC lesions. The patients treated were unfit for, or had refused, surgery due to concerns about physical trauma or facial disfigurement. The topical formulation of liposomal bleomycin resulted easy to apply, well-tolerated, painless, and cost-effective and resulted in excellent cosmetic outcomes (S. Chopra, unpublished data). These features appeared to suggest that liposome-encapsulated bleomycin would be potentially useful in treating skin malignancies in the veterinary species. In the pilot study of Knottenbelt et al (2018), there were 118 horses of mixed age and breed. Authors compared the efficacy of tazarotene and 5-FU alone and in combination with Bleosome as topical treatment for equine cutaneous sarcoids. They found that the therapeutic benefit of the novel formulation of topically applied liposome-encapsulated bleomycin (0.1%) in combination with 5-FU or tazarotene was shown to be effective at 12 months in treating 77 and 78%, respectively, of periocular, facial verrucous or occult sarcoids (Knottenbelt et al. 2018). The success of this twice daily treatment over a period of up to 60 days indicates it is a potential new approach to the treatment of certain types of sarcoid in the horse. Importantly, they also found that Bleosome was easily applied by horse owners and remarkably free of side effects in the patients, especially when compared to alternative standard treatments. These findings support preliminary results in human studies (Knottenbelt et al. 2018).

We conducted a case observation study on the Bleosome efficacy as adjuvant treatment, administered after the CO_2 laser surgical excision, in the management of equine cutaneous sarcoids. Here, the main difference compared to the previously mentioned studies was the application of Bleosome to surgical scars and not on gross lesions. In the majority of the cases, the surgical wound was left healing by secondary intention. Healing by secondary intention occurs when the sides of the wound are not opposed, therefore healing must occur from the bottom of the wound upwards. It occurs in the same four stages as primary intention, including: haemostasis**,** where a large fibrin mesh forms, which fills the wound; inflammation, where an inflammatory response acts to remove any cell debris and pathogens present; proliferation, where a granulation tissue forms at the bottom of the wound. This is an important step, as the epithelia can only proliferate and regenerate once granulation tissue fills the wound to the level of the original epithelium, and once the granulation tissue reaches this

level, the epithelia can completely cover the wound; and lastly, the remodelling phase occurs, where the inflammatory response begins to resolve, and wound contraction can occur. Myofibroblasts are vital cells in secondary intention. They are modified smooth muscle cells that contain actin and myosin, and act to contract the wound; decreasing the space between the dermal edges. They also can deposit collagen for scar healing (Chhabra et al. 2017). We speculated that as granulation tissue, collagen and myofibroblasts during the healing process are not organised in thightly structure, such as the one of the *stratum corneum*, the efficacy of penetration of Bleosome through the surgical site could be greater compared to what we found in section 3 in intact skin. Moreover, in this section, we observed that Bleosome is able to penetrate through the inner layers of a sarcoids *in vitro*. Hence, we assumed that the disorganised architecture proper of the granulation tissue might be an easy barrier for Bleosome to trepass and reach the residual cancer cells, compared to the densely compacted aggregation of fibroblasts proper of the sarcoid.

To date, 12 patients fulfilled the inclusion criteria; there were 7 males and 5 females and the mean age of the horses was 7.7 years. 5 patients experienced a complete remission at the time of writing, with an mean follow-up of 14.8 months. 3 patients failed to follow up; however, all of them were reported to be free of recurrence during the last updates, which occurred after 3 months in 1 and 6 months in 2 cases. 4 patients experienced recurrences. Of those, 1 had recurrent lesions at the time of the first treatment at the Dick Vet Equine Hospital and 3 had multiple sarcoids at the initial presentation. Previously, horses affected with multiple sarcoids and with recurrent lesions have been shown to have a poorer prognosis following treatment (Lane 1977). Types of recurrent lesions were fibroblastic in 1 cases, mixed and occult in 1 case, verrucous and verrucous and nodular in the last 2 patients. The presence of verrucous sarcoids was significantly associated with a higher rate of sarcoid recurrence in the study of Compston et al. (2016). Previously poor results have been reported for periocular verrucous sarcoids. The reasons for this are unclear. Histological examination of verrucous sarcoids has shown increased levels of hyperkeratosis, rete pegs and 'picket fence' appearance at the dermoepidermal junction compared with other types of sarcoid except for mixed varieties. These histological characteristics may indicate that verrucous sarcoids extend further into the dermal layer than other types of sarcoid, which could have an influence on excisional margins (Compston et al. 2016). Sites of recurrence varied among all the horses. Follow-ups were conducted

by photos sent by owners, phone, e-mail or clinical re-check. Length of Bleosome treatment was 4 weeks, 2 patients received the topical application for longer (6 weeks) according to the clinician's instructions. One patient, who experienced a recurrence, only received Bleosome treatment for 2 weeks, as the horse was reluctant to being handled and having the cream applied. However, following the recurrence of 3 lesions, she received a course of 4 weeks of Bleosome and she seemed to tolerate the treatment well during the second administration.

The treatment was well tolerated in all the patients, according to the lack of clinical signs associated with pain or discomfort reported by the owners and to the lack of adverse cutaneous reactions at the site of the surgical excision following the Bleosome application. One patient experienced some swelling on the site of the surgical excision during the first week post-surgery. However, it was unlikely due to the Bleosome administration, as the lesion appeared as a minor complication following the surgical procedure and was treated accordingly. Furthermore, this horse had other sarcoids removed in other areas of the body that were treated with Bleosome without showing any side effects. All the other patients treated with Bleosome did not show any pain or adverse reactions to the treatment.

The clinical study we conducted was still on-going at the time of the writing and thus, data shown should be considered as a preliminary insight into the efficacy of the Bleosome as adjuvant treatment in the management of equine cutaneous sarcoids. However, the major limitations so far, include the low number of patients enrolled, that prevents any significant statistical analysis at this stage of the study. Additional bias will occur when long-term follow-up cannot be obtained for all animals, and recall bias is unavoidable when using telephone and mailing communication. Owner-reported data on follow-up were used to obtain information on recurrence. Although it was expected that most owners would be capable of identifying evident lesions, some occult sarcoid types may have been missed in particular locations, such as the inguinal region. Furthermore, at this stage, this was a one-harm study, without a 'control' group of horses treated with CO_2 laser surgical excision only, used as comparison. However, this has the advantage to be a prospective study and in our future plans there are the recruitment of more patients, the inclusion of a 'control' arm, represented by horses treated at the Dick Vet Equine Hospital with the surgical

excision without the Bleosome treatment, and the on-going follow-ups of the patients already treated.

However, to date, our results showed that Bleosome was very well tolerated by the patients and was effective in maintaining the disease-free status in some patients who bore recurrent and/ or multiple sarcoids, sometimes located in area of the body where it is difficult to achieve clear margins with surgery due to anatomical restrictions. Furthermore, the cases who experienced recurrences had lesions that were previously treated at the time of the first check and types of sarcoids and location which are reported in literature to be difficult to treat and more prone to relapse.

5.6 Conclusions, limitations and future directions

This study was aimed to evaluate the ability of Bleosome in penetrating through equine sarcoids and to investigate the efficacy and safety of the treatment as adjuvant therapy in the management of equine cutaneous sarcoids, as part of the comparative study on the potential of Bleosome against NMSC in human and veterinary species.

We treated living sarcoids explants, excised from patients as part of their therapeutic protocol, with F-Bleosome, and assessed that the fluorescent liposomal bleomycin was able to penetrate through the lesion, reaching the bottom of the tumour, after a single administration lasted 6 hours. We established a method to detect the fluorescence intensity within every distance from the outermost surface of the analysed section, calculating the depth at which F-Bleosome particles were visualised. However, the next step would be enriching the tumour-penetration analysis by adding further sarcoids excised and treated in the same manner, of other pathological types, in order to strengthen and confirm our findings.

Subsequently, we conducted a case observation study in order to evaluate the efficacy and safety of Bleosome as adjuvant treatment for equine sarcoids. We treated 11 patients with Bleosome after the CO2 laser surgical excision and 1 patient received concomitant Bleosome and tazarotene treatment without surgical excision. To date, we observed that 5 patients (41.6%) were in complete remission, 4 patients (33.3%) experienced recurrences and 3 (25%) were lost of follow up. The number of patients

evaluated so far was too low to yield statistically significant conclusions and a complete analysis will be performed at the end of the case study. However, there were no adverse reactions reported and the treatment was overall well tolerated.

Overall, we showed the ability of Bleosome in penetrating deep through sarcoids *in vitro* and obtained promising outcomes in the application of Bleosome *in vivo* to date, suggesting the safety and non-invasiveness of the treatment as adjuvant agent for the management of equine cutaneous sarcoids.

Chapter 6 General conclusions

6.1 Summary of findings

Bleomycin is a chemotherapeutic agent which produces cancer cell death mainly by generating DNA single and double-strand breaks (SSB and DSB), and, to some extent, RNA damage as well (J. Chen and Stubbe 2005b). However, current knowledge in the literature indicates that its mechanism of action may be cell-type dependent (Chen and Stubbe 2005). Moreover, as bleomycin is a large and hydrophilic molecule, it cannot easily diffuse across the plasma membrane from the extracellular compartment to the inside of cancer cells, and its passage through the external cutaneous body barrier is restricted (Roy and Horwitz 1984; Lyman et al. 1986). Moreover, when administer systemically, bleomycin has severe intrinsic toxicity (Sleijfer 2001). However, there is evidence suggesting that this drug is highly valued in the treatment of a range of malignancies in human and veterinary medicine, and the target class of tumours, shared between men and animals, are non-melanoma skin cancers (NMSC). To avoid the unwanted side effects following systemic treatment with bleomycin, it has been used as a topical agent for the management of NMSC in human and veterinary species, administering this drug by means of electrochemotherapy (ECT) (Glass et al. 1997; Rodrıguez-Cuevas et al. 2001; Spugnini and Baldi 2019; Tozon, Tamzali, and Cemažar 2017). This therapeutic strategy achieved promising outcomes; however, it can be invasive and painful, and usually requires the patients to undergo general anaesthesia (Impellizeri et al. 2016).

To overcome these issues liposomes loaded with a chemotherapy payload have been proposed as a novel minimally invasive approach to directly and effectively target cancer cells (Utku 2011).

The theoretical benefit of nanocarrier-mediated drugs include greater solubility, longer duration of exposure, selective delivery of entrapped drug to the site of action, superior therapeutic index and the potential to overcome resistance associated with the regular anticancer agent (Zamboni 2008). Within the different types of liposomes, ultra-deformable (UD) or flexible liposomes demonstrated to be the optimal carriers

for the delivery of entrapped active principles through the skin (Cevc and Blume 1992). However, there is still a lack of consensus about the mechanism exploited by these nanoparticles in passing through the several layers of the skin (Honeywell-Nguyen and Bouwstra 2003(B)). For all these reasons, the idea behind the Bleosome was that entrapping of bleomycin within UDs would allow the encapsulated drug to penetrate through the skin, reaching the topical cutaneous tumour, skipping the blood stream and thus, reducing systemic toxicological risks. Moreover, UD liposomes, as small, lipophilic particles, would enable the cellular uptake of the entrapped bleomycin, being potentially effective in penetrating the plasma membrane.

This study focused on the evaluation of the efficacy and safety of the Bleosome as novel, non-invasive treatment for NMSC in veterinary cancer medicine, using companion animals as both target and model for human medicine.

Our first aim was to investigate the ability of Bleosome to penetrate through human, canine and equine skin; to determine the mechanism exploited by UD liposomes to improve the passage of bleomycin through cutaneous layers; and to investigate whether liposomes enable the cellular uptake of the entrapped drug.

Therefore, we sought to explore the mechanism of skin penetration of Bleosome by treating canine, equine and human skin explants with our compound of interest and visualising directly both the liposomes and the entrapped bleomycin within skin layers. In order to perform this study, transmission electron microscope (TEM) and multiphoton microscope (MP) were both used as complimentary techniques: the former allowed the direct visualisation of liposomes, whereas the latter allowed the direct visualisation of encapsulated bleomycin particles within skin samples. Firstly, we treated canine skin sections with Bleosome over a time course, and we sought to visualise the UD liposomes within skin using the TEM, comparing the final images with those from the untreated skin explants, used as control. In doing so, we found the presence of the UD nanoparticles through the *stratum corneum* in the treated samples only. Our results suggested that the nanoparticles are able to penetrate through the *stratum corneum* and reside between corneocytes, but they could not reach layers deeper than this outermost stratum, even after several hours of application of the compound (up to 8 hours of treatment). We performed several replicates of this experiment, optimising the experimental settings in terms of time and modality of skin

treatment. To explore the possibility that the amount of applied compound played the main role in enhancing the penetration of liposomes deeper through the skin, we treated skin explants with repeated application of the compound every 60 minutes, passing from 0.1 ml to 0.4 ml of Bleosome per skin section. Again, we found that UDs were confined in the *stratum corneum* and not in the deeper underlying cellular layers.

Therefore, we concluded that UD liposomes within Bleosome, are able to penetrate through the first outermost layer of the skin; crossing and intercalating between the keratinocytes of the *stratum corneum*, but they are not able to pass beyond this layer. Other studies in literature were concordant with this finding. Bouwstra et al. (2003) conducted a similar experiment using the electron microscopy, and demonstrated that after topical application, flexible liposomes were found intercalated between the outermost skin layers, but no vesicles could be found in layers deeper than the *stratum corneum* (Bouwstra et al. 2003). Authors claimed that, according to Cevc and Blume (2002), the osmotic force resulting from the hydration gradient in the skin is the dominant force for partitioning of vesicles into the *stratum corneum*. However, same authors have noticed that even in a fully hydrated state the water content in the lowest *stratum corneum* layers close to the viable epidermis is much lower than in the central regions of the *stratum corneum*. Therefore, it is expected that as a result of the osmotic force, the vesicle ingredients will not penetrate beyond the level of the lowest layers in the *stratum corneum* (Bouwstra et al. 2003).

Having established the fate of UD liposomes after cutaneous application of Bleosome, we moved to the visualisation of the entrapped bleomycin molecules through the skin. Hence, we treated skin explants from different species according to the same experimental settings of the previous study, but we utilised a different imaging technique. Our preliminary penetration study visualising treated skin explants with the fluorescent microscope demonstrated that the fluorescence of the drug itself was not sufficient to allow a proper visualisation of bleomycin. Thus, we coupled the bleomycin to Bodipy-FL, a green fluorescent fluorophore. To the best of our knowledge, this is the first time that Bodipy-FL has been conjugated to bleomycin, and our main concern was that binding the fluorophore to the bleomcyin molecule, could produce a reduction of its overall efficacy. Therefore, we conducted a viability assays, comparing the efficacy of fluorescently labelled Bleosome (F-Bleosome) with the unlabelled compound and we proved that the F-Bleosome retained the same

efficacy of the non-fluorescent counterpart. Confident in the functionality of F-Bleosome, we directly visualised the penetration of the drug through skin explants of different species.

Canine, equine and human skin sections were treated with F-Bleosome over a time course to assess the extent of penetration of bleomycin-encapsulated liposomes within animal skin. Furthermore, we compared this innovative topical treatment with the standard non-encapsulated bleomycin, labelled with the same fluorophore (F-bleomycin). Our analysis showed that F-Bleosome penetrated significantly deeper through the skin than the free F-bleomycin, and that this was consistent within equine, canine and human skin sections. Furthermore, F-Bleosome penetrated significantly deeper through cutaneous layers over time of treatment; following 4 and 6 hours of administration, the drug molecules were found at a significant greater depth compared to the first 10 minutes of treatment in all the three species.

In all the three species examined, there was a significant difference in the position of F-Bleosome molecules within the skin at each time point of treatment, while this was not the case of the F-bleomycin particles. These findings indicate that the length of treatment is closely related to the ability of F-Bleosome to cross several innermost cutaneous layers, hence, this is an important aspect to be considered when translating this therapy into clinical application.

Moreover, image analysis revealed that, within the canine and equine skin sections treated with F-Bleosome, the deepest drug particles were found at ~300 and 271 µm after 4 hours of treatment and at 800 and 430 µm respectively after 6 hours, which is definitely deeper than the average thickness of the epidermis of both species as previously reported (Theerawatanasirikul et al. 2012; Jorgensen et al. 2018).

To further confirm these findings, examining the images after 4 and 6 hours of treatment, in equine, canine and human sections, F-Bleosome molecules were found intercalated in skin structures at the same level of the cellular nuclei. The first nucleated layer of the skin, starting from the outermost *stratum corneum*, is the *stratum spinosum*, which, in human skin, has an approximate thickness of 100 µm (Horikoshi et al. 2005). Furthermore, the epidermis is an avascular component of the skin (Horikoshi et al. 2005); and in some 3-D images, it is possible to identify few F-Bleosome molecules, located close to structures that appear to be small blood vessels.

This might reinforce the hypothesis that the encapsulated bleomycin is able to penetrate beyond not only the hard outermost corneocytes but also the epidermis. Integrating the findings of the MP and the TEM, we concluded that Bleosome is able to reach the deeper layers of the epidermis and the underlying dermis, according to mechanism number 2 proposed by Verma et al. (2003) acting as penetration enhancer. Of note, liposomes might interact with the hard external keratinocytes, finding their way between lipidic extracellular matrix and lastly being disrupted. This would enable the release of the entrapped bleomycin, rendering the drug free to diffuse across the deeper layers of the dermis and beyond. Our hypothesis is that after 10 minutes, Bleosome consists of bleomycin still encapsulated in liposomes, and this is the main reason why drug molecules are found only in a superficial level, at a depth similar to the one of the free drug, in well-defined, small, round-shaped particles, hence, likely still engulfed in UD nanoparticles. After 4 and 6 hours, once passed beyond the *stratum corneum* the entrapped drug is released out of liposomes and free to expand, to aggregate with other molecules and penetrate in the cellular and vascular deeper dermal layer.

To the best of our knowledge, this is the first study that has investigated the fate of bleomcycin encapsulated within liposomes after topical skin application, through direct visualisation of both UD liposomes and the entrapped drug in live-tissue samples. Our findings support the greater ability of Bleosome to penetrate through the skin, when compared to the free bleomycin, and speculate that UD liposomes, when loaded with bleomycin, act as penetration enhancer, interacting with the *stratum corneum* and releasing the payload after 4 hours of treatment.

To evaluate whether liposomes improve the cellular uptake of bleomycin, we treated two different types of canine cancer cell lines, for short and long time of treatment, with F-Bleosome and F-free bleomycicn, as comparison, and we visualised them in live-cell imaging setting, using the confocal laser scanning microscope (CLSM) and quantified the amount of drug taken-up by fluorescence activated cell sorting (FACS). Our findings showed that bleomycin encapsulated in UD liposomes was internalised by cells more efficiently than the free bleomycin after 2 and 24 hours of treatment, in both types of canine cancer cells treated. Moreover, after 24 hours of treatment, imaging and FACS analysis confirmed that the difference in concentration of Bleosome and free bleomycin inside cells was even greater compared to earlier time

point of treatment, with Bleosome being taken-up more than free-bleomycin. Furthermore, the cellular uptake was dependent on the length of treatment for both free and encapsulated bleomycin; images and FACS confirmed the significantly higher level of green fluorescence within cells after 24 hours of treatment compared to the earlier time point in C2 and CML10 cells treated with both compounds. Of note, the different pattern of fluorescent signal from F-Bleosome between the two time points, led us to hypothesise that liposomal bleomycin particles fuse together in particular cytoplasmic areas, especially after several hours of treatment, or that liposomes accumulate within cellular organelles, such as lysosomes, as part of the endocytic pathway for the cellular internalisation. To further explore this latter hypothesis, we investigated the role of lysosomes within Bleosome treatment, however, due to technical limitations, we could not obtain conclusive results about the involvement of this pathway. However, our observations led us to assume a possible involvement of lysosomes in the Bleosome cellular uptake, and, as this finding has been already speculated in literature, further studies should be conducted to validate this hypothesis. Overall, our results showed that bleomycin, when encapsulated in UD liposomes passes through plasma membrane and is internalised by cancer cells more efficiently than its free counterpart, in two different cancer cell lines. Further studies are required to establish the fate of Bleosome after the cellular internalisation and its translocation to the cellular nucleus, the target of its toxicity.

In literature, there are *in vivo* and *in vitro* evidence about the efficacy of bleomycin as an effective treatment in a range of tumours in human medicine. Therefore, our second major aim was to compare the efficacy of Bleosome in achieving the same outcomes in a range of human and animal neoplasms. To this extend we performed viability and colony formation assays *in vitro* using human, canine and feline cancer cell lines.

The results of cytotoxicity and colony formation assays confirmed that Bleosome is able to kill different types of cancer cell lines *in vitro* at different drug concentrations. However, when its efficacy was compared with the free bleomycin, it appeared that the encapsulated drug was less potent than the free form. The same findings were confirmed when Bleosome was tested for inhibiting cells growth and reproducibility. This finding is in accordance with the literature. Studies demonstrated that encapsulating bleomycin molecules inside vesicles naturally partitioned them away from as well as hindered their presentation to keratinocytes. The compartmentalisation

of the cytotoxin in UDs most likely limits the amount of drug available to the cells *in vitro* (Lau et al. 2005). However, given our results on improved Bleosome cellular uptake, these findings can be refuted treating for instance, cancer cells for longer time. The encapsulated form of bleomycin is internalised in the cell cytoplasm better than the free counterpart, however, it is stored in particular areas (likely lysosomes) and its releasing out from these structures might be delayed, leading to a delayed nuclear uptake and thus, a delayed killing effect. Hence, further studies over longer time of treatment are worth to be conducted, to better elucidate the effective potential of liposomal bleomycin compared to its free form.

We established that Bleosome was able to kill several types of human, canine and feline cancer cell lines and had an insight into its cellular uptake. Hence, subsequently, we aimed to have a better understanding of the molecular effects underlying the mechanism of action of Bleosome at cellular level. Bleomycin produces SSB and DSB (Chen and Stubbe 2005). The sensitivity of cancer cells to bleomycin is reported to be variable and tumour-type dependent (Chen and Stubbe 2005). It is currently unknown why this drug is more efficient against some malignancies rather than others. Studies propose that this variability is related to upregulation of alternative DNA damage and repair signalling pathways (Chen and Stubbe 2005; Pron et al. 1999). As bleomycin main toxicity is achieved by the production of DSB, it is likely that specific DS-lesion repair pathways are involved in this, such as non-homologous end joining (NHEJ) and homologous recombination repair (HRR) (Chen and Stubbe 2005). To this extent, we explored the activation of these two main pathways by means of western blot and qRT PCR, treating with Bleosome canine mast cell tumour (C2) and canine metastatic melanoma (CML10) cell lines, over a time course. We found that all the genes tested resulted in differential expression levels between the two cell lines, following 8 hours of treatment. In particular, we observed an upregulation of HRR in C2 cells, whereas the response of CML10 did not include the activation of any of the tested signalling. However, CML10 has a higher IC_{50} than C2; this suggested that some other mechanisms might be involved in the drug resistance, and that more than one pathway might be activated within the same cell line. However, these preliminary findings confirm the hypothesis of a cell-type dependent response to bleomycin, in its free and encapsulated form and that the activation of the molecular response to the treatment might be activated after 8 hours.

All these reasons led us to investigate the whole transcriptome modification following Bleosome treatment, in order to have a better understanding of the cellular mechanisms triggered by the drug. Hence, we performed next-generation sequencing (NGS) on C2 and CML10 cells. After having proven that cellular response to the treatment was affected more by the timing of treatment rather than by the concentration of the drug, cells were treated with relative Bleosome IC_{50} concentrations for 8 and 24 hours. These time points were chosen based on our previous finding with qRT-PCR, where the most significant variations in gene expressions was found after 8 and 24 hours. Due to technical issues with C2, we excluded this cell lines from the analysis and our results focused on CML10 cells only. In this study, data showed that the majority of differentially expressed genes were found in the contrast between cells treated with Bleosome for 24 hours and untreated cells, suggesting that the major changes in gene expression occurred after prolonged length of treatment.

When cells were treated with Bleosome for 8 hours, the most upregulated genes included growth factors and oncogenes (such as RAB20 and EGR4). Interestingly, after 24 hours of treatment with Bleosome, the most representative upregulated genes compared with untreated cells, were involved in the regulation of extracellular matrix and maintenance of tumour microenvironment, such as IRF5 and PLAUR, but also in the inhibition of cell proliferation and in tumour suppression (HYAL1, ARNT2 and DUSP5). This is an interesting finding as it may indicate that after prolonged time of treatment, melanoma cancer cells are no longer able to rapidly divide and grown; however, to sustain their vitality, they could rely on their tumour microenvironment, which could play a major role in the resistance to the Bleosome, and a valuable target to consider for combined treatments. When the two time points of treatment were compared to the untreated canine melanoma cells**,** another important finding was that the in cells, after both 24 and 8 hours, overexpressed genes responsible for inflammation and modulation of immune response were found. This supported the hypothesis of the formation of a unique tumour microenvironment, which, after Bleosome application, might be the key element in the resistance to the treatment. (Tang and Wang 2016). Current literature supports the role of the tumour microenvironment in the resistance to chemotherapy. Classic cytotoxic chemotherapy targets rapidly proliferating cells. Stromal secretion of ligands promoting proliferation is one of the reasons why cancer cells proliferate rapidly. Chemotherapy cannot

eliminate 100% of cancer cells partially owing to the presence of intrinsic resistant phenotypes within the cancer cell population. Moreover, the tumour microenvironment can promote cancer cell survival and proliferation in a treatment-naive setting and in response to treatment, which does not eliminate nonproliferating stromal cells (Valkenburg, De Groot, and Pienta 2018). Looking at the downregulated elements after Bleosome administration, in the group of cells treated for 8 hours, the majority of genes were involved in cellular metabolism of lipoprotein and endocytosis (LIPG, LDLR, MSMO1), while after 24 hours, key regulator of mitosis and chromosome stability were lost. These findings indicate that following Bleosome treatment, cells have impaired functions in cell cycle progression and cellular division but they can notably promoted by the tumour microenvironment. Chemotherapy-induced DNA damage in the tumour microenvironment causes a stress response in stromal cells, which then secrete many factors that promote cancer cell survival, proliferation, invasion, and metastasis (Valkenburg, De Groot, and Pienta 2018). For example, in a prostate cancer model, DNA damage induced by docetaxel or mitoxantrone caused increased expression of GDNF in stromal cells, which promoted tumour cell proliferation, invasion, and chemotherapy resistance in a paracrine fashion (Huber et al. 2015). Docetaxel and mitoxantrone also caused increased stromal secretion of WNT16, which promotes prostate cancer cell survival in the presence of chemotherapeutic agents (Sun et al. 2012). Similarly, in a lymphoma model, doxorubicin led stromal cells to secrete IL-6 and TIMP1, both of which supported cancer cell survival in the thymus (Gilbert and Hemann 2010). However, mechanisms inhibiting mitosis and cell cycle progression were notably present, indicating an impaired ability in cellular division, confirming that Bleosome treatment affect the ability of this cells to divide, proliferate and exert their function.

To better evaluate the functional significance of these data, we performed pathway analysis using GSEA, Reactome and IPA tools. Our results revealed a set of mechanisms dysregulated in untreated and CML10 cells treated with Bleosome for 8 and 24 hours. For instance, when cells were treated with Bleosome, at both, time points and compared to the untreated, we found that the majority of the upregulated pathways were involved in inflammation and immune response. Among those, a plethora of toll-like receptor (TLR) signalling pathways were found along with processes involved in inflammation and immune response. Interestingly, when interrogating the pathways differentially regulated after 24 hours of treatment compared to the 8 hour time point,

we found that autophagy was also upregulated. We also noted that downregulated pathways were mostly related to DNA synthesis, DNA damage repair and mitotic checkpoints.

The main mechanism of action of bleomycin is to generate DNA DSBs (Chen and Stubbe 2005). DSBs are extremely hazardous lesions for all DNA-bearing organisms and the mechanisms of DSB repair are highly conserved. So far, other authors reported that extended cell-cycle arrest/senescence, apoptosis and mitotic cell death are the most common cellular responses to bleomycin treatment and that bleomycin was found to induce G2/M cell cycle arrest in cancer cell lines (Wang et al. 2013). Thus, they concluded that although the mechanism of bleomycin resistance is unclear, the ability for bleomycin-induced DNA damage to be repaired is the most likely one (Wang et al. 2013).

Our results can open novel perspectives on the putative mechanism of action and of resistance to the treatment, as we have evidence that the DSBs induced by Bleosome are not repaired in canine melanoma cells, and that cell cycle checkpoint and HRR are inhibited.

Taking our findings together, we speculate that after Bleosome treatment, melanoma cancer cells are still metabolically active and produce signals of cell growth. However, importantly, the DNA damage produced by Bleosome cannot be repaired, as the cell cycle progression is arrested, mitotic check points are inhibited along with DNA synthesis and DNA DSB repair mechanisms. We also speculate that cells can respond to the stress of the Bleosome treatment with autophagy. We assessed by viability assays the efficacy of Bleosome in killing CML10 cells, however, in the proteomic study, we did not identify clear markers of cellular apoptosis or other processes directly related to cellular death; thus we hypothesise that autophagy can be a mechanism leading to cellular death after Bleosome treatment. Moreover, in order to survive after the treatment, cells may rely on tumour microenvironment, triggering mostly inflammatory processes and dysregulating immune system, and thus, creating a protective tumour microenvironment. This finding open novel compelling insights into the molecular resistance of Bleosome and bleomycin, highlighting the important role of the tumour stroma in supporting cancer cell survival and recurrence, upon exposure to therapies that target these cells. To combat this resistance, therefore, combining the Bleosome treatment with drugs that target stromal components could be a fundamental next step to consider within preclinical and clinical development.

Bleomycin hydrolase (BLMH), also, has been reported in literature as a possible mechanism of resistance to the bleomycin, although this remains controversial (Chen and Stubbe 2005). Our RNA sequencing results did not reveal any significant difference in the expression of BLMH after Bleosome treatment. To expand on this, we evaluated the expression and protein level of BLMH in cells treated with increasing doses and at various time points after treatment with Bleosomes. We found that either western blot and qRT PCR did not reveal any significant differences in the amount of the enzyme expressed by several cancer cell lines. Moreover, the level of BLMH remained steady not only within the dose titration, but also when compared to the basal level within the respective cells untreated. Furthermore, we evaluated this enzyme at the tumour level by treating equine sarcoids and healthy skin with Bleosome and investigating by IHC differences in the protein levels of BLMH. We showed that the level of BLMH did not changes significantly in the tumour before and after treatment. These results, together with the transcriptomic data, suggest that the level of BLMH does not increase after Bleosome treatment. Although BLMH it is supposed to be involved in the bleomycin resistance, its role is still controversial according to the literature. Blocking its activity, some studies showed that mammalian cells became more sensitive to the bleomycin (Sebti et al. 1991), although others found a lack of connection between this enzyme and the outcome of the treatment (Ramotar and Wang 2003). Our results at both molecular at tumour level did not find any connection between the treatment and the level of BLMH, however, the western blot analysis revealed, in all the cell lines tested, the presence of a second band at a slightly higher molecular weight of the BLMH protein. This might indicate that BLMH is activated post-translationally after the Bleosome treatment.
Hence, further studies are needed to better understand its role in relation to bleomycin and Bleosome treatment, and for future investigation, it would be interesting exploring more in detail the activity more than just the level of this enzyme.

Lastly, we aimed to investigate Bleosome as a non-invasive treatment for NMSC in veterinary species, *in vivo*. Previously, we assessed the efficacy of Bleosome to penetrate through healthy skin; here we utilised similar technique to establish if Bleosome was also able to penetrate through cutaneous sarcoids of horses. With the help of the confocal laser scanning microscope (CLSM) and the F-Bleosome we optimised an innovative technique to visualise the presence of the drug within a living

tumour tissue, excised from patients. We showed that the majority of F-Bleosome, after a single application, resides within the superficial layers of the neoplasm but some F-Bleosome particles were found within the whole depth of each section with the deepest drug particles found very close to the bottom of the lesion (1.6 cm depth). We speculated that after a single application, the majority of the compound reaches mostly the outermost cellular layer of the lesion, leading the Bleosome to be more effective in killing the superficial cells. Hence, this can lead to shrink the tumour in a centripetal manner, decreasing its mass thanks to sequentially repeated application. Further studies can be performed treating the lesion for longer time and/or with repeated application of the compound, visualising the treated lesion over a time course, to gain better understanding of the timing and action of Bleosome within the sarcoid. However, at this preliminary stage, we performed the experiment treating the tumour with an amount sufficient to cover completely external surface, without exploring the optimal therapeutical dose. Moreover, we treated the lesion only once, for a length of 6 hours, and observed that few particles of F-Bleosome were able to reach the bottom layer of the tumour. This information might have important repercussions in the application of the Bleosome on equine patients in clinics, not only because it supports the penetration power of the chemotherapy compound, but also because it suggests that multiple topical applications could be of a great benefit, increasing the number of Bleosome particles within deeper layers of the tumour. This is an important preliminary assessment that enables further studies focused on finding the optimal therapeutic dose of Bleosome to apply on patients *in vivo*. Furthermore, to the best of our knowledge, this was the first time that the topical penetration of a chemotherapeutic was assessed by its direct visualisation within a live-tumour model. This compelling finding not only further confirms our previous data on the efficacy of Bleosome in penetrating through healthy animal and human skin, but may also drive to the development of other innovative similar studies on drug discovery.

A part of this PhD project involved also a case observation study on the efficacy and safety of the Bleosome administration, in combination with other treatment, as part of the therapeutic protocol for equine sarcoids, which was conducted in collaboration with the clinicians of the Dick Vet Equine Hospital of the University of Edinburgh, in particular with Dr Richard Reardon. This study is still on going and results presented in this thesis are preliminary data collected until the time of writing, and should, therefore, be considered as preliminary observations.

The aim of this case observation series was to investigate whether Bleosome could extend the length of remission or achieve long-term cure of equine sarcoids after CO_2 laser excision. To date, 12 patients bearing single or multiple cutaneous sarcoids underwent surgical excision of the tumours by CO_2 laser, followed by 4 or 6 weeks course of Bleosome topical application on the site of the scar, twice a day. Within the group of patients, there were 7 males and 5 females and the mean age of the horses was 7.7 years. Types, location and number of sarcoids treated varied among animals and about half of the patients were presented with lesions that recurred or failed any other previous treatment. 5 patients (41.6%) experienced a complete remission at the time of writing, with a mean follow-up of 14.8 months. 3 patients (25%) failed to follow up; however, all of them were reported to be free of recurrence during the latest updates, which occurred after 3 months in 1 and 6 months in 2 cases. 4 patients (33.3%) experienced recurrence. Overall, the mean follow-up was 12 months. Of note, most of the lesions that recurred after the treatment were types of sarcoids considered at high risk of relapse according to previous studies. None of the patients experienced any adverse effects and, overall, the treatment was very well tolerated.

6.2 Limitations of the study and potential future studies

This study has several limitations. Animal and human skin samples used in this project were collected immediately after the euthanasia, in the case of dogs and horses, and at the time of surgical excision for the human samples. Subcutaneous fat was removed, to facilitate handling later, and the skin samples were stored at -20 ◦C or, in some cases at - 70 ◦C, according to the guidance documents for the conduct of the skin absorption studies (Nakadate 1991; Davies, Ward, and Heylings 2004). These guidance documents claim that animal and human skin can be stored for several months at -20°C. No changes in human skin permeability have been reported in frozen skin stored for up to 466 days. This documents advice to test the viability of the skin before performing a test on permeation/penetration of a compound through the skin. However, the suggested tests to control the quality of the skin have shown to produce different results when applied on the same skin samples in literature, generating doubts on the optimal test to adopt in order to exclude damaged skin (Zhang et al. 2018). Furthermore, several studies have now shown that freezing skin samples does not alter

the skin permeability compared to fresh samples (Barbero and Frasch 2016). Publications involving skin penetration and permeation experiments routinely do not assess the viability of skin sections frozen at -20°C before performing the tests (Mills, Magnusson, and Cross 2003; Cross, Anderson, and Roberts 1998; Yousef et al. 2019; de Oliveira et al. 2020). Therefore, there is established precedence to support our methodology. Furthermore, well preserved frozen biospecimens are reported to be ideal for evaluating the genome, transcriptome, and proteome. Frozen biospecimen degradation can be influenced by factors independent of the collection methodology including tissue type, premortem agonal changes, and warm ischemia time during surgery. Rapid stabilization of tissues by snap freezing immediately can mitigate artifactually altered gene expression and protein phosphorylation profiles. If data is not available for a particular tissue type, a practical goal is snap freezing within 20 minutes. Tissue storage at -70°C can preserve DNA and protein for years but RNA can show degradation at 5 years, and it is reported to decrease the risk of proteins cross-linking when compared to paraffin embedded tissues (Shabinkhani et al. 2014). Of note, this literature support the rationale of using skin explants, immediately snap-frozen following the collection and stored at -20°C and -70°C, as suitable tool to test the ability of Bleosome to penetrate to skin, resembling an *in vivo* model.

In the first part of the study, we optimised a method to directly visualise liposomes and the entrapped bleomycin through skin and sarcoid tumours in live-tissue explants. To this extent, the TEM and the MP provided integrative data, however the TEM analysis was only applied to canine skin. In future, the fate of nanoparticles through equine and human skin should be assessed by TEM. Images obtained with MP were analysed using Imaris software. This program has pre-set tools for analysing images, and we optimised these settings to assess the degree of penetration of F-Bleosome. However, many issues arose including compensation for variability in depth of single skin explants imaged, and the exact dimension and size of the drug particles. We developed a novel Imaris protocol to overcome some of these experimental hurdles. The program successfully identified the majority of F-Bleosome particles but in a minority of cases was unable to differentiate F-Bleosome particles from the autofluorescent structures of the skin, producing the need to manually adjust the count in limited circumstances. Thus, an important improvement could be achieved by designing a personalised script in MATLAB (the programming language used by Imaris), which will allow to meet the remained pending questions and help in

differentiating better the F-Bleosome molecules from the autofluorescent structures of the skin. However, this is the first study, to the best of our knowledge, that successfully visualised directly both the entrapped drug and liposomes within skin, using live-tissues, and we obtained innovative and important information about not only the efficacy of the drug and the mechanism of penetration of Bleosome but also on the methodology to be employed to answer these important research questions. Therefore, new and exciting trials can be conducted to gain more detailed information about the skin penetration of this and other compounds. For instance, liposomal nanoparticles could be labelled with an alternative fluorescent probe to that of the entrapped drug, to enable a direct comparison of the position of the liposomes and the encapsulated bleomycin in the skin using MP.

Subsequently, we observed that the cellular uptake of Bleosome is time-dependent and proved that the ability of Bleosome to cross the plasma membrane and to reach the inside of the cells is superior to that of the free drug. However, during our cytotoxicity assay, we observed that Bleosome is slightly less efficient at killing cancer cells compared to the free drug. We speculated that the encapsulated form of bleomycin may be hindered in its ability to translocate into the nucleus. Further live-cell imaging studies, optimising the labelling of cellular organelles, could further the mechanism of cellular uptake, confirming the involvement of the endocytic pathways, and can enable a better evaluation of the nuclear passage of the drug. Moreover, labelling also the liposomal membrane can elucidate the timing and mechanism of release of the entrapped bleomycin.

The second part of this study was focused on assessing the molecular response to the Bleosome treatment on cancer cell lines, with a particular emphasis on the molecular basis of the mechanism of resistance to the treatment and on exploring the hypothesis of a cell-type dependant response. In this study we used the C2 cells and the CML10 cells, as they showed, by western blotting and qRT-PCR that HRR was the dominant response to bleomycin-induced DNA damage in C2 but not in CML10, confirming the different molecular mechanisms activated in different cell types. To improve the biological significance of the data we used biological replicates at different passages rather than technical replicates. Unfortunately, analysis of the data generated by RNA Seq revealed that C2 cells did not form homogeneous groups according to the time points of treatment; moreover, when considering the number of cell passages, we

found a significant variation in gene expression in samples derived from cells from different passages. This may indicate that the C2 cell line has a mutational load. A recent study about the whole genome sequencing of canine cancer cell lines shows that these cells have a mutated TP53, the gene encoding for p53; hence, this accelerates accumulation of mutations over time leading to the high variance of these cells at different passage number (Das et al. 2020). This should be taken into account for future studies within this cell line, and noted that C2 cells should be used with a given cell passage number window, to avoid significant heterogeneity derived by mutations. However, we did obtain important and novel findings from the sequencing of CML10 cells. Hence, we are confident that performing replicates of the experiment using other canine cancer cell lines, derived from other types of NMSC, would be compelling in order to compare the cellular effects of Bleosome on different cell lines, and to evaluate whether there would be significant differences. Furthermore, the ideal condition for a further transcriptomic profiling of Bleosome-treated samples, would be to utilise skin tumours excised from patients, rather than cell lines. One part of the tumour can be used as the untreated control, and another part can be treated with Bleosome, in order to observe the modification in molecular signalling at the tumour level.

Lastly, our preliminary investigation on the efficacy and safety of Bleosome as adjuvant treatment in the management of equine sarcoids showed promising outcomes to date; however, it is not possible to drawn any conclusion from our data so far, as this study is still under completion and we aim to fully analyse results at the end of case observation study. To date, one of the major shortcomings of this case observation series is the low number of patients involved. Furthermore, as the Dick Vet Equine Hospital is a referral centre, many owners live far away and regular visits for follow-ups can be very difficult in most cases. This led to photographic and telephone updates conducted by referring veterinarians or by the owners. This naturally creates a bias in establishing the exact response to the treatment, as it is influenced by different personal point of views and by personal feelings of the owners. Moreover, one patient did not undergo surgical excision of the sarcoid, like all the others, but received Bleosome as part of a topical treatment. Lastly, this study was not stratified according to the type, location and number of tumours. This can generate variable results, as some types of sarcoids naturally carry worse prognosis than others. However, the study was on going at the time of the writing, and more patients were recruited and

follow-ups are still being collected. Therefore, these results should be considered as preliminary observations and as a first stage of a study on the efficacy and safety of the Bleosome treatment as part of the therapeutic protocol for equine cutaneous sarcoids. The planned next steps in the future are to continue recruiting patients to be treated with Bleosome as adjuvant post-operative treatment, to improve the statistical power of the study and to confirm the lack of side effects of the treatment. Moreover, at this stage, we conducted an observational study. Observational studies and randomised controlled trials are the main types of studies used to evaluate treatments. In the latter, patients are assigned to active or control group by chance (through randomization) in order to reduce errors or bias and to remark only the differences due to the treatment. On the contrary, observational studies do not require randomization: differences in outcomes are only observed after a particular therapy has been opted for. Although randomized controlled trials are considered to be more reliable than observational studies when evaluating treatment effectiveness, meta-analyses that confronted the results on different interventions typologies from both types of studies did not systematically show significant differences in the estimates of the effects (Concato et al. 2000). However, more often observational studies (compared to randomized controlled trials) tend to overestimate the effects of the treatment and show more variability in the estimates of the effects because of residual confounding (Concato et al. 2000). Therefore, we are planning to compare the results of the Bleosome treatment with a 'control arm', represented by horses treated with CO_2 laser excision without post-operative Bleosome treatment, to better evaluate whether the Bleosome treatment is effective at prolonging the disease-free interval, and in achieving long lasting clinical remission.

6.3 Conclusions and future perspectives

NMSC are a class of tumour that share similar behaviour and outcome in some cases in both humans and animals. Advances in cancer research are focusing on precise and minimal invasive approach-based medicine. In this study, we evaluated the efficacy and safety of Bleosome as topical treatment for cutaneous neoplasms, conducting a transversal *in vitro*, *ex vivo* and *in vivo* study, using animals as target and model for human medicine. We have preliminary evidence on the efficacy of the penetration of

Bleosome through healthy skin and cutaneous tumour models, as well as the improved cellular uptake of bleomycin when encapsulated in UD liposomes. We showed how the DNA damage generated by the Bleosome at the cellular level is not repaired in a canine metastatic melanoma cell line, and speculate that the tumour microenvironment may play a significant role in the resistance to the treatment in this particular cell line. We also have evidence indicating that the cellular response to Bleosome is cell-type dependent and that the use of Bleosome as part of the treatment for equine sarcoids has the potential to improve the outcome and well-being of patients, without producing any painful or systemic consequences.

These findings support advanced research on the ability of Bleosome to target a wider range of neoplasms *in vitro*. Similarly, understanding of the cellular mechanisms leading to the acquisition of resistance to Bleosome treatment, would allow the evaluation of combination therapies to use alongside the non-invasive form of liposomal bleomycin. Of note, we conducted a translational study, from *in vitro* experiments to the application of the Bleosome *in vivo*, using human and animal samples. In doing so, we supported the preliminary findings on the safety of Bleosome in human medicine with our case observation study on horses, highlighting the benefits of comparative research between human and veterinary medicine. Within this 'one-health' approach, future studies on the molecular mechanisms of the action of Bleosome and emergence of resistance can improve the formulation and drive the personalised use of the Bleosome in human and veterinary medicine.

Chapter 7 References

Abraham, A. T., X. Zhou, and S. M. Hecht. 2001. "Metallobleomycin-Mediated Cleavage of DNA Not Involving a Threading-Intercalation Mechanism." *Journal of the American Chemical Society* 123 (22): 5167–75. https://doi.org/10.1021/ja002460y.

Absalon, M. J., W. Wu, J. W. Kozarich, and J.A. Stubbe. 1995. "Sequence-Specific Double-Strand Cleavage of DNA by Fe-Bleomycin. 2. Mechanism and Dynamics." *Biochemistry* 34 (6): 2076–86. https://doi.org/10.1021/bi00006a030.

Acosta, A. M., and S. K. Shrihari. 2016. "Mitogen-Activated Protein Kinase Signaling Pathway in Cutaneous Melanoma: An Updated Review." *Archives of Pathology and Laboratory Medicine* 140 (11): 1290–96. https://doi.org/10.5858/arpa.2015-0475-RS.

Alam, M., L.H. Goldberg, S. Silapunt, E.S. Gardner, S.S. Strom, A.W. Rademaker, D.J. and Margolis. 2011. "Delayed Treatment and Continued Growth of Nonmelanoma Skin Cancer." *Journal of the American Academy of Dermatology* 64 (5): 839–48. https://doi.org/10.1016/j.jaad.2010.06.028.

Alavi, M., K. Naser, and S. Mohsen. 2017. "Application of Various Types of Liposomes in Drug Delivery Systems." *Advanced Pharmaceutical Bulletin*. Iran. https://doi.org/10.15171/apb.2017.002.

Alavi, S. E., K.M. Maedeh, A. Fatemeh, M. Fatemeh, and A. Azim. 2013. "Drug Delivery of Hydroxyurea to Breast Cancer Using Liposomes." *Indian Journal of Clinical Biochemistry : IJCB* 28 (3): 299–302. https://doi.org/10.1007/s12291-012-0291-y.

Alnasif N., C. Zoschke, E. Fleige, R. Brodwolf, A. Boreham, E. Rühl, K.M. Eckl, et al. 2014. "Penetration of Normal, Damaged and Diseased Skin - An in Vitro Study on Dendritic Core-Multishell Nanotransporters." *Journal of Controlled Release* 185 (1): 45–50. https://doi.org/10.1016/j.jconrel.2014.04.006.

Alomrani, A. H., M.G. El Maghraby, F.G. Alanazi, M.A. Al-Mohanna, A.A. Ayodele,

and I.A. Alsarra. 2011. “Liposomes for Enhanced Cytotoxic Activity of Bleomycin.” *Drug Development Research* 72 (3): 265–73. https://doi.org/10.1002/ddr.20394.

Alshehri, A., A. Grabowska, and S. Stolnik. 2018. “Pathways of Cellular Internalisation of Liposomes Delivered SiRNA and Effects on SiRNA Engagement with Target MRNA and Silencing in Cancer Cells.” *Scientific Reports* 8 (1): 3748. https://doi.org/10.1038/s41598-018-22166-3.

Amadori, D., and L. Marconato. 2012. *Oncologia Medica Veterinaria e Comparata*. Manuali Pratici Di Veterinaria. Poletto. https://books.google.co.uk/books?id=nlYUnAEACAAJ.

Amaravadi, R., A.C. Kimmelman, and E. White. 2016. “Recent Insights into the Function of Autophagy in Cancer.” *Genes and Development* 30 (17): 1913–30. https://doi.org/10.1101/gad.287524.116.

Angelos, J A, E. Marti, S. Lazary, and L.E. Carmichael. 1991. “Characterization of BPV-like DNA in Equine Sarcoids.” *Archives of Virology* 119 (1–2): 95–109. https://doi.org/10.1007/bf01314326.

Anthony, M L. 2000. “Surgical Treatment of Nonmelanoma Skin Cancer.” *AORN Journal* 71 (3): 552-554,556-558,560-570. https://doi.org/10.1016/s0001-2092(06)61577-9.

Aouida, M., L. Anick, H. Wang, and D. Ramotar. 2004. “Characterization of a Transport and Detoxification Pathway for the Antitumour Drug Bleomycin in Saccharomyces Cerevisiae.” *Biochemical Journal* 384 (1): 47–58. https://doi.org/10.1042/BJ20040392.

Araujo, L., M. Pires de Campos, J.A. Thomazine, and R. Fonseca Vianna Lopez. 2010. “Development of Microemulsions to Topically Deliver 5-Aminolevulinic Acid in Photodynamic Therapy.” *European Journal of Pharmaceutics and Biopharmaceutics : Official Journal of Arbeitsgemeinschaft Fur Pharmazeutische Verfahrenstechnik e.V* 75 (1): 48–55. https://doi.org/10.1016/j.ejpb.2010.01.008.

Arlander, S. J H, B.T. Greene, C.L. Innes, and R.S. Paules. 2008. “DNA Protein

Kinase-Dependent G2 Checkpoint Revealed Following Knockdown of Ataxia-Telangiectasia Mutated in Human Mammary Epithelial Cells." *Cancer Research* 68 (1): 89–97. https://doi.org/10.1158/0008-5472.CAN-07-0675.

Arndt, D., R. Zeisig, D. Bechtel, and I. Fichtner. 2001. "Liposomal Bleomycin: Increased Therapeutic Activity and Decreased Pulmonary Toxicity in Mice." *Drug Delivery: Journal of Delivery and Targeting of Therapeutic Agents* 8 (1): 1–7. https://doi.org/10.1080/107175401300002685.

Barbero, A. M., and H. F. Frasch. 2016. "Effect of Frozen Human Epidermis Storage Duration and Cryoprotectant on Barrier Function Using Two Model Compounds." *Skin Pharmacology and Physiology* 29 (1): 31–40. https://doi.org/10.1159/000441038.

Barrera, M. V., and E. Herrera. 2007. "[Topical chemotherapy for actinic keratosis and nonmelanoma skin cancer: current options and future perspectives]." *Actas dermo-sifiliograficas* 98 (8): 556–62.

Barry, B. W. 1991. "Modern Methods of Promoting Drug Absorption through the Skin." *Molecular Aspects of Medicine* 12 (3): 195–241. https://doi.org/10.1016/0098-2997(91)90002-4.

Bennett, R. A., P. S. Swerdlow, and L. F. Povirk. 1993. "Spontaneous Cleavage of Bleomycin-Induced Abasic Sites in Chromatin and Their Mutagenicity in Mammalian Shuttle Vectors." *Biochemistry* 32 (12): 3188–95. https://doi.org/10.1021/bi00063a034.

Bergh, B. A. van den, J. Vroom, H. Gerritsen, H. E. Junginger, and J. A. Bouwstra. 1999. "Interactions of Elastic and Rigid Vesicles with Human Skin in Vitro: Electron Microscopy and Two-Photon Excitation Microscopy." *Biochimica et Biophysica Acta* 1461 (1): 155–73. https://doi.org/10.1016/s0005-2736(99)00176-5.

Bergvall, K. E. 2013. "Sarcoids." *The Veterinary Clinics of North America. Equine Practice* 29 (3): 657–71. https://doi.org/10.1016/j.cveq.2013.09.002.

Bertino, G.,Sersa G., F. De Terlizzi, A. Occhini, C. C. Plaschke, A. Groselj, C. Langdon, et al. 2016. "European Research on Electrochemotherapy in Head and

Neck Cancer (EURECA) Project: Results of the Treatment of Skin Cancer." *European Journal of Cancer* 63: 41–52. https://doi.org/10.1016/j.ejca.2016.05.001.

Betts, J Gordon, P. Desaix, E. Johnson, J. E Johnson, O. Korol, D. Kruse, B. Poe, et al. 2013. "Anatomy & Physiology." https://open.umn.edu/opentextbooks/BookDetail.aspx?bookId=169.

Bouwstra, J. A, P L. Honeywell-Nguyen, G. S Gooris, and M. Ponec. 2003. "Structure of the Skin Barrier and Its Modulation by Vesicular Formulations." *Progress in Lipid Research* 42 (1): 1–36. https://doi.org/10.1016/s0163-7827(02)00028-0.

Bozzuto, G., and A. Molinari. 2015. "Liposomes as Nanomedical Devices." *International Journal of Nanomedicine* 10: 975–99. https://doi.org/10.2147/IJN.S68861.

Brostrom, H. 1995. "Equine Sarcoids. A Clinical and Epidemiological Study in Relation to Equine Leucocyte Antigens (ELA)." *Acta Veterinaria Scandinavica* 36 (2): 223–36.

Bugaut, H., M. Bruchard, H. Berger, V. Derangère, L. Odoul, R. Euvrard, S. Ladoire, et al. 2013. "Bleomycin Exerts Ambivalent Antitumor Immune Effect by Triggering Both Immunogenic Cell Death and Proliferation of Regulatory T Cells." *PLoS ONE* 8 (6). https://doi.org/10.1371/journal.pone.0065181.

Burger, R. M., J. Peisach, and S. B. Horwitz. 1981. (A) "Activated Bleomycin. A Transient Complex of Drug, Iron, and Oxygen That Degrades DNA." *Journal of Biological Chemistry* 256 (22): 11636–44.

Burger, R. M. 1998. (B) "Cleavage of Nucleic Acids by Bleomycin." *Chemical Reviews* 98 (3): 1153–69. https://doi.org/10.1021/cr960438a.

Burgoyne, P. S., S. K. Mahadevaiah, and J.M.A. Turner. 2007. "The Management of DNA Double-Strand Breaks in Mitotic G2, and in Mammalian Meiosis Viewed from a Mitotic G2 Perspective." *BioEssays* 29 (10): 974–86. https://doi.org/10.1002/bies.20639.

Burma, S., Benjamin P. Chen, M. Murphy, A. Kurimasa, and D. J. Chen. 2001. "ATM

Phosphorylates Histone H2AX in Response to DNA Double-Strand Breaks." *Journal of Biological Chemistry* 276 (45): 42462–67. https://doi.org/10.1074/jbc.C100466200.

Burns, C. A, and M. D. Brown. 2005. "Imiquimod for the Treatment of Skin Cancer." *Dermatologic Clinics* 23 (1): 151–64, vii. https://doi.org/10.1016/j.det.2004.08.007.

Burns, E. M, and N. Yusuf. 2014. "Toll-like Receptors and Skin Cancer." *Frontiers in Immunology* 5 (March): 135. https://doi.org/10.3389/fimmu.2014.00135.

Campana, L. G., A. J. P. Clover, S. Valpione, P. Quaglino, J. Gehl, C. Kunte, M. Snoj, et al. 2016. "Recommendations for Improving the Quality of Reporting Clinical Electrochemotherapy Studies Based on Qualitative Systematic Review." *Radiology and Oncology* 50 (1): 1–13. https://doi.org/10.1515/raon-2016-0006.

Carstanjen, B., P. Jordan, and O. M. Lepage. 1997. "Carbon Dioxide Laser as a Surgical Instrument for Sarcoid Therapy--a Retrospective Study on 60 Cases." *The Canadian Veterinary Journal = La Revue Veterinaire Canadienne* 38 (12): 773–76.

Cevc, G., and G. Blume. 1992. "Lipid Vesicles Penetrate into Intact Skin Owing to the Transdermal Osmotic Gradients and Hydration Force." *BBA - Biomembranes* 1104 (1): 226–32. https://doi.org/10.1016/0005-2736(92)90154-E.

Cevc, G., and G. Blume. 2001. "New, Highly Efficient Formulation of Diclofenac for the Topical, Transdermal Administration in Ultradeformable Drug Carriers, Transfersomes." *Biochimica et Biophysica Acta* 1514 (2): 191–205. https://doi.org/10.1016/s0005-2736(01)00369-8.

Cevc, G., D. Gebauer, J. Stieber, A. Schatzlein, and G. Blume. 1998. "Ultraflexible Vesicles, Transfersomes, Have an Extremely Low Pore Penetration Resistance and Transport Therapeutic Amounts of Insulin across the Intact Mammalian Skin." *Biochimica et Biophysica Acta* 1368 (2): 201–15. https://doi.org/10.1016/s0005-2736(97)00177-6.

Cevc, G., and G. Blume. 2003. (A) "Biological Activity and Characteristics of Triamcinolone-Acetonide Formulated with the Self-Regulating Drug Carriers,

Transfersomes." *Biochimica et Biophysica Acta* 1614 (2): 156–64. https://doi.org/10.1016/s0005-2736(03)00172-x.

Cevc, G., and Dieter G. 2003. (B) "Hydration-Driven Transport of Deformable Lipid Vesicles through Fine Pores and the Skin Barrier." *Biophysical Journal* 84 (2 I): 1010–24. https://doi.org/10.1016/S0006-3495(03)74917-0.

Cevc, G., and G. Blume. 2004. "Hydrocortisone and Dexamethasone in Very Deformable Drug Carriers Have Increased Biological Potency, Prolonged Effect, and Reduced Therapeutic Dosage." *Biochimica et Biophysica Acta* 1663 (1–2): 61–73. https://doi.org/10.1016/j.bbamem.2004.01.006.

Cevc, G., A. Schätzlein, and H. Richardsen. 2002. "Ultradeformable Lipid Vesicles Can Penetrate the Skin and Other Semi-Permeable Barriers Unfragmented. Evidence from Double Label CLSM Experiments and Direct Size Measurements." *Biochimica et Biophysica Acta - Biomembranes* 1564 (1): 21–30. https://doi.org/10.1016/S0005-2736(02)00401-7.

Chaudhary, S., and S. S. Rajuria. 1995. "EFFECTS OF ELECTROCONVULSIVE THERAPY ON CARDIOVASCULAR SYSTEM." *Medical Journal, Armed Forces India* 51 (1): 31–33. https://doi.org/10.1016/S0377-1237(17)30915-2.

Chen, J., and J. A. Stubbe. 2004. "Bleomycins: New Methods Will Allow Reinvestigation of Old Issues." *Current Opinion in Chemical Biology* 8 (2): 175–81. https://doi.org/10.1016/j.cbpa.2004.02.008.

Chen, J., and J.A. Stubbe. 2005. "Bleomycins: Towards Better Therapeutics." *Nature Reviews. Cancer* 5 (2): 102–12. https://doi.org/10.1038/nrc1547.

Chen, Y., R. Xu, J. Chen, X. Li, and Q. He. 2013. "Cleavage of Bleomycin Hydrolase by Caspase-3 during Apoptosis." *Oncology Reports* 30 (2): 939–44. https://doi.org/10.3892/or.2013.2484.

Chhabra S., N. Chhabra, A. Kaur, N. Gupta. 2017. "Wound Healing Concepts in Clinical Practice of OMFS". *J Maxillofac Oral Surg*.;16(4):403-423. doi:10.1007/s12663-016-0880-z

Chiani, M., M.A. Shokrgozar, K. Azadmanesh, D. Norouzian, M. R. Mehrabi, A.

Najmafshar, and A. Akbarzadeh. 2017. “Preparation, Characterization, and in Vitro Evaluation of Bleomycin-Containing Nanoliposomes.” *Chemical Biology and Drug Design* 89 (4): 492–97. https://doi.org/10.1111/cbdd.12869.

Clark, Z. D., and E. L. Frank. 2016. “Development and Implementation of an HPLC-ECD Method for Analysis of Vitamin C in Plasma Using Single Column and Automatic Alternating Dual Column Regeneration.” *Practical Laboratory Medicine* 6 (December): 25–37. https://doi.org/10.1016/j.plabm.2016.09.001.

Compston, P. C., T. Turner, C. E. Wylie, and R. J. Payne. 2016. “Laser Surgery as a Treatment for Histologically Confirmed Sarcoids in the Horse.” *Equine Veterinary Journal* 48 (4): 451–56. https://doi.org/10.1111/evj.12456.

Concato J., N. Shah, R.I. Horwitz. 2000. Randomized, controlled trials, observational studies, and the hierarchy of research designs. *N Engl J Med*.;342(25):1887-1892. doi:10.1056/NEJM200006223422507

Connor, T. H., R. W. Anderson, P.J. Sessink, L. Broadfield, and L. A. Power. 1999. “Surface Contamination with Antineoplastic Agents in Six Cancer Treatment Centers in Canada and the United States.” *American Journal of Health-System Pharmacy : AJHP : Official Journal of the American Society of Health-System Pharmacists* 56 (14): 1427–32. https://doi.org/10.1093/ajhp/56.14.1427.

Corney, D. C. 2013. “RNA-Seq Using Next Generation Sequencing.” *Materials and Methods* 3 (April). https://doi.org/10.13070/mm.en.3.203.

Croft, D., G. O’Kelly, G. Wu, R. Haw, M. Gillespie, L. Matthews, M. Caudy, et al. 2011. “Reactome: A Database of Reactions, Pathways and Biological Processes.” *Nucleic Acids Research* 39 (Database issue): D691-7. https://doi.org/10.1093/nar/gkq1018.

Cross, S. E., C. Anderson, and M. S. Roberts. 1998. “Topical Penetration of Commercial Salicylate Esters and Salts Using Human Isolated Skin and Clinical Microdialysis Studies.” *British Journal of Clinical Pharmacology* 46 (1): 29–35. https://doi.org/10.1046/j.1365-2125.1998.00045.x.

Daphu, I., S. Horn, D. Stieber, J. K. Varughese, E. Spriet, H. A. Dale, K. Ove Skaftnesmo, R. Bjerkvig, and F. Thorsen. 2014. “In Vitro Treatment of

Melanoma Brain Metastasis by Simultaneously Targeting the MAPK and PI3K Signaling Pathways." *International Journal of Molecular Sciences* 15 (5): 8773–94. https://doi.org/10.3390/ijms15058773.

Das, S., R. Idate, K. E. Cronise, D. L. Gustafson, L, Dawn, Biomedical Sciences, Fort Collins, Fort Collins, Fort Collins, and Anschutz Medical Campus. 2020. "HHS Public Access" 18 (8): 1460–71. https://doi.org/10.1158/1535-7163.MCT-18-1346.Identifying.

Davies, D. J., R. J. Ward, and J. R. Heylings. 2004. "Multi-Species Assessment of Electrical Resistance as a Skin Integrity Marker for in Vitro Percutaneous Absorption Studies." *Toxicology in Vitro* 18 (3): 351–58. https://doi.org/10.1016/j.tiv.2003.10.004.

Deguine, J., and G. M. Barton. 2014. "MyD88: A Central Player in Innate Immune Signaling." *F1000prime Reports* 6: 97. https://doi.org/10.12703/P6-97.

Dolinsek, T., L. Prosen, M. Cemazar, T. Potocnik, and G. Sersa. 2016. "Electrochemotherapy with Bleomycin Is Effective in BRAF Mutated Melanoma Cells and Interacts with BRAF Inhibitors." *Radiology and Oncology* 50 (3): 274–79. https://doi.org/10.1515/raon-2016-0042.

Ducat, E., B. Evrard, O. Peulen, and G. Piel. 2011. "Cellular Uptake of Liposomes Monitored by Confocal Microscopy and Flow Cytometry." *Journal of Drug Delivery Science and Technology* 21 (6): 469–77. https://doi.org/10.1016/S1773-2247(11)50076-0.

Durr, N. J., C. T. Weisspfennig, B. A. Holfeld, and A. Ben-Yakar. 2011. "Maximum Imaging Depth of Two-Photon Autofluorescence Microscopy in Epithelial Tissues." *Journal of Biomedical Optics* 16 (2): 26008. https://doi.org/10.1117/1.3548646.

Ehrenfeld, G. M., L. O. Rodriguez, S. M. Hecht, C. Chang, V. J. Basus, and N. J. Oppenheimer. 1985. "Copper(I)-Bleomycin: Structurally Unique Complex That Mediates Oxidative DNA Strand Scission." *Biochemistry* 24 (1): 81–92. https://doi.org/10.1021/bi00322a013.

Eloy, J. O., M. Claro de Souza, R. Petrilli, J. Palma Abriata Barcellos, R. J. Lee, and

J. Maldonado Marchetti. 2014. “Liposomes as Carriers of Hydrophilic Small Molecule Drugs: Strategies to Enhance Encapsulation and Delivery.” *Colloids and Surfaces. B, Biointerfaces* 123 (November): 345–63. https://doi.org/10.1016/j.colsurfb.2014.09.029.

Elsayed, M.A., O. Y. Abdallah, V. F. Naggar, and N. M. Khalafallah. 2006. “Deformable Liposomes and Ethosomes: Mechanism of Enhanced Skin Delivery.” *International Journal of Pharmaceutics* 322 (1–2): 60–66. https://doi.org/10.1016/j.ijpharm.2006.05.027.

Elsayed, M.A., O.Y. Abdallah, V. F. Naggar, and N. M. Khalafallah. 2007. “Lipid Vesicles for Skin Delivery of Drugs: Reviewing Three Decades of Research.” *International Journal of Pharmaceutics* 332 (1–2): 1–16. https://doi.org/10.1016/j.ijpharm.2006.12.005.

Fleury, S., and R. Fonseca Vianna Lopez. 2011. “Topical Administration of Anticancer Drugs for Skin Cancer Treatment.” *Skin Cancers - Risk Factors, Prevention and Therapy*. https://doi.org/10.5772/27785.

Forrester, H. B., J.Li, D. Hovan, A. N. Ivashkevich, and C. N. Sprung. 2012. “DNA Repair Genes: Alternative Transcription and Gene Expression at the Exon Level in Response to the DNA Damaging Agent, Ionizing Radiation.” *PLoS ONE* 7 (12). https://doi.org/10.1371/journal.pone.0053358.

Franzé, S., G. Donadoni, A. Podestà, P. Procacci, M. Orioli, M. Carini, P. Minghetti, and F. Cilurzo. 2017. “Tuning the Extent and Depth of Penetration of Flexible Liposomes in Human Skin.” *Molecular Pharmaceutics* 14 (6): 1998–2009. https://doi.org/10.1021/acs.molpharmaceut.7b00099.

Froudarakis, M., E. Hatzimichael, L. Kyriazopoulou, K. Lagos, P. Pappas, A. G. Tzakos, V. Karavasilis, D. Daliani, C. Papandreou, and E. Briasoulis. 2013. “Revisiting Bleomycin from Pathophysiology to Safe Clinical Use.” *Critical Reviews in Oncology/Hematology* 87 (1): 90–100. https://doi.org/10.1016/j.critrevonc.2012.12.003.

Fulda, S., E. Meyer, C. Friesen, S. A. Susin, G. Kroemer, and K. M. Debatin. 2001. “Cell Type Specific Involvement of Death Receptor and Mitochondrial Pathways

in Drug-Induced Apoptosis." *Oncogene* 20 (9): 1063–75. https://doi.org/10.1038/sj.onc.1204141.

Galiczynski, E. M, and A. T. Vidimos. 2011. "Nonsurgical Treatment of Nonmelanoma Skin Cancer." *Dermatologic Clinics* 29 (2): 297–309, x. https://doi.org/10.1016/j.det.2011.01.011.

Gerst, R., and M. Hölzer. 2018. "PCAGO: An Interactive Web Service to Analyze RNA-Seq Data with Principal Component Analysis." *BioRxiv*, 433078. https://doi.org/10.1101/433078.

Giardino, R., M. Fini, V. Bonazzi, R. Cadossi, A. Nicolini, and A. Carpi. 2006. "Electrochemotherapy a Novel Approach to the Treatment of Metastatic Nodules on the Skin and Subcutaneous Tissues." *Biomedicine and Pharmacotherapy* 60 (8): 458–62. https://doi.org/10.1016/j.biopha.2006.07.016.

Gilbert, L. A, and M. T. Hemann. 2010. "DNA Damage-Mediated Induction of a Chemoresistant Niche." *Cell* 143 (3): 355–66. https://doi.org/10.1016/j.cell.2010.09.043.

Gill, V. L., P. J. Bergman, K. E. Baer, D. Craft, and C. Leung. 2008. "Use of Imiquimod 5% Cream (Aldara™) in Cats with Multicentric Squamous Cell Carcinoma in Situ: 12 Cases (2002-2005)." *Veterinary and Comparative Oncology* 6 (1): 55–64. https://doi.org/10.1111/j.1476-5829.2007.00144.x.

Glass, L. F., M. Jaroszeski, R. Gilbert, D. S. Reintgen, and R. Heller. 1997. "Intralesional Bleomycin-Mediated Electrochemotherapy in 20 Patients with Basal Cell Carcinoma." *Journal of the American Academy of Dermatology* 37 (4): 596–99. https://doi.org/10.1016/S0190-9622(97)70178-6.

Glass, L. F., N. A. Fenske, M. Jaroszeski, R. Perrott, D. T. Harvey, D. S. Reintgen, and R. Heller. 1996. "Bleomycin-Mediated Electrochemotherapy of Basal Cell Carcinoma." *Journal of the American Academy of Dermatology* 34 (1): 82–86. https://doi.org/10.1016/S0190-9622(96)90838-5.

Gothelf, A., L. M. Mir, and J. Gehl. 2003. "Electrochemotherapy: Results of Cancer Treatment Using Enhanced Delivery of Bleomycin by Electroporation." *Cancer Treatment Reviews* 29 (5): 371–87. https://doi.org/10.1016/S0305-

7372(03)00073-2.

Goto, Y., T. Arigami, M. Kitago, S. L. Nguyen, N. Narita, S. Ferrone, D. L. Morton, R. F. Irie, and D. S. B. Hoon. 2008. “Activation of Toll-like Receptors 2, 3, and 4 on Human Melanoma Cells Induces Inflammatory Factors.” *Molecular Cancer Therapeutics* 7 (11): 3642 LP – 3653. https://doi.org/10.1158/1535-7163.MCT-08-0582.

Grawunder, U., D. Zimmer, P. Kulesza, and M. R. Lieber. 1998. “Requirement for an Interaction of XRCC4 with DNA Ligase IV for Wild- Type V(D)J Recombination and DNA Double-Strand Break Repair in Vivo.” *Journal of Biological Chemistry* 273 (38): 24708–14. https://doi.org/10.1074/jbc.273.38.24708.

Griffin, M., M. Abu-El-Haija, M. Abu-El-Haija, T. Rokhlina, and A. Uc. 2012. “Simplified and Versatile Method for Isolation of High-Quality RNA from Pancreas.” *BioTechniques* 52 (5): 332–34. https://doi.org/10.2144/0000113862.

Grit, M, and D. J. Crommelin. 1993. “Chemical Stability of Liposomes: Implications for Their Physical Stability.” *Chemistry and Physics of Lipids* 64 (1–3): 3–18. https://doi.org/10.1016/0009-3084(93)90053-6.

Guo, F., J. Wang, M. Ma, F. Tan, and N. Li. 2015. “Skin Targeted Lipid Vesicles as Novel Nano-Carrier of Ketoconazole: Characterization, in Vitro and in Vivo Evaluation.” *Journal of Materials Science. Materials in Medicine* 26 (4): 175. https://doi.org/10.1007/s10856-015-5487-2.

He, Y., Y. Lan, Y. Liu, H. Yu, Z. Han, X. Li, and L. Zhang. 2016. “Pingyangmycin and Bleomycin Share the Same Cytotoxicity Pathway.” *Molecules (Basel, Switzerland)* 21 (7). https://doi.org/10.3390/molecules21070862.

Hecht, S. M. 1986. “DNA Strand Scission by Activated Bleomycin Group Antibiotics.” *Federation Proceedings* 45 (12): 2784–91.

Hecht, S. M. 1994. “RNA Degradation by Bleomycin, a Naturally Occurring Bioconjugate.” *Bioconjugate Chemistry* 5 (6): 513–26. https://doi.org/10.1021/bc00030a006.

Hecht, S.M. 2000. “Bleomycin: New Perspectives on the Mechanism of Action.” *Journal of Natural Products* 63 (1): 158–68. https://doi.org/10.1021/np990549f.

Helleday, T., E. Petermann, C. Lundin, B. Hodgson, and R. A. Sharma. 2008. “DNA Repair Pathways as Targets for Cancer Therapy.” *Nature Reviews Cancer* 8 (3): 193–204. https://doi.org/10.1038/nrc2342.

Honeywell-Nguyen, P. L., S. Arenja, and J. A. Bouwstra. 2003 (A). “Skin Penetration and Mechanisms of Action in the Delivery of the D2-Agonist Rotigotine from Surfactant-Based Elastic Vesicle Formulations.” *Pharmaceutical Research* 20 (10): 1619–25. https://doi.org/10.1023/a:1026191402557.

Honeywell-Nguyen, P. L., and J. A. Bouwstra. 2003 (B). “The in Vitro Transport of Pergolide from Surfactant-Based Elastic Vesicles through Human Skin: A Suggested Mechanism of Action.” *Journal of Controlled Release : Official Journal of the Controlled Release Society* 86 (1): 145–56. https://doi.org/10.1016/s0168-3659(02)00415-7.

Horikoshi, T., M. Matsumoto, A. Usuki, S. Igarashi, R. Hikima, H. Uchiwa, S. Hayashi, M. M. Brysk, M. Ichihashi, and Y. Funasaka. 2005. “Effects of Glycolic Acid on Desquamation-Regulating Proteinases in Human Stratum Corneum.” *Experimental Dermatology* 14 (1): 34–40. https://doi.org/10.1111/j.0906-6705.2005.00224.x.

Huber, R. M., J. M. Lucas, L. A. Gomez-Sarosi, I. Coleman, S. Zhao, R. Coleman, and P. S. Nelson. 2015. “DNA Damage Induces GDNF Secretion in the Tumor Microenvironment with Paracrine Effects Promoting Prostate Cancer Treatment Resistance.” *Oncotarget* 6 (4): 2134–47. https://doi.org/10.18632/oncotarget.3040.

Hussain, A., S. Singh, D. Sharma, T. J. Webster, K. Shafaat, and A. Faruk. 2017. “Elastic Liposomes as Novel Carriers: Recent Advances in Drug Delivery.” *International Journal of Nanomedicine* 12: 5087–5108. https://doi.org/10.2147/IJN.S138267.

Impellizeri, J., L. Aurisicchio, P. Forde, and D. M. Soden. 2016. “Electroporation in Veterinary Oncology.” *Veterinary Journal* 217: 18–25.

https://doi.org/10.1016/j.tvjl.2016.05.015.

Ince, B., M. Dadaci, P. Oltulu, Z. Altuntas, and F. Bilgen. 2015. “Effect of Dermal Thickness on Scars in Women with Type III-IV Fitzpatrick Skin.” *Aesthetic Plastic Surgery* 39 (3): 318–24. https://doi.org/10.1007/s00266-015-0466-z.

Ishida, T., H. Harashima, and H. Kiwada. 2002. “Liposome Clearance.” *Bioscience Reports* 22 (2): 197–224. https://doi.org/10.1023/a:1020134521778.

Jain, S., V. Mishra, P. Singh, P. K. Dubey, D. K. Saraf, and S. P. Vyas. 2003. “RGD-Anchored Magnetic Liposomes for Monocytes/Neutrophils-Mediated Brain Targeting.” *International Journal of Pharmaceutics* 261 (1–2): 43–55. https://doi.org/10.1016/s0378-5173(03)00269-2.

Ji, Z., K. T. Flaherty, and H. Tsao. 2013. “Targeting the RAS Pathway in Melanoma Current Therapies for Melanoma” 18 (1): 27–35. https://doi.org/10.1016/j.molmed.2011.08.001.

Jia, Y., S. Hao, G. Jin, H. Li, X. Ma, Y. Zheng, D. Xiao, and Y. Wang. 2019. “Overexpression of ARNT2 Is Associated with Decreased Cell Proliferation and Better Prognosis in Gastric Cancer.” *Molecular and Cellular Biochemistry* 450 (1–2): 97–103. https://doi.org/10.1007/s11010-018-3376-y.

Jonkman, J., and C. M. Brown. 2015. “Any Way You Slice It-A Comparison of Confocal Microscopy Techniques.” *Journal of Biomolecular Techniques : JBT* 26 (2): 54–65. https://doi.org/10.7171/jbt.15-2602-003.

Jorgensen, E., G. Lazzarini, A. Pirone, S. Jacobsen, and V. Miragliotta. 2018. “Normal Microscopic Anatomy of Equine Body and Limb Skin: A Morphological and Immunohistochemical Study.” *Annals of Anatomy = Anatomischer Anzeiger : Official Organ of the Anatomische Gesellschaft* 218 (July): 205–12. https://doi.org/10.1016/j.aanat.2018.03.010.

Kamata, Y., Y. Itoh, A. Kajiya, S. Karasawa, C. Sakatani, S. Takekoshi, R. Y. Osamura, and A. Takeda. 2007. “Quantification of Neutral Cysteine Protease Bleomycin Hydrolase and Its Localization in Rat Tissues.” *Journal of Biochemistry* 141 (1): 69–76. https://doi.org/10.1093/jb/mvm005.

Kamata, Y., M. Yamamoto, F. Kawakami, R. Tsuboi, A. Takeda, K. Ishihara, and T. Hibino. 2011. “Bleomycin Hydrolase Is Regulated Biphasically in a Differentiation- and Cytokine-Dependent Manner: Relevance to Atopic Dermatitis?” *Journal of Biological Chemistry* 286 (10): 8204–12. https://doi.org/10.1074/jbc.M110.169292.

Kane, S. A., S. M. Hecht, J. S. Sun, T. Garestier, and C. Helene. 1995. “Specific Cleavage of a DNA Triple Helix by FeII.Bleomycin.” *Biochemistry* 34 (51): 16715–24. https://doi.org/10.1021/bi00051a021.

Kang, J. H., W. Y. Jang, and Y. T. Ko. 2017. “The Effect of Surface Charges on the Cellular Uptake of Liposomes Investigated by Live Cell Imaging.” *Pharmaceutical Research* 34 (4): 704–17. https://doi.org/10.1007/s11095-017-2097-3.

Knottenbelt, D. C., A. H. Watson, J. W. Hotchkiss, S. Chopra, and A. J. Higgins. 2018. “A Pilot Study on the Use of Ultra-Deformable Liposomes Containing Bleomycin in the Treatment of Equine Sarcoid.” *Equine Veterinary Education*, 1–6. https://doi.org/10.1111/eve.12950.

Knottenbelt, D. C., and D. F. Kelly. 2000. “The Diagnosis and Treatment of Periorbital Sarcoid in the Horse: 445 Cases from 1974 to 1999.” *Veterinary Ophthalmology* 3 (2–3): 169–91. https://doi.org/10.1046/j.1463-5224.2000.00119.x.

Knottenbelt, D. C. 2005. “A Suggested Clinical Classification for the Equine Sarcoid.” *Clinical Techniques in Equine Practice* 4 (4): 278–95. https://doi.org/https://doi.org/10.1053/j.ctep.2005.10.008.

Knottenbelt, D. C.. 2019. “The Equine Sarcoid: Why Are There so Many Treatment Options?” *The Veterinary Clinics of North America. Equine Practice* 35 (2): 243–62. https://doi.org/10.1016/j.cveq.2019.03.006.

Koldamova, R .P., I. M. Lefterov, M. T. DiSabella, C. Almonte, S. C. Watkins, and J. S. Lazo. 1999. “Human Bleomycin Hydrolase Binds Ribosomal Proteins.” *Biochemistry* 38 (22): 7111–17. https://doi.org/10.1021/bi990135l.

Kunimoto, T., M. Hori, and H. Umezawa. 1967. “Modes of Action of Phleomycin, Bleomycin and Formycin on HeLa S3 Cells in Synchronized Culture.” *The*

Journal of Antibiotics 20 (5): 277–81.

Kuo, L. J., and L.X. Yang. 2008. “Gamma-H2AX - a Novel Biomarker for DNA Double-Strand Breaks.” *In Vivo (Athens, Greece)* 22 (3): 305–9.

Kuo, M. T. 1981. “Preferential Damage of Active Chromatin by Bleomycin.” *Cancer Research* 41 (6): 2439–43.

Laemmli, U. K. 1970. “Cleavage of Structural Proteins during the Assembly of the Head of Bacteriophage T4.” *Nature* 227 (5259): 680–85. https://doi.org/10.1038/227680a0.

Laiho, L. H, S. Pelet, T. M. Hancewicz, P.D. Kaplan, and P. T. C. So. 2005. “Two-Photon 3-D Mapping of Ex Vivo Human Skin Endogenous Fluorescence Species Based on Fluorescence Emission Spectra.” *Journal of Biomedical Optics* 10 (2): 24016. https://doi.org/10.1117/1.1891370.

Lane, J. G. 1977. “The Treatment of Equine Sarcoids by Cryosurgery.” *Equine Veterinary Journal* 9 (3): 127–33. https://doi.org/10.1111/j.2042-3306.1977.tb04003.x.

Larson, A.M. 2011. “Multiphoton Microscopy.” *Nature Photonics* 5 (1): 1. https://doi.org/10.1038/nphoton.an.2010.2.

Lau, K. G., Y. Hattori, S. Chopra, E. A. O’Toole, A. Storey, T. Nagai, and Y. Maitani. 2005. “Ultra-Deformable Liposomes Containing Bleomycin: In Vitro Stability and Toxicity on Human Cutaneous Keratinocyte Cell Lines.” *International Journal of Pharmaceutics* 300 (1–2): 4–12. https://doi.org/10.1016/j.ijpharm.2005.04.019.

Lee, Y. S., S. Yoon, M. S. Park, J. H. Kim, J. H. Lee, and C. W. Song. 2010. “Influence of P53 Expression on Sensitivity of Cancer Cells to Bleomycin.” *Journal of Biochemical and Molecular Toxicology* 24 (4): 260–69. https://doi.org/10.1002/jbt.20334.

Leitheiser, C. J., M. J. Rishel, X. Wu, and S. M. Hecht. 2000. “Solid-Phase Synthesis of Bleomycin Group Antibiotics. Elaboration of Deglycobleomycin A(5).” *Organic Letters* 2 (21): 3397–99. https://doi.org/10.1021/ol0002469.

Lokeshwar, V. B, W. H. Cerwinka, T. Isoyama, and B. L. Lokeshwar. 2005. “HYAL1 Hyaluronidase in Prostate Cancer: A Tumor Promoter and Suppressor.” *Cancer Research* 65 (17): 7782–89. https://doi.org/10.1158/0008-5472.CAN-05-1022.

Lopez, R. Fonseca Vianna, N. Lange, R. Guy, and M. V. Lopes Badra Bentley. 2004. “Photodynamic Therapy of Skin Cancer: Controlled Drug Delivery of 5-ALA and Its Esters.” *Advanced Drug Delivery Reviews* 56 (1): 77–94. https://doi.org/10.1016/j.addr.2003.09.002.

Lu, T., Y. Zhang, Y. Kidane, A. Feiveson, L. Stodieck, F. Karouia, G. Ramesh, L. Rohde, and H. Wu. 2017. “Cellular Responses and Gene Expression Profile Changes Due to Bleomycin-Induced DNA Damage in Human Fibroblasts in Space.” *PLoS ONE* 12 (3): 1–19. https://doi.org/10.1371/journal.pone.0170358.

Lyman, S, B Ujjani, K Renner, W Antholine, D H Petering, J W Whetstone, and J M Knight. 1986. “Properties of the Initial Reaction of Bleomycin and Several of Its Metal Complexes with Ehrlich Cells.” *Cancer Research* 46 (9): 4472–78.

MacEwen, E. G., Kurzman, I. D., Rosenthal, R. C., Smith, B. W., Manley, P. A., Roush, J. K., & Howard, P. E. 1989. "Therapy for osteosarcoma in dogs with intravenous injection of liposome-encapsulated muramyl tripeptide". *Journal of the National Cancer Institute*, *81*(12), 935–938

Madathil, M. M., C. Bhattacharya, Z. Yu, R. Paul, M. J. Rishel, and S. M. Hecht. 2014. “Modified Bleomycin Disaccharides Exhibiting Improved Tumor Cell Targeting.” *Biochemistry* 53 (43): 6800–6810. https://doi.org/10.1021/bi501102z.

Maghraby, G. M. El, B. W. Barry, and A. C. Williams. 2008. “Liposomes and Skin: From Drug Delivery to Model Membranes.” *European Journal of Pharmaceutical Sciences* 34 (4–5): 203–22. https://doi.org/10.1016/j.ejps.2008.05.002.

Maghraby, G. M. El, A. C. Williams, and B. W. Barry. 1999. “Skin Delivery of Oestradiol from Deformable and Traditional Liposomes: Mechanistic Studies.” *The Journal of Pharmacy and Pharmacology* 51 (10): 1123–34. https://doi.org/10.1211/0022357991776813.

Maghraby, G. M. El, A. C. Williams, and B. W. Barry. 2001 (A) "Skin Delivery of 5-Fluorouracil from Ultradeformable and Standard Liposomes in-Vitro." *The Journal of Pharmacy and Pharmacology* 53 (8): 1069–77. https://doi.org/10.1211/0022357011776450.

Maghraby, G. M. El, A. C. Williams, and B. W. Barry. 2001 (B). "Skin Hydration and Possible Shunt Route Penetration in Controlled Estradiol Delivery from Ultradeformable and Standard Liposomes." *The Journal of Pharmacy and Pharmacology* 53 (10): 1311–22. https://doi.org/10.1211/0022357011777800.

Marconato, L., J. Buchholz, M. Keller, G. Bettini, P. Valenti, and B. Kaser-Hotz. 2013. "Multimodal Therapeutic Approach and Interdisciplinary Challenge for the Treatment of Unresectable Head and Neck Squamous Cell Carcinoma in Six Cats: A Pilot Study." *Veterinary and Comparative Oncology* 11 (2): 101–12. https://doi.org/10.1111/j.1476-5829.2011.00304.x.

Marconato, L. 2009. *Principi Di Chemioterapia in Oncologia*. Tascabili Di Veterinaria / Collana Diretta Da Vincenzo Appicciutoli. Poletto. https://books.google.co.uk/books?id=hDDHSAAACAAJ.

Martens, A, A De Moor, L Vlaminck, F Pille, and M Steenhaut. 2001. "Evaluation of Excision, Cryosurgery and Local BCG Vaccination for the Treatment of Equine Sarcoids." *The Veterinary Record* 149 (22): 665–69. https://doi.org/10.1136/vr.149.22.665.

Matsuo, T., L. Tan Dat, M. Komatsu, T. Yoshimaru, K. Daizumoto, S. Sone, Y. Nishioka, and T. Katagiri. 2014. "Early Growth Response 4 Is Involved in Cell Proliferation of Small Cell Lung Cancer through Transcriptional Activation of Its Downstream Genes." *PLoS ONE* 9 (11). https://doi.org/10.1371/journal.pone.0113606.

McGrath, J. A., and J. Uitto. 2010. "Anatomy and Organization of Human Skin." *Rook's Textbook of Dermatology*. Wiley Online Books. https://doi.org/doi:10.1002/9781444317633.ch3.

Mekid, H., O. Tounekti, A. Spatz, M. Cemazar, F. Z. El Kebir, and L. M. Mir. 2003. "In Vivo Evolution of Tumour Cells after the Generation of Double-Strand DNA

Breaks." *British Journal of Cancer* 88 (11): 1763–71. https://doi.org/10.1038/sj.bjc.6600959.

Metzker, M. L. 2010. "Sequencing Technologies — the next Generation." *Nature Reviews Genetics* 11 (1): 31–46. https://doi.org/10.1038/nrg2626.

Mills, P. C., B. M. Magnusson, and S. E. Cross. 2003. "Effect of Solute Lipophilicity on Penetration through Canine Skin." *Australian Veterinary Journal* 81 (12): 752–55. https://doi.org/10.1111/j.1751-0813.2003.tb14608.x.

Mir, L.M., and S. Orlowski. 1999. "Mechanisms of Electrochemotherapy." *Advanced Drug Delivery Reviews* 35 (1): 107–18. https://doi.org/10.1016/S0169-409X(98)00066-0.

Mitragotri, S, Y. G. Anissimov, A. L. Bunge, H. F. Frasch, R. H. Guy, J. Hadgraft, Gerald B. Kasting, M. E. Lane, and M. S. Roberts. 2011. "Mathematical Models of Skin Permeability: An Overview." *International Journal of Pharmaceutics* 418 (1): 115–29. https://doi.org/10.1016/j.ijpharm.2011.02.023.

Moser, K., K. Kriwet, A. Naik, Y. N. Kalia, and R. H. Guy. 2001. "Passive Skin Penetration Enhancement and Its Quantification in Vitro." *European Journal of Pharmaceutics and Biopharmaceutics : Official Journal of Arbeitsgemeinschaft Fur Pharmazeutische Verfahrenstechnik e.V* 52 (2): 103–12. https://doi.org/10.1016/s0939-6411(01)00166-7.

Nakadate, M. 1991. "OECD: Organization for Economic Co-Operation and Development." *Japan Journal of Water Pollution Research* 14 (7): 437–43. https://doi.org/10.2965/jswe1978.14.437.

Ndoye, A., and A.T. Weeraratna. 2016. "Autophagy- An Emerging Target for Melanoma Therapy [Version 1; Referees: 2 Approved]." *F1000Research* 5 (0): 1–9. https://doi.org/10.12688/F1000RESEARCH.8347.1.

Newlands, C., R. Currie, A. Memon, S. Whitaker, and T. Woolford. 2016. "Non-Melanoma Skin Cancer: United Kingdom National Multidisciplinary Guidelines." *The Journal of Laryngology & Otology* 130 (S2): S125–32. https://doi.org/10.1017/s0022215116000554.

Noonan, P. S, P. Mohan, A. P. Goodwin, and D. K. Schwartz. 2014. “DNA Hybridization-Mediated Liposome Fusion at the Aqueous Liquid Crystal Interface.” *Advanced Functional Materials* 24 (21): 3206–12. https://doi.org/10.1002/adfm.201303885.

Oliveira, D., D. Fontana de Andrade, E. Gadelha de Oliveira, and R. C. Ruver Beck. 2020. “Liquid Chromatography Method to Assay Tretinoin in Skin Layers: Validation and Application in Skin Penetration/Retention Studies.” *Heliyon* 6 (1): e03098. https://doi.org/10.1016/j.heliyon.2019.e03098.

Pai, V. C, C. Hsu, T. Chan, W. Liao, C. Chuu, W. Chen, C. Li, et al. 2019. “ASPM Promotes Prostate Cancer Stemness and Progression by Augmenting Wnt-Dvl-3-Beta-Catenin Signaling.” *Oncogene* 38 (8): 1340–53. https://doi.org/10.1038/s41388-018-0497-4.

Papahadjopoulos, D., M. Cowden, and H. Kimelberg. 1973. “Role of Cholesterol in Membranes. Effects on Phospholipid-Protein Interactions, Membrane Permeability and Enzymatic Activity.” *Biochimica et Biophysica Acta* 330 (1): 8–26. https://doi.org/10.1016/0005-2736(73)90280-0.

Paszko, E., and M. O. Senge. 2012. “Immunoliposomes.” *Current Medicinal Chemistry* 19 (31): 5239–77. https://doi.org/10.2174/092986712803833362.

Paul, A., G. Cevc, and B. K. Bachhawat. 1995. “Transdermal Immunization with Large Proteins by Means of Ultradeformable Drug Carriers.” *European Journal of Immunology* 25 (12): 3521–24. https://doi.org/10.1002/eji.1830251248.

Peng, G., and S. Lin. 2011. “Exploiting the Homologous Recombination DNA Repair Network for Targeted Cancer Therapy.” *World Journal of Clinical Oncology* 2 (2): 73–79. https://doi.org/10.5306/wjco.v2.i2.73.

Perez, A., M. J. Altube, P. Schilrreff, G. Apezteguia, F. Santana Celes, S. Zacchino, C. Indiani de Oliveira, E. L. Romero, and M. J. Morilla. 2016. “Topical Amphotericin B in Ultradeformable Liposomes: Formulation, Skin Penetration Study, Antifungal and Antileishmanial Activity in Vitro.” *Colloids and Surfaces B: Biointerfaces* 139: 190–98. https://doi.org/10.1016/j.colsurfb.2015.12.003.

Perrotta, R., M. Giordano, and M. Malaguarnera. 2011. “Non-Melanoma Skin Cancers

in Elderly Patients." *Critical Reviews in Oncology/Hematology* 80 (3): 474–80. https://doi.org/10.1016/j.critrevonc.2011.04.011.

Peters, S. R. 2010. *A Practical Guide to Frozen Section Technique*. *A Practical Guide to Frozen Section Technique*. https://doi.org/10.1007/978-1-4419-1234-3.

Pettersson, C., K. Bergvall, and P. Humblot. 2011. "Topical Treatment of Equine Sarcoids: A Clinical Pilot Study Comparing Aldara and Xxterra." *Vet Dermatol* 22 (January).

Pron, G., N. Mahrour, S. Orlowski, O. Tounekti, B. Poddevin, J. Belehradek, and L. M. Mir. 1999. "Internalisation of the Bleomycin Molecules Responsible for Bleomycin Toxicity: A Receptor-Mediated Endocytosis Mechanism." *Biochemical Pharmacology* 57 (1): 45–56. https://doi.org/10.1016/S0006-2952(98)00282-2.

Ramotar, D., and H. Wang. 2003. "Protective Mechanisms against the Antitumor Agent Bleomycin: Lessons from Saccharomyces Cerevisiae." *Current Genetics* 43 (4): 213–24. https://doi.org/10.1007/s00294-003-0396-1.

Rangsimawong, W., P. Opanasopit, T. Rojanarata, and T. Ngawhirunpat. 2015. "Mechanistic Study of Decreased Skin Penetration Using a Combination of Sonophoresis with Sodium Fluorescein-Loaded PEGylated Liposomes with d-Limonene." *International Journal of Nanomedicine* 10: 7413–23. https://doi.org/10.2147/IJN.S96831.

Ranji, M., M. Masoudi Motlagh, F. Salehpour, R. Sepehr, J. S. Heisner, R. K. Dash, and K.S. Camara. 2016. "Optical Cryoimaging Reveals a Heterogeneous Distribution of Mitochondrial Redox State in Ex Vivo Guinea Pig Hearts and Its Alteration During Ischemia and Reperfusion." *IEEE Journal of Translational Engineering in Health and Medicine* 4: 1800210. https://doi.org/10.1109/JTEHM.2016.2570219.

Reed, S. D., A. Fulmer, J. Buckholz, B. Zhang, J. Cutrera, K. Shiomitsu, and S. Li. 2010. "Bleomycin/Interleukin-12 Electrochemogenetherapy for Treating Naturally Occurring Spontaneous Neoplasms in Dogs." *Cancer Gene Therapy* 17 (8): 571–78. https://doi.org/10.1038/cgt.2010.13.

Reinert, T., C. Serodio da Rocha Baldotto, F. Pereira Nunes, and A. Alves de Souza Scheliga. 2013. “Bleomycin-Induced Lung Injury.” *Journal of Cancer Research* 2013: 1–9. https://doi.org/10.1155/2013/480608.

Reschke, C. 2012. “Successful treatment of an equine sarcoid. Case report on a combined surgical and photodynamic therapy.” *Tierarztliche Praxis. Ausgabe G, Grosstiere/Nutztiere* 40 (5): 309–13.

Rhodes, L.E., M.A. de Rie, R. Leifsdottir, R. C. Yu, I. Bachmann, V. Goulden, G.A. E. Wong, M. Richard, A. Anstey, and P. Wolf. 2007. “Five-Year Follow-up of a Randomized, Prospective Trial of Topical Methyl Aminolevulinate Photodynamic Therapy vs Surgery for Nodular Basal Cell Carcinoma.” *Archives of Dermatology* 143 (9): 1131–36. https://doi.org/10.1001/archderm.143.9.1131.

Riviere, J. E. and M. G. Papich. 2009. *Veterinary Pharmacology and Therapeutics.* Ames, Iowa: Wiley-Blackwell.

Robertson, K. A., H.A. Bullock, Y. Xu, R. Tritt, E. Zimmerman, T. M. Ulbright, R. S. Foster, L. H. Einhorn, and M. R. Kelley. 2001. “Altered Expression of Ape1/Ref-1 in Germ Cell Tumors and Overexpression in NT2 Cells Confers Resistance to Bleomycin and Radiation.” *Cancer Research* 61 (5): 2220–25.

Robinson, M. D., D. J. McCarthy, and G. K. Smyth. 2010. “EdgeR: A Bioconductor Package for Differential Expression Analysis of Digital Gene Expression Data.” *Bioinformatics (Oxford, England)* 26 (1): 139–40. https://doi.org/10.1093/bioinformatics/btp616.

Rodrıguez-Cuevas, S., S. Barroso-Bravo, J. Almanza-Estrada, L. Cristóbal-Martınez, and E. González-Rodrıguez. 2001. “Electrochemotherapy in Primary and Metastatic Skin Tumors: Phase II Trial Using Intralesional Bleomycin.” *Archives of Medical Research* 32 (4): 273–76. https://doi.org/10.1016/S0188-4409(01)00278-8.

Romero, E. L., and M. J. Morilla. 2013. “Highly Deformable and Highly Fluid Vesicles as Potential Drug Delivery Systems: Theoretical and Practical Considerations.” *International Journal of Nanomedicine* 8: 3171–86. https://doi.org/10.2147/IJN.S33048.

Rossetti, F. C. 2013. “Confocal Laser Scanning Microscopy as a Tool for the Investigation of Skin Drug Delivery Systems and Diagnosis of Skin Disorders.” In , edited by Lívia Vieira Depieri, Ch. 6. Rijeka: IntechOpen. https://doi.org/10.5772/55995.

Roy, S. N., and S. B. Horwitz. 1984. “Characterization of the Association of Radiolabeled Bleomycin A2 with HeLa Cells.” *Cancer Research* 44 (4): 1541–46.

Rushworth, L. K., A. M. Kidger, L. Delavaine, G. Stewart, S. Van Schelven, J. Davidson, Christopher J. Bryant, et al. 2014. “Dual-Specificity Phosphatase 5 Regulates Nuclear ERK Activity and Suppresses Skin Cancer by Inhibiting Mutant Harvey-Ras (HRasQ61L)-Driven SerpinB2 Expression.” *Proceedings of the National Academy of Sciences of the United States of America* 111 (51): 18267–72. https://doi.org/10.1073/pnas.1420159112.

Scagliarini, A., Giuliano B., F. Savini, A. Spadari, F. Sonvico, A. G. Balducci, S. Calbucci, and G. Colombo. 2012. “Treatment of Equine Sarcoids.” *The Veterinary Record*. England. https://doi.org/10.1136/vr.e6506.

Scheuplein, R. J. 1965. “Mechanism of Percutaneous Adsorption. I. Routes of Penetration and the Influence of Solubility.” *The Journal of Investigative Dermatology* 45 (5): 334–46. https://doi.org/10.1038/jid.1965.140.

Schmid, M.H., and H. C. Korting. 1996. “Therapeutic Progress with Topical Liposome Drugs for Skin Disease.” *Advanced Drug Delivery Reviews* 18 (3): 335–42. https://doi.org/https://doi.org/10.1016/0169-409X(95)00019-4.

Schroeder, B. R., M. I. Ghare, C. Bhattacharya, R. Paul, Z. Yu, Paul A. Zaleski, T. C. Bozeman, M. J. Rishel, and S. M. Hecht. 2014. “The Disaccharide Moiety of Bleomycin Facilitates Uptake by Cancer Cells.” *Journal of the American Chemical Society* 136 (39): 13641–56. https://doi.org/10.1021/ja507255g.

Schummer, P., S. Kuphal, L. Vardimon, A. K. Bosserhoff, and M. Kappelmann. 2016. “Specific C-Jun Target Genes in Malignant Melanoma.” *Cancer Biology and Therapy* 17 (5): 486–97. https://doi.org/10.1080/15384047.2016.1156264.

Sebti, S. M., J. P. Jani, J. S. Mistry, E. Gorelik, and J. S. Lazo. 1991. “Metabolic

Inactivation: A Mechanism of Human Tumor Resistance to Bleomycin." *Cancer Research* 51 (1): 227–32.

Sessink, P. J., K. A. Boer, A. P. Scheefhals, R. B. Anzion, and R. P. Bos. 1992. "Occupational Exposure to Antineoplastic Agents at Several Departments in a Hospital. Environmental Contamination and Excretion of Cyclophosphamide and Ifosfamide in Urine of Exposed Workers." *International Archives of Occupational and Environmental Health* 64 (2): 105–12. https://doi.org/10.1007/bf00381477.

Seynhaeve, A. L.B., B. M. Dicheva, S. Hoving, G. A. Koning, and T.L.M. Ten Hagen. 2013. "Intact Doxil Is Taken up Intracellularly and Released Doxorubicin Sequesters in the Lysosome: Evaluated by in Vitro/in Vivo Live Cell Imaging." *Journal of Controlled Release* 172 (1): 330–40. https://doi.org/10.1016/j.jconrel.2013.08.034.

Shabihkhani, M., Lucey, G. M., Wei, B., Mareninov, S., Lou, J. J., Vinters, H. V., Singer, E. J., Cloughesy, T. F., & Yong, W. H. 2014. "The procurement, storage, and quality assurance of frozen blood and tissue biospecimens in pathology, biorepository, and biobank settings". *Clinical biochemistry*, *47*(4-5), 258–266. https://doi.org/10.1016/j.clinbiochem.2014.01.002

Simonetti, Leonardo D D, Guilherme M Gelfuso, Julie C R Barbosa, and Renata F V Lopez. 2009. "Assessment of the Percutaneous Penetration of Cisplatin: The Effect of Monoolein and the Drug Skin Penetration Pathway." *European Journal of Pharmaceutics and Biopharmaceutics : Official Journal of Arbeitsgemeinschaft Fur Pharmazeutische Verfahrenstechnik e.V* 73 (1): 90–94. https://doi.org/10.1016/j.ejpb.2009.04.016.

Sleijfer, S. 2001. "Bleomycin-Induced Pneumonitis." *Chest* 120 (2): 617–24. https://doi.org/10.1378/chest.120.2.617.

Soneson, C., and M. Delorenzi. 2013. "A Comparison of Methods for Differential Expression Analysis of RNA-Seq Data." *BMC Bioinformatics* 14 (March): 91. https://doi.org/10.1186/1471-2105-14-91.

Spugnini, E. P., M. Pizzuto, M. Filipponi, L. Romani, B. Vincenzi, F. Menicagli, A.

Lanza, et al. 2015. “Electroporation Enhances Bleomycin Efficacy in Cats with Periocular Carcinoma and Advanced Squamous Cell Carcinoma of the Head.” *Journal of Veterinary Internal Medicine* 29 (5): 1368–75. https://doi.org/10.1111/jvim.13586.

Spugnini, E. P., and A. Porrello. 2003. “Potentiation of Chemotherapy in Companion Animals with Spontaneous Large Neoplasms by Application of Biphasic Electric Pulses.” *Journal of Experimental & Clinical Cancer Research : CR* 22 (4): 571–80.

Spugnini, E. P., G. Citro, and A. Baldi. 2009. (A) “Adjuvant Electrochemotherapy in Veterinary Patients: A Model for the Planning of Future Therapies in Humans.” *Journal of Experimental and Clinical Cancer Research* 28 (1): 1–5. https://doi.org/10.1186/1756-9966-28-114.

Spugnini, E. P., B. Vincenzi, G. Citro, G. Tonini, I. Dotsinsky, N. Mudrov, and A. Baldi. 2009. (B) “Electrochemotherapy for the Treatment of Squamous Cell Carcinoma in Cats: A Preliminary Report.” *Veterinary Journal* 179 (1): 117–20. https://doi.org/10.1016/j.tvjl.2007.08.011.

Spugnini, E. P, E. Dragonetti, B. Vincenzi, N. Onori, G. Citro, and A. Baldi. 2006. “Pulse-Mediated Chemotherapy Enhances Local Control and Survival in a Spontaneous Canine Model of Primary Mucosal Melanoma.” *Melanoma Research* 16 (1): 23–27. https://doi.org/10.1097/01.cmr.0000195702.73192.a0.

Spugnini, E. Pierluigi, and A. Baldi. 2019. “Electrochemotherapy in Veterinary Oncology: State-of-the-Art and Perspectives.” *The Veterinary Clinics of North America. Small Animal Practice* 49 (5): 967–79. https://doi.org/10.1016/j.cvsm.2019.04.006.

Stadler, S., C. Kainzbauer, R. Haralambus, W. Brehm, E. Hainisch, and S. Brandt. 2011. “Successful Treatment of Equine Sarcoids by Topical Aciclovir Application.” *Veterinary Record* 168 (7): 187. https://doi.org/10.1136/vr.c5430.

Stewart, A. A., B. Rush, and E. Davis. 2006. “The Efficacy of Intratumoural 5-Fluorouracil for the Treatment of Equine Sarcoids.” *Australian Veterinary Journal* 84 (3): 101–6. https://doi.org/10.1016/j.ijcard.2006.01.001.

Strandberg, L., J. Karolin, L. B. Johansson, M. Fa, S. Aleshkov, and T. Ny. 1994. “Fluorescence Studies on Plasminogen Activator Inhibitor 1: Reactive Centre Cysteine Mutants Remain Active after Fluorophore Attachment.” *Thrombosis Research* 76 (3): 253–67. https://doi.org/10.1016/0049-3848(94)90197-x.

Suarez-Farinas, M., M. A. Lowes, L. C. Zaba, and J. G. Krueger. 2010. “Evaluation of the Psoriasis Transcriptome across Different Studies by Gene Set Enrichment Analysis (GSEA).” *PloS One* 5 (4): e10247. https://doi.org/10.1371/journal.pone.0010247.

Subongkot, T., B. Pamornpathomkul, T. Rojanarata, P. Opanasopit, and T. Ngawhirunpat. 2014. “Investigation of the Mechanism of Enhanced Skin Penetration by Ultradeformable Liposomes.” *International Journal of Nanomedicine* 9 (1): 3539–50. https://doi.org/10.2147/IJN.S65287.

Sun, Y., J. Campisi, C. Higano, T. M. Beer, P. Porter, I. Coleman, L. True, and P. S Nelson. 2012. “Treatment-Induced Damage to the Tumor Microenvironment Promotes Prostate Cancer Therapy Resistance through WNT16B.” *Nature Medicine* 18 (9): 1359–68. https://doi.org/10.1038/nm.2890.

Takeuchi, H., H. Kojima, H. Yamamoto, and Y. Kawashima. 2001. “Evaluation of Circulation Profiles of Liposomes Coated with Hydrophilic Polymers Having Different Molecular Weights in Rats.” *Journal of Controlled Release : Official Journal of the Controlled Release Society* 75 (1–2): 83–91. https://doi.org/10.1016/s0168-3659(01)00368-6.

Tang, L., and K. Wang. 2016. “Chronic Inflammation in Skin Malignancies.” *Journal of Molecular Signaling* 11 (1): 1–13. https://doi.org/10.5334/1750-2187-11-2.

Taylor, S., and G. Haldorson. 2013. “A Review of Equine Sarcoid.” *Equine Veterinary Education* 25 (4): 210–16. https://doi.org/10.1111/j.2042-3292.2012.00411.x.

Theerawatanasirikul, S., G. Suriyaphol, R. Thanawongnuwech, and A. Sailasuta. 2012. “Histologic Morphology and Involucrin, Filaggrin, and Keratin Expression in Normal Canine Skin from Dogs of Different Breeds and Coat Types.” *Journal of Veterinary Science* 13 (2): 163–70. https://doi.org/10.4142/jvs.2012.13.2.163.

Theon, A. P., and J. R. Pascoe. 1995. “Iridium-192 Interstitial Brachytherapy for

Equine Periocular Tumours: Treatment Results and Prognostic Factors in 115 Horses." *Equine Veterinary Journal* 27 (2): 117–21. https://doi.org/10.1111/j.2042-3306.1995.tb03046.x.

Thompson, C. D., B. Matta, and B. J. Barnes. 2018. "Therapeutic Targeting of IRFs: Pathway-Dependence or Structure-Based?" *Frontiers in Immunology* 9: 2622. https://doi.org/10.3389/fimmu.2018.02622.

Thompson, R., R. Gatenby, and S. Sidi. 2019. "How Cells Handle DNA Breaks during Mitosis: Detection, Signaling, Repair, and Fate Choice." *Cells* 8 (9): 1049. https://doi.org/10.3390/cells8091049.

Torchilin, V. 2011. "Tumor Delivery of Macromolecular Drugs Based on the EPR Effect." *Advanced Drug Delivery Reviews* 63 (3): 131–35. https://doi.org/10.1016/j.addr.2010.03.011.

Tounekti, O., A. Kenani, N. Foray, S. Orlowski, and L. M. Mir. 2001. "The Ratio of Single-to Double-Strand DNA Breaks and Their Absolute Values Determine Cell Death Pathway." *British Journal of Cancer* 84 (9): 1272–79. https://doi.org/10.1054/bjoc.2001.1786.

Tozon, N., V. Kodre, G. Sersa, and M. Cemazar. 2005. "Effective Treatment of Perianal Tumors in Dogs with Electrochemotherapy." *Anticancer Research* 25 (2A): 839–45.

Tozon, N., Y. Tamzali, and M. Cemažar. 2017. "Electrochemotherapy in Veterinary Oncology." *Handbook of Electroporation* 3: 1953–67. https://doi.org/10.1007/978-3-319-32886-7_107.

Tran, V., J. Moon, and Y. Lee. 2019. "Liposomes for Delivery of Antioxidants in Cosmeceuticals: Challenges and Development Strategies." *Journal of Controlled Release : Official Journal of the Controlled Release Society* 300 (April): 114–40. https://doi.org/10.1016/j.jconrel.2019.03.003.

Trotta, M., E. Peira, F. Debernardi, and M. Gallarate. 2002. "Elastic Liposomes for Skin Delivery of Dipotassium Glycyrrhizinate." *International Journal of Pharmaceutics* 241 (2): 319–27. https://doi.org/10.1016/s0378-5173(02)00266-1.

Ulrich, G., R. Ziessel, and A. Harriman. 2008. “The Chemistry of Fluorescent Bodipy Dyes: Versatility Unsurpassed.” *Angewandte Chemie - International Edition* 47 (7): 1184–1201. https://doi.org/10.1002/anie.200702070.

Umezawa, H., S. Hori, T. Sawa, T. Yoshioka, and T. Takeuchi. 1974. “A Bleomycin-Inactivating Enzyme in Mouse Liver.” *The Journal of Antibiotics* 27 (6): 419–24. https://doi.org/10.7164/antibiotics.27.419.

Umezawa, H., K. Maeda, T. Takeuchi, and Y. Okami. 1966. “New Antibiotics, Bleomycin A and B.” *The Journal of Antibiotics* 19 (5): 200–209.

Utku, N. 2011. “New Approaches to Treat Cancer - What They Can and Cannot Do.” *Biotechnology Healthcare* 8 (4): 25–27.

Valkenburg, K. C., A. E. De Groot, and K. J. Pienta. 2018. “Targeting the Tumour Stroma to Improve Cancer Therapy.” *Nature Reviews Clinical Oncology* 15 (6): 366–81. https://doi.org/10.1038/s41571-018-0007-1.

Verma, D. D., S. Verma, G. Blume, and A. Fahr. 2003. “Liposomes Increase Skin Penetration of Entrapped and Non-Entrapped Hydrophilic Substances into Human Skin: A Skin Penetration and Confocal Laser Scanning Microscopy Study.” *European Journal of Pharmaceutics and Biopharmaceutics* 55 (3): 271–77. https://doi.org/10.1016/S0939-6411(03)00021-3.

Wang, Q., K. Cui, O. Espin-Garcia, D. Cheng, X. Qiu, Z. Chen, M. Moore, et al. 2013. “Resistance to Bleomycin in Cancer Cell Lines Is Characterized by Prolonged Doubling Time, Reduced DNA Damage and Evasion of G2/M Arrest and Apoptosis.” *PLoS ONE* 8 (12): 1–13. https://doi.org/10.1371/journal.pone.0082363.

Weber, G. C., B. A. Buhren, H. Schrumpf, J. Wohlrab, and P. A. Gerber. 2019. “Clinical Applications of Hyaluronidase.” *Advances in Experimental Medicine and Biology* 1148: 255–77. https://doi.org/10.1007/978-981-13-7709-9_12.

Williams, A. C., and B. W. Barry. 1991. “Terpenes and the Lipid-Protein-Partitioning Theory of Skin Penetration Enhancement.” *Pharmaceutical Research* 8 (1): 17–24. https://doi.org/10.1023/a:1015813803205.

Winkler, C. F., E. A. Sausville, D. C. Ihde, A. B. Fischmann, G. P. Schechter, P. P. Kumar, J. R. Nibhanupdi, J. D. Minna, R. W. Makuch, and J. L. Eddy. 1986. "Combined Modality Treatment of Cutaneous T Cell Lymphoma: Results of a 6-Year Follow-Up." *Journal of Clinical Oncology* 4 (7): 1094–1100. https://doi.org/10.1200/JCO.1986.4.7.1094.

Xu, C., W. Zipfel, J. B. Shear, R. M. Williams, and W. W. Webb. 1996. "Multiphoton Fluorescence Excitation: New Spectral Windows for Biological Nonlinear Microscopy." *Proceedings of the National Academy of Sciences of the United States of America* 93 (20): 10763–68. https://doi.org/10.1073/pnas.93.20.10763.

Xu, W., Y. Wang, Y. Wang, S. Lv, X. Xu, and X. Dong. 2019. "Screening of Differentially Expressed Genes and Identification of NUF2 as a Prognostic Marker in Breast Cancer." *International Journal of Molecular Medicine* 44 (2): 390–404. https://doi.org/10.3892/ijmm.2019.4239.

Xu, Y., S. Parsons, W. K. Hansen, D. A. Williams, and M. Kelley. 1998. "Retroviral Overexpression of the Yeast Apurinic/Apyrimidinic (AP) Endonuclease (Apn1) DNA Repair Enzyme Enhances the Level of Protection of Mammalian Cells against Oxidative and Alkylating Agents." *Cancer Gene Therapy* 5 (November): S16–S16.

Yang, B., E. Yang, H. Liao, Z. Wang, Z. Den, and H. Ren. 2015. "ARNT2 Is Downregulated and Serves as a Potential Tumor Suppressor Gene in Non-Small Cell Lung Cancer." *Tumour Biology : The Journal of the International Society for Oncodevelopmental Biology and Medicine* 36 (3): 2111–19. https://doi.org/10.1007/s13277-014-2820-1.

Yang, C., W. Zang, Z. Tang, Y. Ji, R. Xu, Y. Yang, A. Luo, et al. 2018. "A20/TNFAIP3 Regulates the DNA Damage Response and Mediates Tumor Cell Resistance to DNA-Damaging Therapy." *Cancer Research* 78 (4): 1069–82. https://doi.org/10.1158/0008-5472.CAN-17-2143.

Yoon, S., S. Kim, and D. Nam. 2016. "Improving Gene-Set Enrichment Analysis of RNA-Seq Data with Small Replicates." *PloS One* 11 (11): e0165919. https://doi.org/10.1371/journal.pone.0165919.

Yousef, S. A., Y. H. Mohammed, S. Namjoshi, J. E. Grice, H. A.E. Benson, W. Sakran, and M. S. Roberts. 2019. “Mechanistic Evaluation of Enhanced Curcumin Delivery through Human Skin in Vitro from Optimised Nanoemulsion Formulations Fabricated with Different Penetration Enhancers.” *Pharmaceutics* 11 (12). https://doi.org/10.3390/pharmaceutics11120639.

Yu, M., X. Xu, Q. Zhou, N. Deuitch, and M. Lu. 2019. “Haploinsufficiency of A20 (HA20): Updates on the Genetics, Phenotype, Pathogenesis and Treatment.” *World Journal of Pediatrics : WJP*, October. https://doi.org/10.1007/s12519-019-00288-6.

Yu, Z., M. Schmaltz, T. C. Bozeman, R. Paul, M. J. Rishel, K. S. Tsosie, and S. M. Hecht. 2013. “Selective Tumor Cell Targeting by the Disaccharide Moiety of Bleomycin.” *Journal of the American Chemical Society* 135 (8): 2883–86. https://doi.org/10.1021/ja311090e.

Zamboni, W. C. 2008. “Concept and Clinical Evaluation of Carrier-Mediated Anticancer Agents.” *The Oncologist* 13 (3): 248–60. https://doi.org/10.1634/theoncologist.2007-0180.

Zhang, Q., M. Murawsky, T. LaCount, G. B. Kasting, and S. K. Li. 2018. “Transepidermal Water Loss and Skin Conductance as Barrier Integrity Tests.” *Toxicology in Vitro : An International Journal Published in Association with BIBRA* 51 (September): 129–35. https://doi.org/10.1016/j.tiv.2018.04.009.

Zhu, X., X. Luo, G. Feng, H. Huang, Y. He, W. Ma, C. Zhang, M. Zeng, and H. Liu. 2019. “CENPE Expression Is Associated with Its DNA Methylation Status in Esophageal Adenocarcinoma and Independently Predicts Unfavorable Overall Survival.” *PloS One* 14 (2): e0207341. https://doi.org/10.1371/journal.pone.0207341.

Zygogianni, A., G. Kyrgias, J. Scarlatos, M. Koukourakis, K. Souliotis, J. Kouvaris, N. Kelekis, and V. Kouloulias. 2016. “Potential Role of Electrochemotherapy as Anticancer Treatment for Cutaneous and Subcutaneous Lesions.” *Asian Pacific Journal of Cancer Prevention : APJCP* 17 (8): 3753–57.

Chapter 8 Supplementary data

8.1 Appendix 1 Buffers and Solution

Urea lysis buffer: 7 M urea, 0.1 M DTT, 0.01% Triton X-100, 25 mM NaCl, 20 mM HEPES-KOH pH 7.6.

1.5 M Tris-HCl, pH 8.8: 45.43g Tris base in 200 ml H_2O adjusted to pH 8.8 with 12 M HCl. Made up to 250 ml with dH_2O.

10x SDS-Page Running Buffer (1l): 30.3g Tris base, 144g glycine, 10g SDS in 1l H_2O (dissolved on heat stirrer).

10x Tris-Glycine Buffer (Transfer buffer 1L): 30g Tris base, 144g glycine in 1l dH_2O.

10% SDS: 5g SDS dissolved in 40 mL dH_2O with gentle heated stirring. Bring to 50 ml with dH_2O.

10% APS (Ammonium persulphate): 5g APS dissolved in 40 ml dH_2O with gentle stirring. Bring to 50 ml with dH_2O.

1M DTT (dithiothreitol): 1.5g DTT dissolved in 10 ml dH_2O.

4x SDS (sodium dodecyl sulfate) sample buffer (16 mL): 4 mL 20% SDS, 4 ml 1 M Tris pH 6.8, 5 ml 80% glycerol, 2 ml 0.1 M EDTA and 1 ml 1% bromophenol blue. 1 M DTT is added immediately prior to sample preparation in a 1:4 (DTT:Sample buffer) ratio.

Freezing media: FBS (fetal bovine serum) + 10 % DMSO.

PBS (phosphate buffered saline): Provided by the Central Services Unit (CSU) at The Roslin Institute.

PBS Tween (0.1%): 1 ml of Tween 2000 (Scientific Laboratory Supplies) in 1 L of PBS.

5% milk: 5g of skimmed milk powder (Sigma Aldrich) dissolved on 100 ml PBS Tween (0.1%).

BSA (bovine serum albumin) standard solutions: 10mg/mL BSA stock solution (>99% pure grade, A-7638 Sigma) in dH_2O serially diluted to 0.125mg/ml, 0.25mg/ml, 0.5mg/ml, 1mg/ml, 2mg/ml and 4mg/ml.

8.2 Appendix 2 Supplementary material

8.2.1 Staining program for IHC in material and methods (2.6)

1.	Rinse buffer	2 minutes
2.	Primary antibody	30 minutes
3.	Rinse buffer	2 minutes
4.	Rinse buffer	2 minutes
5.	Endogenous block (peroxidase)	10 minutes
6.	Rinse buffer	2 minutes
7.	Rinse buffer	2 minutes
8.	Labelled polymer	40 minutes
9.	Rinse buffer	2 minutes
10.	Rinse buffer	2 minutes
11.	Chromogen (dab or vector red)	15 minutes
12.	Rinse buffer	2 minutes
13.	Dist. Water rinse	5 minutes

Solutions required:

Tris Buffered Saline + Tween 20 (100 ml in 2 l of dH_2O) (TA-999-TT)

Peroxidase Block (Dako K4007)

Red Vector SK-4805 chromagen (Impact Nova)

Liquid DAB (Dako) + substrate (Chromogen system, K3468)

8.2.2 Information leaflet for donation of human skin as part of the study on the Bleosome penetration through the skin (2.9.1.2)

PARTICIPANT INFORMATION SHEET

"Investigation of the penetration potential of a novel formulation of a drug to treat skin cancer"

We'd like to invite you to take part in our research study. Before you decide, it is important that you understand why the research is being done and what it will involve for you. Please take time to read this information, and discuss it with others if you wish. If there is anything that is not clear, or if you would like more information, please ask us.

What is the purpose of the study?

We are testing the efficacy of Bleosome, a novel cream designed for the treatment of skin tumours. Bleosome is made by encapsulating bleomycin, a chemotherapy agent, into small particles that enhance the penetration of the drug through the skin. Our research is focused on determining how far through the skin Bleosome penetrates and this will give us an indication as to how successful it will be in reaching the deeper layers of the tumour. We have completed this work with dog and horse skin and would now like to do this work with human skin. We are inviting you to be part of this research by donating the excess skin that will be removed during your surgery. In the lab, we will apply Bleosome cream to the skin section and look at it under the microscope to see how far through the skin the drug has travelled.

Why have I been invited?

You are invited because you have planned plastic surgery, which involves the removal of a portion of skin. This surplus of skin is required to enable us to study how effective this treatment is on human skin. We will apply Bleosome cream to the top of the skin explant, and at different time points we will look at the skin section under the microscope to see how far through the skin the drug has travelled. At the end of the experiment, the skin will be destroyed.

Do I have to take part?

Your participation to this study is entirely voluntary.

What will happen to me if I decide to take part?

Beyond agreeing to donate the skin removed during your planned surgery, this study does not require anything further from you. Your therapeutic plan will not be affected.

What should I consider?

If you have known skin problem, please let us know about them.

Are there any possible disadvantages or risks from taking part?

There are no side effects or risks for you associated with your participation in the study; we will collect only skin that is the by-product of your planned surgery.

What are the possible benefits of taking part?

There are no financial benefits in being part of the study.

Will my General Practitioner/family doctor (GP) be informed of my participation?

We will contact your GP and let her/him know about your involvement in the study.

Will my taking part in the study be kept confidential?

All your personal data will be kept strictly confidential, your samples will be stored only fully anonymised and identified by a code rather than by your name.

What will happen to the samples I give?

After the collection, your skin donation will be frozen and transported to our labs. It will be then thawed and treated with Bleosome for several hours, subsequently, the skin will be processed to be observed under the microscope to see how far through the skin the drug has travelled. At the end of the experiment, the skin will be destroyed.

All skin explants will be used for this purpose only and any unused samples will be disposed of six months after collection.

What will happen to the results of this study?

This study has scientific relevance; hence, the results may be shared in the scientific community through publications and/or conferences, this can involve also images taken from your biological samples, before and after the study. However, your personal information will be kept strictly confidential and you will be identified by a number.

Some of the research being undertaken will also contribute to the fulfilment of an educational requirement (e.g. doctoral thesis and academic presentations).

Who is organising and funding the study?

All work will be carried out at The Roslin Institute, the University of Edinburgh. This work is funded by SPS Animal Care Company Ltd.

Further information and contact details:

Please contact by e-mail:

Thank you for considering taking part.

8.2.3 Consent form for donors of human skin as part of the study on the Bleosome penetration through the skin (2.9.1.2)

Consent form for the donation of skin to study the penetration of a novel formulation of a drug to treat skin cancer

This Informed Consent Form (ICF) is for patients undergoing plastic surgery involving skin reduction to donate the skin removed during surgery to be used in a study to determine the penetration of Bleosome cream through the layers of the skin. This product has previously been tested on explants of dog and horse skin and we would like to compare these results to human skin.

The title of our research project is “Investigation of the penetration potential of a novel formulation of a drug to treat skin cancer”.

The Principal Investigator of this project is Prof. David J. Argyle. All work will be carried out at The Roslin Institute. This work is funded by SPS Animal Care Company Ltd.

Part I: Information sheet

I am Giulia Ferrari, and I work for The Roslin Institute. We are doing research on a new drug called Bleosome that we hope will be used to successfully treat skin cancer. Bleosome is a cream that is applied to the tumour. Our research is focused on determining how far through the skin Bleosome penetrates and this will give us an indication as to how successful it will be in reaching the deeper layers of the tumour. We have completed this work with dog and horse skin and would now like to do this work with human skin. We are inviting you to be part of this research by donating the excess skin that will be removed during your surgery. In the lab we will apply Bleosome cream to the skin section and look at it under the microscope to see how far through the skin the drug has travelled.

Purpose of the research

Skin cancer is the most common cancer in the UK, and rates continue to rise. Drugs that could be applied directly to the skin tumour are poorly absorbed and have limited effect. Here we are testing novel formulation of a drug called Bleosome. Bleosome is an established chemotherapy drug, bleomycin, packaged inside a bubble composed of tiny fat molecules, which aid absorption through the skin. The skin is made up of many different layers and our research is focused on determining how far through the skin Bleosome can travel. This is preliminary work to show that the Bleosome cream can penetrate through the skin layers, we will then use this information to find out how well Bleosome penetrates through a tumour, with the aim of establishing a new treatment to fight skin cancer.

Type of Research Intervention

This research will **not** involve any additional procedures. We will use the excess skin removed during your surgery.

Participant selection

We are inviting all adults, without known skin issues, undergoing skin removal surgery to donate skin explants for our study.

Voluntary participation

Your participation is voluntary. Skin removed during your surgery will be disposed of, as is general practise, if you choose not to participate in this study.

Procedures and protocol

Skin removed during your surgery will be frozen. In the laboratory we will cut the skin explant into 2 x 2 x 1 cm dimensions and apply Bleosome cream to the top of the skin; at different time points we will look at the skin section under the microscope to see how far through the skin the drug has travelled. At the end of the experiment, the skin will be destroyed.

All skin explants will be used for this purpose only and any unused samples will be disposed of six months after collection.

Beyond the initial donation patient participation is **not** required.

Side-effects and risks

There are no side-effects or risks. We will only use skin that is the by-product of your planned surgery.

Confidentiality

Information collected about you will be confidential. Any information about you will have a number on it instead of your name.

Sharing the results

This research is of significant scientific value and we will share the results with the scientific community through publications and conferences. All patient information will be confidential.

Part II: Certificate of consent

I have read the foregoing information, or it has been read to me. I have had the opportunity to ask questions about it and any questions that I have asked have been answered to my satisfaction. I consent voluntarily to participate as a participant in this research and that any data generated may be used for scientific publication.

Print Name of Participant_____

Signature of Participant _____

Date _____

Day/month/year

Statement by the researcher/person taking consent

I have accurately read out the information sheet to the potential participant, and to the best of my ability made sure that the participant understands. I confirm that the participant was given an opportunity to ask questions about the study, and all the questions asked by the participant have been answered correctly and to the best of my ability. I confirm that the individual has not been coerced into giving consent, and the consent has been given freely and voluntarily.

A copy of this ICF has been provided to the participant.

Print Name of Researcher/person taking the consent_____

Signature of Researcher /person taking the consent_____

Date _____

Day/month/year

8.2.4 Optimised protocol for IMARIS 9.1.2. (3.3.5.4)

- 3-D images, captured with the multiphoton and automatically stored as ZEN files (AIMApplication documents) are converted into IMARIS FILE.IMS
- Pictures appear in the "Arena" in Imaris software;
- "Groups" are created to compared groups of files;
- "SPOTS" tool is used to identify F-Bleosome and F-free bleomycin molecules and structure emitting high intensity of green fluorescence (such as some nuclei, co-emitting Hoechst staining); within this command, the following settings are used as default for all the file analysed, to customize the function to the purpose of this study:
    - Algorithm Settings: tick "Different Spot Sizes (Region Growing)"
    - Source Channel: Channel 2 – NDD R4
    - Spot Detection: Estimated XY Diameter: 8.30 um, tick "Model PSF-elongation along Z-axys", Estimated Z Diameter: 16.6um, tick Background Subctraction"
    - Filter Type: "Quality", Upper and Lower threshold: The value is automatically set (depending on images. Between 1 and 10%)
    - Spot Regions from: Local Contrast
    - Region Treshold: 0, Diamter from: Region Volume

- "SURFACES" tool is used to identify Hoechst staining objects (mainly nuclei) and autofluorescent skin structures (structures emitting low level of Hoechst staining and low level of green autofluorescence concomitantly; e.g. hair follicles, glands, connective tissue); within this command, the following settings are used as default for all the file analysed, to customize the function to the purpose of this study:
    - Algorithm settings: all unticked
    - Source Channel: Channel 1 – NDD R3, tick "Smooth", Surfaces details: 1.66 um; Thresholding: tick "Background subtraction (local Contrast), Diameter of largest Sphere which fits into the object: 6.23 um
    - Threshold: Lower threshold: 0, Upper threshold: 166
    - Filter Type: Number of Voxels Img=1: Lower threshold: 10, Upper threshold: 65508 (the maximum for each file)

- On "Matlab": "Distance Transformation", tick "Outside Surface Object"
- On "Edit":"Change Data Type",tick"32 bit float";
- On"Matlab":"Find Spot Close to The Surfaces": threshold: "0.5" ;

- “Spots Close to The Surfaces” are the nuclei identified as “spots” (close to other “surfaces”) and autofluorescent green structure. They are turned in MAGENTA colour for ease of observation;
- “Spots Far From the Surfaces” are the objects emitting green fluorescence, far from autoflurescence structure (the majority of F-Bleosome and F-free bleomycin molecules). They are turned in GREEN for ease of observation;
- “Stats” command gives the Area, Volume and Position of the Spots. Highlight “spots far from the surface” and click on STATS----export AREA, VOLUME and POSITION.

8.2.5 Link for the access to the live cell imaging videos of the cellular uptake of F-Bleosome and F-bleomcyin in C2 and CML10 cells (4.4.2)

https://uoe-my.sharepoint.com/:f:/g/personal/s1690685_ed_ac_uk/EsxsQnwjXKdOr9iMJnsooCUBSe4GxtI0_kfPH5mxUvX2vQ?e=FlGVLq

Password: gfthesis2020

- ‘C2 2h F-Bleosome’: video corresponding to C2 cells treated for 2 hours with F-Bleosome
- ‘C2 2h F-Bleomycin’: video corresponding to C2 cells treated for 2 hours with F-Bleomycin
- ‘C2 24h F-Bleosome’: video corresponding to C2 cells treated for 24 hours with F-Bleosome
- ‘C2 24h F-Bleosome’: video corresponding to C2 cells treated for 24 hours with F-Bleomycin
- ‘CML10 2h F-Bleosome’: video corresponding to C2 cells treated for 2 hours with F-Bleosome
- ‘CML10 2h F-Bleomycin’: video corresponding to C2 cells treated for 2 hours with F-Bleomycin
- ‘CML10 24h F-Bleosome’: video corresponding to C2 cells treated for 24 hours with F-Bleosome

- ‘CMl10 24h F-Bleomycin’: video corresponding to C2 cells treated for 24 hours with F-Bleomycin

8.2.6 Dysregulated biological processes assessed by GSEA as part of the functional annotation analysis within the NGS of CML10 cells treated with a time course of Bleosome (4.4.4.3)

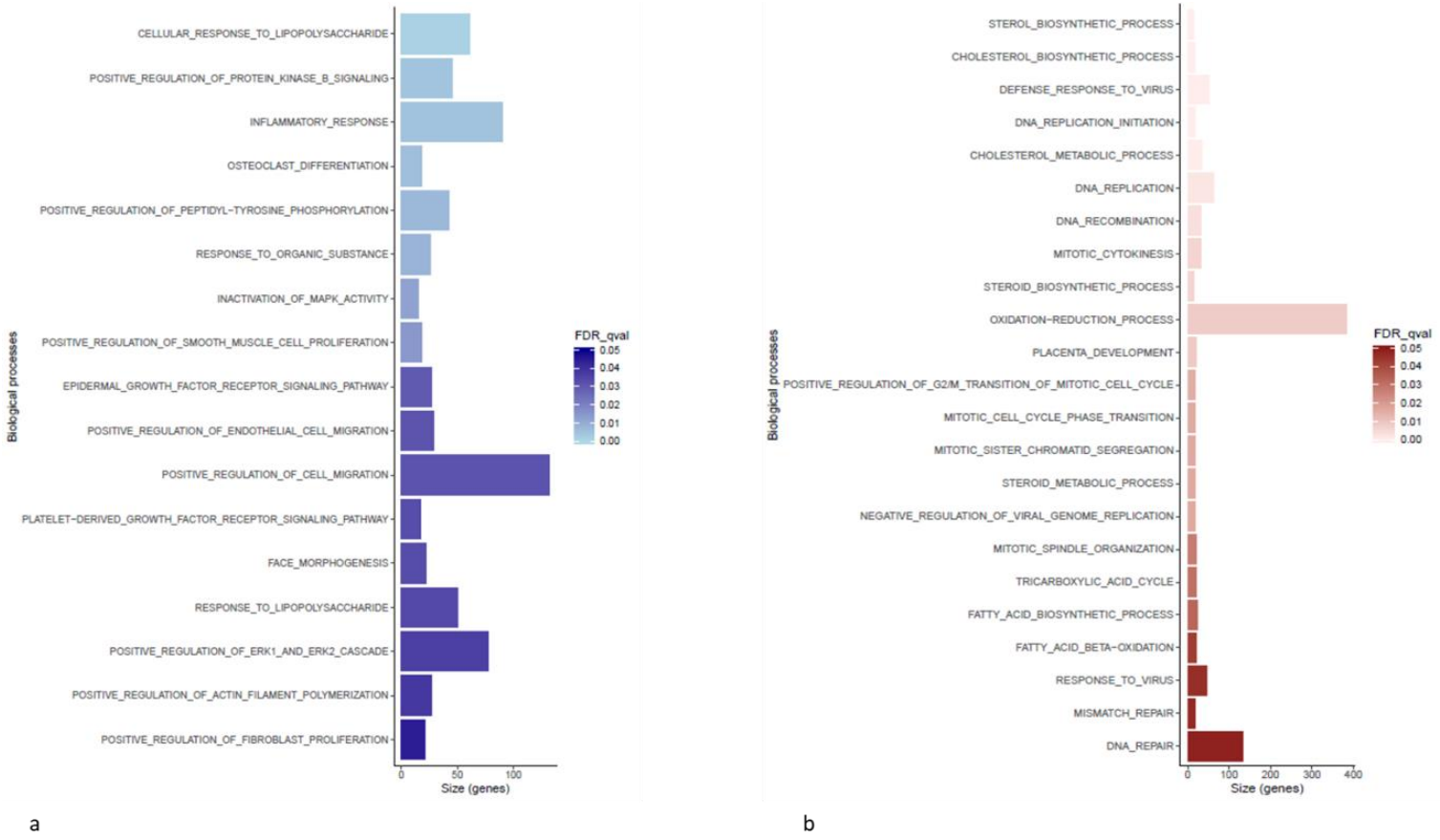

Figure 8.1 *Top most significant (according to FDR<0.05) upregulated (a) and downregulated (b) Biological processes between CML10 cells treated with Bleosome for 8 hours and CML10 cells untreated. Analysis were performed using gene set enrichment analysis (GSEA) software.*

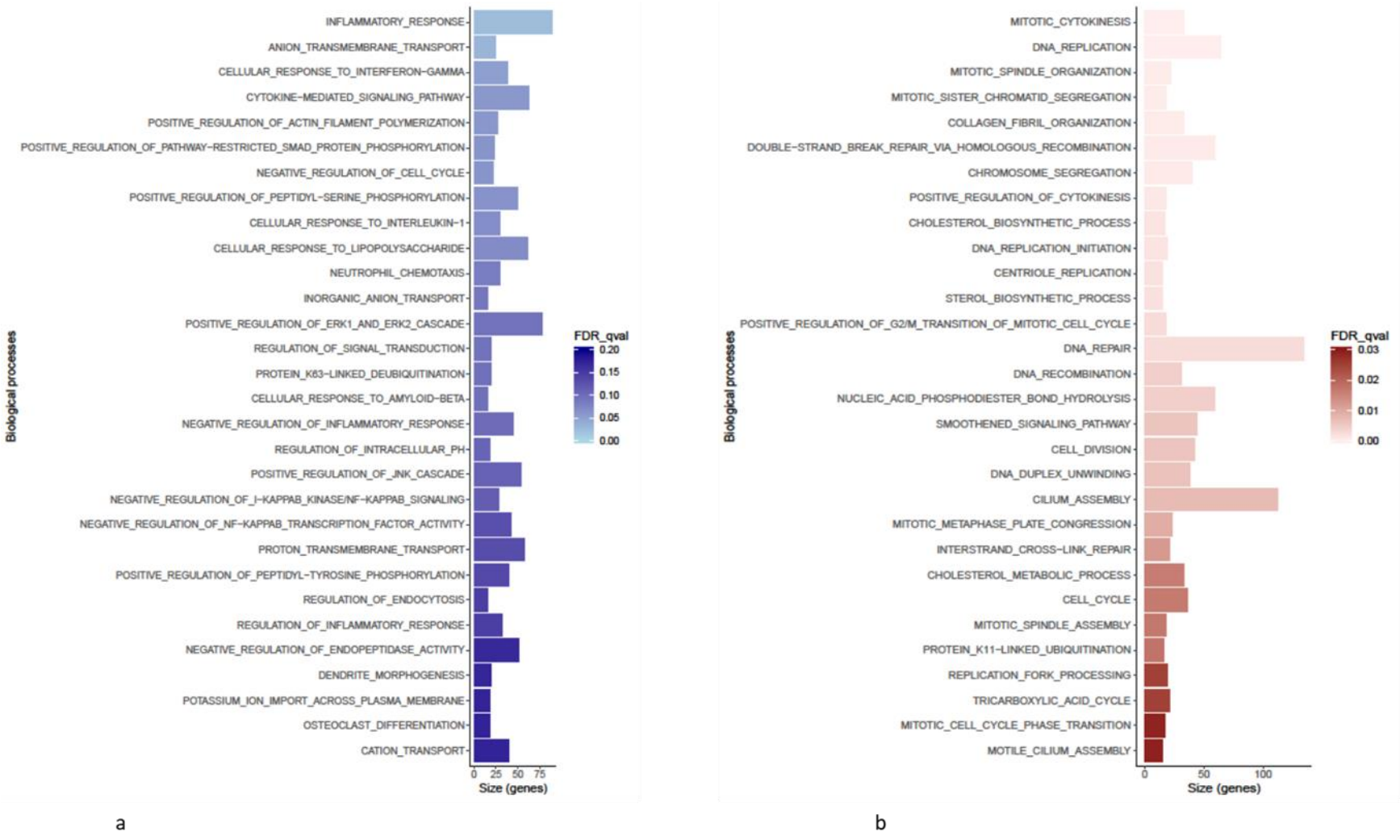

Figure 8.2 *Top most significant (according to FDR<0.05) upregulated (a) and downregulated (b) Biological processes between CML10 cells treated with Bleosome for 24 hours and CML10 cells untreated. Analysis were performed using gene set enrichment analysis (GSEA) software.*

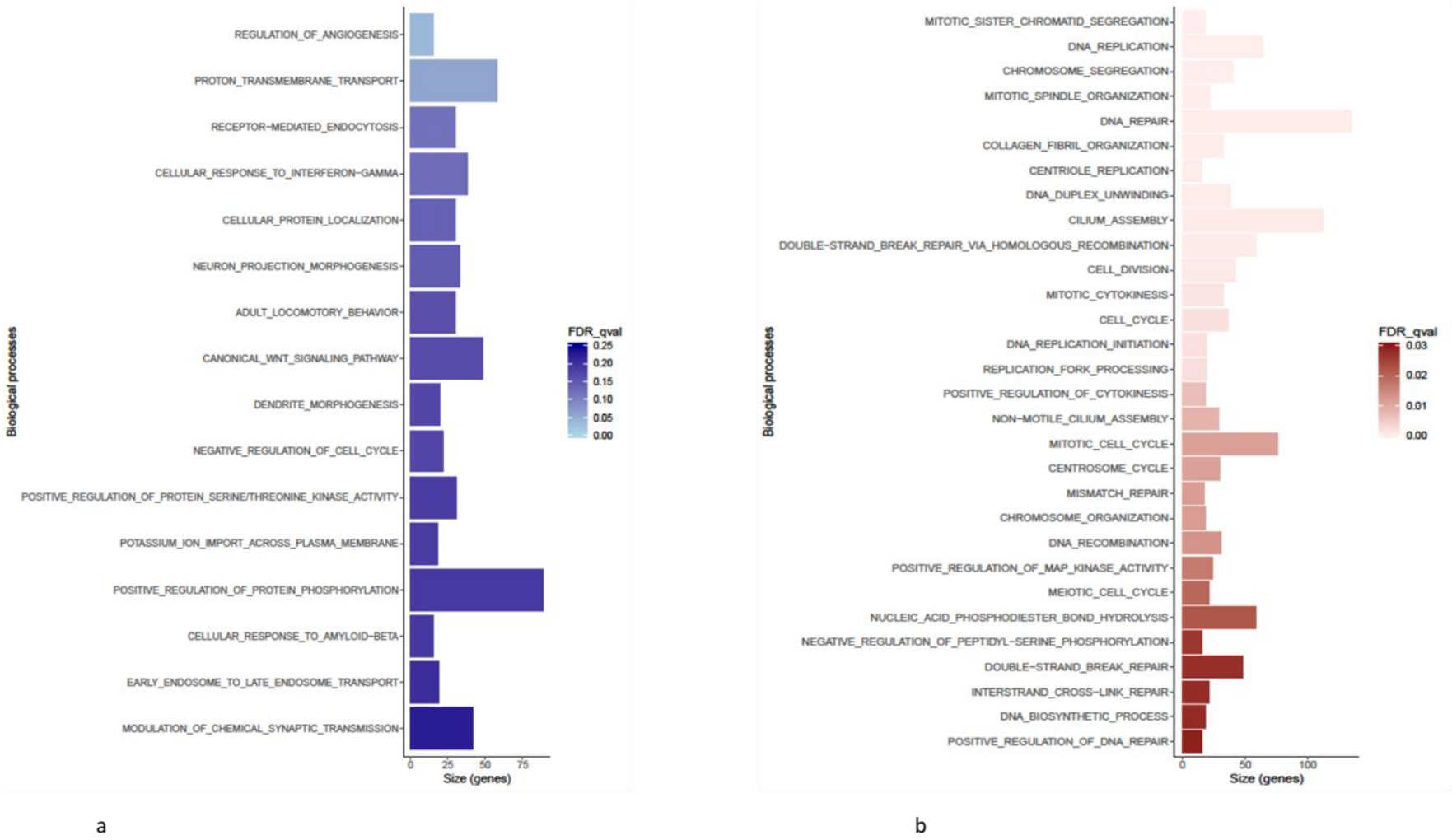

Figure 8.3 *Top most significant (according to FDR<0.05) upregulated (a) and downregulated (b) Biological processes between CML10 cells treated with Bleosome for 24 hours and CML10 cells treated for 8 hours. Analysis were performed using gene set enrichment analysis (GSEA) software.*

8.2.7 Equine melanoma as positive control for IHC slides of equine sarcoids stained with anti-BLMH antibody (4.4.5.2)

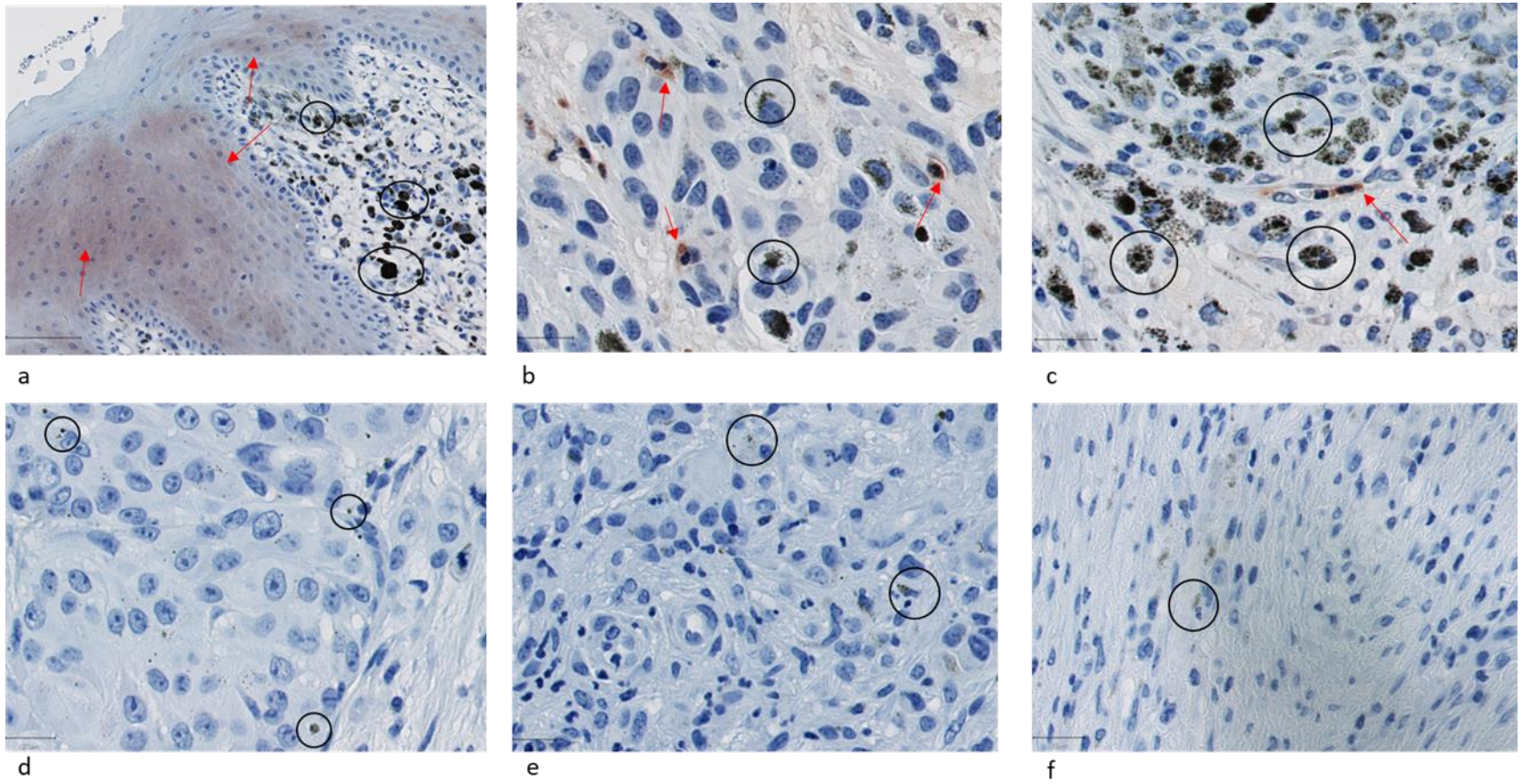

Figure 8.4 *IHC slides of equine melanoma used as positive control for the staining of the anti-BLMH antibody ab204584 (Abcam). (a), (b), (c) are three different area of the lesion stained with the anti-BLMH hydrolase. (d), (e), (f) correspond to the same lesion unstained with the antibody. Red arrows indicate relevant area of antibody staining (Vector Red) and black circles highlight melanin pigments*

8.2.8 Disclosure form and protocol for Bleosome application for equine patients (5.3.2.1)

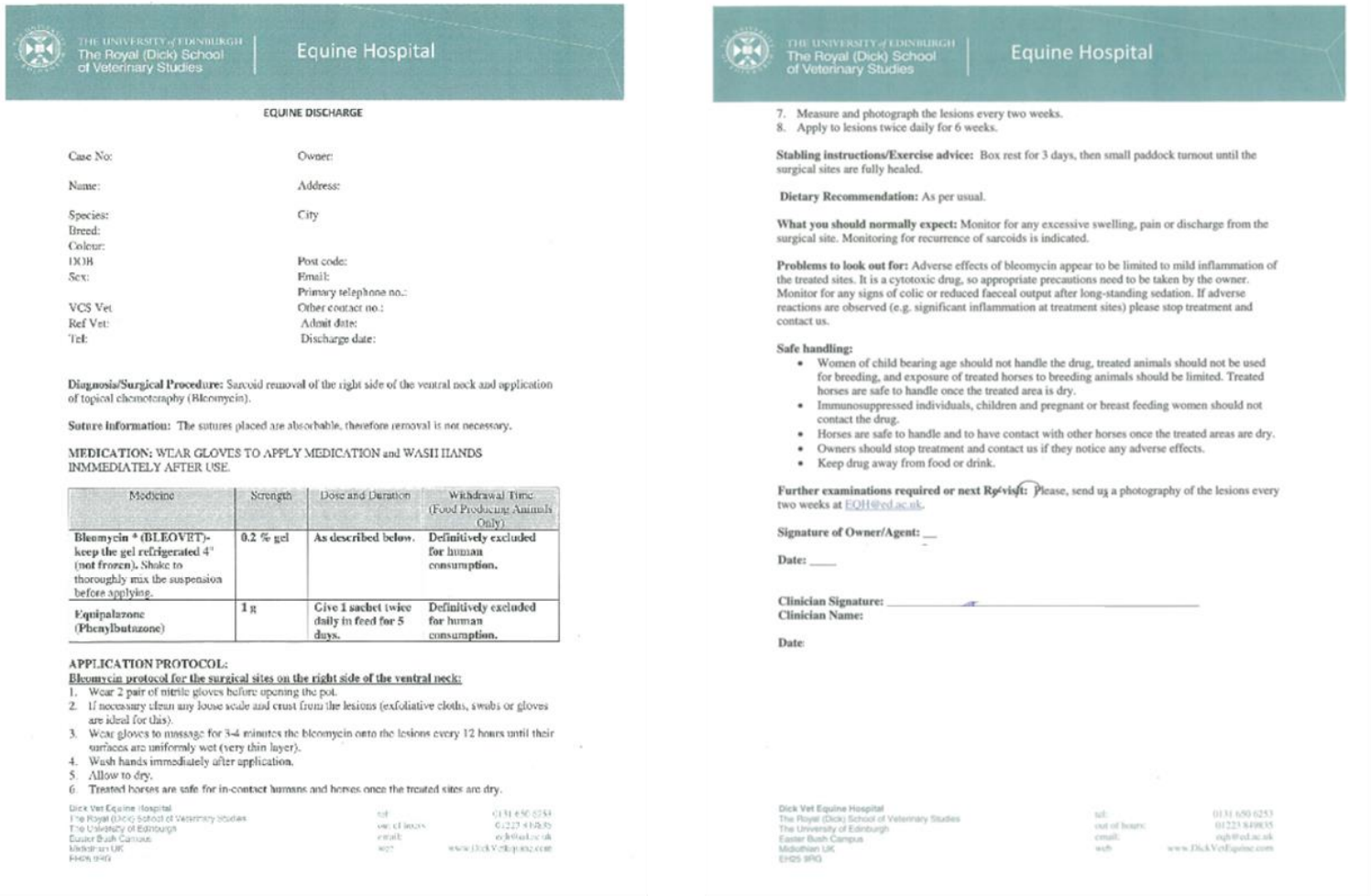

THE UNIVERSITY of EDINBURGH
The Royal (Dick) School of Veterinary Studies | Equine Hospital

EQUINE DISCHARGE

Case No:
Name:
Species:
Breed:
Colour:
DOB
Sex:
VCS Vet
Ref Vet:
Tel:

Owner:
Address:
City
Post code:
Email:
Primary telephone no.:
Other contact no.:
Admit date:
Discharge date:

Diagnosis/Surgical Procedure: Sarcoid removal of the right side of the ventral neck and application of topical chemotoraphy (Bleomycin).

Suture Information: The sutures placed are absorbable, therefore removal is not necessary.

MEDICATION: WEAR GLOVES TO APPLY MEDICATION and WASH HANDS IMMEDIATELY AFTER USE.

Medicine	Strength	Dose and Duration	Withdrawal Time (Food Producing Animals Only)
Bleomycin * (BLEOVET)- keep the gel refrigerated 4° (not frozen). Shake to thoroughly mix the suspension before applying.	**0.2 % gel**	**As described below.**	**Definitively excluded for human consumption.**
Equipalazone (Phenylbutazone)	**1 g**	**Give 1 sachet twice daily in feed for 5 days.**	**Definitively excluded for human consumption.**

APPLICATION PROTOCOL:
Bleomycin protocol for the surgical sites on the right side of the ventral neck:
1. Wear 2 pair of nitrile gloves before opening the pot.
2. If necessary clean any loose scale and crust from the lesions (exfoliative cloths, swabs or gloves are ideal for this).
3. Wear gloves to massage for 3-4 minutes the bleomycin onto the lesions every 12 hours until their surfaces are uniformly wet (very thin layer).
4. Wash hands immediately after application.
5. Allow to dry.
6. Treated horses are safe for in-contact humans and horses once the treated sites are dry.

Dick Vet Equine Hospital
The Royal (Dick) School of Veterinary Studies
The University of Edinburgh
Easter Bush Campus
Midlothian UK
EH25 9RG

tel: 0131 650 6253
out of hours: 07223 418035
email: eqh@ed.ac.uk
web: www.DickVetEquine.com

THE UNIVERSITY of EDINBURGH
The Royal (Dick) School of Veterinary Studies | Equine Hospital

7. Measure and photograph the lesions every two weeks.
8. Apply to lesions twice daily for 6 weeks.

Stabling instructions/Exercise advice: Box rest for 3 days, then small paddock turnout until the surgical sites are fully healed.

Dietary Recommendation: As per usual.

What you should normally expect: Monitor for any excessive swelling, pain or discharge from the surgical site. Monitoring for recurrence of sarcoids is indicated.

Problems to look out for: Adverse effects of bleomycin appear to be limited to mild inflammation of the treated sites. It is a cytotoxic drug, so appropriate precautions need to be taken by the owner. Monitor for any signs of colic or reduced faeceal output after long-standing sedation. If adverse reactions are observed (e.g. significant inflammation at treatment sites) please stop treatment and contact us.

Safe handling:
- Women of child bearing age should not handle the drug, treated animals should not be used for breeding, and exposure of treated horses to breeding animals should be limited. Treated horses are safe to handle once the treated area is dry.
- Immunosuppressed individuals, children and pregnant or breast feeding women should not contact the drug.
- Horses are safe to handle and to have contact with other horses once the treated areas are dry.
- Owners should stop treatment and contact us if they notice any adverse effects.
- Keep drug away from food or drink.

Further examinations required or next Revisit: Please, send us a photography of the lesions every two weeks at EQH@ed.ac.uk.

Signature of Owner/Agent: __

Date: ____

Clinician Signature: _____
Clinician Name:

Date

Dick Vet Equine Hospital
The Royal (Dick) School of Veterinary Studies
The University of Edinburgh
Easter Bush Campus
Midlothian UK
EH25 9RG

tel: 0131 650 6253
out of hours: 07223 418035
email: eqh@ed.ac.uk
web: www.DickVetEquine.com

Figure 8.5 *Discharge form and protocol for Bleosome application with safe handlings guidelines for owners of equine patients enrolled in the Bleosome case observation series*